WATER QUALITY MODELING OF LAKE DIEFENBAKER

A Thesis Submitted to the
College of Graduate and Postdoctoral Studies
in Partial Fulfillment of the Requirements
for the degree of Doctor of Philosophy
in the School of Environment and Sustainability
University of Saskatchewan
Saskatoon

by

AMIR SADEGHIAN

Permission to Use

In presenting this thesis in partial fulfilment of the requirements for a Postgraduate degree from the University of Saskatchewan, I agree that the Libraries of this University may make it freely available for inspection. I further agree that permission for copying of this thesis in any manner, in whole or in part, for scholarly purposes may be granted by the professor or professors who supervised my thesis work or, in their absence, by the Head of the Department or the Dean of the College in which my thesis work was done. It is understood that any copying or publication or use of this thesis or parts thereof for financial gain shall not be allowed without my written permission. It is also understood that due recognition shall be given to me and to the University of Saskatchewan in any scholarly use which may be made of any material in my thesis.

Requests for permission to copy or to make other uses of materials in this thesis/dissertation in whole or part should be addressed to:

Head of the School of Environment and Sustainability
University of Saskatchewan
117 Science Place
Saskatoon, Saskatchewan S7N 5C8
Canada

OR

Dean
College of Graduate and Postdoctoral Studies
University of Saskatchewan
116 Thorvaldson Building, 110 Science Place
Saskatoon, Saskatchewan S7N 5C9
Canada

Abstract

Lake Diefenbaker is one of the most important sources of water in the prairie province of Saskatchewan, Canada. It is a long (181.6 km) and narrow (maximum width 6 km) reservoir formed along the South Saskatchewan River by the construction of the Gardiner and Qu'Appelle River dams in the 1960s. The reservoir has a surface elevation of 556.87 meters above sea level (full supply level) with a maximum depth of 60 m, a surface area of approximately 393 km^2 and a volume of 9.03 km^3. The reservoir and dams are part of a multipurpose hydraulic project, which provides water for irrigation, drinking water, eco-services, hydropower generation, aquaculture and recreation as well as for flood mitigation.

Surface water quality modeling is a useful tool to simulate and predict nutrient dynamics in lakes, reservoirs, and rivers, as well as the fate and transport of sediment and toxic contaminants in freshwater environments. In this study, water quality modeling of Lake Diefenbaker was carried out in order to help understand the mixing regimes and biological processes in the aquatic environment of this strategic reservoir. Based on the study's objectives, the physical and chemical characteristics of the lake and available data, the laterally-averaged two-dimensional model CE-QUAL-W2 hydrodynamic and water quality model was deemed the best model for Lake Diefenbaker. CE-QUAL-W2 was developed by the US Army Corp of Engineers to simulate the hydrodynamics, water quality, aquatic biology and aquatic chemistry in surface waters.

On the one hand, this study provided information on temperature and hydrodynamic behaviors of Lake Diefenbaker as well as sediment and nutrient transport, nutrient uptake and algal activities. On the other hand, it addressed some key and limitations in the application of water quality models. Limitations addressed include studying snow cover effects on the ice surface in winter, applying variable algal stoichiometry, using combined local/global optimization for model calibration, and running the model on High-Performance Cluster (HPC) systems.

Acknowledgment

The person, who conducts the training and imparts his knowledge, is entitled to his own rights. He must be treated with honor and respect during his sessions. The audience must listen to him with full attention and attend to him with devotion. In asking him a question, your voice must be modulated. He must be allowed to answer and should not be interrupted. If anyone ever speaks ill of him in your presence, you must defend him, concealing his faults and emphasizing his virtues. Never sit with him in enmity or show hostility toward him in friendship. Keep away from his enemies, do not make enemies with his friends.

Imam Ali bin Al-Hussein (658 – 713 AD)

Firstly, I would like to express my honest gratitude to my Ph.D. supervisor Dr. Karl-Erich Lindenschmidt for his endless support, patience, motivation, and immense experience. His supervision helped me in all different stages of my research and thesis writing. I also would like to thank my co-supervisor, Professor Howard Wheater for his valuable guidance and encouragement and his insightful comments. My sincere thanks also go to all the members of my advisory committee: Professor Steven Chapra, Dr. Naveed Khaliq, Dr. Kerry Mazurek, Dr. Yanping Li, and Dr. Jeffrey Sereda, for their helpful feedbacks which helped me to obtain results of better quality. I am thankful to my defense external examiner Dr. Luis Camacho Botero for accepting this role and providing constructive feedback.

I would like to acknowledge the Canada Excellence Research Chair in Water Security, School of Environment and Sustainability and the University of Saskatchewan for their financial support. Besides, I would like to thank all the research groups that gave me access to the laboratory and field observation data.

I would like to thank my friends at the Global Institute for Water Security who were with me during my Ph.D. studies. It would be a long list to include all the names, so I apologize for, but I would like to especially thank Badrul Masud, Edward Bam, Moges Mamo, Hammad Javid, Julie Terry, Ali Nazemi, Razi Sheikholeslami, Shervan Gharari, Saman Razavi and Amin HaghNegahdar.

Last but not least, I need to thank my parents, parents-in-law and family members who have helped me unconditionally throughout my entire life. Countless thanks to my wife, Fatemeh Madaeni, for her patience, encouragement, and sacrifice. Without her support, I would not have been able to finish this research work.

In the Name of God, the Most Beneficent, the Most Merciful [1]

[1] Translation to English from Arabic. Calligraphy by Unknown, Source: Iran Calligraphers Association

Contents

Permission to Use i

Abstract ii

Acknowledgment iii

Contents ix

List of Tables x

List of Figures xvii

List of Abbreviations xviii

1 Introduction 1
- 1.1 Background information . . . 1
  - 1.1.1 Extreme events and water quality . . . 8
  - 1.1.2 Sustainability in Canadian prairie reservoirs . . . 10
- 1.2 Objectives and thesis structure . . . 13
  - 1.2.1 Content of the manuscript-style thesis . . . 14

References . . . 16

2 Modeling 24
- 2.1 Model selection . . . 24
  - 2.1.1 Governing equations . . . 26
  - 2.1.2 Bathymetry and model boundaries . . . 31
  - 2.1.3 Water quality data . . . 33
- 2.2 Model application . . . 37
  - 2.2.1 Temperature and hydrodynamics . . . 37
  - 2.2.2 Water quality . . . 38
  - 2.2.3 Sediment transport . . . 39

References . . . 41

3 Lake Diefenbaker temperature model 47
- 3.1 Abstract . . . 48
- 3.2 Introduction . . . 48
  - 3.2.1 Temperature effects . . . 48
  - 3.2.2 Ice cover . . . 49
  - 3.2.3 Lake Diefenbaker . . . 50
- 3.3 Methods . . . 53
  - 3.3.1 Study site description . . . 53

3.3.2 Model Selection . . . 53
3.3.3 Bathymetry . . . 54
3.3.4 Forcing data and boundary conditions . . . 55
3.4 Calculations . . . 61
3.5 Results . . . 62
3.5.1 Bathymetry . . . 62
3.5.2 Temperature simulation . . . 63
3.6 Discussion . . . 73
3.6.1 Sedimentation and erosion . . . 73
3.6.2 Simulations . . . 73
3.6.3 Mixing . . . 74
3.6.4 Temperature . . . 76
3.6.5 Uncertainties . . . 79
3.7 Conclusions . . . 79
3.8 Acknowledgments . . . 81
References . . . 81

4 Sedimentation and erosion in Lake Diefenbaker, Canada: solution for shoreline retreat monitoring 86
4.1 Abstract . . . 86
4.2 Introduction . . . 87
4.3 Methods . . . 90
4.4 Results and Discussion . . . 94
4.5 Conclusions . . . 105
4.6 Acknowledgements . . . 106
References . . . 106

5 Effects of meteorological data: long- and short-term quality controlled measured meteorological data and re-analyzed meteorological data on water temperature calibration 109
5.1 Abstract . . . 110
5.2 Introduction . . . 110
5.3 Methods . . . 112
5.3.1 Environment and Climate Change Canada Database . . . 116
5.3.2 AccuWeather Database . . . 116
5.3.3 MeteoBlue Database . . . 117
5.4 Results and Discussion . . . 118
5.5 Conclusions . . . 123
5.6 Acknowledgements . . . 124
References . . . 124

6 Input data for water quality models: a case study of South Saskatchewan River 128
6.1 Abstract . . . 128
6.2 Introduction . . . 129

6.3 Methods . . . 131
6.4 Results and Discussion . . . 136
6.5 Conclusions . . . 152
6.6 Acknowledgements . . . 154
References . . . 154

7 Water quality modeling of Lake Diefenbaker by using variable chlorophyll *a*/algal biomass ratio 159
7.1 Abstract . . . 159
7.2 Introduction . . . 160
7.3 Methods . . . 164
7.4 Results . . . 168
7.5 Discussion . . . 177
7.6 Conclusion . . . 179
7.7 Acknowledgements . . . 180
References . . . 180

8 Sediment plume model - a comparison between use of measured turbidity data and satellite images for model calibration 184
8.1 Abstract . . . 185
8.2 Introduction . . . 185
8.3 Methods . . . 191
8.3.1 Study site . . . 191
8.3.2 Measurements . . . 193
8.3.3 Model . . . 197
8.4 Results . . . 200
8.5 Discussion . . . 205
8.6 Conclusion . . . 210
8.7 Acknowledgements . . . 211
References . . . 212

9 Synthesis, conclusions and future works 217
9.1 Overviews . . . 217
9.2 Conclusions . . . 220
9.2.1 Bathymetry . . . 220
9.2.2 Temperature and hydrodynamics . . . 221
9.2.3 Meteorological data . . . 222
9.2.4 Water quality data . . . 223
9.2.5 Water quality modeling . . . 223
9.2.6 Sediment transport . . . 225
9.3 Future research . . . 225
References . . . 227

Appendices 230

I Modelling Scenarios to Estimate the Potential Impact of Hydrological Standards on Nutrient Retention in the Tobacco Creek Watershed, Manitoba, Canada **230**
I Abstract . . . 231
II Introduction . . . 232
III Study Site . . . 233
IV Methods and Data . . . 234
IV.1 Water Sampling . . . 234
IV.2 Modelling . . . 235
IV.3 New Channel Design . . . 238
V Results and Discussion . . . 240
V.1 Nitrogen (N) . . . 240
V.2 Phosphorus (P) . . . 241
V.3 Total Suspended Solids (TSS) and Dissolved Organic Carbon (DOC) 243
V.4 Total Sediment Load . . . 245
V.5 Modelling Results . . . 245
V.6 Discussion . . . 248
VI Conclusions . . . 252
References . . . 253

II Modelling Dissolved Oxygen/Sediment Oxygen Demand under Ice in a Shallow Eutrophic Prairie Reservoir **256**
I Abstract . . . 257
II Introduction . . . 257
III Materials and Methods . . . 261
III.1 Site Description . . . 261
III.2 Model Setup . . . 261
III.3 Data Collection and Analysis . . . 263
III.4 Model Customisation . . . 265
III.5 Model Setup and Application . . . 267
IV Results . . . 272
IV.1 Dissolved Oxygen Simulation . . . 272
IV.2 Sediment Oxygen Demand Relationships . . . 272
V Discussion . . . 273
VI Conclusions . . . 280
References . . . 281

III Calibration and optimization **284**

IV pH calculation code subroutine in CE-QUAL-W2 **289**

V Water quality variables in CE-QUAL-W2 **290**

VI Permission for use of published manuscripts **293**
.1 Elsevier License, terms and conditions 293
.2 Springer Licenses, terms and conditions 298
.3 MDPI Open Access 303

List of Tables

2.1 Description of different water quality models, after Vandenberg et al. 2011 . 25

3.1 Ice model equations and parameters 60
3.2 Simulated values for ice calculation in CE-QUAL-W2 model in 2012 – 2013 for Blackstrap Lake 60
3.3 Sedimentation and erosion rates based on comparison of cross sections from the late 1960s/early 1970s and the 2012–2013 cross sections. See Figure 3.2 for locations 63

4.1 Coordinates for new cross sections locations at Lake Diefenbaker's upstream reach 93
4.2 Precision control of Google Maps API data with the Natural Resources Canada control points 98

5.1 Total number of stations is listed as 8,732. However, after removing duplicates, 7,291 stations remain. Data derived from downloading the stations information from Environment and Climate Change Canada website on July 24, 2016 117
5.2 Comparison of measured data from the meteorological stations and MeteoBlue re-analyses data. Source: MeteoBlue (2016) 118

6.1 Variables used in CE-QUAL-W2 from model manual (Cole and Wells, 2013) 137

7.1 Distance between different sections in SSR / RDR / LDF. For locations see Figure 7.1 162
7.2 Statistics for model performance in normal and *Lite* models 173

I.1 Flow calculation table 240
I.2 Brown drain channel geometries at upstream and downstream 240
I.3 Design discharge at upstream site under various return periods 241
I.4 Design discharge at downstream site under various return periods 244
I.5 Model calibration coefficients ranges and final values 251

II.1 W2 Default kinetic coefficients used in this study for the sediment oxygen demand (SOD) and biochemical oxygen demand (BOD) calculations 265

V.1 CE-QUAL-W2 initial and optimal values for different parameters in the *Lite* model. Parameters definitions are from the CE-QUAL-W2 manual (Cole and Wells, 2015) 291
V.2 Derived variables in CE-QUAL-W2 model 292

List of Figures

1.1 Map of the South Saskatchewan River and Lake Diefenbaker 7

3.1 Map of the South Saskatchewan River Basin and Lake Diefenbaker. Locations 1 & 2 are hydrometric stations used for inflow water data. Location # 3 is upstream of Lake Diefenbaker at highway 4, # 4 is downstream of the lake at Gardiner Dam and # 5 is the City of Saskatoon where the outflow data were calculated from 52

3.2 Lake Diefenbaker bathymetry map from the 2013–2013 survey 55

3.3 Model segmentations and locations of observation stations and meteorological stations 57

3.4 Sensitivity analysis results. a: Sensitivity results for Monte-Carlo simulations for the model with 187 & 126 segments. WSC and SHADE are wind sheltering and shading coefficients. EXT and T_{IN} are light extinction coefficient and inflow temperature multipliers in equations 1& 2 64

3.4 Sensitivity analysis results. b: Sensitivity results for Monte-Carlo simulations for the model with 187 & 126 segments. WSC and SHADE are wind sheltering and shading coefficients. EXT and T_{IN} are light extinction coefficient and inflow temperature multipliers in equations 1& 2 65

3.4 Sensitivity analysis results. c: Comparison of model's results for two sensitive parameters (WSC & SHADE) with the 187 and 126 segments in 2011 & 2012. Each sheet is for the depth which is located and the next 15 meters below it. Since the number of samples were not the same at each depth, the sse/n (n is number of samples) was used instead for consistency 66

3.4 Sensitivity analysis results. d: Comparison of model results for two sensitive parameters (WSC & SHADE) for the model with 187 segments at different depths. Each sheet is for the depth which is located and the next 15 meters below it. Since the number of samples were not the same at each depth, the sse/n (n is number of samples) was used instead for consistency 67

3.5 Simulated (lines) vs measured (dots) temperature for observation station 10 (near Elbow) 69

3.6 Comparison of model original ice model with the modified ice code in both Blackstrap Lake and Lake Diefenbaker in winter 2012/2013 71

3.7 Quantitative contribution of different sources to the lake's heat budget. The parameter on the right (bed, tributary, evaporation and ice) has a scale of one tenth of those on the left (surface heat exchange, inflow, outflow and net). The "surface heat exchange" is the sum of all the shortwave and longwave solar radiation terms and conductive and evaporative fluxes. "Bed" is the heat exchange between sediment and water at the bottom of the lake. The "inflow" and "tributary" show the amount of heat added to the lake by the SSR and Swift Current Creek, respectively. The "outflow" and "evaporation" are the equivalent amounts of heat removed from the lake due, respectively, to water discharged via the outflow and evaporation. "Ice" represents the heat lost at the ice–water interface. The "net" component is the sum of all the components 72
3.8 Simulated longitudinal contours of water temperature for Lake Diefenbaker in May, June and July 2011. The figure on top shows the heat plume from the SSR inflow water. The windrose has also been included to show the effects of wind on shifting the thermocline (middle and bottom figures). The colorbar shows the values for both the wind speed and water temperature. The complete simulation profiles are available at: http://giws.usask.ca/proposals/LakeDiefenbakerTemperatureModel.avi 75
3.9 Net radiation at Lake Diefenbaker surface in 2012. a: Net radiation at Lake Diefenbaker surface in 2012 based on original code (Eq. 3.5) (no cloud cover). b: Net radiation on Lake Diefenbaker surface in 2012 based on modified ice code code (Eq. 3.8 and 3.9) ((no cloud cover). c: Difference in net radiation on Lake Diefenbaker surface in 2012 between original ice code and modified ice code ($RN_{modified}$ - $RN_{original}$). Positive values show less cooling in winter and negative values show less ice melting in spring compared to the original code 78

4.1 Location map of Lake Diefenbaker, and 1:50,000 topographic map sheets based on the National Topographic System (NTS) of Canada 88
4.2 1968–1972 cross section ranges locations for Lake Diefenbaker. The cross sections (ranges) 1–20 were on Lake Diefenbaker and cross sections 21–37 were on the South Saskatchewan River upstream of reservoir 91
4.3 Cross section ranges locations used for Google Maps Elevation API for Lake Diefenbaker's upstream. These cross sections are located between ranges 20 and 8 in Figure 4.2. The base map is taken from Google Satellite 92
4.4 Ranges 15, 17, 18 and 19 cross sections for 1944, 1968–1972 and 2012–2013. See Figure 4.2 for locations. (2012–13* are interpolated cross sections). The cross sections (ranges) 1–20 were on Lake Diefenbaker and cross sections 21–37 were on the South Saskatchewan River upstream of reservoir 95
4.5 Ranges 20, 21, 23 and 24 cross sections for 1944, 1968–1972 and 2012–2013. See Figure 4.2 for locations. (2012–13* are interpolated cross sections) 96
4.6 Maps of Natural Resources Canada control points used for precision control and comparison with Google Maps Elevation API data. Map obtained from GeoGratis Web Services, Natural Resources Canada 99

4.7 Cross sections for locations at Lake Diefenbaker's upstream shown in Figure 4.3 104

5.1 Map of South Saskatchewan River SSR, Red Deer River RDRand Lake Diefenbaker. The meteorological stations for the three databases are shown in graph on top. The graph in bottom shows the location of filed observation stations used for model calibration 113
5.2 Sensitivity analysis of Lake Diefenbaker temperature model performance based on three different meteorological databases. The figure shows effects of wind sheltering coefficient on model performance for all the measurements based on the best run for each meteorological station 119
5.3 Sensitivity analysis of Lake Diefenbaker temperature model performance based on three different meteorological databases. The figure shows effects of solar radiation shading on model performance for all the measurements based on the best run for each meteorological station 120
5.4 Sensitivity analysis of Lake Diefenbaker temperature model performance based on three different meteorological databases. The figure shows the model overall performance for all the measurements based on the best run for each meteorological station 121
5.5 Comparing the temperature profiles from the results of different meteorological databases with the measured data. The stations in the top left corner start from upstream towards the dams downstream 122

6.1 Map of the South Saskatchewan River and Red Deer River. The hydrometric stations are marked by red triangles on the map 132
6.2 Discharge and water temperature data in South Saskatchewan River (SSR) at Medicine Hat station and Red Deer River (RDR) at Bindloss station for 2011 – 2014 135
6.3 Correlations between different water quality variables in the South Saskatchewan River (SSR) at the Medicine Hat station and the Red Deer River (RDR) at the Bindloss station 138
6.4 Daily time-series for different water quality variables: a) specific conductance, b) total dissolved solids, c) total dissolved phosphorus, d) phosphate. The concentrations of these variables are based on the averaged first-order and second-order polynomial fitting method in the South Saskatchewan River (SSR) at the Medicine Hat station and the Red Deer River (RDR) at the Bindloss station for 2011 – 2014 139
6.5 Daily time-series for different water quality variables: a) total phosphorous, b) nitrate plus nitrite, c) ammonia, d) total dissolved nitrogen. The concentrations of these variables are based on the averaged first-order and second-order polynomial fitting method in the South Saskatchewan River (SSR) at the Medicine Hat station and the Red Deer River (RDR) at the Bindloss station for 2011 – 2014 141

6.6 Daily time-series for different water quality variables: a) particulate nitrogen, b) total nitrogen, c) chlorophyll *a*, d) algal biomass. The concentrations of these variables are based on the averaged first-order and second-order polynomial fitting method in the South Saskatchewan River (SSR) at the Medicine Hat station and the Red Deer River (RDR) at the Bindloss station for 2011 – 2014 143
6.7 Daily time-series for different water quality variables: a) dissolved organic carbon, b) particulate organic carbon, c) dissolved organic matter, d) particulate organic matter. The concentrations of these variables are based on the averaged first-order and second-order polynomial fitting method in the South Saskatchewan River (SSR) at the Medicine Hat station and the Red Deer River (RDR) at the Bindloss station for 2011 – 2014 145
6.8 Daily time-series for different water quality variables: a) total organic carbon, b) total organic matter, c) labile/refractory dissolved organic matter, d) labile/refractory particulate organic matter. The concentrations of these variables are based on the averaged first-order and second-order polynomial fitting method in the South Saskatchewan River (SSR) at the Medicine Hat station and the Red Deer River (RDR) at the Bindloss station for 2011 – 2014 147
6.9 Daily time-series for different water quality variables: a) labile/refractory dissolved organic matter - phosphorus, b) labile/refractory particulate organic matter - phosphorus, c) labile/refractory dissolved organic matter - nitrogen, d) labile/refractory particulate organic matter - nitrogen. The concentrations of these variables are based on the averaged first-order and second-order polynomial fitting method in the South Saskatchewan River (SSR) at the Medicine Hat station and the Red Deer River (RDR) at the Bindloss station for 2011 – 2014 149
6.10 Daily time-series for different water quality variables: a) total suspended solids, b) Inorganic suspended solids, c) Dissolved oxygen, d) reactive silica. The concentrations of these variables are based on the averaged first-order and second-order polynomial fitting method in the South Saskatchewan River (SSR) at the Medicine Hat station and the Red Deer River (RDR) at the Bindloss station for 2011 – 2014 151
6.11 Daily time-series for different water quality variables: a) total alkalinity, b) pH, c) total inorganic carbon. The concentrations of these variables are based on the averaged first-order and second-order polynomial fitting method in the South Saskatchewan River (SSR) at the Medicine Hat station and the Red Deer River (RDR) at the Bindloss station for 2011 – 2014 153

7.1 South Saskatchewan River (SSR) and Lake Diefenbaker (LDF), Alberta and Saskatchewan, Canada. The segmentations show different waterbodies (black lines) and branches (red lines) used by the CE-QUAL-W2 model. Blue triangles with red filling show locations of observation stations 163
7.2 LDF model segmentation for the normal (fine) and *Lite* (coarse) models in CE-QUAL-W2 168

7.3 Lake Diefenbaker segmentation and layering for the normal (fine) and *Lite* (coarse) models . . . 169
7.4 Simplified flow diagram of the components and interactions within the the CE-QUAL-W2 model based on CE-QUAL-W2 manual, (Cole and Wells, 2013). LDOM, RDOM, LPOM, RPOM are labile/refractory dissolved/particulate organic matter . . . 171
7.5 Model performance for the *Lite* model based on fixed ACHLA. OBS stands for observation values and SIM for simulated values . . . 172
7.6 Top and left: nitrogen limiting for algal growth. Top and right: phosphorus limiting. Middle and left: nutrients (nitrogen and phosphorus) limiting. Middle and right: light limiting. Bottom: ACHLA values based on limiting conditions. All the sub-plots show the values at the depth of 2 m from the surface . . . 175
7.7 Model performance for the *Lite* model based on variable ACHLA. OBS stands for observation values and SIM for simulated values . . . 176
7.8 Simplified nitrogen cycle in water . . . 178

8.1 Lake Diefenbaker (LDF), Saskatchewan, Canada. The reservoir is divided into four sections (waterbodies) which allow use of four different meteorological stations along the reservoir. Solid red lines show locations of waterbodies in the model. The dotted red line at the Elbow shows the location at which the Qu'Appelle River Dam branch merges to the main channel in the model. Red circles show locations of stations with turbidity data measurements. . . . 189
8.2 Discharge values at South Saskatchewan River (SSR), Red Deer River (RDR), inflow to Lake Diefenbaker (LDF), outflow from LDF and water level elevation at the Gardiner Dam. The SSR and RDR merge 171 km upstream of the LDF inlet. . . . 192
8.3 Recorded air temperature (top) and wind speed (bottom) at the Elbow station. The vertical strips show cloud amount with darker bands meaning more clouds. . . . 193
8.4 Water temperature on July 1^{st}, 2013 in Lake Diefenbaker when the flood peak arrived at the reservoir. . . . 194
8.5 Vertical turbidity profiles collected at 12 stations along Lake Diefenbaker in June and July 2013. . . . 195
8.6 Satellite images obtained from MODIS for Lake Diefenbaker during the 2013 flood event. Land areas around Lake Diefenbaker blurred by 70% to better show the reservoir area. The images with green marker and date are real satellite images. The image with red marker (July 31^{st}) is interpolated. . . . 196
8.7 Estimating the TSS concentration at LDF upstream based on C_{IN} and discharge. 199
8.8 Sensitivity analysis for parameters SSS (m/day) and τ_{cr} (dynes/cm^2) for observations with TSS values larger than 15 mg/l. SSS ranged between zero and 6. τ_{cr} ranged between zero and 4 . . . 202

8.9 Simulated TSS ranges for different SSS (m/day) values. The bands show the ranges that the model calculated the TSS concentrations by using the SSS values in the specified ranges for different days/locations. Small SSS over-predict TSS at downstream several order of magnitudes 203
8.10 Simulated TSS values at the water surface for different SSS (m/day) values. The color-bar is in logarithmic scale to capture trends in both upstream with large TSS concentrations and downstream with small concentrations 204

I.1 The Tobacco creek watershed is located in southern Manitoba. the brown drain is at sites 17 and 11 while the main drain is sites 4, 6. 7, and 5 235
I.2 Channel geometry of the Brown drain in tobacco creek 236
I.3 Flow and water level in the Brown drain during the year 2013. outliers in the data are marked with a red cross 237
I.4 St. Adolphe design storms (environment Canada, 1967 – 2000) 238
I.5 Channel profiles for different return period rainfalls 239
I.6 Rating curve for outflowing water at downstream 239
I.7 Nitrogen concentrations at Site 17 in the Brown drain during the year 2013 . 241
I.8 Nitrogen concentrations at Site 17 in the Brown drain during the year 2013 . 242
I.9 Phosphorus concentrations at Site 17 in the Brown drain during the year 2013 243
I.10 Phosphorus concentrations at Site 11 in the Brown drain during the year 2013 244
I.11 DOC, TSS, and discharge at site 17 of the Brown drain during the year 2013 245
I.12 DOC, TSS, and discharge at site 11 of the Brown drain during the year 2013 246
I.13 Total sediment load at site 17 in the Brown drain 247
I.14 Total sediment load at site 11 in the Brown drain 248
I.15 Simulated and observed nutrient concentrations 249

II.1 Buffalo Pound Lake, Saskatchewan, Canada. Mean depth is 3.8 m with a maximum depth of 5.98 m. Mean residence time is highly variable (6 to 30 months). Flow is in a southeast direction. The black reservoir outline is to the provided scale. The digital elevation model (DEM) shows bathymetry for the main body of the lake downstream of the underpass 262
II.2 Results of the water temperature model. Compares predicted temperatures in the same grid cell as the Buffalo Pound Water Treatment Plant weekly observations. Note that CE-QUAL-W2 converts the negative water temperature modelled at the start of each winter to equivalent ice thickness. Root mean square error = 1.46 (to 2 dp); mean absolute error = 1.12 (to 2 dp) 268

II.3 The dissolved oxygen (DO) model using variable sediment oxygen demand (SOD) rates found through a semi-automated calibration procedure to match weekly predicted and observed DO concentrations (WTP weekly DO). These SOD rates are maximum values, as used by CE-QUAL-W2. The black line represents the best fit we could achieve by Monte Carlo analyses using a constant SOD rate (root mean square error = 1.94 (to 2 dp); mean absolute error = 1.43 (to 2 dp). Ice-cover days shown here in blue stripes are observed data from the Buffalo Pound Water Treatment Plant. Predicted DO concentrations using the variable SOD have root mean square error = 1.58 (to 2 dp); mean absolute error = 1.1 (to 2 dp) 269

II.4 Observed dissolved oxygen (DO) and biochemical oxygen demand (BOD) inflow data, and in-reservoir Chlorophyll-a (Chla) concentrations in BPL. The DO and BOD data are monthly measurements at the upstream boundary (BOD as the standard five-day BOD at 20 °C), and the Chla data are from the long-term weekly dataset, provided by the Buffalo Pound Water Treatment Plant, at the downstream sample point 271

II.5 Dissolved oxygen (DO) model using summer sediment oxygen demand (SOD) rates based on the maximum summer Chlorophyll-a. The end of season peak and winter decay are found through a semi-automated calibration procedure to match weekly observed DO concentrations (WTP weekly DO). Ice-cover days shown here are the observed data from the Buffalo Pound Water Treatment Plant, and snow data are from Environment Canada. Snow on the ground is measured on the last day of each month. Predicted DO have root mean square error = 1.47 (to 2 dp); mean absolute error = 1.09 (to 2 dp) 273

II.6 Relationships between SOD (day^{-1}), and observed BPL measurements, after the final DO model simulation: (**a**) Predicted peak SOD and average open water BOD inflows (R^2 = 0.85); (**b**) Back-calculated winter SOD decay, and observed maximum summer Chla concentrations of the previous summer (R^2 = 0.88) 274

II.7 A comparison of the maximum SOD rates that we input into the model (blue) against the temperature adjusted rates that the model is actually using based on W2 default values for the four temperature-rate multipliers (green). Also shown is the temperature adjusted rates for the fixed SOD simulations . . . 278

III.1 Optimization method procedure. a: PSO+LM runs for the model with 126 segments in 2011 and 2012. The figure shows the distribution of parameters that are selected by algorithms which is different from the uniform distribution in Monte-Carlo simulations. The size of the circles is also an indicator of errors. The bigger the circles the larger the SSE. b: Model parameter distribution for best PSO+LM run. In each year the total runs are 35 including 24 PSO (red circles) and 11 LM runs (blue circles) 287

List of Abbreviations[2]

AB	Alberta
ACHLA	Ratio between algal biomass and chlorophyll *a*
ALG	Algae, mg/L organic matter (dry weight)
ALK	Alkalinity mg/L as $CaCO_3$
BOD	Biological Oxygen Demand
C	Carbon
CBOD	Carbonaceous biochemical oxygen demand, mg/L O_2
Chla	Chlorophyll *a*
DO	Dissolved oxygen, mg/L O_2
DOC	Dissolved Organic Carbon
DOM	Dissolved Organic Matter
DON	Dissolved Organic Nitrogen
DOP	Dissolved Organic Phosphorous
EXT	Light extinction coefficient
HPC	High-performance computing
ISS	Inorganic suspended solids, mg/L
LDF	Lake Diefenbaker
LDOM	Labile dissolved organic matter, mg/L organic matter
$LDOM_N$	Total N in labile dissolved organic matter
$LDOM_P$	Total P in labile dissolved organic matter
LPOM	Labile particulate organic matter, mg/L organic matter
$LPOM_N$	Total N in labile particulate organic matter
$LPOM_P$	Total P in labile particulate organic matter
N	Nitrogen
NH_4	Ammonia, mg/L as N
NO_3	Nitrate, mg/L as N
OM	Organic matter
P	Phosphorous
PO_4	Phosphate, mg/L as P
POC	Particulate Organic Carbon
POM	Particulate Organic Matter
PON	Particulate Organic Nitrogen
POP	Particulate Organic Phosphorous
PSO	Particle Swarm Optimization

[2]In the digital (PDF) version, when the mouse cursor appears over these abbreviations, a pop-up window containing the complete form of the associated word will be displayed.

RDOM	Refractory dissolved organic matter, mg/L organic matter
$RDOM_N$	Total N in refractory dissolved organic matter
$RDOM_P$	Total P in refractory dissolved organic matter
RDR	Red Deer River
RMSE	Root mean square error
RPOM	Refractory particulate organic matter, mg/L organic matter
$RPOM_N$	Total N in refractory particulate organic matter
$RPOM_P$	Total P in refractory particulate organic matter
SHADE	Shading coefficient
Si	Silica
SK	Saskatchewan
SOD	Sediment Oxygen Demand
SRB	Saskatchewan River Basin
SS	Suspended solids, mg/L
SSE	Sum of squared errors
SSR	South Saskatchewan River
SSRB	South Saskatchewan River Basin
SSS	Suspended solids settling rate
τ_{cr}	Critical shear stress for sediment resuspension
TDP	Total Dissolved Phosphorous
TDS	Total dissolved solids, mg/L
TIC	Total inorganic carbon mg/L as C
T_{IN}	Inflow temperature coefficient
TIP	Total Inorganic Phosphorous
TN	total Nitrogen
TOC	Toxic Organic Chemicals
TP	Total Phosphorous
TSS	Total suspended solids, mg/L
WSC	wind sheltering coefficient
WWTP	Wastewater Treatment Plant

Chapter 1
Introduction

Surface water quality modeling is a useful tool to simulate and predict nutrient dynamics in lakes, reservoirs, and rivers, as well as to determine the fate and transport of sediment and toxic contaminants in freshwater environments. In this study, water quality modeling of Lake Diefenbaker was carried out to help understand the mixing regimes and biological processes in the aquatic environment of this strategic waterbody. Lake Diefenbaker is one of the most important sources of water in the prairie province of Saskatchewan, Canada. It is a long (181.6 km) and narrow (maximum width 6 km) reservoir formed along the South Saskatchewan River by the construction of the Gardiner and Qu'Appelle River dams in the 1960s. The reservoir and dams are part of a multipurpose hydraulic project, which provides water for irrigation, drinking water, eco-services, hydropower generation, aquaculture and recreation. The reservoir is also used for flood mitigation and as a receptacle for treated wastewater. On the one hand, this study provides information on temperature and hydrodynamic behaviors of Lake Diefenbaker, as well as sediment and nutrient transport, nutrient uptake and algal activities. On the other hand, some key limitations and knowledge gaps in applying water quality models are discussed and the solutions are addressed including calibrating the model when using limited input data at boundaries, applying combined local/global optimization for faster model calibration, considering effects of snow cover on the ice surface in winter, running the model on High Performance Cluster (HPC) systems and applying variable chlorophyll a/algal biomass ratio in water quality model simulations.

1.1 Background information

Water resources problems are becoming more complex as we go forward in uncertain future. Demands on and competition for water resources are increasing; at the same time, we are facing more uncertainties in predicting future conditions of our changing environment (Wheater and Gober, 2013). Expected climate and land use change effects in the future are higher air temperatures and, consequently, higher water temperatures, transport of

excessive nutrient loads to rivers, changes in dissolved oxygen concentrations in water, and degradation of water quality (Delpla et al., 2009; Ficklin et al., 2013; Jeppesen et al., 2009; Morrison et al., 2002; van Vliet et al., 2013). These negative environmental impacts will have economic costs as water treatment requirements rise in line with increasing reserves of poor water quality (Muller, 2007). This is especially true of our drinking water supplies in reservoirs, lakes and rivers that may suffer greatly from these expected changes (Bates, 2009; Muller, 2007).

Water quality processes are temperature dependent (Cole and Wells, 2015), and the impacts of higher water temperatures are going to be very diverse (Delpla et al., 2009; Murdoch et al., 2000; Whitehead et al., 2009). In general, solutes are more soluble at higher temperatures, while gases are less (Ji, 2008). For example, warming water temperatures increase chemical reaction rates, decomposition rates, the sediment oxygen demand and biochemical oxygen demand rates as well as algal kinetic rates (Cole and Wells, 2015). In contrary, the dissolved oxygen concentration decreases because gases are less soluble at higher temperatures (Ji, 2008; Matear et al., 2000). Phytoplankton growth is highest in summer because of the availability of light and thermal energy (Eppley, 1972). Dead algae and detritus are added to the water and sediment as organic matter (Cole and Wells, 2015). Algal mortality and settling to sediment increases sediment oxygen demand (Terry et al., 2017), and decomposition of the organic matter consumes oxygen in the water. Productivity (phosphorus and Chlorophyll concentrations), therefore, directly influences the amount of organic matter added to water (algae use inorganic nutrients and convert them to organic matter), and is a function of temperature (Hosseini et al., 2017a; Terry et al., 2017). Ji (2008) summarized the main effects of the temperature in waterbodies as the following: affecting stratification and mixing; dissolved oxygen solubility; biological and physiological processes (metabolic and reproductive rates); reaeration; sorption of organic chemicals and particulate matter; aquatic species tolerance rates; and economic values (cooling towers).

Higher air temperatures can also impact water quality indirectly through influencing ice phenology (Hosseini et al., 2017a,b). Rivers and lakes of high latitude regions experience several months of thick ice cover (Lindenschmidt, 2017), as much as one meter thick, that in some places connect separated lands to each other. Under the ice, lakes and reservoirs have different physical, chemical and biological characteristics than ice-free conditions as

a result of different light and temperature levels (Agbeti and Smol, 1995). Many water quality actions are at their lowest in near-freezing temperatures - although they still exist (Ji, 2008). The ice layer on the surface of a lake works as a barrier for solar radiation penetration, which is the primary source of heat, energy and light to the water (Jacoby and Welch, 2004; Scheffer, 2004). Snow cover on the ice surface reduces light and heat penetration even further (Sadeghian et al., 2015). Snow has a high albedo in relation to open water conditions (Grenfell and Maykut, 1977). Under-ice, there is also the possibility of inverse stratification where the top layer of water near the ice is colder than the bottom layers due to water temperature density differences (Jacoby and Welch, 2004).

The oxygen levels of ice-covered lakes are largely dependent on the lake's productivity during the ice-free period, the sediment oxygen demand over winter (Babin and Prepas, 1985; Hosseini et al., 2016; Terry et al., 2017), and the duration of ice-cover (Scheffer, 2004). The bottom temperature affects the sediment oxygen demand by influencing chemical reaction rates, and under-ice heat fluxes from the sediment bed become important. In open-water, dissolved oxygen is added to the water column freely by aeration at the water-air boundary and by photosynthesis within the water column (Cole and Wells, 2015). In winter, ice cover prevents aeration of the water at the surface; therefore, photosynthesis becomes the primary producer of dissolved oxygen in water (Ji, 2008). The lack of light under-ice reduces photosynthesis to minimal levels, and so oxygen levels can become dangerously low over a prolonged ice-cover period. Where there are high concentrations of organic matter in the lake, care should be taken to avoid anoxic conditions (Barica and Mathias, 1979). Clearing any snow-cover may help by allowing more light penetration and higher photosynthesis by algae (Dubourg et al., 2015). Understanding how increasing air and water temperatures will impact a waterbody is therefore of considerable importance for a water manager.

The quality of water in a lake or reservoir is additionally linked to the activities in its watershed (Lee et al., 2009). In the Canadian prairies, where the majority of water in the lakes comes from upstream watersheds, the effects are even higher. The larger the upstream watershed compared to the surface area of a lake, the stronger the effects on water quality (Mehaffey et al., 2005). This means for small prairie lakes, with large watersheds, the upstream land management practices impact greatly on water quality as well as quantity. Excessive nutrients levels and pollution (toxic substances) are among the major problems

for water resources management (Wetzel, 2001).

Eutrophication sits on the top of the list of challenges (Wetzel, 2001). Eutrophication results from overproduction of a waterbody and the existence of undesirable forms of algae such as cyanobacteria that are usually limited by nutrients availability in water (Smith et al., 1999). Generally, the limiting factor in fresh waters is phosphorus and in marine waters is nitrogen (Correll, 1999). Problems associated with eutrophication include decreasing light intensities and dissolved oxygen levels, and increasing turbidity and nutrient concentration (Karadvzic et al., 2010). Any excessive changes in a waterbody can put further stresses on the sensitive biological communities (Brierley and Kingsford, 2009). In example, cyanobacteria are highly tolerant to stressed environments because they can float and sink in the water column depending on light and nutrient availability (Ji, 2008). The floating and sinking help the cyanobacteria to adapt and still grow in less favorable conditions faster than other algae giving them competitive advantage over the other species (Scheffer, 2004). Cyanobacteria prevent light from penetrating to the water by creating scums on the surface of water which reduce the oxygen production by photosynthesis (Ji, 2008). The high amounts of cyanobacteria then lead to further degradation of water quality, hypoxia and fish kills, bad odor and recreational problems (McInnes and Quigg, 2010; Paerl, 2006; Paerl et al., 2001).

In order to deal with all the previously mentioned water quality problems, monitoring ecological and environmental changes due to different land/water management and pollution control practices, and predicting the repercussions for water quality is critical (McIntyre et al., 2005). Monitoring allows water resources managers to get advance warning of potential problems. Monitoring is, generally, associated with field observations at regional and local scales. Chlorophyll *a* concentrations and Secchi depth are early indicators of eutrophication followed by total phosphorus, total nitrogen, dissolved oxygen, biochemical oxygen demand, organic matter concentrations and sediment oxygen demand as more comprehensive water quality variables are needed for a complete monitoring program (Ji, 2008). Dissolved oxygen is the only water quality variable that can represent the health and quality of water in the absence of other variables (Ji, 2008).

Generally, the temporal sampling frequencies and spatial distribution of stations in water quality databases are not satisfactory enough to carry out an accurate evaluation of the

environment on which responsible agencies can make management decisions. Also, there are many external factors that must be taken into consideration because of their influence on the outcomes on management decisions. These factors include effects of climate change (Gosling and Arnell, 2016), land use changes (El-Khoury et al., 2015), increasing populations (Vörösmarty et al., 2000), industrial development (Aulakh et al., 2009), mining activities (Schmidt et al., 2012), wastewater treatment plant affluents (Bunzel et al., 2013), agricultural tillage practices (Kachi et al., 2016) and fish, poultry and livestock farming (Herbst et al., 2012). The biggest problem with these activities is their contribution to both point source and nonpoint source contamination (e.g., pesticides) and nutrients (mainly phosphorus and nitrogen) discharged into waterbodies (Chislock et al., 2013; Wu and Chen, 2013). Hence, monitoring programs, especially for large scale regions, need to be linked to other sources of information to minimize the risk of overestimation and underestimation due to propagations of errors. Computer models can help to cover the limitations of the monitoring programs, and in a better understanding of the complexities of the environmental systems by incorporating different sources of information to interpretable numerical and visual forms.

Water quality models are useful tools for studying the physical, chemical and biological processes and mechanisms in rivers and lakes (Sadeghian et al., 2014). They can be used to compensate for limitations in water quality data and to consider effects of different sources of uncertainties (Chapra, 2008). They are useful for simulating and predicting nutrient and algae dynamics as well as the fate and transport of toxins. Water quality models are also used to address characteristics of the waterscape including complex geomorphology (Missaghi and Hondzo, 2010), complicated boundary conditions (Jin et al., 2007), and multidimensional internal processes (Kopmann and Markofsky, 2000). A typical water quality model might use hourly climate data, daily flow data and monthly chemical and biological data, but is often expected to produce high-resolution results (e.g., hourly) (Hughes and Slaughter, 2016; James, 2016; Leon et al., 2011). As a result, some modelers are tempted to move towards more complex models with higher dimensions [e.g., two and three-dimensional (2D and 3D)], but at the cost of higher uncertainty levels due to over-parameterization (Freni et al., 2011). To represent the uncertain boundary conditions, especially of future, water quality models are required to be linked to hydrological models (Rode et al., 2010).

The Canadian prairie and its main watershed, the Saskatchewan River Basin (SRB), are unique in having many extremes; extreme temperatures (-40 – +40 °C), extreme events (the 1999 – 2004 droughts and 2011 and 2013 floods) and extreme statistics (80% of SRB runoff from the Rocky Mountain, 80% of Canada's agriculture in the prairies, 75% of Canada's irrigated agriculture in Alberta and Saskatchewan, 82% of SRB water for irrigated agriculture) (c.f. Wheater and Gober, 2013; Wheater, 2015). The occurrence of all these extremes in the SRB watershed makes the area a suitable choice for researchers to study the key challenges and pressures on water resources including the effects of climate and land-use changes; pollution; agricultural and industrial developments; and economic developments (Sadeghian et al., 2015; Wheater, 2015). Gober and Wheater (2014) listed the main governance concerns in the SRB to be the provision of water to the inhabitants; hazard protection; meeting drinking, agriculture and industry requirements; and water allocation issues between Alberta:Saskatchewan:Manitoba.

Lake Diefenbaker is situated in the SRB. The South Saskatchewan River (SSR) is a long river (1,392 km) (Sheelanere et al., 2013) flowing North-east through the provinces of Alberta and Saskatchewan in Canada (Figure 1.1). Near the Alberta-Saskatchewan border, the Red Deer River (RDR) merges with the SSR. Approximately 171 kilometers downstream of the SSR and RDR confluence is the inlet to Lake Diefenbaker at Saskatchewan's Highway 4. Lake Diefenbaker is a strategic reservoir formed by the construction of two earth-filled dams (the Gardiner Dam and the Qu'Appelle River Dam) in the SSR valley. The reservoir is 181 km long with increasing depth from 8 m at its upstream, to 60 m at the Gardiner Dam, with a volume capacity of 9.03 km^3 at full-level (Sadeghian et al., 2015). Most of the inflow (∼98%) comes from the SSR, and the main outflow (∼98%) is through the Gardiner Dam. The reservoir provides water storage capacity for irrigation, drinking water, recreation, eco-services, hydropower generation, fish farming and waste receptacles. It also plays a key role in flood mitigation (WSA, 2012).

In recent years, algal blooms, an indicator of eutrophication, have been observed in some parts of the lake (Giesy et al., 2009). Potential causes are pollution from lagoons and runoff, the inflow of excessive nutrients, nutrient remobilization from the bottom sediments and nutrient pulses from the hypolimnion to epilimnion due to upwelling or flood plumes (Sadeghian et al., 2014). Although historical studies have been limited, a significant

Figure 1.1: Map of the South Saskatchewan River and Lake Diefenbaker

experimental program has combined expertise in limnology and toxicology to investigate nutrient loads, the lake's physical and biological processes, sediment properties and the potential for nutrient release from 2011 – 2014 (c.f. North et al., 2015a). This period coincided with massive inflows of both nitrogen (N) and phosphorus (P), with almost 90% retention of P within the lake system (North et al., 2015b).

This makes the reservoir an ideal place to study the temperature and mixing regimes, nutrient and water quality variable pools, and sediment transport using a comprehensive water quality model which can address concerns regarding the shifts in the aquatic structure of the reservoir's ecosystem in light of future climate and land-use changes.

1.1.1 Extreme events and water quality

Extreme weather events, such as drought and flooding, are happening more frequently as a result of climate and land use changes, and management practices (Gober and Wheater, 2014). Both droughts and floods lead to concerns about transport of pollutants to waterbodies, and intensify the challenge of reservoir management (Birch, 1885; Cánovas et al., 2008; Foster and Charlesworth, 1996). The pollutants may originate from point sources or nonpoint sources. Point sources need a minimum river flow to dilute and mix the pollutant with the water, otherwise all the available dissolved oxygen can be consumed and anoxia conditions occur (Scheffer, 2004). Hence, low flows during drought conditions become problematic where the release of point source pollutants are set at a constant rate in respect to normal flow rates (Ji, 2008).

In contrast, the concentrations of pollutants from nonpoint sources can increase several orders of magnitude during high flow conditions during flooding with large uncertainties on the amounts of pollutants and nutrients that are transported into rivers and lakes (Shen et al., 2008; Whitworth et al., 2012). Extreme floods can extend to the banks and nearby lands, and when the waters drain back from the submerged areas to the streams there is a high potential for pesticide, other organic chemical contamination and nutrients to enter the water (Bainbridge et al., 2009). Land erosion during flooding can increase this pollutant load and bring particulate sediments to the waterbody (Borah and Bera, 2003). Large quantities of suspended solids can influence the water quality by changing

the sediment-water interactions and the ecological balance (Walling, 1977). Suspended Sediments (SS) contribute to the turbidity of the water and change light penetration, water density and nutrient availability (Dubourg et al., 2015; Schallenberg and Burns, 2004). Reduced light availability in water leads to decreasing photosynthesis rates and, consequently, decreases the oxygen production (Urabe et al., 2002). In addition, the reduced light penetration influences the water temperature by providing less thermal energy which, in turn, can affect biological activities and chemical reaction rates in water (Caissie, 2006).

The time of the year when a flood occurs significantly influences the impacts on the receiving waterbody (Whitworth et al., 2012). The existence of vegetation cover, soil frosts (low infiltration rates), and length of time from application of fertilizer, and more importantly the thermal and stratification conditions of a lake may all affect the nutrient loads (Ji, 2008; Wetzel, 2001). Depending on the inflow water density gradient (a function of water temperature and dissolved and suspended solids), the incoming flow could enter a lake in three different ways (Romero and Imberger, 2003). Warmer river waters usually have a lower density than the lake's water and enter along the top of the lake's water as overflow (Alavian et al., 1992). The heavier river waters which are mainly due to cold and sediment-laden flood waters enter along the lakebed as underflow or density currents (Fink et al., 2016). At the point where the density of the underflow become lower than the density of the water at the lakebed, the flow spreads into the upper layers as interflow until the mixing balances the density gradient (Alavian et al., 1992).

When floodwaters enter a lake as overflow, high amounts of nutrients become available in the euphotic zone (the upper part in lakes that receive enough quantity of light for photosynthesis) (Jacoby and Welch, 2004). Adequate light and large volumes of nutrients boost algal activities and can lead to algal blooms and eutrophication (Smith, 1986). When the water enters as underflow, the water goes to the bottom and nutrients become unavailable for algal uptake because the light intensity and temperature are low at the bottom (Ji, 2008). As a result, the sediment load contributes fewer problems in the short term (Vincent et al., 1991). Interflow effects can be either contributing or noncontributing to eutrophication depending on the thermal and stratification conditions and euphotic depth.

Flood mitigation in a reservoir is difficult because the actions can influence the water supply (WSA, 2012). The flood control efficiency of a reservoir is mainly dependent on its storage capacity as well as the size of the contributing watershed (Ji, 2008). A high ratio of drainage area to the surface area (e.g., in many reservoirs) leads to greater potential for sediment and nutrient loads (Wild and Loucks, 2014). Also, large reservoirs have the ability to store the flood water and gradually release the water through the spillways (Verstraeten and Poesen, 2000). Lake Diefenbaker has a good capacity for controlling flood intensities downstream of the Gardiner Dam (WSA, 2012). In the summer of 2013, flooding produced an inflow peak of 5,200 m^3/s to Lake Diefenbaker, but the release rates from the Gardiner Dam were adjusted based on downstream river capacities at 2,000 m^3/s (Sadeghian et al., 2017).

Modeling SS transport can provide valuable information on contaminant transport characteristics and rates (Langeveld et al., 2005). In Chapter 8, a sediment transport model is built and calibrated based on summer 2013 flood, the largest recorded flood for Lake Diefenbaker, since its impoundment in 1967. Measured turbidity data collected from stations along the reservoir over the course of two months (June and July 2013), and MODIS satellite images were used to validate the sediment model for better understanding of the settling and resuspension rates of the suspended sediments in the reservoir.

1.1.2 Sustainability in Canadian prairie reservoirs

Our actions are limited to the technologies and developments of the time. Although there has been dramatic growth in understanding natural phenomena during the past century, our knowledge is still very limited. Pollution, climate change, and more frequent floods are among the consequences of our actions in the past century. Today, the influences of our actions are even broader in space and time. Therefore, our responsibilities are also higher. Teamwork and knowledge sharing are the best tools for overcoming our limitations. Hence, a sustainable approach needs the participation of many, where everyone has a similar definition in mind and shares a common goal (Samaddar et al., 2015).

Sustainability has a very broad meaning. Before defining sustainability, we need to understand the environment's characteristics, the needs of both the environment and

humans as well as governance practices in each region (Mihelcic et al., 2017). Sustainability of water resources is best described by the term "water security". Water security leads to access to good quality water for the environment and all the users and is best defined by Wheater and Gober (2013) as "*sustainable use and protection of water resources, safeguarding access to water functions and services for humans and the environment, and protection against water-related hazards (flood and drought)*".

For a sustainable management of water resources in reservoirs and lakes, land protection, and nutrient load management are two main emphasized measures (Wetzel, 2001). In waterbodies that are surrounded by wetlands or grasslands, vegetation keeps higher amounts of nutrients in the soil because of less erosion and more plant uptake (Ji, 2008). In contrast, urban development changes flow characteristics and leads to higher loads of nutrients and pollutants on waterbodies (Wheater and Evans, 2009). Recommended actions are controlling and limiting pollutant and nutrient loads, good land management practices, and conducting both impact and risk assessments (Huang and Xia, 2001; Ji, 2008; Wheater and Gober, 2013). In addition to land management practices, (Wetzel, 2001) suggested nutrient limiting through the diversion of waste and storm waters; hypolimnetic water removal; phosphorus precipitation and inactivation; sediment oxidation/removal; and water column aeration. Use of "low regret" practices which are management practices that lead to better quality of water even if the expected stressed future conditions never happen is a beneficial management approach (Wheater and Gober, 2013).

Many management practices are site specific. For example, controlling point source pollution may not show a notable effect on the water quality of shallow lakes where wind forces contribute to a high sediment resuspension (Ji, 2008). Similarly, the wind may not affect a small, deep lake's water quality due to a short fetch on the lake surface that wind can disturb (Ji, 2008). The main parameters affecting in-lake processes across all sites include meteorological conditions; flow and hydrodynamic conditions; sediment load and particle size distribution; vegetation type and distribution; biological properties in bed and water column; contributing watershed size; and governance practices (Schultze, 2012).

Reservoir management is complex and needs consideration of many different elements and conditions, as well as a comprehensive understanding of influential factors and different

users' requirements. For example, more than 90% of Lake Diefenbaker's inflow come from the South Saskatchewan River Basin (c.f. Sadeghian et al., 2015), where the water quality and reservoir's health are a representation of activities in the watershed upstream (WSA, 2012). Reservoirs are different from natural lakes in many respects including morphology, biological zones, external loading and management objectives (Ji, 2008). Different withdrawal depths at dams is one of the main factors that distinguish reservoirs from lakes (Ji, 2008). Dam operations can change the downstream ecosystem in many ways. At various depths, water has different temperature, oxygen and nutrients levels (Scheffer, 2004). In winter and summer, water temperature differences between the downstream river and the release from the dam can create stresses for fish and other organisms (Lessard and Hayes, 2003). Similarly, sediment and nutrient concentration differences can produce anomalies (Kim et al., 2003). Reservoirs work as a sink for sediment, and suspended solids are significantly lower in dam outflow compared with inflow water in the river upstream (Dean and Gorham, 1998; Friedl et al., 2004; Mulholland and Elwood, 1982). A very low nutrient level discharge from the dams can significantly affect the growths of the phytoplankton community (Friedl et al., 2004).

Hydropower generation in reservoirs has many advantages. One of the most obvious benefits is the flexibility in power generation (WSA, 2012). Power generation can change very quickly based on demands. A drawback to hydropower is rapid changes in water elevation, which create problems for boat operation, pipe withdrawals, and shoreline birds (Beam, 1983; Moog, 1993; WSA, 2012). Water level fluctuations are one of the key challenges in reservoir management. In some cases, these changes are useful. For example, the lowering of water levels in shallow rivers or lakes allows for the better establishment of macrophyte communities, which reduce erosion by dampening high flow velocities and stabilizing the soil with the plants' roots (Ji, 2008). Some negative consequences include higher phosphorus release from re-flooded sediments, and losing nearby wetlands and habitats for waterfowl communities (Cooke et al., 2016). In winter, under ice-cover conditions, excessive drawdown can lead to a low volume of water, and insufficient oxygen levels resulting in massive fish kills (Cooke et al., 2016). Water level management in reservoir is an important and complex task to meet power generation, flood protection, drinking water and industrial needs, and environmental health.

Plans for protecting reservoirs are practical when they are based on future boundary conditions (Beven, 2012). Therefore, we need to understand the fundamental processes that affect the physical, chemical and biological properties of a reservoir (Sadeghian et al., 2014). Before starting planning, we need monitoring and measurement programs. In large and complex systems like Lake Diefenbaker, it is not possible to understand the system through field and laboratory studies alone; hence, water quality modeling is crucial. In our complex changing climate and environment, linking water quality models to watershed models, using scenario-based modeling, and making decisions under uncertainty are essential techniques for an accurate action plan (Wheater and Gober, 2013).

Water quality modeling is an art which requires an interdisciplinary knowledge of hydrodynamics, aquatic biology and chemistry, numerical methods, computers and coding, statistics, data assembly and reconstruction, and their integration (Cole and Wells, 2015). Water quality modeling is only possible with team-working and collaboration with other teams working on bathymetry surveying, in-situ measurements, field sampling, laboratory analysis, and data archiving.

1.2 Objectives and thesis structure

The main objective of this thesis is to successfully build a water quality model of Lake Diefenbaker, Saskatchewan, Canada.
The overall objectives of this research include the following:

- To understand the mixing regime and biological processes in the aquatic environment of Lake Diefenbaker;
- To determine which key factors can lead to increased or decreased eutrophication of the lake;
- To determine short-term and long-term water quality changes associated with different water management actions;
- To understand how nutrient transformation and retention changes with the varying flow in such a large system; and

- To develop a tool for representing Lake Diefenbaker's surface water in order to support water quality management and decision making.

In Chapter 2, the model selection, setup and application are presented. In Chapter 3, the temperature and hydrodynamic processes in Lake Diefenbaker are discussed. Also, a historical study of sedimentation rates in the reservoir is presented. A method for better and faster calibration by using combined global/local optimization techniques and considering the snow cover effects on the ice surface are included in the calculations. In Chapters 4, 5 and 6, three main inputs to the model: the bathymetry, meteorological data, and water quality variables are discussed respectively. In Chapter 7, a complete water quality model of Lake Diefenbaker is presented. Also, to improve the calculation of chlorophyll *a* concentrations, variable chlorophyll *a*/algal biomass ratios are considered in the simulations. Finally, in Chapter 8, the sediment transport model of Lake Diefenbaker is built for the 2013 Calgary flood and is calibrated using turbidity measurements and recorded satellite images from MODIS.

Prior to building a complex and computationally intensive model for Lake Diefenbaker, two small sites, in the region, were selected for constructing pre-models. These sites were the Blackstrap Lake in Saskatchewan (presented in Chapter 3) and the Brown drain within the Tobacco Creek watershed in Manitoba (presented in appendix Chapter I). Also, during the modeling process, some limitations were found with the model that required attention especially for using the model in the cold regions. Hence, a post-modeling of the Lake Diefenbaker water quality model for addressing the limitations with regard to the winter sediment oxygen demand were conducted (presented in appendix Chapter II).

1.2.1 Content of the manuscript-style thesis

Chapter 3 is a published manuscript in the journal of Great Lakes Research. Chapter 4 is a published manuscript in the journal of Environmental Monitoring and Assessment. Chapter 5 is submitted to the journal of Hydrologic Engineering. An excerpt of chapter 6 is submitted as a technical note to the journal of Environmental Engineering. Chapter 7 is submitted to the journal of Environmental Modelling & Software. Chapter 8 is published in the journal of Environmental Science and Pollution Research. Appendix Chapter I is published in the journal of Water Resources Management. Appendix Chapter II is published

in the journal of Water. As per the College of Graduate and Postdoctoral Studies guidelines for manuscript style theses, the student is the lead author on at least one manuscript.

Chapter 3: Sadeghian, A., de Boer, D., Hudson, J. J., Wheater, H., and Lindenschmidt, K. E. (2015). Lake Diefenbaker temperature model. *Great Lakes Research*, 41:8–21. DOI: 0.1016/j.jglr.2015.10.002

Chapter 4: Sadeghian, A., de Boer, D., and Lindenschmidt, K. E. (2017). Sedimentation and erosion in Lake Diefenbaker, Canada: solution for shore-line retreat monitoring. *Environmental Monitoring and Assessment*, 189:507. DOI: 10.1007/s10661-017-6217-7

Chapter 5: Sadeghian, A., Hudson, J. J., and Lindenschmidt, K. E. Effects of meteorological data: long- and short-term quality controlled measured meteorological data and re-analyzed meteorological data on water temperature calibration.

Chapter 6: Sadeghian, A., and Lindenschmidt, K. E. Input data for water quality models: a case study of South Saskatchewan River.

Chapter 7: Sadeghian, A., Chapra, S., Hudson, J. J., Wheater, H., and Lindenschmidt, K. E. Improving in-lake water quality modeling using variable chlorophyll a/algal biomass ratios.

Chapter 8: Sadeghian, A., Hudson, J. J., Wheater, H., and Lindenschmidt, K. E. (2017). Sediment plume model - a method for tracking the transport of suspended solids during an extreme flood event. *Environmental Science and Pollution Research*, 24(24):19583–19598. DOI: 10.1007/s11356-017-9616-y

Chapter I: Weber, D., Sadeghian, A., Luo, B., Waiser, M., Lindenschmidt, K.E., 2017. Modelling scenarios to estimate the potential impact of drainage standards on nutrient retention in a Canadian prairie watershed. *Water Resources Management*, 31 (4), 1305-1321. http://dx.doi.org/10.1007/s11269-017-1578-9

Chapter II: Terry, J., Sadeghian, A., Lindenschmidt, K.E., 2017. Modelling dissolved oxygen/sediment oxygen demand under ice in a shallow eutrophic prairie reservoir. *Water*, 9 (2), 131. http://dx.doi.org/10.3390/w9020131

The permissions to use the complete manuscript of chapter 3 from the publisher (ELSEVIER), chapters 4, 8 and I from the publisher (SPRINGER) are included in Appendix VI. The journal of Water is an open access journal, and the open access license and policy from the publisher (MDPI) are included in Appendix VI.

References

Agbeti, M. D. and Smol, J. P. (1995). Winter limnology: a comparison of physical, chemical and biological characteristics in two temperate lakes during ice cover. *Hydrobiologia*, 304(3):221–234.

Alavian, V., Jirka, G. H., Denton, R. A., Johnson, M. C., and Stefan, H. G. (1992). Density currents entering lakes and reservoirs. *Journal of Hydraulic Engineering*, 118(11):1464–1489.

Aulakh, M. S., Khurana, M. P. S., and Singh, D. (2009). Water pollution related to agricultural, industrial, and urban activities, and its effects on the food chain: Case studies from Punjab. *Journal of New Seeds*, 10(2):112–137.

Babin, J. and Prepas, E. (1985). Modelling winter oxygen depletion rates in ice-covered temperate zone lakes in Canada. *Canadian Journal of Fisheries and Aquatic Sciences*, 42(2):239–249.

Bainbridge, Z. T., Brodie, J. E., Faithful, J. W., Sydes, D. A., and Lewis, S. E. (2009). Identifying the land-based sources of suspended sediments, nutrients and pesticides discharged to the Great Barrier Reef from the Tully–Murray Basin, Queensland, Australia. *Marine and Freshwater Research*, 60(11):1081–1090.

Barica, J. and Mathias, J. A. (1979). Oxygen depletion and winterkill risk in small prairie lakes under extended ice cover. *Journal of the Fisheries Board of Canada*, 36(8):980–986.

Bates, B. (2009). *Climate Change and Water: IPCC technical paper VI*. World Health Organization.

Beam, J. H. (1983). The effect of annual water level management on population trends of white crappie in Elk City Reservoir, Kansas. *North American Journal of Fisheries Management*, 3(1):34–40.

Beven, K. (2012). Causal models as multiple working hypotheses about environmental processes. *Comptes Rendus Geoscience*, 344(2):77–88.

Birch, R. (1885). The effect of the drought of 1884 upon the pollution of the river Thames below London. *Minutes of the Proceedings of the Institution of Civil Engineers*, 81(1885):295–298.

Borah, D. and Bera, M. (2003). Watershed-scale hydrologic and nonpoint-source pollution models: Review of mathematical bases. *Transactions of the ASAE*, 46(6):1553.

Brierley, A. S. and Kingsford, M. J. (2009). Impacts of climate change on marine organisms and ecosystems. *Current biology*, 19(14):R602–R614.

Bunzel, K., Kattwinkel, M., and Liess, M. (2013). Effects of organic pollutants from wastewater treatment plants on aquatic invertebrate communities. *Water Research*, 47(2):597–606.

Caissie, D. (2006). The thermal regime of rivers: a review. *Freshwater Biology*, 51(8):1389–1406.

Cánovas, C., Hubbard, C., Olías, M., Nieto, J., Black, S., and Coleman, M. L. (2008). Hydrochemical variations and contaminant load in the Rio Tinto (Spain) during flood events. *Journal of Hydrology*, 350(1):25–40.

Chapra, S. C. (2008). *Surface water-quality modeling*. Waveland press.

Chislock, M. F., Doster, E., Zitomer, R. A., and Wilson, A. (2013). Eutrophication: causes, consequences, and controls in aquatic ecosystems. *Nature Education Knowledge*, 4(4):10.

Cole, T. M. and Wells, S. A. (2015). *CE-QUAL-W2: A two-dimensional, laterally averaged, hydrodynamic and water quality model*. Department of Civil and Environmental Engineering, Portland State University, Portland, OR, 3.72 edition.

Cooke, G. D., Welch, E. B., Peterson, S., and Nichols, S. A. (2016). *Restoration and management of lakes and reservoirs*. CRC press.

Correll, D. (1999). Phosphorus: a rate limiting nutrient in surface waters. *Poultry Science*, 78(5):674–682.

Dean, W. E. and Gorham, E. (1998). Magnitude and significance of carbon burial in lakes, reservoirs, and peatlands. *Geology*, 26(6):535–538.

Delpla, I., Jung, A.-V., Baures, E., Clement, M., and Thomas, O. (2009). Impacts of climate change on surface water quality in relation to drinking water production. *Environment International*, 35(8):1225–1233.

Dubourg, P., North, R. L., Hunter, K., Vandergucht, D. M., Abirhire, O., Silsbe, G. M., Guildford, S. J., and Hudson, J. J. (2015). Light and nutrient co-limitation of phytoplankton communities in a large reservoir: Lake Diefenbaker, Saskatchewan, Canada. *Journal of Great Lakes Research*, 41:129–143.

El-Khoury, A., Seidou, O., Lapen, D., Que, Z., Mohammadian, M., Sunohara, M., and Bahram, D. (2015). Combined impacts of future climate and land use changes on discharge, nitrogen and phosphorus loads for a Canadian river basin. *Journal of environmental management*, 151:76–86.

Eppley, R. W. (1972). Temperature and phytoplankton growth in the sea. *Fish. Bull*, 70(4):1063–1085.

Ficklin, D. L., Stewart, I. T., and Maurer, E. P. (2013). Effects of climate change on stream temperature, dissolved oxygen, and sediment concentration in the Sierra Nevada in California. *Water Resources Research*, 49(5):2765–2782.

Fink, G., Wessels, M., and Wüest, A. (2016). Flood frequency matters: Why climate change degrades deep-water quality of peri-alpine lakes. *Journal of Hydrology*, 540:457–468.

Foster, I. and Charlesworth, S. (1996). Heavy metals in the hydrological cycle: trends and explanation. *Hydrological processes*, 10(2):227–261.

Freni, G., Mannina, G., and Viviani, G. (2011). Assessment of the integrated urban water quality model complexity through identifiability analysis. *Water Research*, 45(1):37–50.

Friedl, G., Teodoru, C., and Wehrli, B. (2004). Is the Iron Gate I reservoir on the Danube River a sink for dissolved silica? *Biogeochemistry*, 68(1):21–32.

Giesy, J. P., Li, P. D. S., and Khim, J. S. (2009). Water quality analysis report. Technical report, Toxicology Centre, University of Saskatchewan.

Gober, P. and Wheater, H. (2014). Socio-hydrology and the science–policy interface: a case study of the Saskatchewan River basin. *Hydrology and Earth System Sciences*, 18(4):1413–1422.

Gosling, S. N. and Arnell, N. W. (2016). A global assessment of the impact of climate change on water scarcity. *Climatic Change*, 134(3):371–385.

Grenfell, T. C. and Maykut, G. A. (1977). The optical properties of ice and snow in the Arctic Basin. *Journal of Glaciology*, 18(80):445–463.

Herbst, D. B., Bogan, M. T., Roll, S. K., and Safford, H. D. (2012). Effects of livestock exclusion on in-stream habitat and benthic invertebrate assemblages in montane streams. *Freshwater biology*, 57(1):204–217.

Hosseini, N., Chun, K. P., and Lindenschmidt, K.-E. (2016). Quantifying spatial changes in the structure of water quality constituents in a large prairie river within two frameworks of a water quality model. *Water*, 8(4):158.

Hosseini, N., Chun, K. P., Wheater, H., and Lindenschmidt, K.-E. (2017a). Parameter sensitivity of a surface water quality model of the lower South Saskatchewan River–comparison between ice-on and ice-off periods. *Environmental Modeling & Assessment*, 22(4):291–307.

Hosseini, N., Johnston, J., and Lindenschmidt, K.-E. (2017b). Impacts of climate change on the water quality of a regulated prairie river. *Water*, 9(3):199.

Huang, G. H. and Xia, J. (2001). Barriers to sustainable water-quality management. *Journal of Environmental Management*, 61(1):1–23.

Hughes, D. and Slaughter, A. (2016). Disaggregating the components of a monthly water resources system model to daily values for use with a water quality model. *Environmental Modelling & Software*, 80:122–131.

Jacoby, J. and Welch, E. (2004). *Pollutant effects in freshwater: applied limnology*. CRC Press.

James, R. T. (2016). Recalibration of the Lake Okeechobee Water Quality Model (LOWQM) to extreme hydro-meteorological events. *Ecological Modelling*, 325:71–83.

Jeppesen, E., Kronvang, B., Meerhoff, M., Søndergaard, M., Hansen, K. M., Andersen, H. E., Lauridsen, T. L., Liboriussen, L., Beklioglu, M., Özen, A., et al. (2009). Climate change effects on runoff, catchment phosphorus loading and lake ecological state, and potential adaptations. *Journal of Environmental Quality*, 38(5):1930–1941.

Ji, Z.-G. (2008). *Hydrodynamics and water quality: modeling rivers, lakes, and estuaries*. John Wiley & Sons.

Jin, K.-R., Ji, Z.-G., and James, R. T. (2007). Three-dimensional water quality and SAV modeling of a large shallow lake. *Journal of Great Lakes Research*, 33(1):28–45.

Kachi, N., Kachi, S., Bousnoubra, H., et al. (2016). Effects of irrigated agriculture on water and soil quality (case perimeter Guelma, Algeria). *Soil & Water Res*, 11:97–104.

Karadvzic, V., Subakov-Simic, G., Krizmanic, J., and Natic, D. (2010). Phytoplankton and eutrophication development in the water supply reservoirs Garaši and Bukulja (Serbia). *Desalination*, 255(1):91–96.

Kim, L.-H., Choi, E., and Stenstrom, M. K. (2003). Sediment characteristics, phosphorus types and phosphorus release rates between river and lake sediments. *Chemosphere*, 50(1):53–61.

Kopmann, R. and Markofsky, M. (2000). Three-dimensional water quality modelling with TELEMAC-3D. *Hydrological Processes*, 14(13):2279–2292.

Langeveld, J., Veldkamp, R., and Clemens, F. (2005). Suspended solids transport: an analysis based on turbidity measurements and event based fully calibrated hydrodynamic models. *Water Science and Technology*, 52(3):93–101.

Lee, S.-W., Hwang, S.-J., Lee, S.-B., Hwang, H.-S., and Sung, H.-C. (2009). Landscape ecological approach to the relationships of land use patterns in watersheds to water quality characteristics. *Landscape and Urban Planning*, 92(2):80–89.

Leon, L. F., Smith, R. E., Hipsey, M. R., Bocaniov, S. A., Higgins, S. N., Hecky, R. E., Antenucci, J. P., Imberger, J. A., and Guildford, S. J. (2011). Application of a 3D hydrodynamic–biological model for seasonal and spatial dynamics of water quality and phytoplankton in Lake Erie. *Journal of Great Lakes Research*, 37(1):41–53.

Lessard, J. L. and Hayes, D. B. (2003). Effects of elevated water temperature on fish and macroinvertebrate communities below small dams. *River research and applications*, 19(7):721–732.

Lindenschmidt, K.-E. (2017). RIVICE—A Non-Proprietary, Open-Source, One-Dimensional River-Ice Model. *Water*, 9(5):314.

Matear, R., Hirst, A., and McNeil, B. (2000). Changes in dissolved oxygen in the Southern Ocean with climate change. *Geochemistry, Geophysics, Geosystems*, 1(11).

McInnes, A. S. and Quigg, A. (2010). Near-annual fish kills in small embayments: casual vs. causal factors. *Journal of Coastal Research*, 26(5):957–966.

McIntyre, N., Jackson, B., Wade, A., Butterfield, D., and Wheater, H. (2005). Sensitivity analysis of a catchment-scale nitrogen model. *Journal of Hydrology*, 315(1):71–92.

Mehaffey, M., Nash, M., Wade, T., Ebert, D., Jones, K., and Rager, A. (2005). Linking land cover and water quality in New York City's water supply watersheds. *Environmental Monitoring and Assessment*, 107(1):29–44.

Mihelcic, J. R., Naughton, C. C., Verbyla, M. E., Zhang, Q., Schweitzer, R. W., Oakley, S. M., Wells, E. C., and Whiteford, L. M. (2017). The grandest challenge of all: The role of environmental engineering to achieve sustainability in the world's developing regions. *Environmental Engineering Science*, 34(1):16–41.

Missaghi, S. and Hondzo, M. (2010). Evaluation and application of a three-dimensional water quality model in a shallow lake with complex morphometry. *Ecological Modelling*, 221(11):1512–1525.

Moog, O. (1993). Quantification of daily peak hydropower effects on aquatic fauna and management to minimize environmental impacts. *River Research and Applications*, 8(1-2):5–14.

Morrison, J., Quick, M. C., and Foreman, M. G. (2002). Climate change in the Fraser River watershed: flow and temperature projections. *Journal of Hydrology*, 263(1):230–244.

Mulholland, P. J. and Elwood, J. W. (1982). The role of lake and reservoir sediments as sinks in the perturbed global carbon cycle. *Tellus*, 34(5):490–499.

Muller, M. (2007). Adapting to climate change: water management for urban resilience. *Environment and Urbanization*, 19(1):99–113.

Murdoch, P. S., Baron, J. S., and Miller, T. L. (2000). Potential effects of climate change on surface-water quality in North America. *JAWRA Journal of the American Water Resources Association*, 36(2):347–366.

North, R. L., Davies, J.-M., Doig, L., Hudson, J. J., and Lindenschmidt, K.-E. (2015a). Special issue on characterization and dynamics of a large multi-purpose prairie reservoir: Lake Diefenbaker, Saskatchewan, Canada. *Journal of Great Lakes Research*, 41:1–164.

North, R. L., Johansson, J., Vandergucht, D., Doig, L. E., Liber, K., Lindenschmidt, K.-E., Baulch, H., and Hudson, J. J. (2015b). Evidence for internal phosphorus loading in a large prairie reservoir (Lake Diefenbaker, Saskatchewan). *J. Great Lakes Res.*, 41(Supplement 2):91–99.

Paerl, H. W. (2006). Assessing and managing nutrient-enhanced eutrophication in estuarine and coastal waters: Interactive effects of human and climatic perturbations. *Ecological Engineering*, 26(1):40–54.

Paerl, H. W., Fulton, R. S., Moisander, P. H., and Dyble, J. (2001). Harmful freshwater algal blooms, with an emphasis on cyanobacteria. *The Scientific World Journal*, 1:76–113.

Rode, M., Arhonditsis, G., Balin, D., Kebede, T., Krysanova, V., Van Griensven, A., and Van der Zee, S. E. (2010). New challenges in integrated water quality modelling. *Hydrological Processes*, 24(24):3447–3461.

Romero, J. R. and Imberger, J. (2003). Effect of a flood underflow on reservoir water quality: Data and three-dimensional modeling. *Archiv für Hydrobiologie*, 157(1):1–25.

Sadeghian, A., de Boer, D., Hudson, J. J., Wheater, H., and Lindenschmidt, K.-E. (2015). Lake Diefenbaker temperature model. *Journal of Great Lakes Research*, 41:8–21.

Sadeghian, A., Hudson, J., Wheater, H., and Lindenschmidt, K. (2014). Water quality modeling of Lake Diefenbaker. *Water news. Can Water Res Assoc*, 33(2):17–20.

Sadeghian, A., Hudson, J., Wheater, H., and Lindenschmidt, K.-E. (2017). Sediment plume model—a comparison between use of measured turbidity data and satellite images for model calibration. *Environmental Science and Pollution Research*, 24(24):19583–19598.

Samaddar, S., Yokomatsu, M., Dayour, F., Oteng-Ababio, M., Dzivenu, T., Adams, M., and Ishikawa, H. (2015). Evaluating effective public participation in disaster management and climate change adaptation: Insights from northern Ghana through a user-based approach. *Risk, Hazards & Crisis in Public Policy*, 6(1):117–143.

Schallenberg, M. and Burns, C. W. (2004). Effects of sediment resuspension on phytoplankton production: teasing apart the influences of light, nutrients and algal entrainment. *Freshwater Biology*, 49(2):143–159.

Scheffer, M. (2004). *Ecology of shallow lakes*. Springer Science & Business Media.

Schmidt, T. S., Clements, W. H., Wanty, R. B., Verplanck, P. L., Church, S. E., San Juan, C. A., Fey, D. L., Rockwell, B. W., DeWitt, E. H., and Klein, T. L. (2012). Geologic processes influence the effects of mining on aquatic ecosystems. *Ecological Applications*, 22(3):870–879.

Schultze, M. (2012). *The filling and remediation of pit lakes in former open cast lignite mines*. PhD thesis, Thesis, der Technischen Universität Carolo-Wilhelmina zu Braunschweig.

Sheelanere, P., Noble, B. F., and Patrick, R. J. (2013). Institutional requirements for watershed cumulative effects assessment and management: Lessons from a Canadian trans-boundary watershed. *Land Use Policy*, 30(1):67–75.

Shen, Z., Hong, Q., Yu, H., and Liu, R. (2008). Parameter uncertainty analysis of the non-point source pollution in the daning river watershed of the three gorges reservoir region, china. *Science of the total environment*, 405(1):195–205.

Smith, V. H. (1986). Light and nutrient effects on the relative biomass of blue-green algae in lake phytoplankton. *Canadian Journal of Fisheries and Aquatic Sciences*, 43(1):148–153.

Smith, V. H., Tilman, G. D., and Nekola, J. C. (1999). Eutrophication: impacts of excess nutrient inputs on freshwater, marine, and terrestrial ecosystems. *Environmental pollution*, 100(1):179–196.

Terry, J. A., Sadeghian, A., and Lindenschmidt, K.-E. (2017). Modelling dissolved oxygen/sediment oxygen demand under ice in a shallow eutrophic prairie reservoir. *Water*, 9(2):131.

Urabe, J., Kyle, M., Makino, W., Yoshida, T., Andersen, T., and Elser, J. (2002). Reduced light increases herbivore production due to stoichiometric effects of light/nutrient balance. *Ecology*, 83(3):619–627.

van Vliet, M. T., Franssen, W. H., Yearsley, J. R., Ludwig, F., Haddeland, I., Lettenmaier, D. P., and Kabat, P. (2013). Global river discharge and water temperature under climate change. *Global Environmental Change*, 23(2):450–464.

Verstraeten, G. and Poesen, J. (2000). Estimating trap efficiency of small reservoirs and ponds: methods and implications for the assessment of sediment yield. *Progress in Physical Geography*, 24(2):219–251.

Vincent, W. F., Gibbs, M. M., and Spigel, R. H. (1991). Eutrophication processes regulated by a plunging river inflow. *Hydrobiologia*, 226(1):51–63.

Vörösmarty, C. J., Green, P., Salisbury, J., and Lammers, R. B. (2000). Global water resources: vulnerability from climate change and population growth. *Science*, 289(5477):284–288.

Walling, D. (1977). Limitations of the rating curve technique for estimating suspended sediment loads, with particular reference to British rivers. *Erosion and solid matter transport in inland waters*, pages 34–48. IAHS Publication 122.

Wetzel, R. G. (2001). *Limnology: lake and river ecosystems*. Gulf Professional Publishing, 3rd edition.

Wheater, H. and Evans, E. (2009). Land use, water management and future flood risk. *Land Use Policy*, 26:S251–S264.

Wheater, H. and Gober, P. (2013). Water security in the Canadian Prairies: science and management challenges. *Philosophical Transactions of the Royal Society of London A: Mathematical, Physical and Engineering Sciences*, 371(2002):20120409.

Wheater, H. S. (2015). Water security-science and management challenges. *Proceedings of the International Association of Hydrological Sciences*, 366:23.

Whitehead, P., Wilby, R., Battarbee, R., Kernan, M., and Wade, A. J. (2009). A review of the potential impacts of climate change on surface water quality. *Hydrological Sciences Journal*, 54(1):101–123.

Whitworth, K. L., Baldwin, D. S., and Kerr, J. L. (2012). Drought, floods and water quality: drivers of a severe hypoxic blackwater event in a major river system (the southern Murray–Darling Basin, Australia). *Journal of Hydrology*, 450:190–198.

Wild, T. B. and Loucks, D. P. (2014). Managing flow, sediment, and hydropower regimes in the Sre Pok, Se San, and Se Kong Rivers of the Mekong basin. *Water Resources Research*, 50(6):5141–5157.

WSA (2012). *State of Lake Diefenbaker*. Water Security Agency. Available at: https://www.wsask.ca/Global/Lakes%20and%20Rivers/Dams%20and%20Reservoirs/Operating%20Plans/Developing%20an%20Operating%20Plan%20for%20Lake%20Diefenbaker/State%20of%20Lake%20Diefenbaker%20Report%20-%20October%2019%202012.pdf, Accessed: 21 May 2015.

Wu, Y. and Chen, J. (2013). Investigating the effects of point source and nonpoint source pollution on the water quality of the East River (Dongjiang) in South China. *Ecological Indicators*, 32:294–304.

Chapter 2
Modeling

2.1 Model selection

The modeling work for this research includes two parts, the hydrodynamic model and water quality model. The hydrodynamic model mainly deals with the physical characteristics of the reservoir, while the water quality model considers the chemical and biological characteristics. River and lake hydrodynamics are important determinants of water quality. Hydrodynamic models consider variables that affect water density and circulation, such as temperature, total dissolved solids and total suspended solids (Hall, 2008).

To address all the fundamental processes that contribute to water quality in lakes and reservoirs, the model framework needed to be sufficiently rigorous (Vandenberg et al., 2011). A model was required that works with both the river and reservoir systems. Potential models for this study include Water Quality Analysis Simulation Program (WASP) by Environmental Protection Agency (EPA), Environmental Fluid Dynamics Code (EFDC) by Virginia Institute of Marine Science, MIKE3 and MIKE21 by Danish Hydraulic Institute (DHI), and CE-QUAL-W2 by US Army and Portland State University. These models are the most cited and applied water quality models at academic and industry levels and recommended by many environmental agencies such as Environment and Climate Change Canada and the United States Environmental Protection Agency. The WASP model (Ambrose et al., 1983; Connolly and Winfield, 1984; Di Toro et al., 1983) can be used in 1D, 2D and 3D; however, since the model only solves water quality equations it needs to be couple with another model for the hydrodynamics and transport. Hence, for consistency, the model was not consider for this study. The EFDC (Hamrick, 1996) and MIKE3 (Cesana and Siwek, 2001) models are sophisticated 3D models which meet all the requirements for this study. The EFDC model uses horizontal curvilinear segmentation and vertical sigma layering while the MIKE3 model uses triangular mesh grids. Both models were tried on Lake Diefenbaker. However, the lengthy computational times make them impractical for this study which includes uncertainty analyses. The whole system, from the hydrometric

Table 2.1: Description of different water quality models, after Vandenberg et al. 2011

Model type	Description	Capabilities	Limitations	Example of models
0-D chemical	Water and mass balances assuming full mixing of water within the lake; balances can be made within separate cells to account for stratification	These tools are usually user-developed, made on a case-by-case basis, and should normally be quick to run	No spatial representation; applicable to fully-mixed systems such as shallow lakes	Excel, Goldsim, Matlab, Stella
1D physical and chemical	Modelling formulations that allow discretization of geometry as a function of depth	Will typically provide basic representation of lake hydrodynamics (including stratification) and water quality, are relatively quick to run	Lack of horizontal discretization makes these mainly applicable to lakes with small surface area relative to depth	DYRESM coupled with CAEDYM, PHREEQC
2D physical and chemical	Two modelling formulations are available: laterally-averaged and depth-averaged	Models available with relatively detailed representation of lake hydrodynamic and water quality components	Laterally-averaged models are applicable mostly to long and narrow lakes; depth-averaged models are applicable to shallow lakes	Laterally averaged CE-QUAL-W2 ,MIKE21
3D physical and chemical	Models provide longitudinal, lateral and depth discretization, and therefore can be used for any geometry.	Models available with detailed representation of hydrodynamic and water quality processes; geochemical models can be coupled to 3D hydrodynamic models	Requires significant user and computational time to operate and develop; existing data not always sufficient for 3D representation	ELCOM coupled with CAEDYM, EFDC coupled with HEM3D, MIKE3, GEMSS, MODFLOW

stations at South Saskatchewan River (SSR) and Red Deer River (RDR) to the dams, is 602 km. The reservoir has a maximum depth of 60 m, so to capture the correct hydrodynamics and variations in the longitudinal and vertical directions, a two-dimensional model was required (lateral values are averaged). The third dimension was not necessary as the river and reservoir have a narrow width, and the gradients of importance are expected to be in the vertical and horizontal directions. The MIKE21 (DHI, 2002) model is a 2D model. However, the averaging of the third dimension is over the vertical direction which is more suitable for natural lakes with large surface area to depth ratios. Since Lake Diefenbaker is a narrow and deep reservoir, the MIKE21 model could not represent all the physical characteristic of the reservoir. Hence, the model was selected among the laterally averaged models which are well suited to long and narrow waterbodies (Table. 2.1).

Based on the study's objectives, and the physical and chemical characteristics of the lake and available data, the CE-QUAL-W2 hydrodynamic and water quality model was deemed the best model for Lake Diefenbaker. The CE-QUAL-W2 is a 2D laterally averaged water quality model over 40 years in development, and has been successfully tested on numerous systems worldwide. The US Army Corps of Engineers launched the model in 1975 (Edinger and Buchak, 1975). The model was developed by Edinger and Buchak for about 10 years (Buchak and Edinger, 1984; Edinger and Buchak, 1978), and, in 1984 was handed over to

the next team led by Tom Cole. The majority of work on the fundamental theories of the work took place during the next 20 years (Cole and Buchak, 1995; Cole and Wells, 2003a,b, 2006). After 30 years of progress, the US Corps of Engineers stopped model development, and passed the model to Portland State University. The university's model development is still continuing with an emphasis on computational efficiency, easier usage through a GUI (graphical user interface) and more efficient and accurate numerical schemes (Cole and Wells, 2008, 2013, 2015a,b).

CE-QUAL-W2 can simulate water temperature, hydrodynamics, dissolved and particulate suspended solids, dissolved oxygen, nutrients, organic matter and algae, therefore fulfilling all research objectives. Due to several decades of development, the model has an up-to-date comprehensive user manual, covering both the theoretical and practical aspects of the model, and an active user forum. The best feature is that the source code is freely available with clear comments allowing the extension and application of new formulations and algorithms. In the next section, a summary of the governing equations from the user manual (Cole and Wells, 2013) is presented.

2.1.1 Governing equations

The governing hydrodynamic equations are derived based on three-dimensional equations for the continuity and momentum (conservation of the fluid mass and conservation of momentum, respectively) which are laterally averaged. A summary of the equations after averaging and simplifications based on the model assumptions are presented here (Eq. 2.1, 2.2, and 2.3). The x-momentum equation (Eq. 2.2) can be solved using either a fully explicit, which is based on solving the partial differential terms using an explicit finite difference technique, or an explicit/implicit finite difference solution technique. In the latter form, the implicit technique would only be used for solving the vertical transport of momentum term, which reduces the time step limitation for numerical stability, but all other terms for the solution of the horizontal momentum equation should be used by the explicit scheme. The free water surface equation (Eq. 2.4) is the continuity equation integrated over the depth from the water surface to the bottom and is solved by substituting the momentum equation. The equation of state (Eq. 2.5) relates density to temperature (t_w), concentration of dissolved substances (Φ_{TDS}), and concentration of particulate substances

(Φ_{ISS}). Since the lake has freshwater, salinity calculations can be excluded from density calculations.

Continuity equation

$$\frac{\delta UB}{\delta x} + \frac{\delta WB}{\delta z} = qB \tag{2.1}$$

x- momentum equation

$$\frac{\delta UB}{\delta t} + \frac{\delta UUB}{\delta x} + \frac{\delta WUB}{\delta z} = gB\frac{\delta \eta}{\delta x} - \frac{gB}{\rho}\int_{\eta}^{z}\frac{\delta \rho}{\delta x}dz + \frac{1}{\rho}\frac{\delta B\tau_{xx}}{\delta x} + \frac{1}{\rho}\frac{\delta B\tau_{xz}}{\delta z} \tag{2.2}$$

z-momentum equation

$$0 = g - \frac{1}{\rho}\frac{\delta P}{\delta z} \tag{2.3}$$

Free surface equation

$$B_{\eta}\frac{\delta \eta}{\delta t} = \frac{\delta}{\delta x}\int_{\eta}^{h} UBdz - \int_{\eta}^{h} qBdz \tag{2.4}$$

Equation of State

$$\rho = f(t_w, \Phi_{TDS}, \Phi_{ISS}) \tag{2.5}$$

where:

U = horizontal velocity, m s^{-1}

W = vertical velocity, m s^{-1}

B = channel width

q = net lateral inflow per unit volume of cell, T^{-1}

P = pressure

τ_x = x-direction lateral average shear stress

τ_y = y-direction lateral average shear stress

ρ = density

η = water surface

By considering the U and W the averaged values of velocity in horizontal and vertical directions and the Φ as the averaged concentration, the mass transport equation is become:

Water Quality Transport

$$\frac{\delta B\Phi}{\delta t} + \frac{\delta UB\Phi}{\delta x} + \frac{\delta WB\Phi}{\delta z} - \frac{\delta\left(BD_x\frac{\delta\Phi}{\delta x}\right)}{\delta x} - \frac{\delta\left(BD_z\frac{\delta\Phi}{\delta z}\right)}{\delta z} = q_\Phi B + S_\Phi B \tag{2.6}$$

where:

Φ = laterally averaged constituent concentration, g m^{-3}

D_x = longitudinal temperature and constituent dispersion coefficient, m^2 s^{-1}

D_z = vertical temperature and constituent dispersion coefficient, m^2 s^{-1}

q_Φ = lateral inflow or outflow mass flow rate of constituent per unit volume, g m^{-3} s^{-1}

S_Φ = laterally averaged source/sink term, g m^{-3} s^{-1}

The rate of heat exchange is defined as:

Heat budget

$$H_{aw} = -K_{aw}(T_w - T_e) \tag{2.7}$$

where:

H_{aw} = rate of surface heat exchange, W m^{-2}

K_{aw} = coefficient of surface heat exchange, W m^{-2} $°C^{-1}$

T_w = water surface temperature, °C

T_e = equilibrium temperature, °C

In the equation 2.7, seven separate heat exchange processes (Eq. 2.8) are summarized in the coefficient of surface heat exchange and equilibrium temperature.

$$H_n = H_s + H_a + H_e + H_c - (H_{sr} + H_{ar} + H_{br}) \tag{2.8}$$

where:

H_n = the net rate of heat exchange across the water surface, W m^{-2}

H_s = incident short wave solar radiation, W m^{-2}

H_a = incident long wave radiation, W m^{-2}

H_{sr} = reflected short wave solar radiation, W m^{-2}

H_{ar} = reflected long wave radiation, W m^{-2}

H_{br} = back radiation from the water surface, W m^{-2}
H_e = evaporative heat loss, W m^{-2}
H_c = heat conduction, W m^{-2}

Since some of the terms in equation 2.8 are surface temperature dependent and others are measurable or computable input variables, the equilibrium temperature, T_e, is defined as the temperature at which the net rate of surface heat exchange is zero.

The evaporation and water heat lost is defined as a wind function:

Evaporation

$$f(W) = a + bW^c \tag{2.9}$$

where:
f(W) = wind speed function, W m^{-2} mm Hg^{-1}
a = empirical coefficient, 9.2 default
b = empirical coefficient, 0.46 default
c = empirical coefficient, 2 default
W = wind speed at 2 m above the ground, m s^{-1}

Lake Diefenbaker is located in a cold region and ice cover has an important role in heat budget of the water until late spring or early summer. The ice cover prevents absorption of the short wave solar radiation, and it is an essential part of the Lake Diefenbaker temperature model. The ice formation requires a negative water temperature at the surface. When the surface water temperature drops to freezing point, ice begins to form on the water surface (Eq. 2.10).

Ice cover

$$\theta_0 = \frac{-T_{Wn}\rho_W C_{Pw} h}{\rho_i L_f} \tag{2.10}$$

where:
θ_0 = thickness of initial ice formation during a timestep, m
T_{Wn} = local temporary negative water temperature, °C

h = layer thickness, m

ρ_W = density of water, kg m^{-3}

C_{Pw} = specific heat of water, J kg^{-1} $°C^{-1}$

ρ_i = density of ice, kg m^{-3}

L_f = latent heat of fusion, J kg^{-1}

The negative water surface temperature is then converted to equivalent ice thickness and equivalent heat is added to the heat source and sink term for water. The heat balance for the water-ice-air system is:

$$\rho_i L_f \frac{\Delta h}{\Delta t} = h_{ai}(T_i - T_e) - h_{wi}(T_w - T_m) \tag{2.11}$$

where:

$\Delta h/\Delta t$ = change in ice thickness (h) with time (t), m s^{-1}

h_{ai} = coefficient of ice-to-air heat exchange, W m^{-2} $°C^{-1}$

h_{wi} = coefficient of water-to-ice heat exchange through the melt layer, W m^{-2} $°C^{-1}$

T_i = ice temperature, °C

T_{ei} = equilibrium temperature of ice-to-air heat exchange, °C

T_w = water temperature below ice, °C

T_m = melt temperature, 0 °C

Numerical solution

The **Q**uadratic **U**pstream **I**nterpolation for **C**onvective **K**inetics with **E**stimated **S**treaming **T**erms (QUICKEST) method is used for solving the convection-diffusion equation. The QUICKEST scheme proposed by (Leonard, 1979) is an explicit third-order horizontal/vertical transport scheme designed for highly advective unsteady flows and gives better results compared to lower order schemes like UPWIND (Lin and Falconer, 1997). The problem with the QUICKEST scheme is the unphysical overshoot and undershoot near sharp changes of concentration. Hence, the ULTIMATE scheme (Leonard, 1991) is coupled with the QUICKEST as a universal limiter in the model for overcoming this problem.

Numerical stability

Defining the time steps for calculations is a key factor. Large time steps lead to stability violation and very small time steps increase the computation time. The CE-QUAL-W2 model works with dynamic time steps. For the times or regions with too many fluctuations in flow, the model uses a smaller time step and increases that when a small time step is not necessary. To have the stability, the spatial and temporal steps (Δx and Δt) should be fine enough. The timestep adjustment is based on the characteristics of the waterbody. For river systems, the timesteps can be selected as low as 0.1 seconds and for lake systems as low as 1 second. To avoid too small timesteps and save computational time the timesteps can increase when the variations are small over time. This is controlled by using a maximum timesteps limit (Cole and Buchak, 1995) as:

$$\Delta t \leq \frac{1}{2(\frac{A_x}{\Delta X^2} + \frac{A_z}{\Delta Z^2}) + \frac{Q}{V} + \frac{\sqrt{\frac{\Delta\rho}{\rho}\frac{gH}{2}}}{\Delta X}} \tag{2.12}$$

where

Δt = timestep, sec

A_x = longitudinal eddy viscosity, $m^2\ s^{-1}$

A_z = vertical eddy viscosity, $m^2\ s^{-1}$

Q = total flow into or out of a cell, $m^3\ s^{-1}$

V = cell volume, m^3

g = gravitational acceleration, $m\ s^{-2}$

H = maximum waterbody depth, m

ρ = water density, $kg\ m^{-3}$

$\Delta\rho$ = surface to bottom water density difference, $kg\ m^{-3}$

2.1.2 Bathymetry and model boundaries

Lake Diefenbaker is an artificial reservoir whose morphology consists of an indented shoreline originating from river valley pathways of tributaries flowing into the South Saskatchewan River. The curvy shape makes the bathymetry particularly complicated with many variations requiring a complex structure of the model discretization. Early bathymetry data are available from surveys carried out after the construction of the dams in the 1970s and

1980s. To obtain more recent information, new surveys were carried out on the reservoir in 2012 and 2013. In order to check the accuracy and applicability of the new data and to investigate historical sedimentation rates, these recent data were compared with contour maps from the 1980s and cross section data from the 1970s (SWRC, 1968, 1969, 1970, 1971, 1972).

High rates of sedimentation and bank erosion have changed the bathymetry and, consequently, diminished the reservoir volume capacity over time. Therefore, the bathymetric model was constructed by applying the natural neighbor interpolation method to the 2012 – 2013 survey data. To evaluate the effect of grid spacing on model performance, the model results from different bathymetry files with different longitudinal and vertical resolutions were compared.

The inflow to and outflow from the reservoir were highly uncertain. Near the Alberta-Saskatchewan border (∼331 km upstream of the dams), the RDR merges with the SSR. The closest hydrometric stations for inflow water were at the Medicine Hat and Bindloss stations, 203 km and 47 km upstream of the SSR and RDR confluence (374 km and 218 km to the reservoir), respectively. The outflow from the reservoir was not measured, and the closest station downstream of the Gardiner Dam was in the city of Saskatoon, 120 km away. The nearest meteorological stations were also several kilometers away from the reservoir, and there was not even one single buoy station on this large strategic waterbody. Two approaches have been used and compared to determine the effects of inflow water on model accuracy by routing the inflows to the reservoir inlet and by extending upstream boundaries to the hydrometric stations. The effects of meteorological data were also studied by comparing the temperature model results using three different meteorological databases.

There are some preliminary guidelines to estimate and interpolate the flow and climate data at the reservoir (Pomeroy and Shook, 2012). However, the same routing methods could not be used to estimate the nutrient input data for Lake Diefenbaker because comparable guidelines for predicting the chemical and biological constituents had not been developed by biologists and engineers. The reason is that many factors such as sedimentation, erosion, retention and point (e.g., waste water treatment plants) and nonpoint source loadings (e.g., agriculture field surface runoff and groundwater infusion) could significantly change nutrient

concentrations in the inflow to Lake Diefenbaker via the SSR. The best approach found to estimate the state variable concentrations at the Lake Diefenbaker inlet was to first build the daily water quality database by correlating the water quality variables with the date, Julian day, discharge and water temperature (see Chapter 6) at the hydrometric stations.

2.1.3 Water quality data

The statistical properties for water quality data are different from those of existing hydrological data due to the smaller number of samples available, both spatially and temporally (Helsel and Cohn, 1988). In climate databases, the data are available with differing frequencies varying from yearly, monthly, daily, hourly to even shorter frequencies; however, for a water quality database, a typical frequency is once per month. Also, the spatial distribution of data is more limited for water quality data. The small spatiotemporal resolution of water quality data may not produce correct statistic metrics (Mayer and Butler, 1993), so an expert interpretation of the results is necessary (Arhonditsis and Brett, 2004).

To have the best choice of water quality parameters, we can look at the input data requirements for CE-QUAL-W2, which is a comprehensive water quality model. The CE-QUAL-W2 model uses data from several groups of inorganic and organic nutrients, phytoplankton and zooplankton. The CE-QUAL-W2 has 28 state variables, 23 derived water quality variables and 73 water quality fluxes (Cole and Wells, 2015a). Most of these variables are directly available from water quality databases, but there are a number of variables that are calculated from a series of equations or based on the correlations with other variables.

The CE-QUAL-W2 model needs all 28 state variables, as water quality input data, for a complete analysis of the system (Chapter 6). In the water quality database for Lake Diefenbaker, there were no data available for the state variables iron, carbonaceous biochemical oxygen demand (CBOD), particulate silica and zooplankton. The remaining 24 variables were taken directly from the database or derived based on relationships with the other water quality variables. Below is a short description of the most important water

quality variables and their effects on model results.

Phosphorus

Inorganic phosphorus (PO_4), an essential component of algal production (Pote and Daniel, 2000), is the most common limiting nutrient for algal production in freshwaters; hence many restoration programs limit the discharge of this nutrient to freshwaters (Ortolani, 2014). However, because of the strong absorptive characteristics of phosphorus, the potential influences of buried phosphorus in sediment can remain for some time; hence many restoration programs suggest using total phosphorus (TP) instead or in addition to PO_4 for long-term rehabilitation (Havens and Walker Jr, 2002). Total dissolved phosphorus (TDP) is the sum of organic phosphorus compounds which come from algal excretion (Kuenzler, 1970)) and inorganic phosphorus (PO_4). Water quality models require the inorganic fraction (PO_4) for simulating algal behaviors; however, because PO_4 has strong correlations with TDP, when the observations are not available, TDP measurements can be used instead of PO_4.

Nitrogen

The CE-QUAL-W2 model uses nitrate (NO_3) plus nitrite (NO_2) as a single state variable (Cole and Wells, 2015a). There are strict drinking water guidelines for NO_3 concentrations because of severe health problems associated with elevated levels of NO_3 in drinking water (Metzler and Stoltenberg, 1950). High NO_3 concentrations can promote eutrophication in nitrogen limited waters (McIsaac et al., 2001) and increase phosphorus internal loading from anaerobic sediments (Jensen and Andersen, 1992). Ammonium (NH_4) in addition to NO_3 are the primary sources of inorganic nitrogen used in algal photosynthesis for making chlorophyll pigments (Turpin, 1991). A study by McCarthy et al. (1977) showed that in non-limiting conditions NH_4 is preferred over NO_3 by algae. To study the effects of the watershed on the quality of water, total dissolved nitrogen (TDN) is a reliable measurement as it is transported easily by water and shows a quick response to precipitation, which is a good indicator of land use and climate changes (Gallo et al., 2015). Particulate nitrogen (PN) has two main contributors: phytoplankton (eutrophic systems) and detritus (oligotrophic systems) (Caperon et al., 1976). The inorganic nutrients, especially the

nitrogen and phosphorus, become aqueous when they are taken up by phytoplankton; hence many monitoring studies also measure total nitrogen (TN) and total phosphorus to consider the entire pool of nutrients (Guildford and Hecky, 2000).

Algae

Algae are a major component of every water quality model and are affected by and as well affect the physical, chemical and biological characteristics of waterbodies. Algae require the physical conditions of thermal energy, light and particular water movement patterns for growth. Also, algae need nutrients mainly inorganic carbon, PO_4, NH_4, NO_3 and dissolved silica. Algae are producers of dissolved oxygen through photosynthesis and an oxygen consumer through respiration and also through decay of excreted organic matter and dead algae (Cole and Wells, 2015a). The measurements of algal biomass are usually available in the form of chlorophyll *a* which needs to be converted into biomass (Wiltshire et al., 1998). Modelers use different approaches by using static or variable stoichiometric ratios for converting chlorophyll *a* concentrations into algal biomass (chapter 7). There are three species of algae that are used more frequently in water quality models: diatom, green algae, and cyanobacteria. Berger and Wells (2005) used species fractions of 60% for diatoms, 30% for greens algae, and 10% for blue-greens algae (cyanobacteria).

Organic matter

The amount of organic compound that passes through a 0.45 μm glass fiber filter is defined as the dissolved organic carbon (DOC) and the amount of residue retained by the filter is the particulate organic carbon (POC) (Evans et al., 2005). The DOC and POC need to be converted to dissolved organic matter (DOM) and particulate organic matter (POM) prior to use in the CE-QUAL-W2 model. Dissolved organic matter is an oxygen consumer variable in the water quality models and decays to inorganic carbon, PO_4, and NH_4. The organic matter from mortality and excretion of phytoplankton added to DOM concentrations. Similar to DOM, the POM is also an oxygen consumer and also mineralizes into inorganic carbon, PO_4, and NH_4. The main difference is that the POM is only from phytoplankton mortality (no excretion), and a portion of POM deposits into the sediment which may either return to the water column or remain buried permanently. To convert

organic carbon into organic matter, the organic carbon needs to be divided by the carbon to biomass ratio ($\delta c = 0.45$). Total organic carbon (TOC) is calculated as the sum of DOC and POC. Similar to DOC and POC, total organic carbon is converted into the organic matter by dividing the organic carbon by the carbon to biomass ratio.

Organic matter partitioning

Both the DOM and POM have two forms: labile and refractory. The labile organic matter has a short decay rate of a few days to weeks, while the refractory organic matter has a longer decay rate of up to years (Ji, 2008). Therefore, the labile compounds are removed faster from the water than the refractory portion. When there are no data available for partitioning between the labile and refractory DOM/POM (LDOM, RDOM, LPOM, and RPOM), reasonable fractions of labile and refractory groups need to be considered. The phosphorus and nitrogen portions of the organic matter are used as state variables in the CE-QUAL-W2 model. The phosphorus/nitrogen portion of organic matter is calculated based on guidelines available in Chapter 6.

Suspended solids

Total dissolved solids (TDS) and total suspended solids (TSS) concentrations affect the density in water. Total dissolved solids which is a state variable in the CE-QUAL-W2 model, has strong linear relationships with specific conductance (Thomas, 1986). The non-filterable residue is the weighing of the residue left on a 0.45 μm glass fiber filter after filtering water, and is the standard method for measuring total suspended solids concentration (Zhang and Zhu, 2006).

Dissolved oxygen

Dissolved oxygen (DO) has interactions with many water quality variables in water and represents the physical, chemical and biological characteristics of a waterbody very well (Sánchez et al., 2007). Dissolved oxygen is a water quality index in many regions (e.g., Boyacioglu, 2007; Cude, 2001; Kannel et al., 2007). Dissolved oxygen concentration is simple to calibrate but difficult to validate because many components interact with oxygen,

with many parameters contributing to oxygen production and consumption.

Silica

Dissolved silica is an essential nutrient for the growth of diatoms which considered a favorable form of algae. Dissolved silica is used for the development of the diatom skeleton (Cole and Wells, 2015a). In silica limiting conditions, the diatom is succeeded by green algae and cyanobacteria which are less desirable (Koszelnik and Tomaszek, 2008).

Alkalinity

Alkalinity buffers the pH of water and can decrease the effects of toxins on aquatic organisms (Laurén and McDonald, 1986). In water quality models, alkalinity and total inorganic carbon (TIC) are used for prediction of the pH of water which in turn affects the chemical and biological reaction rates (Cole and Wells, 2015a).

2.2 Model application

2.2.1 Temperature and hydrodynamics

Anticipated increases in air temperature due to climate change may also influence in-lake processes. To make valid predictions regarding the impact of climate change on the thermal structure of reservoirs and to determine the potential effects of management strategies, a temperature and mixing model of Lake Diefenbaker was utilized for the period 2011 – 2014.

Since the reservoir is characterized as a deep waterbody, the occurrence of upwelling bringing nutrient-rich water from the reservoir's bottom layers to the surface water layer is another component of the transport of nutrients. Therefore, the energy balance of the reservoir was also considered in determining the mixing regime and stratification behavior. In the upstream reaches of Lake Diefenbaker, the density current and turbulent inflowing water from the South Saskatchewan River are dominant forces of water circulation; further downstream towards the Gardiner and Qu'Appelle Dams, wind stress and surface heat fluxes become the primary forces for water-column mixing. The vertical water temperature profile determines the stratification of the reservoir's water layers, which influence the

circulation patterns in the lake.

A new ice algorithm was also used, incorporating the effect of snow on the ice surface. In particular, the study presented in Chapter 3 provides a novel quantitative analysis of the contribution of different heat sources and sinks to the reservoir's heat budget, providing invaluable information for reservoir management practices in response to climate change and uncertainty. Of particular interest is the high input of heat from the reservoir's main inflow, the South Saskatchewan River, which has a large impact on the heat budget.

2.2.2 Water quality

Water quality models are useful tools for simulating and predicting nutrient dynamics as well as the fate and transport of toxins in freshwaters. In CE-QUAL-W2, the transport of constituents is expressed as a balance of sources and sinks including kinetic reactions with specific rates of transformation (Cole and Wells, 2013). The model solves a two-dimensional advection-diffusion equation for water temperature and other water quality parameters such as nutrients, suspended solids, biological oxygen demand and algal dynamics. If data is available, other groups such as macrophytes, zooplankton and epiphyton can be included in the model setup.

Algal concentrations are good representative of the health of aquatic systems, hence they are a component of any water quality models. Algae have many interactions with the inorganic and organic pools of nutrients in water. Therefore, the quality of the input data is critical for obtaining a correct algae simulation. As a result of low quality input data, most water quality models simulate algal behavior only moderately well, and poorly in most cases (Arhonditsis et al., 2006). In addition to the quality of input data, the other primary reason leading to poor algal results is using fixed growth, mortality, respiration, excretion, and settling rates for algae in models. In reality, algae adjust these ratios based on nutrient and light availability and temperature conditions (Ji, 2008). Algal biomass measurements are difficult to make so limnologists prefer measuring chlorophyll a concentrations (Ji, 2008). Since water quality models simulate algae as biomass, algae is converted to chlorophyll a by multiplying it with a chlorophyll a/algal biomass ratio. In most models, the chlorophyll a/algal biomass ratio is held constant during simulations, while, in reality, it changes

dynamically through time and space based on light and nutrient availability (Chapra, 2008).

In Chapter 7 of this study, a water quality modeling exercise was implemented on the prairie reservoir, Lake Diefenbaker, where the measurements confirmed that algae adjust their chlorophyll a/algal biomass ratios based on phosphorus availability (Abirhire et al., 2015). A top-down approach was considered by first developing a large, complex model and gradually simplifying it. With some modifications to the source code of the CE-QUAL-W2 model, the chlorophyll a/algal biomass ratio parameter was modified to change based on the nutrient and light limiting conditions in the water column. The final version of the model with the variable chlorophyll a/algal biomass ratio was the most simplified model that could be used to reproduce measurements for several water quality variables during the time frame 2011 – 2013. A minimum of either nitrogen or phosphorus limitation was applied as the nutrient limiting rate and then the light limiting effects were incorporated into the calculations of the chlorophyll a/algal biomass ratio.

2.2.3 Sediment transport

In Chapter 8, a sediment transport model was built and calibrated based on the largest recorded flood for Lake Diefenbaker, since its impoundment in 1967. In June 2013, there was heavy rainfall for two consecutive days on the frozen and snow-covered ground in the higher elevations of western Alberta, Canada (Sutherland, 2016). The runoff from the rainfall and melted snow caused one of the largest recorded inflows to the headwaters of the SSR and caused heavy damage to population centers, particularly High River and Calgary, and devastation in the surrounding areas (De Vynck and Polson, 2013; Welsch and De Vynck, 2013). The gauges recorded discharge with peaks of 4,500 m^3/s at the Medicine Hat station (SSR) and 950 m^3/s at the Bindloss station (RDR), which merge 171 km from the Lake Diefenbaker inlet. The 2013 Alberta flood brought highly turbid water into the reservoir (Hudson and Vandergucht, 2015), where the sediment settling and resuspension rates were unknown, leading to concerns regarding water quality.

In a sediment transport model, the use of suspended solids (SS) concentrations is preferred over turbidity because it is a state variable in the model, while the turbidity needs to be converted to SS for comparisons. However, a fundamental limitation with SS is maintaining

a consistent sampling program of sediment with a temporal frequency that is adequate to capture the variations between seasons and events such as floods (Stroud et al., 2009). The acquisition of data, from which decisions are often based is frequently inadequate, and this may lead to underestimation or overestimation and, ultimately, to poor management and policy decisions (Littlewood, 1992). Therefore, a practical alternative is using turbidity measurements (Gippel, 1995). Sonde-based turbidity measurements correlate the light scattering in water with SS concentrations, and are easier, faster and less expensive to operate compared with suspended solids sampling. Hence, sondes provide SS readings at finer temporal and spatial scales. The results will be very close to the direct measurements when the sensors are calibrated properly, according to particle size variations (Gippel, 1995). The measured turbidity data collected from stations along the reservoir over the course of two months (June and July 2013) were used to validate the sediment model quantitatively.

In addition, MODIS satellite images were used to qualitatively calibrate the model based on near-surface suspended solids and to track the sediment plume front. Use of satellite images is not a new technique in studying near surface conditions in waterbodies. Sakmont Engineering (1987) was one of the first groups who looked at satellite images of the South Saskatchewan River Basin and suggested incorporation of NOAA-VHRR and LANDSAT images for consistent data with reasonable resolutions. For Lake Diefenbaker, the first use of satellite images was in estimating chlorophyll *a* concentrations using MODIS and LANDSAT data (Giesy et al., 2009), with further work completed by Hecker et al. (2012) and Yip (2015).

Satellite images are generally are being used in two primary fields: phytoplankton dominated systems, which are based on absorption of light at the water surface, and inorganic sediments systems, which are based on scattering of light at the water surface (Budd and Warrington, 2004; Myint and Walker, 2002). The focus of this study is the second category. Turbid waters exhibit strong relationships between sediment concentrations and reflected bands because the SS properties, such as particle size distribution, exert considerable control over the reflectance and scattering (Binding et al., 2005).

Lake Diefenbaker is a long (180 km) and narrow reservoir where the width increases from about 800 m upstream to about 4,000 m downstream. MODIS data with the finest resolution (i.e. 250 m) would have three pixels for the upstream part and about 16 pixels

downstream. The chlorophyll *a* concentrations are generally higher downstream, and the upstream area is more light limited because of higher SS concentrations (Dubourg et al., 2015). Therefore, studies based on the use of satellite images were mainly concentrated on estimating chlorophyll *a* concentrations downstream. Attempts could not find any study that correlates SS or turbidity data with reflectance bands from satellite images for Lake Diefenbaker.

The measured turbidity and satellite images data allowed to develop the dispersion and diffusion transport models of Lake Diefenbaker using the two-dimensional hydrodynamic and water quality model CE-QUAL-W2. The model is capable of tracing the flood's sediment plume movements through the reservoir. This results in better understanding of the settling and resuspension rates of the suspended sediments in the reservoir.

References

Abirhire, O., North, R. L., Hunter, K., Vandergucht, D. M., Sereda, J., and Hudson, J. J. (2015). Environmental factors influencing phytoplankton communities in Lake Diefenbaker, Saskatchewan, Canada. *Journal of Great Lakes Research*, 41:118–128.

Ambrose, R. B., Hill, S. I., and Mulkey, L. A. (1983). *User's manual for the chemical transport and fate model TOXIWASP, Version 1.* Environmental Research Laboratory, Office of Research and Development, US Environmental Protection Agency.

Arhonditsis, G. B., Adams-VanHarn, B. A., Nielsen, L., Stow, C. A., and Reckhow, K. H. (2006). Evaluation of the current state of mechanistic aquatic biogeochemical modeling: citation analysis and future perspectives. *Environmental science & technology*, 40(21):6547–6554.

Arhonditsis, G. B. and Brett, M. T. (2004). Evaluation of the current state of mechanistic aquatic biogeochemical modeling. *Marine Ecology Progress Series*, 271:13–26.

Berger, C. and Wells, S. (2005). Lake Whatcom Water Quality Model. Technical Report EWR-03-05, Maseeh College of Engineering and Computer Science, Department of Civil and Environmental Engineering, Portland State University, Portland, Oregon.

Binding, C., Bowers, D., and Mitchelson-Jacob, E. (2005). Estimating suspended sediment concentrations from ocean colour measurements in moderately turbid waters; the impact of variable particle scattering properties. *Remote sensing of Environment*, 94(3):373–383.

Boyacioglu, H. (2007). Development of a water quality index based on a European classification scheme. *Water Sa*, 33(1):101–106.

Buchak, E. M. and Edinger, J. E. (1984). Generalized, longitudinal-vertical hydrodynamics and transport: Development, programming, and applications. Technical report, prepared for US Army Corps of Engineers Waterways Experiment Station, Vicksburg, MS.

Budd, J. W. and Warrington, D. S. (2004). Satellite-based sediment and chlorophyll a estimates for Lake Superior. *Journal of Great Lakes Research*, 30:459–466.

Caperon, J., Harvey, W. A., and Steinhilper, F. A. (1976). Particulate organic carbon, nitrogen, and chlorophyll as measures of phytoplankton and detritus standing crops in Kaneohe Bay, Oahu, Hawaiian Islands. *Pacific Science*.

Cesana, C. and Siwek, R. (2001). *Manual for MIKE3*. Danish Hydraulic Institute (DHI).

Chapra, S. C. (2008). *Surface water-quality modeling*. Waveland press.

Cole, T. M. and Buchak, E. (1995). *CE-QUAL-W2: A two-dimensional, laterally averaged, hydrodynamic and water quality model*. US Army Engineer Waterways Experiment Station, Vicksburg, MS, 2.0 edition.

Cole, T. M. and Wells, S. A. (2003a). *CE-QUAL-W2: A two-dimensional, laterally averaged, hydrodynamic and water quality model*. US Army Engineer Waterways Experiment Station, Vicksburg, MS, 3.1 edition.

Cole, T. M. and Wells, S. A. (2003b). *CE-QUAL-W2: A two-dimensional, laterally averaged, hydrodynamic and water quality model*. US Army Engineer Waterways Experiment Station, Vicksburg, MS, 3.2 edition.

Cole, T. M. and Wells, S. A. (2006). *CE-QUAL-W2: A two-dimensional, laterally averaged, hydrodynamic and water quality model*. US Army Engineer Waterways Experiment Station, Vicksburg, MS, 3.5 edition.

Cole, T. M. and Wells, S. A. (2008). *CE-QUAL-W2: A two-dimensional, laterally averaged, hydrodynamic and water quality model*. Department of Civil and Environmental Engineering, Portland State University, Portland, OR, 3.6 edition.

Cole, T. M. and Wells, S. A. (2013). *CE-QUAL-W2: A two-dimensional, laterally averaged, hydrodynamic and water quality model*. Department of Civil and Environmental Engineering, Portland State University, Portland, OR, 3.71 edition.

Cole, T. M. and Wells, S. A. (2015a). *CE-QUAL-W2: A two-dimensional, laterally averaged, hydrodynamic and water quality model*. Department of Civil and Environmental Engineering, Portland State University, Portland, OR, 3.72 edition.

Cole, T. M. and Wells, S. A. (2015b). *CE-QUAL-W2: A two-dimensional, laterally averaged, hydrodynamic and water quality model*. Department of Civil and Environmental Engineering, Portland State University, Portland, OR, 4.0 edition.

Connolly, J. P. and Winfield, R. P. (1984). *A user's guide for WASTOX, a framework for modeling the fate of toxic chemicals in aquatic environments*. Environmental Research Laboratory, Office of Research and Development, US Environmental Protection Agency.

Cude, C. G. (2001). Oregon water quality index a tool for evaluating water quality management effectiveness. *JAWRA Journal of the American Water Resources Association*, 37(1):125–137.

De Vynck, G. and Polson, J. (2013). Suncor among Calgary offices closed amid severe Alberta floods. Available at: http://business.financialpost.com/news/suncor-among-calgary-offices-closed-amid-severe-alberta-floods, Accessed: 3 October 2016.

DHI, D. (2002). *MIKE 21 Coastal Hydraulics and Oceanography, the Hydrodynamics Module Reference Manual.* Danish Hydraulic Institute (DHI).

Di Toro, D. M., Fitzpatrick, J. J., Thomann, R. V., et al. (1983). *Documentation for water quality analysis simulation program (WASP) and model verification program (MVP).* Environmental Research Laboratory, Office of Research and Development, US Environmental Protection Agency.

Dubourg, P., North, R. L., Hunter, K., Vandergucht, D. M., Abirhire, O., Silsbe, G. M., Guildford, S. J., and Hudson, J. J. (2015). Light and nutrient co-limitation of phytoplankton communities in a large reservoir: Lake Diefenbaker, Saskatchewan, Canada. *Journal of Great Lakes Research*, 41:129–143.

Edinger, J. and Buchak, E. (1975). *A hydrodynamic, two-dimensional reservoir model: The computational basis.* US Army Engineer Division, Ohio River. Cincinnati, OH.

Edinger, J. and Buchak, E. (1978). Reservoir longitudinal and vertical implicit hydrodynamics. In *Proc. Int. Conf. on environmental effects of hydraulic engineering works, American society of civil engineers, Knoxville, TN.*

Evans, C., Monteith, D., and Cooper, D. (2005). Long-term increases in surface water dissolved organic carbon: observations, possible causes and environmental impacts. *Environmental Pollution*, 137(1):55–71.

Gallo, E. L., Meixner, T., Aoubid, H., Lohse, K. A., and Brooks, P. D. (2015). Combined impact of catchment size, land cover, and precipitation on streamflow and total dissolved nitrogen: A global comparative analysis. *Global Biogeochemical Cycles*, 29(7):1109–1121.

Giesy, J. P., Li, P. D. S., and Khim, J. S. (2009). Water quality analysis report. Technical report, Toxicology Centre, University of Saskatchewan.

Gippel, C. J. (1995). Potential of turbidity monitoring for measuring the transport of suspended solids in streams. *Hydrological processes*, 9(1):83–97.

Guildford, S. J. and Hecky, R. E. (2000). Total nitrogen, total phosphorus, and nutrient limitation in lakes and oceans: Is there a common relationship? *Limnology and Oceanography*, 45(6):1213–1223.

Hall, E. (2008). Hydrodynamic modeling of Lake Ontario. Master's thesis, Queen's University, Kingston, Ontario, Canada.

Hamrick, J. M. (1996). *User's manual for the environmental fluid dynamics computer code*. Department of Physical Sciences, School of Marine Science, Virginia Institute of Marine Science, College of William and Mary.

Havens, K. E. and Walker Jr, W. W. (2002). Development of a total phosphorus concentration goal in the TMDL process for Lake Okeechobee, Florida (USA). *Lake and Reservoir Management*, 18(3):227–238.

Hecker, M., Khim, J. S., Giesy, J. P., Li, S.-Q., and Ryu, J.-H. (2012). Seasonal dynamics of nutrient loading and chlorophyll a in a northern prairies reservoir, Saskatchewan, Canada. *Journal of Water Resource and Protection*, 4(04):180.

Helsel, D. R. and Cohn, T. A. (1988). Estimation of descriptive statistics for multiply censored water quality data. *Water Resources Research*, 24(12):1997–2004.

Hudson, J. J. and Vandergucht, D. M. (2015). Spatial and temporal patterns in physical properties and dissolved oxygen in Lake Diefenbaker, a large reservoir on the Canadian Prairies. *Journal of Great Lakes Research*, 41:22–33.

Jensen, H. S. and Andersen, F. O. (1992). Importance of temperature, nitrate, and pH for phosphate release from aerobic sediments of four shallow, eutrophic lakes. *Limnology and Oceanography*, 37(3):577–589.

Ji, Z.-G. (2008). *Hydrodynamics and water quality: modeling rivers, lakes, and estuaries*. John Wiley & Sons.

Kannel, P. R., Lee, S., Lee, Y.-S., Kanel, S. R., and Khan, S. P. (2007). Application of water quality indices and dissolved oxygen as indicators for river water classification and urban impact assessment. *Environmental Monitoring and Assessment*, 132(1):93–110.

Koszelnik, P. and Tomaszek, J. A. (2008). Dissolved silica retention and its impact on eutrophication in a complex of mountain reservoirs. *Water, air, and soil pollution*, 189(1-4):189–198.

Kuenzler, E. J. (1970). Dissolved organic phosphorus excretion by marine phytoplankton. *Journal of Phycology*, 6(1):7–13.

Laurén, D. J. and McDonald, D. (1986). Influence of water hardness, pH, and alkalinity on the mechanisms of copper toxicity in juvenile rainbow trout, Salmo gairdneri. *Canadian Journal of Fisheries and Aquatic Sciences*, 43(8):1488–1496.

Leonard, B. P. (1979). A stable and accurate convective modelling procedure based on quadratic upstream interpolation. *Computer methods in applied mechanics and engineering*, 19(1):59–98.

Leonard, B. P. (1991). The ultimate conservative difference scheme applied to unsteady one-dimensional advection. *Computer methods in applied mechanics and engineering*, 88(1):17–74.

Lin, B. and Falconer, R. A. (1997). Tidal flow and transport modeling using ULTIMATE QUICKEST scheme. *Journal of hydraulic engineering*, 123(4):303–314.

Littlewood, I. G. (1992). *Estimating contaminant loads in rivers: a review*. Institute of Hydrology Hydrology (Centre for Ecology & Hydrology), Crowmarsh Gifford, Wallingford, Oxfordshire, OX1O 8BB.

Mayer, D. and Butler, D. (1993). Statistical validation. *Ecological modelling*, 68(1-2):21–32.

McCarthy, J. J., Taylor, W. R., and Taft, J. L. (1977). Nitrogenous nutrition of the plankton in the Chesapeake Bay. 1. nutrient availability and phytoplankton preferences. *Limnol. Oceanogr*, 22(6):996–1011.

McIsaac, G. F., David, M. B., Gertner, G. Z., and Goolsby, D. A. (2001). Eutrophication: Nitrate flux in the Mississippi river. *Nature*, 414(6860):166–167.

Metzler, D. F. and Stoltenberg, H. A. (1950). The public health significance of high nitrate waters as a cause of infant cyanosis and methods of control. *Transactions of the Kansas Academy of Science (1903-)*, 53(2):194–211.

Myint, S. and Walker, N. (2002). Quantification of surface suspended sediments along a river dominated coast with NOAA AVHRR and SeaWiFS measurements: Louisiana, USA. *International Journal of Remote Sensing*, 23(16):3229–3249.

Ortolani, V. (2014). Land use and its effects on water quality using the BASINS model. *Environmental earth sciences*, 71(5):2059–2063.

Pomeroy, J. and Shook, K. (2012). Review of Lake Diefenbaker operations, 2010–2011. Available at: http://www.usask.ca/hydrology/papers/Pomeroy_Shook_2012.pdf.

Pote, D. and Daniel, T. (2000). Analyzing for total phosphorus and total dissolved phosphorus in water samples. *Methods of Phosphorus Analysis for Soils, Sediments, Residuals, and Water*, pages 94–97.

Sakmont Engineering (1987). A satellite imagery survey of land use in the effective drainage area of the South Saskatchewan River Basin. technical report d.2. Technical report, Consulting Hydraulic Engineers. Saskatoon, Saskatchewan.

Sánchez, E., Colmenarejo, M. F., Vicente, J., Rubio, A., García, M. G., Travieso, L., and Borja, R. (2007). Use of the water quality index and dissolved oxygen deficit as simple indicators of watersheds pollution. *Ecological Indicators*, 7(2):315–328.

Stroud, J. R., Lesht, B. M., Schwab, D. J., Beletsky, D., and Stein, M. L. (2009). Assimilation of satellite images into a sediment transport model of Lake Michigan. *Water resources research*, 45(2).

Sutherland, S. (2016). Three years later: What caused the 2013 Alberta floods? Available at: https://www.theweathernetwork.com/news/articles/why-was-southern-alberta-so-vulnerable-to-flooding-in-2013/29800, Accessed: 3 October 2016.

SWRC (1968). Delta formation and sedimentation in Lake Diefenbaker. Annual project report, Saskatchewan Water Resources Commission.

SWRC (1969). Delta formation and sedimentation in Lake Diefenbaker. Annual project report, Saskatchewan Water Resources Commission.

SWRC (1970). Delta formation and sedimentation in Lake Diefenbaker. Annual project report, Saskatchewan Water Resources Commission.

SWRC (1971). Delta formation and sedimentation in Lake Diefenbaker. Annual project report, Saskatchewan Water Resources Commission.

SWRC (1972). Delta formation and sedimentation in Lake Diefenbaker. Annual project report, Saskatchewan Water Resources Commission.

Thomas, A. (1986). Specific conductance as an indicator of total dissolved solids in cold, dilute waters. *Hydrological Sciences Journal*, 31(1):81–92.

Turpin, D. H. (1991). Effects of inorganic N availability on algal photosynthesis and carbon metabolism. *Journal of Phycology*, 27(1):14–20.

Vandenberg, J., Lauzon, N., Prakash, S., and Salzsauler, K. (2011). Use of water quality models for design and evaluation of pit lakes. *McCullough CD,(Ed)*, pages 63–80.

Welsch, E. and De Vynck, G. (2013). Alberta floods spread as water subsides in Calgary. Available at: http://www.bloomberg.com/news/articles/2013-06-24/alberta-floods-spread-as-water-subsides-in-oil-hub-of-calgary, Accessed: 3 October 2016.

Wiltshire, K. H., Harsdorf, S., Smidt, B., Blöcker, G., Reuter, R., and Schroeder, F. (1998). The determination of algal biomass (as chlorophyll) in suspended matter from the Elbe estuary and the German Bight: A comparison of high-performance liquid chromatography, delayed fluorescence and prompt fluorescence methods. *Journal of Experimental Marine Biology and Ecology*, 222(1):113–131.

Yip, H. (2015). An assessment of present and historical (1984–2012) Lake Diefenbaker water clarity and chlorophyll-a concentration using Landsat imagery. Master's thesis, University of Saskatchewan.

Zhang, Z. and Zhu, J. (2006). Characteristics of solids, BOD 5 and VFAs in liquid swine manure treated by short-term low-intensity aeration for long-term storage. *Bioresource technology*, 97(1):140–149.

Chapter 3
Lake Diefenbaker temperature model

This chapter is a published paper in the journal of Great Lakes Research.

Sadeghian, A., de Boer, D., Hudson, J. J., Wheater, H., and Lindenschmidt, K. E. (2015). Lake Diefenbaker temperature model. *Journal of Great Lakes Research*, 41:8–21. DOI: 0.1016/j.jglr.2015.10.002

The document has been reformatted from the original version for inclusion in the thesis, and no content has changed from the published version. The permission to use the manuscript in this thesis from the publisher (ELSEVIER) is included in Appendix VI.

Contributions of the candidate and co-authors

The candidate's contributions are follows: developing the bathymetry for Lake Diefenbaker and the Upper South Saskatchewan River; setting up and calibrating the Lake Diefenbaker temperature model; applying the combined global/local optimization method (based on PSO and LM) for the Lake Diefenbaker temperature model calibration; adding an algorithm to the CE-QUAL-W2 model for considering snow cover effects on the ice surface in winter; wring the manuscript. Karl-Erich Lindenschmidt was the supervisor and designed the whole study, and helped the candidate through the research process and manuscript writing. Howard Wheater was the co-supervisor and designed the overall vision of the research at the Global Institute for Water Security (GIWS). He supported the candidate financially as well as provided guidance in research and contributed comments on all the manuscripts. Dirk de Boer provided the Lake Diefenbaker survey data for building the bathymetry and by contributing comments. Jeff Hudson provided the Sonde and Laboratory data for model calibration and by contributed comments.

3.1 Abstract

Many water quality processes in lakes and reservoirs are temperature dependent. Water temperature affects stratification and mixing, dissolved oxygen solubility, biological and physiological processes and aquatic species tolerance rates. Anticipated increases in air temperature due to climate change may also influence in-lake processes. In order to make valid predictions regarding the impact of climate change on the thermal structure of reservoirs and to determine the potential effects of management strategies, a hydrodynamic model of Lake Diefenbaker was utilized for the period 2011 – 2012. Lake Diefenbaker is a long (181 km) and narrow (average width of 2.2 km) reservoir in Saskatchewan, Canada formed along the South Saskatchewan River (SSR) by the construction of the Gardiner and Qu'Appelle River dams in the 1960s. The reservoir and dams provide water for irrigation, drinking water, eco-services, hydropower generation, aquaculture and recreation, and are also used for flood mitigation. The model was calibrated using Monte-Carlo and combined global and local optimization techniques, which provided insights into parameter sensitivity and identifiability of relevance for monitoring needs. A new ice algorithm was also used, incorporating the effect of snow on the ice surface. In particular, this study provides a novel quantitative analysis of the contribution of different heat sources and sinks to the lake's heat budget, providing invaluable information for reservoir management practices in response to climate change and uncertainty. Of particular interest is the high input of heat from the lake's main inflow, the South Saskatchewan River, which has a high impact on the heat budget.

3.2 Introduction

3.2.1 Temperature effects

More frequent and extreme events can be the consequences of climate change and land management practices (Wheater and Evans, 2009). Higher flood peaks lead to higher erosion rates and, consequently, to higher suspended sediment concentrations and turbidity in surface waters. Climate change also affects annual air temperature. Anticipated increases in air temperature on the Canadian Prairies (Khaliq et al., 2015) may influence in-lake processes as well as the magnitude and timing of inflowing waters to lakes. For many aquatic species, this timing is very important, as their reproduction and migration is based

on water temperature (Ji, 2008).

Many water quality processes are temperature dependent. In general, solids are more soluble at higher temperatures, while gases are less soluble (Ji, 2008). For example, increasing water temperature will increase kinetic rates, decomposition rates, biological and sediment oxygen demand (BOD and SOD, respectively) and algal metabolism. On the other hand, dissolved oxygen concentrations will diminish in higher temperature waters. Many species have a small tolerance to low oxygen concentrations (hypoxia). During anoxic conditions, increased nutrient and heavy metal release from the sediments (e.g., phosphorus remobilisation) can increase eutrophication and toxic conditions in water bodies (Ji, 2008).

Water temperature affects stratification and mixing, dissolved oxygen solubility, biological and physiological processes (metabolic and reproductive rates), reaeration, sorption of organic chemicals and particulate matter and aquatic species tolerance rates (Ji, 2008). Surface water temperatures also impact industrial activities, such as surface water abstraction for cooling and water treatment.

3.2.2 Ice cover

In high latitude regions, rivers and lakes are subject to several months of continuous ice cover. Under ice conditions, these water bodies have different physical, chemical and biological characteristics. Changes in light and temperature levels are the key factors, as compared to ice-free conditions (Agbeti and Smol, 1995). Many water quality processes that are temperature dependent decrease their rates substantially in near freezing conditions, but do not cease (Ji, 2008). Water quality under ice is largely dependent on the magnitude of overall lake productivity and sediment oxygen demand (Babin and Prepas, 1985; Hosseini et al., 2016). Heat fluxes from the bottom sediments are particularly important in very cold waters in winter (Ji, 2008), impacting sediment oxygen demand and, subsequently, other biological and chemical reactions and transformations.

Solar radiation is the primary source of heat energy in lakes (Ji, 2008). An ice cover on a surface water body acts as a barrier to solar radiation impinging the water column. Snow cover on the ice surface reduces light penetration further. Consequently, light levels in the

aquatic environment are very low due to the already low solar radiation available in winter and the reduction of light transmission to the water body due to the ice and snow cover (Agbeti and Smol, 1995).

The ice cover also blocks wind, which substantially reduces mixing as well as further cooling of the water at the surface. Some mixing still occurs due to the differential pressure of the wind on the ice cover (Bengtsson, 1996).

Unfortunately, many water quality models are limited in capability for winter simulations because the snow pack on the ice surface is not taken into consideration. The absence of snow in an ice model increases heat conduction through the ice, leading to overestimation of ice thicknesses and ice-on periods (Kheyrollah Pour et al., 2012), especially during extremely cold air temperatures (down to -40 °C) and windy conditions.

3.2.3 Lake Diefenbaker

Much of the Saskatchewan River Basin (SRB) lies within the Canadian Prairie region, which experiences many weather extremes and a wide range in weather variability during the year. Examples are the wide yearly range in air temperature (-40 to +40 °C) as well as extreme dry and wet conditions (1999 – 2004 drought period and 2011 and 2013 large-scale flooding). Eighty percent of the Saskatchewan River's runoff stems from its headwaters in the Rocky Mountains. Eighty percent of Canada's agricultural land lies within the Prairies, with 82% of Canada's irrigated agriculture in the river basin (c.f. Wheater and Gober, 2013; Wheater, 2015). Lake Diefenbaker (Figure 3.1a) is one of the most important water sources in Saskatchewan, with most of its inflow stemming from the upper South Saskatchewan River (SSR) (WSA, 2012a). The reservoir receives high loads of phosphorus from the SSR with 1,533 and 616 tons per year in 2011 and 2012, respectively (North et al., 2015). The phosphorus load is primarily in particulate form (North et al., 2015; Saskatchewan Environment and Public Safety, 1988) and not readily available for immediate uptake by aquatic organisms such as algae. As a result, the reservoir acts as a sink for phosphorus (P), retaining 86% and 84% of the incoming phosphorus in the years 2011 and 2012, respectively (North et al., 2015). During low hypolimnetic oxygen conditions in summer, there is a high potential for the phosphorus

to be released from the bottom sediments in a more accessible dissolved form (North et al., 2015). The release rate of P can be greatly affected by temperature. Algal blooms, an indicator of eutrophication, have already been observed in some parts of the reservoir in late summer and early fall (Abirhire et al., 2015; Giesy et al., 2009; WSA, 2012a).

According to recent Regional Climate Model (RCM) studies on future climate change impacts (Khaliq et al., 2015; Mearns et al., 2012), the South Saskatchewan River Basin (SSRB) is expected to become warmer, based on average air temperature. These future differences in air temperature will affect the timing and intensity of precipitation, evaporation and ice melting and frequency of droughts and floods (Gober and Wheater, 2014). These changes would alter the lake's heat balance and, consequently, affect thermally dependent components such as dissolved oxygen concentration and lake productivity (Hudson and Vandergucht, 2015; Jankowski et al., 2006; Peeters et al., 2002).

Concerns over climate change, water security and environmental sustainability have enhanced the motivation to use a numerical model for studying the thermal behavior of Lake Diefenbaker. The hydrological, morphological and ecological variations of the reservoir were captured in the model setup and an important aim of the simulations was to help us better understand the complexity of the system as well as the key factors that lead to changes in the lake's aquatic ecosystem.

The broad objectives of this study are to provide insights into the physical and thermal response of Lake Diefenbaker through data and modelling analysis; more specifically: (i) to study the behavior of thermal zonation and stratification, (ii) to quantify the influence of different contributing sources to the reservoir heat budget, (iii) to understand and represent the effects of snow cover on the ice surface in the heat budget, and (iv) to provide a brief discussion on sedimentation rates and the changing geomorphology of Lake Diefenbaker. A necessary tool for this analysis is a 2D temperature model of the reservoir, and the paper also reports improved model algorithms for representation of snow and ice cover effects and the development and application of advanced fast algorithms for model calibration.

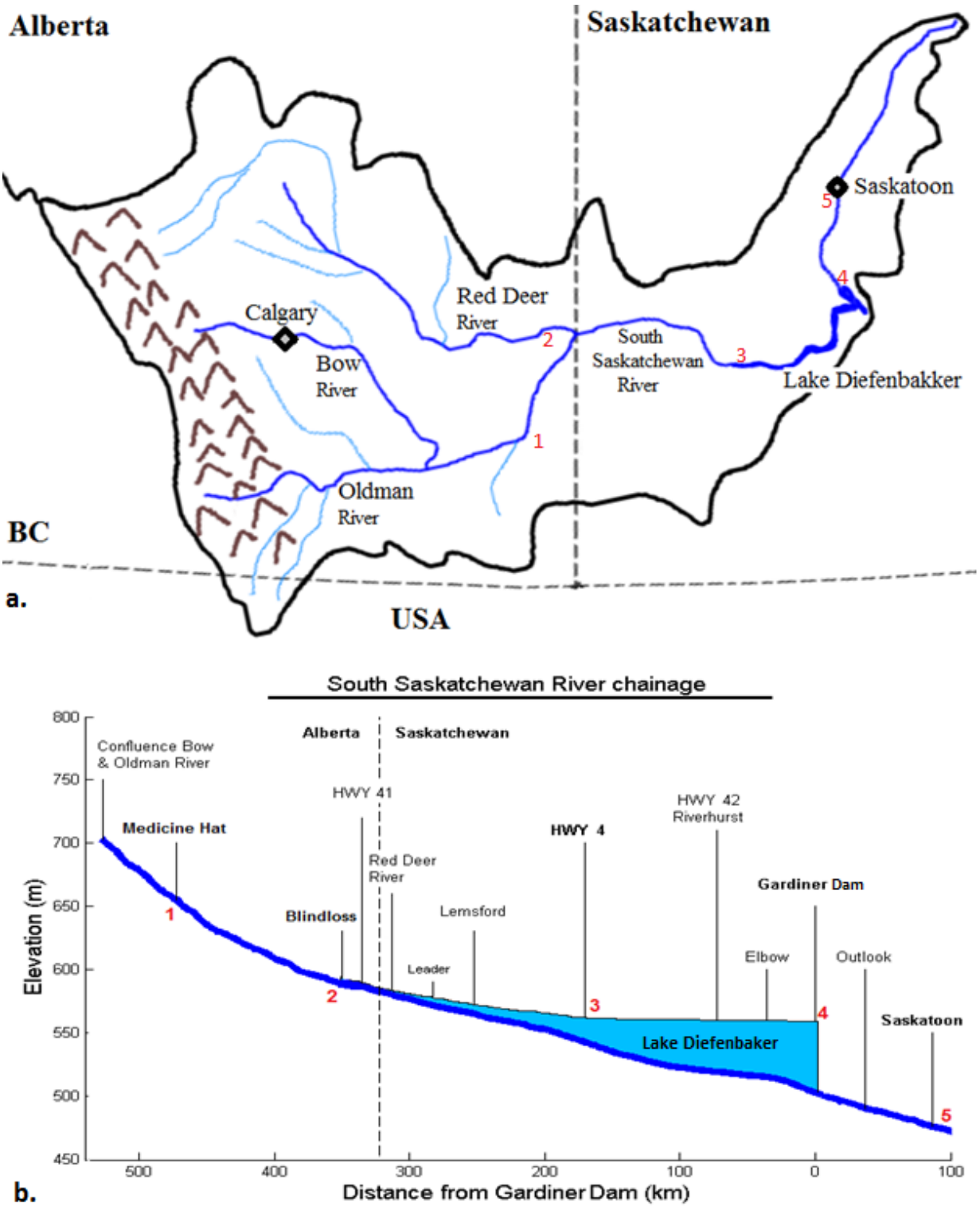

Figure 3.1: Map of the South Saskatchewan River Basin and Lake Diefenbaker. Locations 1 & 2 are hydrometric stations used for inflow water data. Location # 3 is upstream of Lake Diefenbaker at highway 4, # 4 is downstream of the lake at Gardiner Dam and # 5 is the City of Saskatoon where the outflow data were calculated from

3.3 Methods

3.3.1 Study site description

Lake Diefenbaker was formed along the SSR by the construction of the Gardiner and Qu'Appelle River dams in the 1960s. The reservoir is a part of the South Saskatchewan River Basin (SSRB), which originates in the Rocky Mountains in Alberta. The SSR has strong seasonal variations with maximum and minimum recorded discharges of 3940 m^3/s and 14.2 m^3/s, respectively (Environment Canada, 2013). Three principal headwater sub-basins, the Oldman, Bow, and Red Deer River basins, drain into the SSR, which contributes about 98% of the inflowing water to the lake (WSA, 2012b). Smaller contributions of about 1% each stem from precipitation and the local Swift Current Creek tributary (WSA, 2012a).

Lake Diefenbaker is a long (181.6 km) and narrow (maximum width 6 km) reservoir with a surface elevation of 556.87 meters above sea level (full supply level) (Figure 3.1b). It has a maximum depth of 60 m, a surface area of approximately 393 km^2 and a volume of 9.03 km^3. With a mean inflow rate of 254 m^3/s (Environment Canada, 2013), the reservoir has an average residence time of 1.2 years. The reservoir and dams are part of a multipurpose hydraulic project, which provides water for irrigation, drinking water, eco-services, hydropower generation, aquaculture and recreation. The reservoir is also used for flood mitigation and as a receptacle for treated wastewater (Sadeghian et al., 2014).

3.3.2 Model Selection

Lake Diefenbaker is a deep and narrow waterbody in which hydrodynamic variations in the lateral direction are expected to be smaller compared to those in the longitudinal and vertical directions. Hence, the 2D laterally-averaged CE-QUAL-W2 (Cole and Wells, 2013) model was chosen for this study to model the hydrodynamics and water quality of the lake. CE-QUAL-W2 was originally developed by the U.S. Army Corps of Engineers and extended by Portland State University.

CE-QUAL-W2 was selected based on our study objectives, the physical and chemical characteristics of the reservoir and the availability of data. Other reasons include the direct

coupling between hydrodynamics and water quality and its applicability to both rivers and lakes (the model can be extended to include the Upper South Saskatchewan River). In addition, the model is well documented and the source code is freely available, enabling the modeler to modify or amend process descriptions directly within the algorithm (e.g., extended ice model for cold climate regions). Moreover, it has been successfully applied to Canadian lakes, e.g., hydrodynamic model of Lake Erie (Boegman et al., 2001).

One of the limitations of CE-QUAL-W2 is that it uses only one meteorological station for each waterbody. For such a long reservoir (approximately 182 km), use of several stations is preferred; however, the flat topography of the land encompassing the reservoir justified the use of only one station. Moreover, the ice model does not account for snow cover effects on the ice surface, which is a key limitation for regions with a long ice-cover period. Hence, this component of the model was extended to account for the insulating effects of snow on ice.

3.3.3 Bathymetry

Early bathymetry data are available from surveys carried out after the construction of the dams in the 1970s and 1980s. To obtain more recent information, new surveys were carried out on the reservoir in 2012 and 2013. In order to check the accuracy and applicability of the new data and to investigate historical sedimentation rates, these recent data were compared with contour maps from the 1980s and cross section data from the 1970s (SWRC, 1968, 1969, 1970, 1971, 1972). High rates of sedimentation and bank erosion have changed the bathymetry and, consequently, diminished the reservoir volume capacity over time. Therefore, the bathymetric model was constructed by applying the natural neighbor interpolation method to the 2012 – 2013 survey data. Lake volumes were calculated using 3D Analyst Tools (Surface Volume in ArcToolbox) in ArcGIS (Figure 3.2). Details are available in Chapter 4.

The total volume for the lake, from highway 4 (HWY 4) to the dams, was calculated to be 9.03 km^3 at a water level elevation of 556.9 m (full supply level), with a corresponding total surface area of 393.55 km^2. This yields an average depth (= volume / area) of 22.94 m at full supply level. The length of the lake from HWY 4 to the Gardiner Dam is about 163

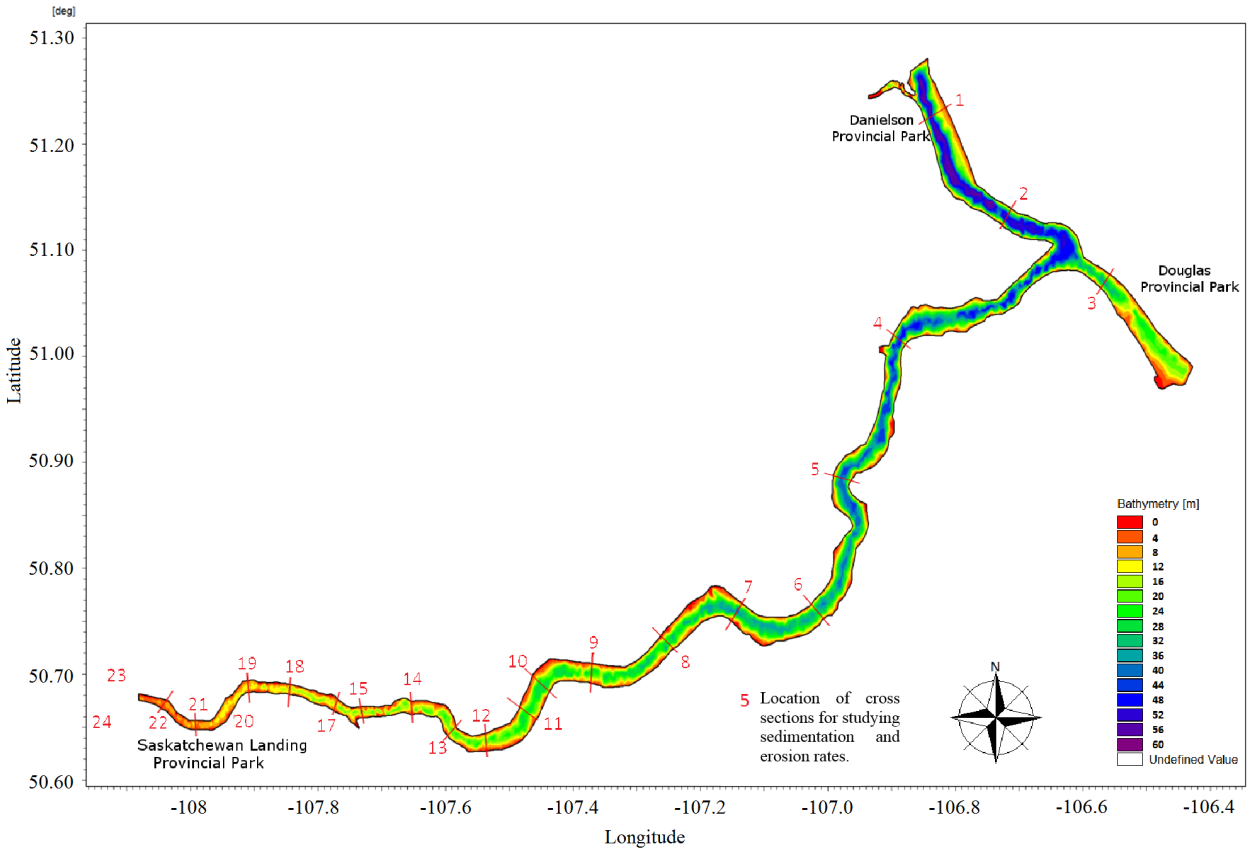

Figure 3.2: Lake Diefenbaker bathymetry map from the 2013–2013 survey

km. The Qu'Appelle arm represents an additional 19 km.

In order to evaluate the effect of grid spacing on model performance, the model results from two bathymetry files with different longitudinal resolutions were compared. The finer resolution bathymetry consisted of 187 longitudinal segments (170 – 3,200 meters long), and the coarser resolution had 126 segments (600 – 4,200 meters long). More smoothing of the flow-path changes was carried out on the second file, which also contained longer segments for the areas where there were no significant changes in the flow path.

3.3.4 Forcing data and boundary conditions

Highway 4, approximately 162 km upstream of the Gardiner Dam, was considered to be the upstream boundary of the reservoir in the model. There are no hydrometric stations close to this point in Saskatchewan; therefore, the SSR inflow was calculated based on two

stations in Alberta. The SSR inflow is the sum of two hydrometric gauge stations: "Red Deer River near Bindloss" (#05CK004) (about 150 km upstream of HWY 4) and "South Saskatchewan River at Medicine Hat" (#05AJ001) (about 300 km upstream of HWY 4) (Figure 3.1b). The inflow was routed based on the Water Security Agency's (WSA) time-lag guidelines, as described in Hudson and Vandergucht (2015).

Discharge data for Swift Current Creek, the main local tributary, were obtained from the hydrometric station "Swift Current Creek near Leinan" (#5HD039). The Qu'Appelle River dam outflow data were obtained from the hydrometric station "Elbow Diversion Canal at Drop Structure" (#05JG006). The Gardiner Dam outflow data were obtained from the hydrometric station "South Saskatchewan River at Saskatoon "(#05HG001). Flows were lagged by one day as suggested by Pomeroy and Shook (2012). The outflow of the Gardiner dam is via the metalimnetic withdrawal supplying the hydroelectric turbines (Phillips et al., 2015) or through the spillway. Due to lack of data, all the outflow water was considered as overflow. A sensitivity analysis showed that different withdrawal depths affect the reservoir's heat budget only slightly, by about one degree in June and July. Water levels were obtained from the station "Lake Diefenbaker at Gardiner Dam" (#05HF003).

The inflow temperature was estimated based on correlations between the average weekly air temperature and daily stream temperature, as suggested by Morrill et al. (2005). A linear relationship was found between weekly averaged air temperatures at the "Leader Airport" meteorological station (WMO ID: 71459) and water temperatures from the monitoring station M3 (# 1 in Figure 3.3):

$$y = 0.85x + T_{IN} \tag{3.1}$$

where y is the stream water temperature (°C), x is the weekly air temperature (°C), and T_{IN} is the inflow temperature coefficient (°C). T_{IN} = 4.8 °C provided a very good coefficient of determination (R^2 = 0.93). Measured water temperature profile data were provided by the Limnology Laboratory of the University of Saskatchewan. There were 16 sampling stations extending across the whole reservoir (Figure 3.3) with 57 days of sonde-profile measurements data collected in both summer and fall of 2011 and 2012 (30 days in 2011 and 27 days in 2012). A Yellow Springs Instrument (YSI) sonde, (model 6600 V2) with the

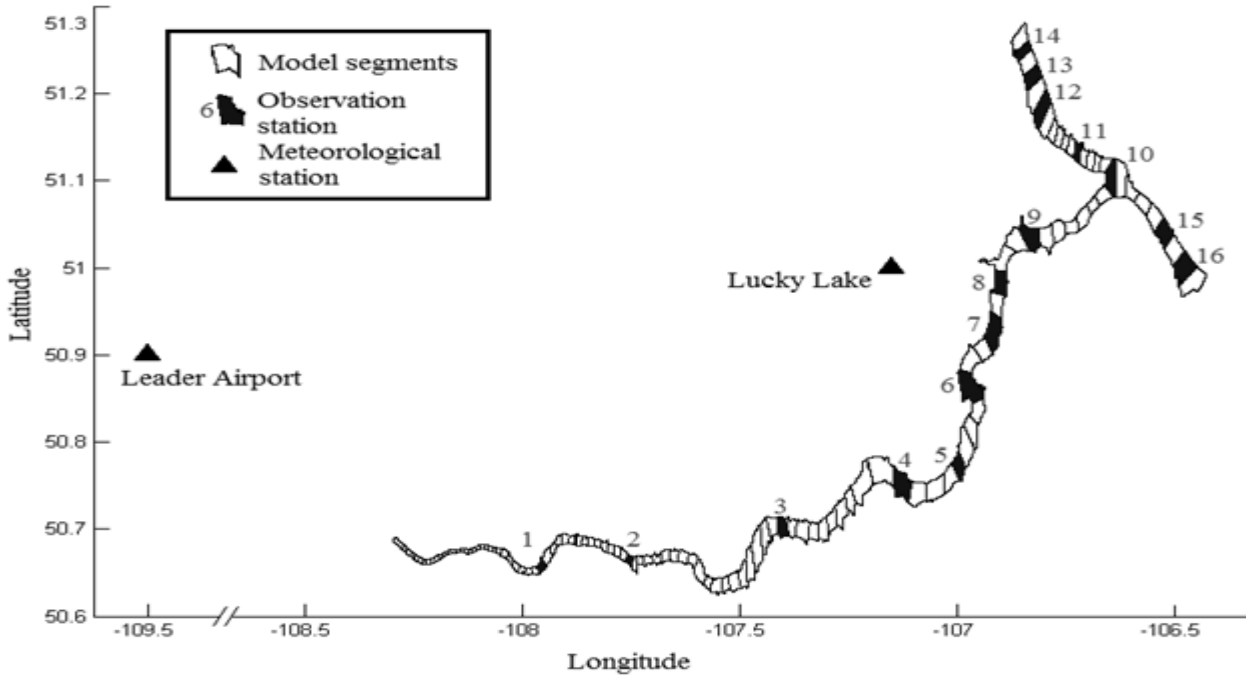

Figure 3.3: Model segmentations and locations of observation stations and meteorological stations

accuracy of ± 0.15 °C and the resolution of 0.01 °C were used for all the measurements. Details of the sampling are provided in Hudson and Vandergucht (2015).

The surface of Lake Diefenbaker freezes over completely in winter. In early spring, after the ice has melted, the reservoir water temperature profile is assumed to be homothermic since the vertical temperature gradients due to convection and turnover are small. A uniform temperature of 4 °C throughout the water column at the beginning of April provides a convenient point in time to initialize the water temperature simulations (Beletsky and Schwab, 2001; Hondzo and Stefan, 1993a,b; Peeters et al., 2002).

Hourly meteorological data (air temperature, dew point temperature, wind speed and wind direction) were obtained from the Lucky Lake station (WMO ID: 71455) located west of the reservoir (Figure 3.3). Since this is a land station, a wind sheltering coefficient (WSC) was applied to transfer wind speed measurements to the reservoir surface.

Solar radiation is an important component of heat flux and is required for temperature simulations of lakes (Beletsky and Schwab, 2001). Global short wave radiation at the surface was calculated based on latitude and time of year, as verified by the National Oceanic and Atmospheric Administration (NOAA) "The NCEP/NCAR Reanalysis 1" solar radiation database.

The light extinction coefficient is the rate of attenuation of solar radiation as it passes vertically through the water column. It controls the amount of solar radiation penetrating the water column and has an impact on stratification and thermal mixing (Jankowski et al., 2006). Values of the light extinction coefficient were calculated empirically from monthly measurements of the Secchi depth, the depth of water at which the Secchi disk is no longer visible from above the water surface:

$$\epsilon = \frac{EXT}{Z_{SD}} \tag{3.2}$$

where ϵ is the light extinction coefficient (m^{-1}), Z_{SD} is the Secchi depth (m) and EXT is the extinction coefficient (a constant). Values for EXT depend on lake water characteristics and typically range between 1.3 (e.g., Lindenschmidt, 1998) and 1.7 (e.g., French et al., 1982).

On average, the surface of Lake Diefenbaker is covered with ice for five months of the year (December-May). Ice layers work as a barrier to solar radiation, wind effects and further cooling of the water. The ice thickness, formation and melting times are important influences on the heat budget, mixing regime and water quality processes in the lake. Physical properties such as albedo and surface temperature change the attenuation of solar radiation in ice and snow, which strongly affects the reservoir's heat balance (Patterson and Hamblin, 1988). Ice models are necessary to calculate the heat transfer between ice and water. The current version of CE-QUAL-W2 includes an ice model; however, its application is limited due to its omission of a snow pack on the ice cover. In order to include snow effects on the ice surface, two empirical coefficients were added to the ice algorithm to mimic the reduction in heat conduction through the ice, from the water to the air. Although further development would be desirable, this simple adaptation to the algorithm greatly improved ice thickness and ice-on period calculations. Table 3.1 summarizes the governing equations

for calculating ice thickness.

For this current study, ice thickness data from Lake Diefenbaker were not sampled during the winter period of 2011 – 2012. Therefore, the ice coefficients were calibrated using an extensive data set from Blackstrap Lake, a smaller reservoir located approximately 70 km north of Lake Diefenbaker, and then transferred to the Lake Diefenbaker model. The transfer was verified for Lake Diefenbaker using data collected during 2012 – 2013. Ice data, including ice thicknesses and the extent of the ice cover period, were obtained onsite by the Global Institute for Water Security (GIWS) at the Elbow station (site # 10 in Figure 3.3). These data were used to fine-tune the calibration of the extended ice.

In the model, ice thickness has three components (Eq. 3.3): one equation for ice growth and two for melting at the air-ice and ice-water interfaces. The first step was to correct the overestimated ice thickness (θ_g). θ_g changes with ice temperature and is a function of solar radiation, air temperature, evaporation (R_E), conduction (R_C) and back radiation from black surfaces (R_B) (Eq. 3.4 – 3.7 in Table 3.1). The average values of ice calculation components in Table 3.2 reveal that R_B has a significant effect on the results by yielding very large thickness values for very low ice temperatures. Therefore, the coefficient α was added to correct R_B (Eq. 3.8). α is assigned values between zero and one and was calibrated to equal 0.63 for Lake Diefenbaker. On some days, R_B becomes too small and consequently R_N becomes positive. Positive values of R_N act as a melting process, which is not intended for θ_g (θ_g is only for ice growth). Therefore, R_N should have a maximum value of zero to prevent ice melting. During times when the ice is melting ($T_i > 0°C$), the model reverts back to the original equation (Eq. 3.5).

The ice melt algorithm contains two parts as described in Equation 3.3. The values for ice melt at the air-ice interface θ_A and melt at the ice-water interface θ_W are listed in Table 3.2. The values for θ_A are mainly zero during the ice-covered period; however, at the time of melting they may have extremely high values, leading to rapid melting of the ice cover. θ_A is allowed to have larger values than θ_W, using the coefficient β (Eq. 3.9) to allow increased melting at the air-ice interface during warmer days in spring with no snow remaining on the ice cover. β was calibrated to be equal to 50 for Lake Diefenbaker. A value of Jday (Julian day) > 90 restricts the criteria to the melt period.

Table 3.1: Ice model equations and parameters

$$\theta = \theta_g - \theta_A - \theta_W \tag{3.3}$$

$$\theta_g = \frac{\Delta_t \times RK1 \times (-T_i)}{\theta_g \times \rho_{IRL1}} \tag{3.4}$$

$$R_N = R_{N1} - R_B - R_E - R_C \tag{3.5}$$

$$\Delta_{ti} = R_N + \frac{RK1 \times (-T_i)}{\theta} \tag{3.6}$$

$$T_i = T_i + \Delta_{ti} \tag{3.7}$$

$$R_N = R_{N1} - \alpha R_B - R_E - R_C; \& \ \{T_i < 0 \text{ and } R_N < 0 \text{ and } 0 < \alpha < 1\} \tag{3.8}$$

$$\theta_A = max(\theta_A, \beta \times \theta_W) \text{ for Jday} > 90 \tag{3.9}$$

θ =ice thickness (m)
θ_g =ice growth (m)
θ_A = ice melt at ice and air surface (m)
θ_W =ice melt at water and ice surface (m)
RK_1= ice conductivity (2.12 W/m/°C)
Δ_t = changes in time (second)
ρIRL_1= constant (305492412)
T_i= ice temperature (°C)
R_N = ice heat balance (W/m^2)
R_{N1} = heat due to solar radiation (W/m^2). f (air temperature, solar radiation and ice albedo)
R_B = heat lost due to back radiation from black surface (W/m2)
R_E = heat lost due to evaporation (W/m^2)
R_C = heat lost due to conduction (W/m^2)
Δ_{ti}= changes in ice temperature (°C)
Jday = Julian day (continuous count of days since the beginning of the year)
α = coefficient for controlling back radiation (ice thickness)
β = coefficient for controlling θ_A (ice melting)

Table 3.2: Simulated values for ice calculation in CE-QUAL-W2 model in 2012 – 2013 for Blackstrap Lake

Ranges in 2012/13	T_{ice}	R_N	R_{N1}	R_B	R_E	R_C	θ_g (m/hr)	θ_A (m/hr)	θ_W (m/hr)
Minimum	-20	-138	158	226	-76	-290	0	-2.46	-9.3 e-5
Maximum	0	426	440	361	113	100	1.6 e-3	0	0
Average	-4.3	-15	218	289	14	19			

Ice formation typically occurs at the end of November/ beginning of December (Jday > 300).

3.4 Calculations

Based on initial model runs and literature guidelines, several parameters were identified as influential on model results. Among them, wind and solar radiation were the most important for the mixing and heat budget, respectively. Within the model, these two meteorological variables were adjusted using the parameters WSC (wind sheltering coefficient) and SHADE (shading coefficient). Considering the high fluctuations in discharge of the inflow and the high flows in late spring and early summer, the effect of inflow temperature was also of interest. The light extinction coefficient is important as it controls the amount of solar radiation penetrating through the water column.

Heat conduction between the lake bed and the water column is also important, particularly in shallower lakes (Lindenschmidt and Hamblin, 1997), but was not incorporated in the calibration since the reservoir is relatively deep. Therefore, four coefficients were used for sensitivity analyses: WSC, SHADE, T_{IN} and EXT. Initial values for the other coefficients and constants were taken from the literature.

Values for WSC and SHADE were used directly in the model, whereas inflow temperature and the light extinction were calculated using T_{IN} and EXT, as described in Equations 3.1 and 3.2, respectively. WSC has a range between 40% and 120% of measured wind speed at the meteorological station. SHADE ranged between 50% and 100% of incoming short wave solar radiation. EXT in Equation 3.2 varied between 1.3 and 1.7. Based on historical data from the Saskatchewan Environment Environmental Management System (SEEMS), the average observed Secchi depth in Lake Diefenbaker ranged from 6 meters in winter to 3 meters in summer, yielding extinction coefficient values ranging from 0.21 – 0.28 for winter to 0.43 – 0.56 for summer. T_{IN} varied between 2 °C and 6 °C in Equation 3.1, setting the inflow temperature range to 0 – 25 °C.

The global sensitivity analysis was based on a Monte Carlo analysis of 1000 runs, to evaluate model performance, with each simulation having parameters randomly selected

from a uniform distribution within defined ranges. Model performances were determined by calculating the differences between measured and simulated temperature values of each Monte Carlo simulation based on the objective functions Sum of Squared Error (SSE) and Root Mean Square Error (RMSE):

$$SSE = \sum (O - S)^2 \tag{3.10}$$

$$RMSE = \sqrt{\frac{\sum (O - S)^2}{n}} \tag{3.11}$$

where O is the measured value and S is the model output time-series for vertical temperature profiles at the 16 stations shown in Figure 3.3, and n is the number of samples.

Also, a coupled global [Particle Swarm Optimization (PSO)] and local [Levenberg-Marquardt (LM)] optimization method (PSO+LM) was tested and utilized to calibrate the model more efficiently. In short, the global optimization method (PSO) finds the optimal regions for each variable based on model performance. Then, these optimal regions are transferred to the local optimization algorithm (LM) for fine-tuning. The model sensitivity analysis and optimization procedure are explained in detail in Appendix III.

3.5 Results

3.5.1 Bathymetry

Comparisons between the more detailed cross sections from the late 1960s/early 1970s and the 2012 – 2013 survey indicate that the pre-lake cross sections are generally consistent with the more detailed, later cross sections, and provide an indication of changes in the general shape of the cross section (Chapter 4).

Sedimentation rates from the late 1960s to 2013 decreased rapidly from 0.18 m year^{-1} at Range 24 to 0.02 m year^{-1} at Range 15 to lower, negligible values downstream (Table 3.3). This pattern of rapid decrease in the sedimentation rate downstream along the lake is consistent with observations of sedimentation rates in the early years as reported by Yuzyk (1983). High sedimentation rates, especially in the upstream part, have significantly

Table 3.3: Sedimentation and erosion rates based on comparison of cross sections from the late 1960s/early 1970s and the 2012–2013 cross sections. See Figure 3.2 for locations

	average sediment m	deposition rate m y^{-1}
Range 24	7.5	0.18
Range 23	6.8	0.16
Range 21	6.2	0.16
Range 20	4.0	0.10
Range 19	4.1	0.10
Range 18	2.1	0.05
Range 15	1.4	0.03
Ranges downstream of range 15	low to negligible sediment deposition rates	

changed the depth and shape of the lake bathymetry over time.

3.5.2 Temperature simulation

The results of the temperature simulations at various locations and vertical depths, using different parameter settings, were compared with the measured values. Dotty plots were used for identification of the parameter responses to the objective function (SSE). The plots are useful for understanding parameter sensitivity to changes within the defined ranges and the boundary condition adjustments (Wagener et al., 2004). They also provide insight into the identifiability of these parameters and the associated effects of varying model spatial resolution.

In the Monte Carlo analysis, the best parameter settings were chosen based on the minimum sum of squared error between measured data and model results (Figures 3.4a and 3.4b). For WSC and SHADE a distinct minimum in the parameter space illustrates that the optimum parameters are quite well identified, but for EXT and T_{IN} this is not the case, i.e., optimal performance can be achieved with any feasible value of these parameters. Further work is needed to investigate potential parameter interdependencies that could explain part of this effect, but for model optimization the implication is that specified values could be used for these two parameters. The ranges found in the calibration of both model resolutions (187 and 126 segments) for both years (2011 and 2012) show very similar values.

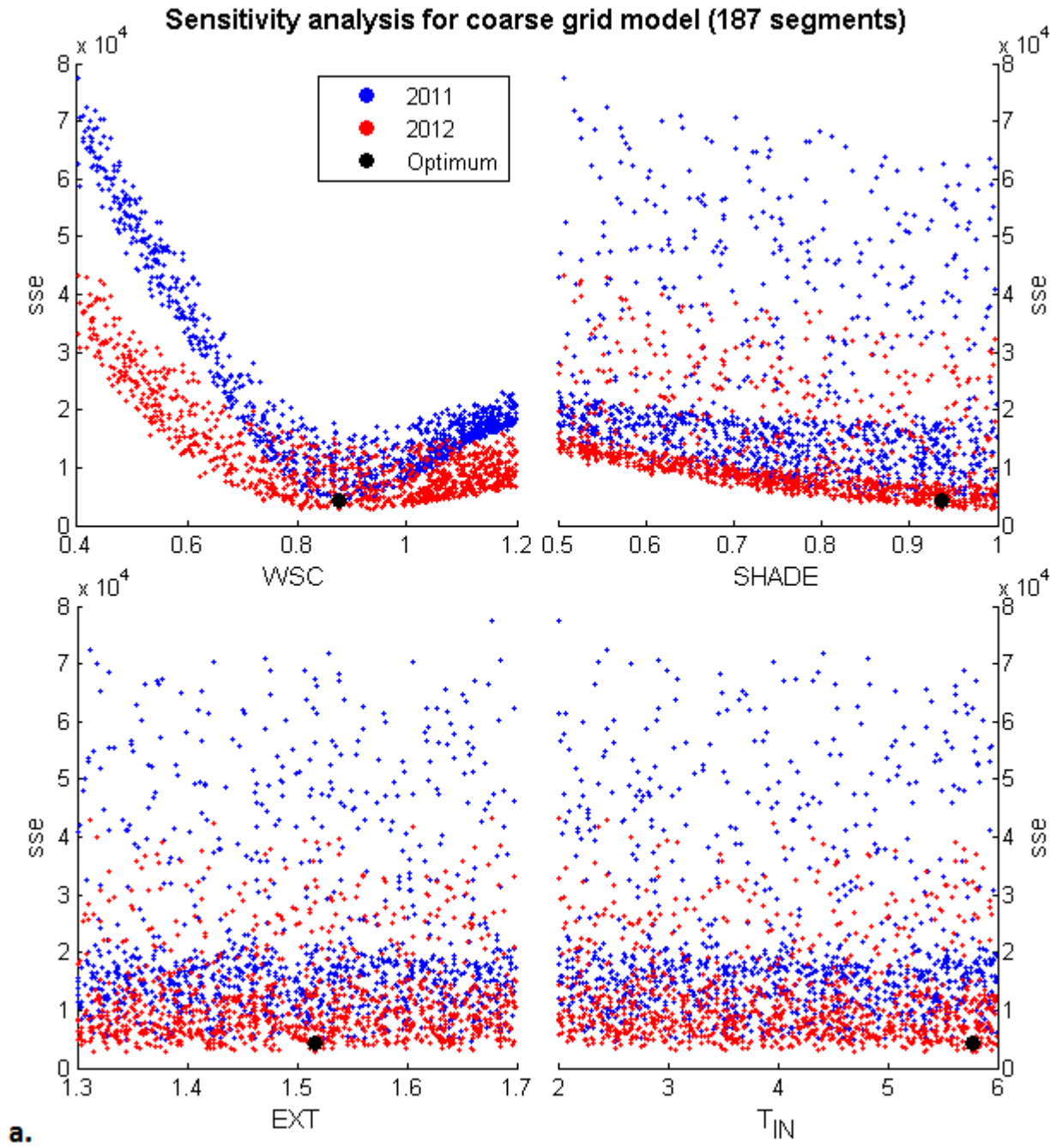

Figure 3.4: Sensitivity analysis results. a: Sensitivity results for Monte-Carlo simulations for the model with 187 & 126 segments. WSC and SHADE are wind sheltering and shading coefficients. EXT and T_{IN} are light extinction coefficient and inflow temperature multipliers in equations 1& 2

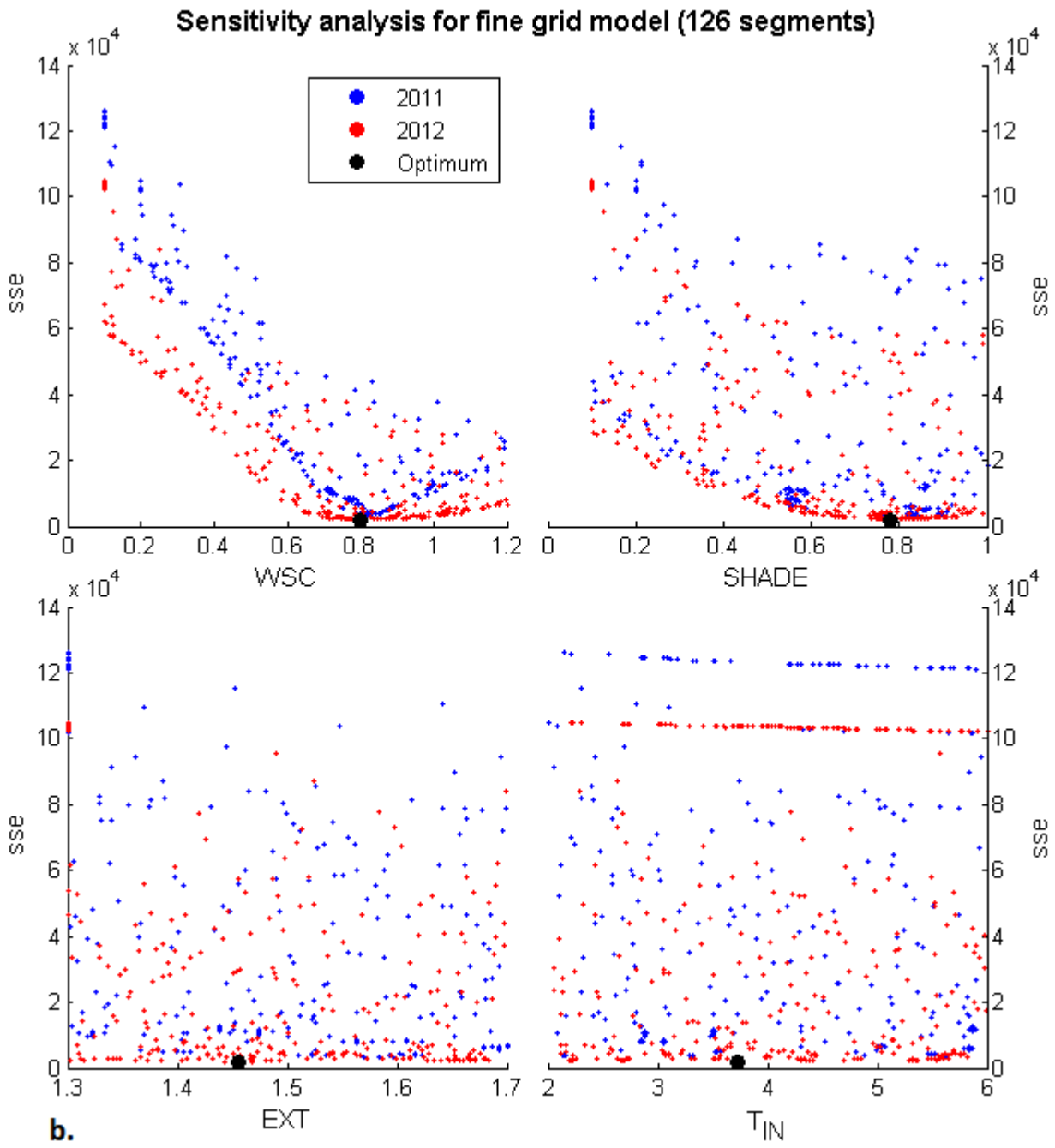

Figure 3.4: Sensitivity analysis results. b: Sensitivity results for Monte-Carlo simulations for the model with 187 & 126 segments. WSC and SHADE are wind sheltering and shading coefficients. EXT and T_{IN} are light extinction coefficient and inflow temperature multipliers in equations 1& 2

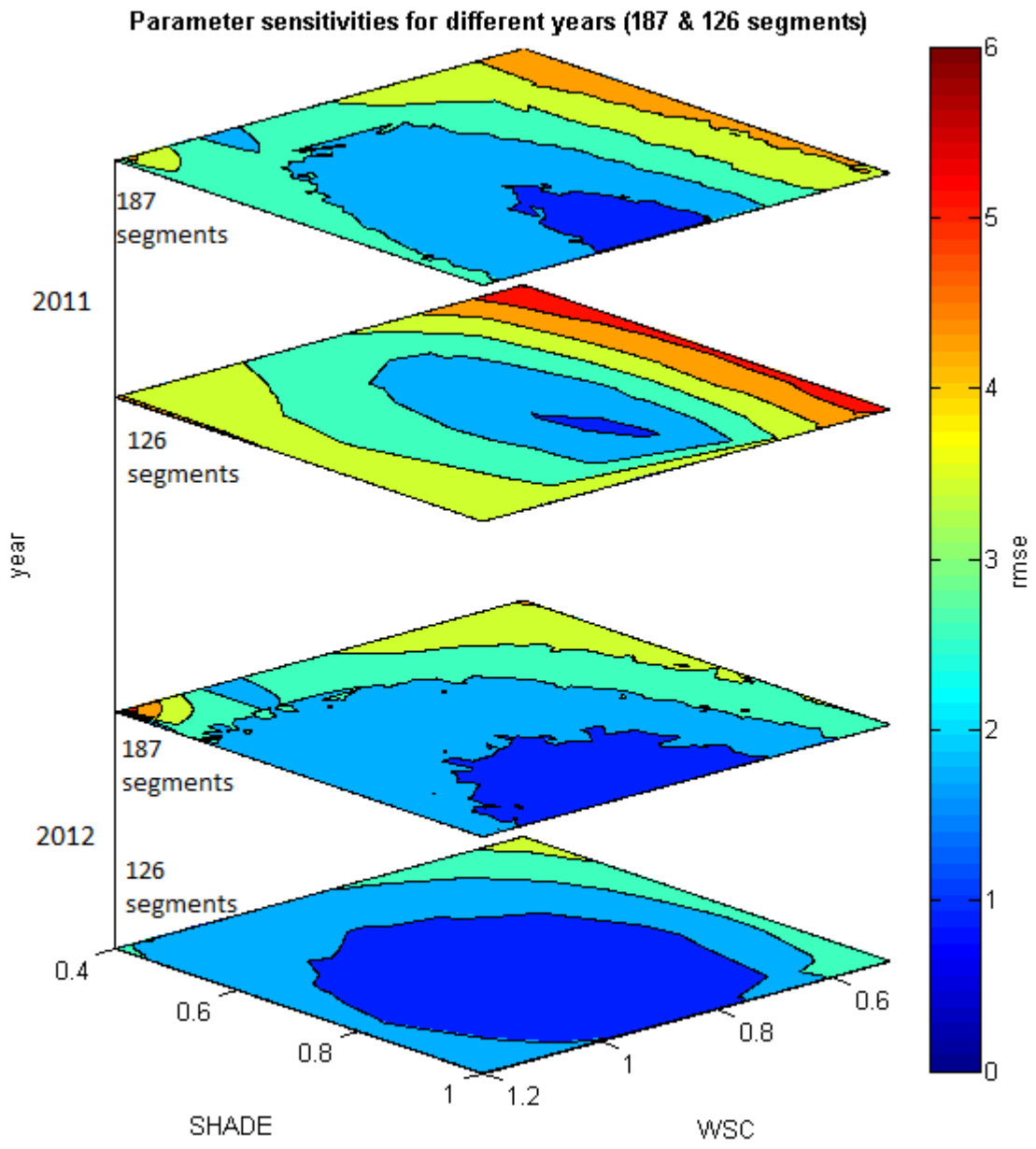

c.

Figure 3.4: Sensitivity analysis results. c: Comparison of model's results for two sensitive parameters (WSC & SHADE) with the 187 and 126 segments in 2011 & 2012. Each sheet is for the depth which is located and the next 15 meters below it. Since the number of samples were not the same at each depth, the sse/n (n is number of samples) was used instead for consistency

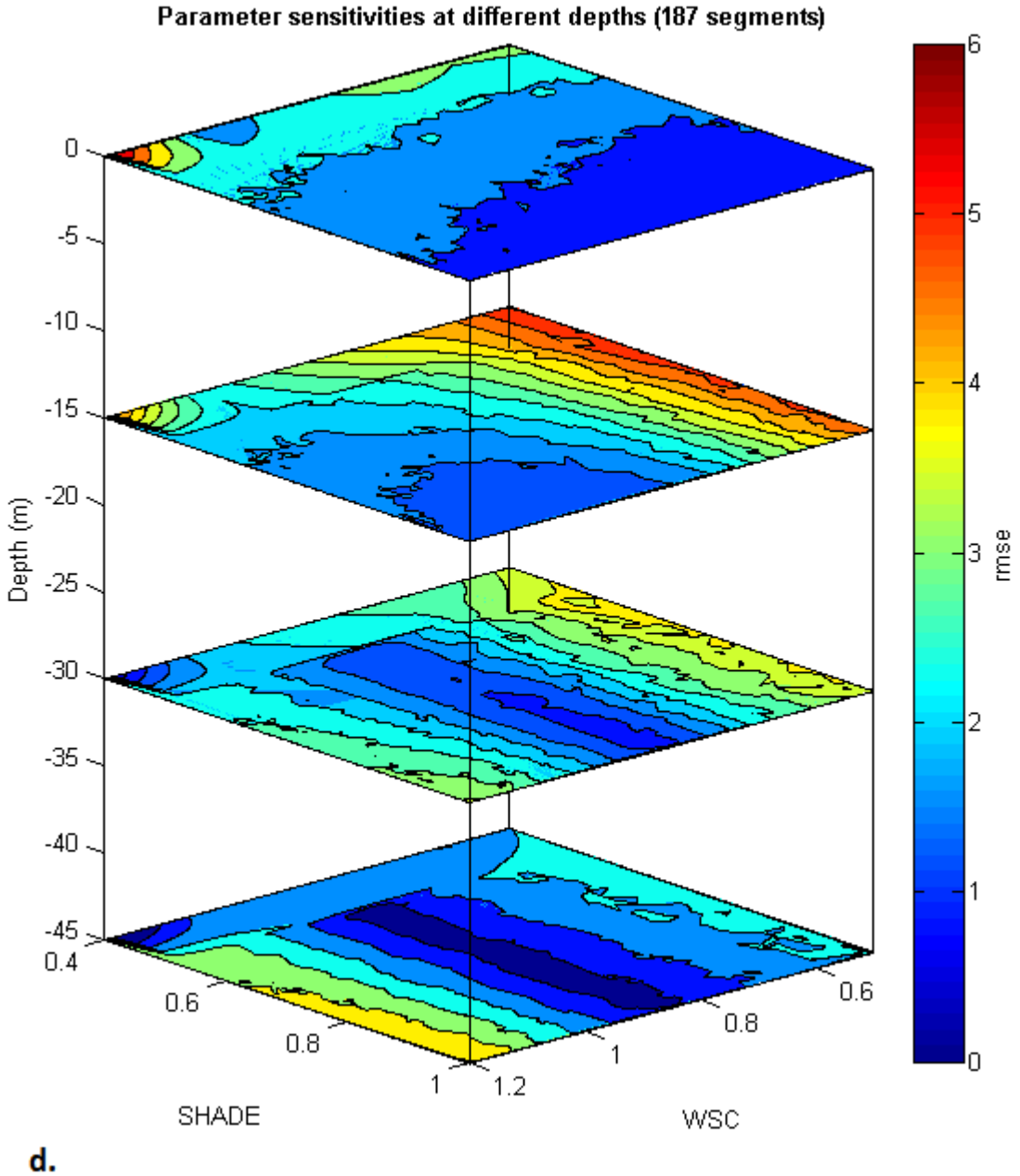

Figure 3.4: Sensitivity analysis results. d: Comparison of model results for two sensitive parameters (WSC & SHADE) for the model with 187 segments at different depths. Each sheet is for the depth which is located and the next 15 meters below it. Since the number of samples were not the same at each depth, the sse/n (n is number of samples) was used instead for consistency

Comparing the results from the 187 and 126 segment models (Figures 3.4a and 3.4b), no significant difference in performance was observed. The model with 187 segments used finer grids and the calculations were continuous from 2011 to 2012. In the model with 126 segments, the calculations for 2011 and 2012 were independent, since in early spring the lake had homothermal conditions of 4 °C. Although the results from these two grid resolutions were not distinguishable, the computational times were significantly less for the coarser grid.

As noted above, the models are sensitive to both WSC and SHADE parameters. In the models with 126 and 187 segments, a fairly similar proportion of the parameter space yielded good performance (Figure 3.4c), implying that the coarser grid model can be used for quicker simulation times without having to compromise accuracy and parameter sensitivity. Lindenschmidt (2006) provides a discussion on the effects of model complexity on parameter sensitivity and modelling accuracy. In the interest of computational efficiency, future studies will be based on the model with 126 segments.

In order to study the model performance at different depths, the reservoir was divided into four vertical layers, each 15 meters thick (Figure 3.4d). Measurements and simulation results at depths 0, 15, 30 and 45 m correspond to the values at depth ranges 0 – 15 m, 15 – 30, 30 – 45 and 45 – 60 meters, respectively. All the measurements within each range were sorted in one column and compared to the simulated values at the corresponding location and depth. Since the number of samples were not the same in each depth range, RMSE values were used instead of SSE to normalize the SSE values. For the top layer, SHADE is more sensitive due to the effects of solar radiation and overflow discharges. Conversely, WSC is more influential on the second layer indicating the effect of wind on mixing in the lower layers. WSC still has an impact on the lower lake layers, whereas SHADE's influence is diminished at the lake bottom.

The PSO+LM optimization method performed exceptionally well. The code found the best parameter settings after only 41 runs. In order to assure that these results were not by chance, the runs were repeated several times until a total of 1000 runs had been completed. Therefore, the results were used for both sensitivity analysis and accuracy control of the codes and the methodology (Figure III.1a). On average, after 24 PSO runs, the results

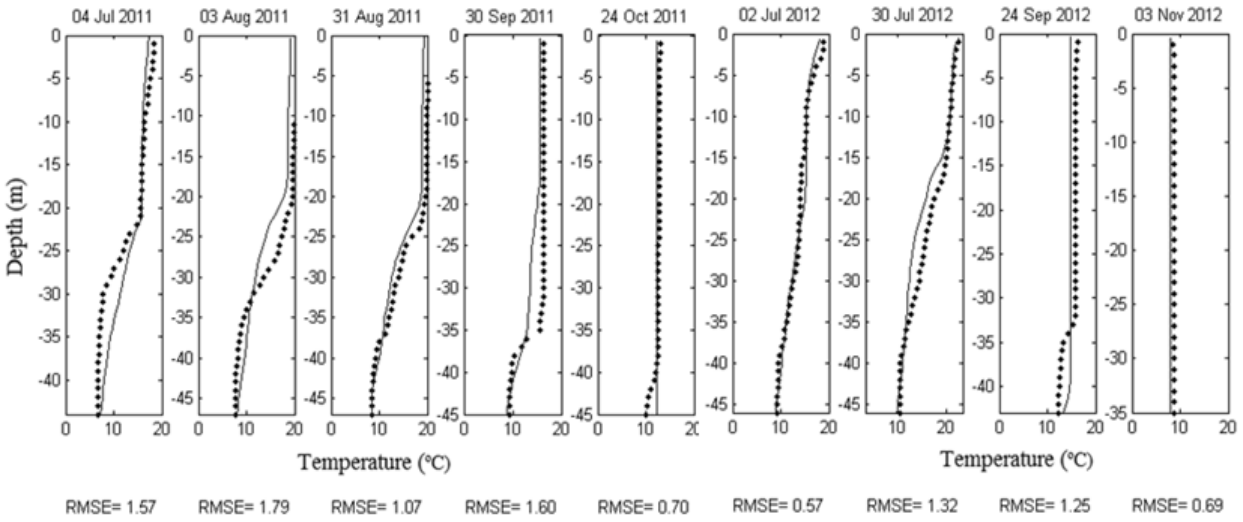

Figure 3.5: Simulated (lines) vs measured (dots) temperature for observation station 10 (near Elbow)

were passed to LM to find the best parameter settings after 20 to 30 iterations (Figure III.1b). The blue circles are parameter values generated by PSO and the red circles are values fine-tuned by LM. There were only two cases where the results from LM were not convincing and LM returned the parameter values to PSO for further exploration of new areas in the parameter space.

As an example, the measured temperature values (dots) were compared with the simulated values (lines) for the stratification and destratification periods near Elbow (Station # 10) (Figure 3.5). The water is thermally stratified in summer and early fall. Early in November the water temperature begins to decrease, leading to the breaking down of the thermal stratification. The discrepancy between measured and simulated temperatures increases when the thermocline location is not calculated correctly, where there are steep temperature gradients (Peeters et al., 2002). A strong wind event can move the thermocline several meters vertically, so using daily meteorological data can produce errors when the reservoir is stratified at windy days. The inclusion of hourly meteorological data, daily hydrometric data and accurate calculations of the water level during the simulations reduced this problem significantly.

In order to extend the description of the thermal regimes over the entire year, water temperatures in winter also required calibration. Temperature data were not available for the winters of 2011 and 2012, but ice data from the 2012 – 2013 winter were available. With $\alpha = 0.63$ and $\beta = 50$ (Tables 3.2 and 3.3), values calibrated by the Blackstrap Lake model, the simulated ice thickening and melting fit the observations reasonably well (Figure 3.6). With the correct ice thicknesses and ice-on durations, solar radiation and wind effects on the ice cover and water column can be estimated. This allows the temperature to be generated for the whole year.

Novel in this work is the quantification and illustration of the effect of different contributing heat sources and sinks to the lake heat budget (Figure 3.7). The values are calculated as the total amount of thermal energy divided by the lake volume. They show the monthly average amount of heat added to or removed from the lake each day. The "surface heat exchange" is the sum of all the shortwave and longwave solar radiation terms and conductive and evaporative fluxes. "Bed" is the heat exchange between sediment and water at the bottom of the lake. The "inflow" and "tributary" show the amount of heat added to the lake by the SSR and Swift Current Creek, respectively. The "outflow" and "evaporation" are the equivalent amounts of heat removed from the lake due, respectively, to water discharged via the outflow and evaporation. "Ice" represents the heat lost at the ice –water interface. The "net" component is the sum of all the components.

The parameters on the right (bed, tributary, evaporation and ice) have a scale one tenth of those on the left (surface heat exchange, inflow, outflow and net). Therefore, their effects are much smaller on the overall lake heat budget. It is interesting to note the large amount of heat input by the inflowing SSR. For example, the inflow water increases the whole lake water temperature by about 0.25 degrees every day in June 2011 and the outflow decreases it by 0.22 degrees. Summing all the components, the lake temperature increases by about 0.14 degrees for each day in June 2011. The three main parameters that influence the heat budget are the surface heat exchanges, inflow and outflow. Since this is a reservoir and outflows are regulated, reservoir management practices can significantly influence the thermal and, consequently, water quality conditions of the lake.

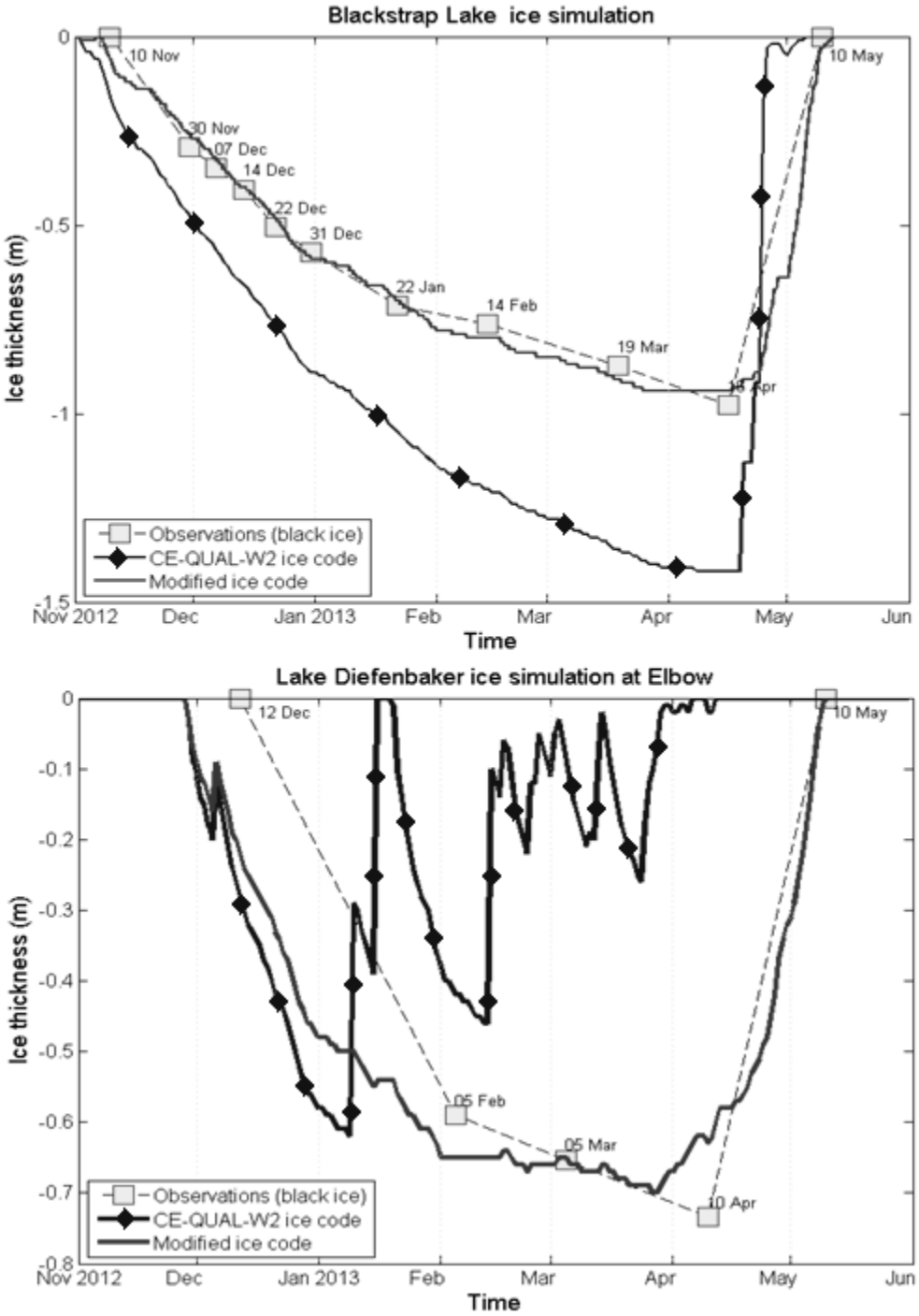

Figure 3.6: Comparison of model original ice model with the modified ice code in both Blackstrap Lake and Lake Diefenbaker in winter 2012/2013

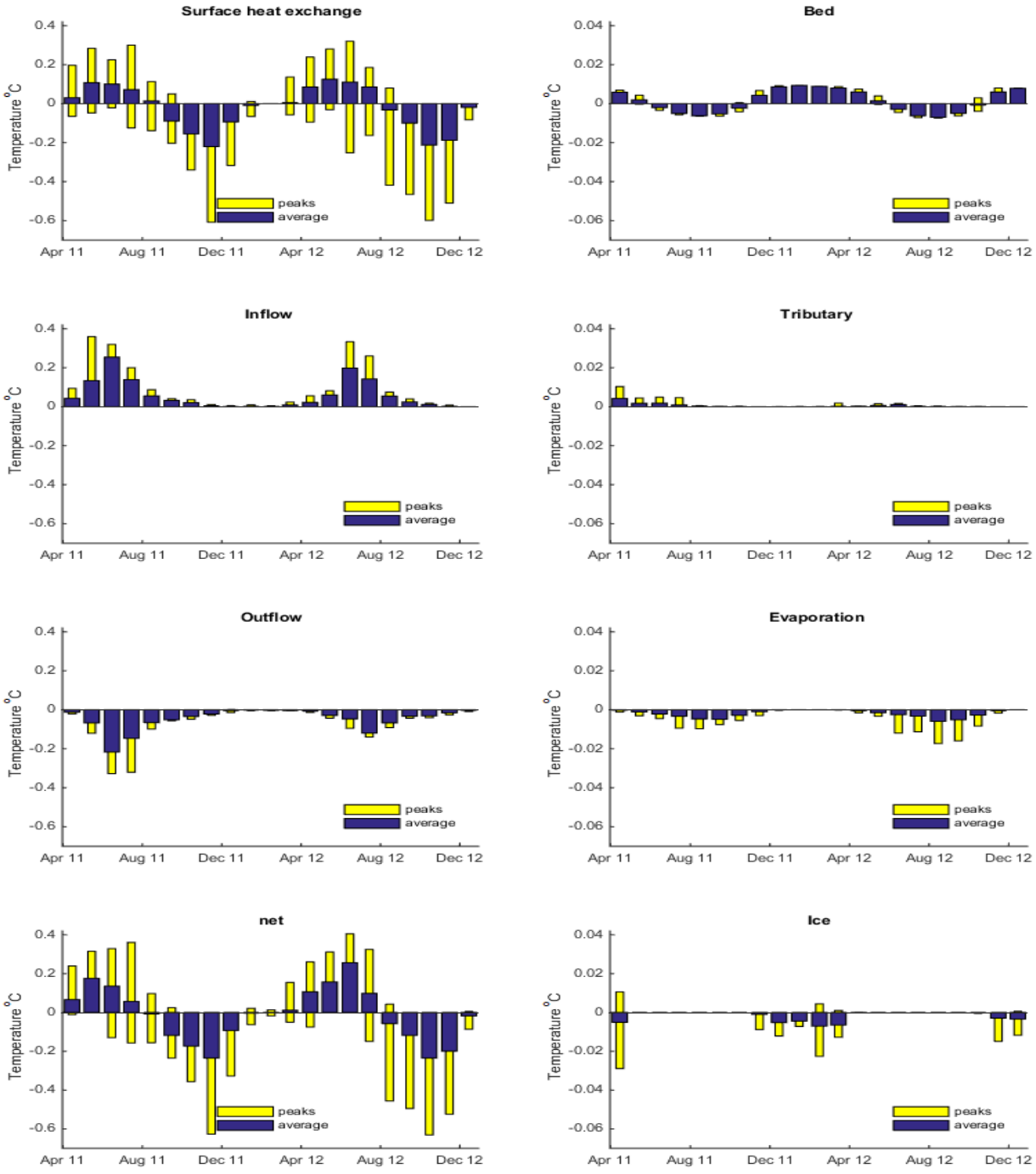

Figure 3.7: Quantitative contribution of different sources to the lake's heat budget. The parameter on the right (bed, tributary, evaporation and ice) has a scale of one tenth of those on the left (surface heat exchange, inflow, outflow and net). The "surface heat exchange" is the sum of all the shortwave and longwave solar radiation terms and conductive and evaporative fluxes. "Bed" is the heat exchange between sediment and water at the bottom of the lake. The "inflow" and "tributary" show the amount of heat added to the lake by the SSR and Swift Current Creek, respectively. The "outflow" and "evaporation" are the equivalent amounts of heat removed from the lake due, respectively, to water discharged via the outflow and evaporation. "Ice" represents the heat lost at the ice–water interface. The "net" component is the sum of all the components

3.6 Discussion

3.6.1 Sedimentation and erosion

After the construction of the Gardiner and Qu'Appelle dams (1959 – 1967), studies were carried out from 1968 to 1972 mapping several cross sections of Lake Diefenbaker. Van Everdingen (1967) investigated bank erosion near Riverhurst Ferry (# 4 in Figure 3.2) as water levels rose in the early years of operation of Lake Diefenbaker in the mid-1960s. He concluded that the relatively weak surficial materials surrounding the lake resulted in the widening of the lake by as much as 100 m on both sides. The eroded sediment accumulated in the lake, decreasing live and dead storage, the former by an estimated 7.4%. Along the lake shoreline, erosion and sediment deposition resulted in extensive shallows that slope towards deeper water at an angle of about 3 degrees. Van Everdingen (1967) also concluded that the sediment load of the SSR was unlikely to be a significant contributor to sedimentation in the lower reaches of Lake Diefenbaker, given the length of the reservoir and the rapid deposition of the load at the lake's inlet.

Ashmore and Day (1988) analyzed Water Survey of Canada sediment load data for the 1962 – 1970 period from the SSR near Lemsford, located upstream of the lake. They provided an estimate of a mean seasonal sediment load of 6.02 million t year^{-1}, with a standard error of 18.3%, flowing into the lake. They estimated the mean seasonal sediment load of Swift Current Creek, the only sizeable tributary flowing into Lake Diefenbaker, to be 67,000 t year^{-1}, with a standard error of 52.2% for the 1965 – 1970 period. Since the completion of the Gardiner and Qu'Appelle River dams, Lake Diefenbaker has functioned as an effective sediment trap. As a result, accumulation of sediment transported into the lake from upstream, in combination with local shoreline erosion and redistribution of sediment, has led to substantial changes in the spatial pattern of erosion and deposition in the lake.

3.6.2 Simulations

The combined global/local optimization, suggested by Vesselinov and Harp (2012), was tested on a polynomial test function and a synthetic plume tracing experiment. In this study, the method was modified for a real case study of the 2D hydrodynamic modelling of Lake Diefenbaker. The PSO method was chosen as a global optimization method and

LM as a local optimization method. One weakness of both the PSO and LM methods is the generation of repeated parameter settings. In a polynomial test function, each iteration takes a fraction of a second, so it is not considered a drawback. However, a single run of the CE-QUAL-W2 model takes approximately three hours; hence, the PSO and LM methods require large computational resources and expenditures. Another problem arises during the transition from PSO to LM and vice versa. Each PSO or LM may generate parameter settings which have already been tested by the other algorithm. These limitations were overcome by adding a history of previous runs to both codes. The new code yielded very convincing results, and the calculation time for model calibration has decreased dramatically.

3.6.3 Mixing

Wind significantly affects the mixing regime (Figures 3.4a and 3.4b). Therefore, daily and weekly wind roses were added to the longitudinal contours, extending across the main channel to the Gardiner dam and Qu'Appelle River dam arms, which were drawn for 2011 and 2012 at six-hour intervals. The animations (http://giws.usask.ca/proposals/LakeDiefenbakerTemperatureModel.avi) provide a powerful tool for evaluating the reservoir's behavior in greater detail in both space and time. For example, there are times in summer when heavy winds shift the thermocline by up to 20 meters vertically (chainage 90 and 130 km in Figure 3.8). The energy of such internal waves (waves due to the density gradient within a fluid medium) can entrain low oxygen, high nutrient water from the hypolimnion to the epilimnion (upwelling), as well as change the light environment (Bocaniov et al., 2014). The Rappbode Reservoir in Germany is very similar to Lake Diefenbaker in terms of maximum and mean depth, water level fluctuations, residence time and shape. Bocaniov et al. (2014) found that a high wind velocity of approximately 6 m/s (almost half the intensity shown in the bottom panel of figure 3.8) increased the hypolimnion/epilimnion mixing by 9% in this reservoir. The mixing increases up to 35% as the average wind speed increases to 14 m/s (equal to the intensity showed in the bottom panel of Figure 3.8).

Moreover, upwelling may lead to high algal growth at certain locations. Low flow, high temperature and high nutrient concentrations provide optimum conditions for algal growth (Osgood and Nürnberg, 2002). Low flow and high temperature conditions in summer, if

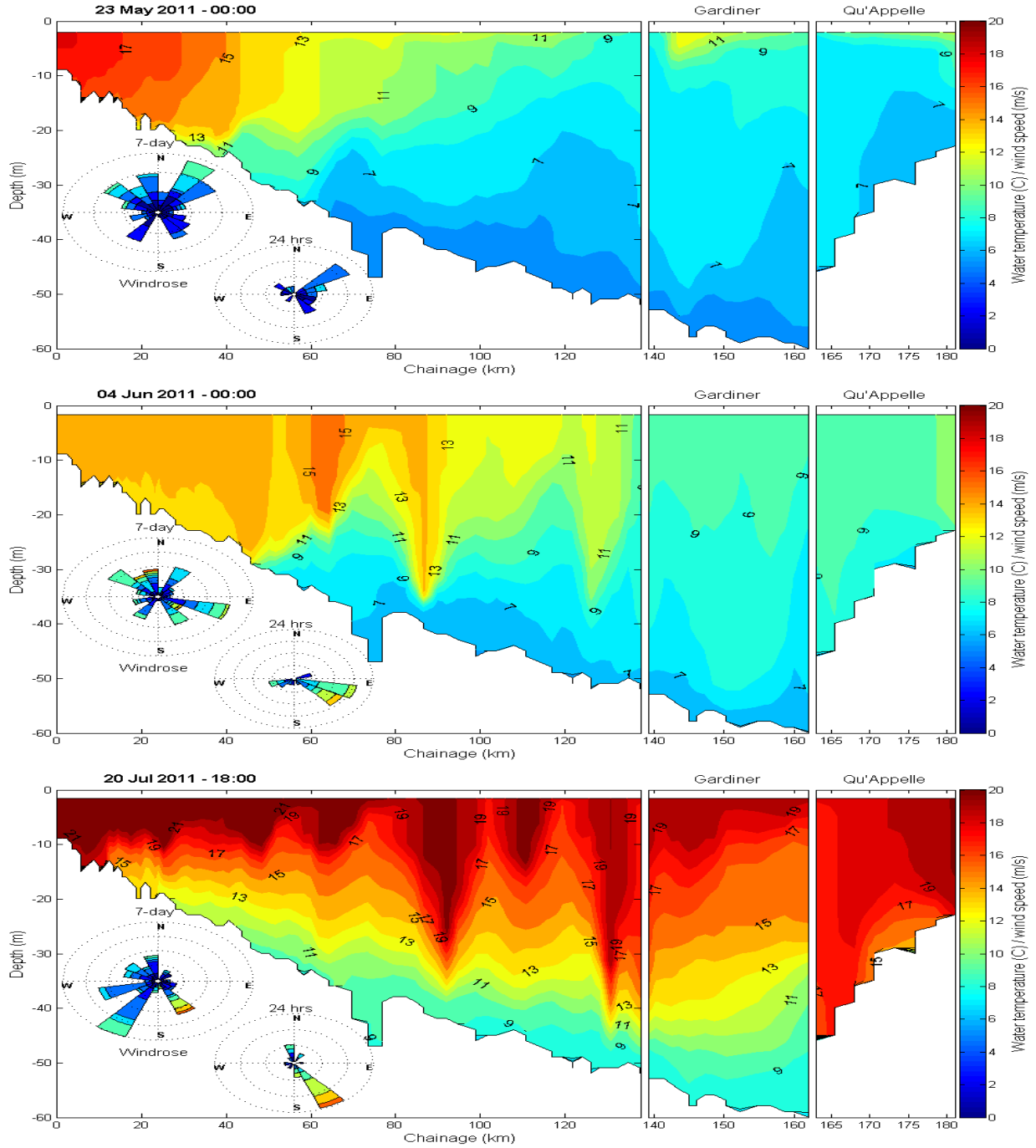

Figure 3.8: Simulated longitudinal contours of water temperature for Lake Diefenbaker in May, June and July 2011. The figure on top shows the heat plume from the SSR inflow water. The windrose has also been included to show the effects of wind on shifting the thermocline (middle and bottom figures). The colorbar shows the values for both the wind speed and water temperature. The complete simulation profiles are available at: http://giws.usask.ca/proposals/LakeDiefenbakerTemperatureModel.avi

accompanied by a prolonged stratification, can lead to hypoxia and subsequent internal loading from sediments. For example, the arm of the Qu'Appelle River Dam has a very low discharge. In contrast to other parts of the lake that have a stronger stratification during summer, this arm stratifies and destratifies several times during the summer and fall (Hudson and Vandergucht, 2015; North et al., 2015). Polymictic behavior can either increase algal growth by increasing internal P loading (North et al., 2015) or inhibit the growth by limiting light and deepening the mixing depth (Dubourg et al., 2015). Hence, this lake arm may be an ideal location to evaluate various management practices, especially in late summer. For example, discharges from the Elbow sewage effluent lagoons should not take place at a time when the water is stratified.

3.6.4 Temperature

Solar radiation is the main source of thermal energy to the reservoir. Due to the relatively high latitude of the reservoir's location, there are significant differences between solar radiation energy and length of day in summer and winter in this region. The minimum day length is less than 8 hours (on December 21^{st}) and the maximum is more than 16 hours (on June 21^{st}). The magnitude and extent of shortwave radiation is very low in winter and increases dramatically from the beginning of May. It reaches a peak of approximately 800 W/m^2 with a clear sky in July. In winter, the short wave radiation values reach above 100 W/m^2 for only a few hours around noon with clear sky conditions.

In 2012, the sum of both short wave and long wave radiation was above 1000 W/m^2 around noon (clear sky) for about four months (May – September 2012) with a maximum value of 1200 W/m^2 in July. This is a considerable amount of energy, with high capacity to increase water temperatures. Long daylight hours and high energy input are conducive to the growth of cyanobacteria in high latitude prairie reservoirs and lakes (Scheffer, 2004). Cloudy conditions can affect the amount of short wave and long wave radiation considerably; however, these data were not available. Data on cloud cover may alter the calculation of the amount of energy that reaches the water surface.

Negative values of net radiation energy on the reservoir surface values indicate that the reservoir loses heat at the surface (cooling). From mid-February, the mid-day energy

balance is positive at the surface and the water becomes warmer (Figure 3.9). Differences between the net radiation energy values calculated by the original code (Eq. 3.5 and Figure 3.9a) and the modified ice code (Eq. 3.8 and 3.9, and Figure 3.9b), are most prevalent for winter and spring. The differences yield to lower negative values (less cooling) in winter and less positive values in spring (less ice melting) (Figure 3.9c).

Snow cover over the ice is not uniform. It has a heterogeneous and patchy structure. Wind makes the snow cover more dissimilar, forming snow dunes on the ice surface. Wind forces can be strong enough to push the ice cover below the phreatic zone, allowing water to flow through cracks in the ice and flood the ice cover, particularly along the shore. This can lead to large scale flooding on the lee shore side of strong wind events. Furthermore, wind forces can form large accumulations of snow on the ice surface. These processes (patchiness, heterogeneous snow, effects of wind and snow dunes, compaction of snow, etc.) have been integrated into the two empirical coefficients added to the ice model, resulting in significant improvement in the calculation of ice thickness and ice cover duration. A more physically-based description of the snow pack on the ice cover may further improve these simulations. However, the focus of this research was to lay a foundation for water quality modeling rather than building an ice model. Hence, the current ice algorithm fulfills the model requirements as a tool for determining the ice thickness for thermal calibration.

Inflow and outflow are also very influential on the lake's overall heat budget, as indicated by both the statistics and plots (Figures 3.7 and 3.8). The total energy added to the reservoir by the inflow is more than the heat lost from the outflow. For example, in 2012 the inflow increased the whole lake water temperature by 15.84 °C and the outflow decreased it by 10.83 °C. The sum of all the surface heat exchanges yielded -4.48 °C. The bed, ice, evaporation and tributary temperature increases or decreases were 0.76, -0.73, -0.66 and 0.08 °C, respectively. The sum of all these components yielded a net heat budget of zero for 2012. The inflowing water temperature to Lake Diefenbaker from the SSR is strongly correlated to the air temperature. Therefore, the predicted changes in global air temperatures would raise the stream water temperatures. The importance of the inflowing water to Lake Diefenbaker's heat budget reveals the potential effects of climate change on the lake's temperature regime and water quality.

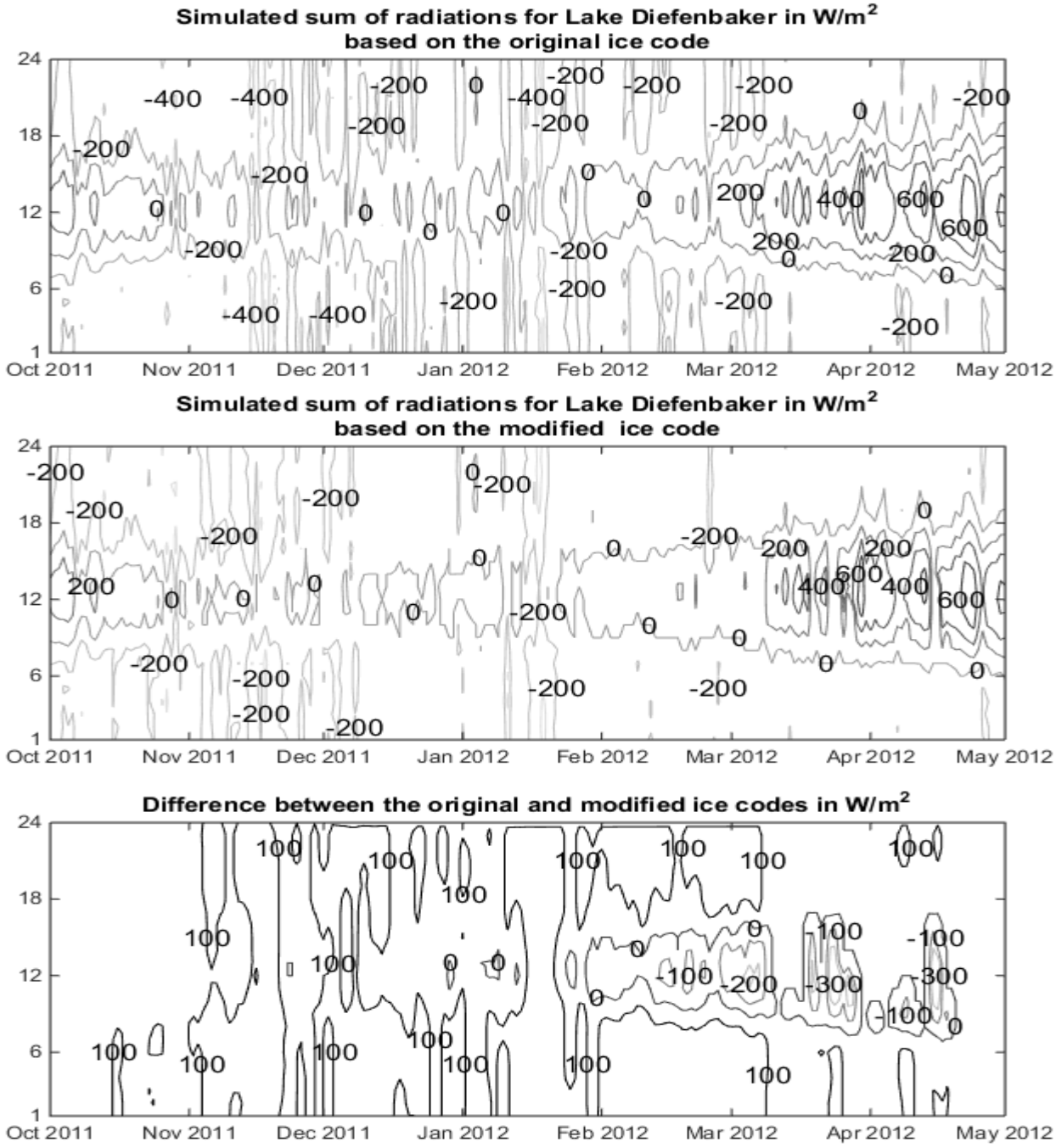

Figure 3.9: Net radiation at Lake Diefenbaker surface in 2012. a: Net radiation at Lake Diefenbaker surface in 2012 based on original code (Eq. 3.5) (no cloud cover). b: Net radiation on Lake Diefenbaker surface in 2012 based on modified ice code code (Eq. 3.8 and 3.9) ((no cloud cover). c: Difference in net radiation on Lake Diefenbaker surface in 2012 between original ice code and modified ice code ($RN_{modified}$ - $RN_{original}$). Positive values show less cooling in winter and negative values show less ice melting in spring compared to the original code

3.6.5 Uncertainties

Lake Diefenbaker is an artificial reservoir constructed by damming the South Saskatchewan River; hence, it has more shoreline indentations than natural lakes. This complexity in the reservoir's bathymetry and geometry, in addition to the fact that the upstream portion of the reservoir has more riverine features (e.g., shallower, higher velocity, more erosion, and sedimentation) makes simulating the reservoir more challenging. The uncertainty in forcing data and parameter values during the simulations helps to explain the source of discrepancies between simulated and measured values.

Since the model variables are highly sensitive to wind, we suggest that instrumentation be installed on the lake surface to capture wind speed and direction more accurately. A data-collecting buoy is to be deployed on Lake Diefenbaker as part of the GIWS's mission to support water resource studies in the Saskatchewan River Basin. In addition to wind measurements, the buoy will also measure air temperature, surface water temperature, heat fluxes and incoming short wave solar radiation.

3.7 Conclusions

A two-dimensional laterally-averaged numerical model was applied to Lake Diefenbaker for the period 2011 – 2012 in order to study the changes in lake thermal structure. The model was able to successfully simulate the basic features of the thermal structure of the lake, including spring isothermal conditions, summer stratification and the overturn in late fall, as well as water temperature in both the epilimnion and hypolimnion. A novel contribution of this work is the application of a lake temperature model to explore the impact of an inflowing tributary on the heat budget of a reservoir. The 2011 – 2012 simulations showed that the higher flows and warmer temperatures of the SSR in late spring and early summer, along with the short residence time of Lake Diefenbaker, caused the stratification to occur earlier in this season. The lower discharge of the inflow in fall does not significantly change the timing of the fall turnover.

The Monte-Carlo sensitivity analysis demonstrated the high sensitivity of the wind sheltering and shading coefficients. The light extinction coefficient and inflow water temperature were rather insensitive to changes within the defined ranges in calibration parameter values. Differences in results from using models with either 126 or 187 segments were minimal; however, the model with coarser grids (126 segments) showed less sensitivity to the WSC and SHADE parameters on model variables. The PSO+LM optimization method was able to find the best parameter settings after 41 iterations (on average), significantly reducing calculation times. Using continuous versus non-continuous simulations for the 2011 – 2012 period did not have any effect on results.

The original ice algorithm yielded extremely poor ice thickness, formation and breakup simulations. The modified ice code calculated these terms with improved accuracy, albeit empirically. A physically-based model that considers snow cover, snow compaction, snow melting, refreezing and other parameters may be more suitable and will be a focus of future work.

The high sensitivity of model results to wind speed measurements and the effect of wind on mixing and occurrences of upwelling have highlighted the need for onsite measurements of wind for accurate calibration. The installation of a data-collecting buoy on the surface of Lake Diefenbaker is highly recommended.

A hydrodynamic model may forecast algal bloom formation without having data on nutrients and oxygen concentrations. The model recognized several areas that were sensitive to strong winds (e.g., chainage 90 and 130 km in Figure 3.8). In these areas, strong winds can bring nutrient-rich sediment to the water column. Secondly, areas with low flow and high temperature were identified, particularly in the Qu'Appelle River arm.

Since the construction of Lake Diefenbaker, many studies have been carried out covering different fields of research, but there has never been a study quantifying the effects of different heat sources to the heat budget. The current temperature model can provide a comprehensive synopsis for researchers and water managers to assist in determining and forecasting changes associated with different management practices in the SSR basin and the reservoir. It could also provide the Saskatchewan Water Security Agency (SWSA), the

main water management agency in Saskatchewan, with valuable information to guide future flow management practices.

3.8 Acknowledgments

This work received financial support from the Canada Excellence Research Chair in Water Security through the Global Institute for Water Security. We thank Environment Canada for providing the meteorological and hydrometric data. The sonde-profile data were provided by the Limnology Laboratory at the University of Saskatchewan. The bathymetry data were surveyed by the Department of Geography and Planning at University of Saskatchewan. The authors thank Paul Jones for providing the boat and truck to carry out the bathymetry surveys and Franny Rawlyk and Bryce Geeraert for assisting with the fieldwork.

References

Abirhire, O., North, R. L., Hunter, K., Vandergucht, D. M., Sereda, J., and Hudson, J. J. (2015). Environmental factors influencing phytoplankton communities in Lake Diefenbaker, Saskatchewan, Canada. *Journal of Great Lakes Research*, 41:118–128.

Agbeti, M. D. and Smol, J. P. (1995). Winter limnology: a comparison of physical, chemical and biological characteristics in two temperate lakes during ice cover. *Hydrobiologia*, 304(3):221–234.

Ashmore, P. and Day, T. (1988). Spatial and temporal patterns of suspended-sediment yield in the Saskatchewan River basin. *Canadian Journal of Earth Sciences*, 25(9):1450–1463.

Babin, J. and Prepas, E. (1985). Modelling winter oxygen depletion rates in ice-covered temperate zone lakes in Canada. *Canadian Journal of Fisheries and Aquatic Sciences*, 42(2):239–249.

Beletsky, D. and Schwab, D. J. (2001). Modeling circulation and thermal structure in lake michigan: Annual cycle and interannual variability. *Journal of Geophysical Research*, 106(C9):19745–19771.

Bengtsson, L. (1996). Mixing in ice-covered lakes. *Hydrobiologia*, 322(1-3):91–97.

Bocaniov, S. A., Ullmann, C., Rinke, K., Lamb, K. G., and Boehrer, B. (2014). Internal waves and mixing in a stratified reservoir: insights from three-dimensional modeling. *Limnologica-Ecology and Management of Inland Waters*, 49:52–67.

Boegman, L., Loewen, M., Hamblin, P., and Culver, D. (2001). Application of a two-dimensional hydrodynamic reservoir model to Lake Erie. *Canadian Journal of Fisheries and Aquatic Sciences*, 58(5):858–869.

Cole, T. M. and Wells, S. A. (2013). *CE-QUAL-W2: A two-dimensional, laterally averaged, hydrodynamic and water quality model*. Department of Civil and Environmental Engineering, Portland State University, Portland, OR, 3.71 edition.

Dubourg, P., North, R. L., Hunter, K., Vandergucht, D. M., Abirhire, O., Silsbe, G. M., Guildford, S. J., and Hudson, J. J. (2015). Light and nutrient co-limitation of phytoplankton communities in a large reservoir: Lake Diefenbaker, Saskatchewan, Canada. *Journal of Great Lakes Research*, 41:129–143.

Environment Canada (2013). Measuring river flows. Available at: http://www.ec.gc.ca/eau-water/default.asp?lang=En&n=45BBB7B8-1.

French, R. H., Cooper, J. J., and Vigg, S. (1982). Secchi disc relationships1. *Water Resources Bulletin*, 18(1):121–123.

Giesy, J. P., Li, P. D. S., and Khim, J. S. (2009). Water quality analysis report. Technical report, Toxicology Centre, University of Saskatchewan.

Gober, P. and Wheater, H. (2014). Socio-hydrology and the science–policy interface: a case study of the Saskatchewan River basin. *Hydrology and Earth System Sciences*, 18(4):1413–1422.

Hondzo, M. and Stefan, H. G. (1993a). Lake water temperature simulation model. *Journal of Hydraulic Engineering*, 119(11):1251–1273.

Hondzo, M. and Stefan, H. G. (1993b). Regional water temperature characteristics of lakes subjected to climate change. *Climatic Change*, 24(3):187–211.

Hosseini, N., Chun, K. P., and Lindenschmidt, K.-E. (2016). Quantifying spatial changes in the structure of water quality constituents in a large prairie river within two frameworks of a water quality model. *Water*, 8(4):158.

Hudson, J. J. and Vandergucht, D. M. (2015). Spatial and temporal patterns in physical properties and dissolved oxygen in Lake Diefenbaker, a large reservoir on the Canadian Prairies. *Journal of Great Lakes Research*, 41:22–33.

Jankowski, T., Livingstone, D. M., Bührer, H., Forster, R., and Niederhauser, P. (2006). Consequences of the 2003 european heat wave for lake temperature profiles, thermal stability, and hypolimnetic oxygen depletion: Implications for a warmer world. *Limnology and Oceanography*, 51(2):815–819.

Ji, Z.-G. (2008). *Hydrodynamics and water quality: modeling rivers, lakes, and estuaries*. John Wiley & Sons.

Khaliq, M., Sushama, L., Monette, A., and Wheater, H. (2015). Seasonal and extreme precipitation characteristics for the watersheds of the Canadian Prairie provinces as simulated by the NARCCAP multi-RCM ensemble. *Climate Dynamics*, 44(1-2):255–277.

Kheyrollah Pour, H., Duguay, C., Martynov, A., and Brown, L. (2012). Simulation of surface temperature and ice cover of large northern lakes with 1-D models: a comparison with MODIS satellite data and in situ measurements. *Tellus A*, 64.

Lindenschmidt, K.-E. (1998). *On the effect of artificial aeration on the phytoplankton populations of the Lake Tegel, Berlin.* PhD thesis, Technical University of Berlin.

Lindenschmidt, K.-E. (2006). The effect of complexity on parameter sensitivity and model uncertainty in river water quality modelling. *Ecological Modelling*, 190(1):72–86.

Lindenschmidt, K.-E. and Hamblin, P. (1997). Hypolimnetic aeration in Lake Tegel, Berlin. *Water Research*, 31(7):1619–1628.

Mearns, L. O., Arritt, R., Biner, S., Bukovsky, M. S., McGinnis, S., Sain, S., Caya, D., Correia Jr, J., Flory, D., Gutowski, W., et al. (2012). The North American regional climate change assessment program: overview of phase I results. *Bulletin of the American Meteorological Society*, 93(9):1337–1362.

Morrill, J. C., Bales, R. C., and Conklin, M. H. (2005). Estimating stream temperature from air temperature: implications for future water quality. *Journal of Environmental Engineering*, 131(1):139–146.

NCEP/NCAR Reanalysis 1 (2013). The NCEP/NCAR 40-Year Reanalysis Project: March, 1996 BAMS.

North, R. L., Johansson, J., Vandergucht, D., Doig, L. E., Liber, K., Lindenschmidt, K.-E., Baulch, H., and Hudson, J. J. (2015). Evidence for internal phosphorus loading in a large prairie reservoir (Lake Diefenbaker, Saskatchewan). *J. Great Lakes Res.*, 41(Supplement 2):91–99.

Osgood, D. and Nürnberg, G. (2002). Lake Mitchell alum treatment system: Final report and recommendations. Available at: http://www.mitchellsd.govoffice3.com/vertical/Sites/%7B738741A8-CB7B-4010-B6EF-9EFB2C81B90D%7D/uploads/osgood_report_2002.pdf.

Patterson, J. and Hamblin, P. (1988). Thermal simulation of a lake with winter ice cover. *Limnology and Oceanography*, 33(3):323–338.

Peeters, F., Livingstone, D. M., Goudsmit, G.-H., Kipfer, R., and Forster, R. (2002). Modeling 50 years of historical temperature profiles in a large central European lake. *Limnology and Oceanography*, 47(1):186–197.

Phillips, I. D., Pollock, M. S., Bowman, M. F., McMaster, D. G., and Chivers, D. P. (2015). Thermal alteration and macroinvertebrate response below a large Northern Great Plains reservoir. *Journal of Great Lakes Research*, 41:155–163.

Pomeroy, J. and Shook, K. (2012). Review of Lake Diefenbaker operations, 2010–2011. Available at: http://www.usask.ca/hydrology/papers/Pomeroy_Shook_2012.pdf.

Sadeghian, A., Hudson, J., Wheater, H., and Lindenschmidt, K. (2014). Water quality modeling of Lake Diefenbaker. *Water news. Can Water Res Assoc*, 33(2):17–20.

Saskatchewan Environment and Public Safety (1988). *Lake Diefenbaker and upper South Saskatchewan River: water quality study 1984 – 85.* Water Quality Branch and Environment Canada, Inland Waters Directorate, Water Quality Branch. Available at: http:/library2.usask.ca/gp/sk/en/scanned/lake.diefenbaker.water.study.1988.pdf.

Scheffer, M. (2004). *Ecology of shallow lakes*. Springer Science & Business Media.

SWRC (1968). Delta formation and sedimentation in Lake Diefenbaker. Annual project report, Saskatchewan Water Resources Commission.

SWRC (1969). Delta formation and sedimentation in Lake Diefenbaker. Annual project report, Saskatchewan Water Resources Commission.

SWRC (1970). Delta formation and sedimentation in Lake Diefenbaker. Annual project report, Saskatchewan Water Resources Commission.

SWRC (1971). Delta formation and sedimentation in Lake Diefenbaker. Annual project report, Saskatchewan Water Resources Commission.

SWRC (1972). Delta formation and sedimentation in Lake Diefenbaker. Annual project report, Saskatchewan Water Resources Commission.

Van Everdingen, R. (1967). *Diefenbaker Lake: Effects of Bank Erosion on Storage Capacity*. Technical bulletin no. 10. Canada. Department of Energy, Mines and Resources. Inland Waters Branch.

Vesselinov, V. V. and Harp, D. R. (2012). Adaptive hybrid optimization strategy for calibration and parameter estimation of physical process models. *Computers & Geosciences*, 49:10–20.

Wagener, T., Wheater, H. S., and Gupta, H. V. (2004). *Rainfall-runoff modelling in gauged and ungauged catchments*. World Scientific.

Wheater, H. and Evans, E. (2009). Land use, water management and future flood risk. *Land Use Policy*, 26:S251–S264.

Wheater, H. and Gober, P. (2013). Water security in the Canadian Prairies: science and management challenges. *Philosophical Transactions of the Royal Society of London A: Mathematical, Physical and Engineering Sciences*, 371(2002):20120409.

Wheater, H. S. (2015). Water security-science and management challenges. *Proceedings of the International Association of Hydrological Sciences*, 366:23.

WSA (2012a). *Area and capacity curves for Lake Diefenbaker*. Number Plan No. J5-1(33). Water Security Agency.

WSA (2012b). *State of Lake Diefenbaker*. Water Security Agency. Available at: https://www.wsask.ca/Global/Lakes%20and%20Rivers/Dams%20and%20Reservoirs/Operating%20Plans/Developing%20an%20Operating%20Plan%20for%20Lake%20Diefenbaker/State%20of%20Lake%20Diefenbaker%20Report%20-%20October%2019%202012.pdf, Accessed: 21 May 2015.

Yuzyk, T. R. (1983). *Lake Diefenbaker, Saskatchewan: a case study of reservoir sedimentation*. Inland Waters Directorate, Environment Canada.

Chapter 4

Sedimentation and erosion in Lake Diefenbaker, Canada: solution for shoreline retreat monitoring

This chapter is a published manuscript in the journal of Environmental Monitoring and Assessment.

Sadeghian, A., de Boer, D., and Lindenschmidt, K. E. (2017). Sedimentation and erosion in Lake Diefenbaker, Canada: solution for shore-line retreat monitoring. *Environmental Monitoring and Assessment*, 189:507. DOI: 10.1007/s10661-017-6217-7

The document has been reformatted from the original version for inclusion in the thesis, and no content has changed from the published version. The permission to use the manuscript in this thesis from the publisher (SPRINGER) is included in Appendix VI.

Contributions of the candidate and co-authors

The candidate's contributions are follows: developing the bathymetry for Lake Diefenbaker and the Upper South Saskatchewan River; utilizing and analyzing the Google Maps Elevation API data; wring the manuscript. Karl-Erich Lindenschmidt was the supervisor and designed the whole study, and helped the candidate through the research process and manuscript writing. Dirk de Boer provided the Lake Diefenbaker survey data for building the bathymetry and by contributing to writing parts of the manuscript.

4.1 Abstract

This study looks into sedimentation and erosion rates in Lake Diefenbaker, a prairie reservoir, in Saskatchewan, Canada, which has been in operation since 1968. First, we looked at the historical data in all different formats over the last 70 years, which includes data from more than 20 years before the formation of the lake. The field observations

indicate high rates of shoreline erosion, especially in the upstream portion as a potential region for shoreline retreat. Because of the great importance of this waterbody to the province, monitoring sedimentation and erosion rates is necessary for maintaining the quality of water especially after severe floods which are more common due to climate change effects. Second, we used Google Maps Elevation API, a new tool from Google that provides elevation data for cross sections drawn between two points, by drawing 24 cross sections in the upstream area extending 250 m from each bank. This feature from Google can be used as an easy and fast monitoring tool, is free of charge, and provides excellent control capabilities for monitoring changes in cross-sectional profiles.

4.2 Introduction

Reservoir sedimentation is a significant problem in many parts of the world. The continual accumulation of sediment in a reservoir decreases the storage capacity, thus reducing the lifespan of the reservoir (e.g., Graf et al., 2010; Juracek, 2015). In addition, the trapping of sediment in a reservoir leads to a reduction in sediment loads downstream, resulting in downstream impacts such as changes in channel pattern (e.g., Juracek, 2015; Nelson et al., 2013), reduced sediment input to the downstream river reaches and deltas (e.g., Meade and Moody, 2010; Walling, 2006; Yu et al., 2013) and enhanced coastal erosion (e.g., Kemp et al., 2014; Syvitski et al., 2005). In a study of reservoir sedimentation in the UK, it was estimated that each year, on average, 203.5 m^3/km^2 of reservoir storage is filled with sediment, which is equivalent to 112.3 t km^{-2} $year^{-1}$ of sediment (Butcher et al., 1992). The estimates of Butcher et al. (1992) were based on data from 69 reservoirs with sediment loads in the range of 3.4 – 397.8 t km^{-2} $year^{-1}$. These sedimentation rates can be much higher in rivers in North America because of their much larger discharges and sediment loads.

On the Canadian prairies, the South Saskatchewan River (SSR) follows the pre-glacial valley emerging from under the ice as the Laurentide Ice Sheet retreated in a north-easterly direction towards, ultimately, Hudson Bay. As the ice retreated, the Paleo-South Saskatchewan River occupied its former valley, but as the ice stagnated and blocked drainage towards the northeast, flow was diverted in an easterly direction along the ice margin, creating a series of spillways more or less parallel to the ice margin (Christiansen,

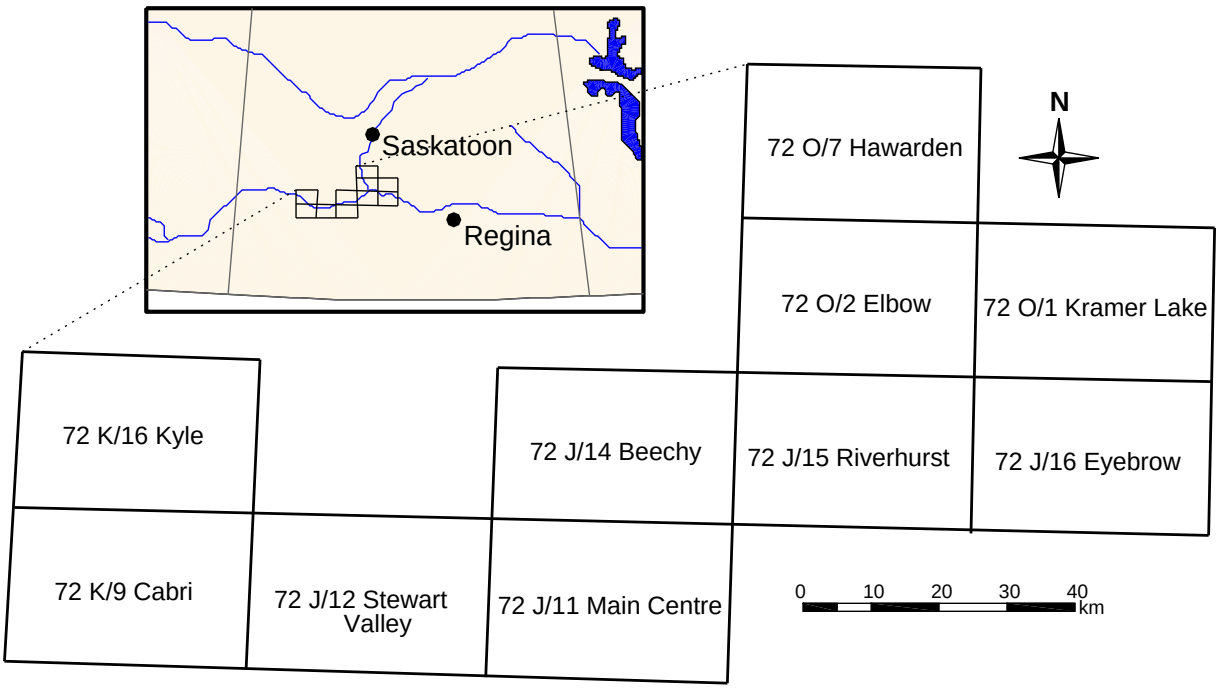

Figure 4.1: Location map of Lake Diefenbaker, and 1:50,000 topographic map sheets based on the National Topographic System (NTS) of Canada

1979; Klassen, 1989).

Lake Diefenbaker is a human-made reservoir formed by damming the SSR south of Saskatoon near the town of Outlook (Figure 4.1). Lake Diefenbaker is a strategic waterbody for water resources management in Saskatchewan, Canada. It has a length of about 140 km from the inlet at Highway 4 until it bifurcates near the village of Elbow into the Gardiner Dam arm and Qu'Appelle Dam arm. Each arm is about 20 km in length, making the total length of the reservoir about 180 km. Construction of the Gardiner Dam and the Qu'Appelle Dam started in 1959 and was completed in 1967. Since 1968, when normal operation of Lake Diefenbaker as a reservoir began (Smith and Wigham, 1989), water levels in the lake have been managed for a combination of flood control, power generation, water supply, irrigation, recreation and ecological considerations, such as providing nesting habitat along the shoreline for the piping plover (WSA, 2012). About 98% of the inflow to the lake comes from the South Saskatchewan River which has an average annual flow ranging from 145 m^3/s to 507 m^3/s in dry and wet years (WSA, 2012) and a maximum recorded daily

inflow of 5,200 m^3/s which occurred in the summer of 2013 (Sadeghian et al., 2017).

The surficial deposits and bedrock of the region consist mostly of till (20 – 100 m) deposited on top of the shales, sandstones, and mudstones of the Bearpaw (up to 241 m) and Judith River formations (up to 66 m) (Schmid et al., 2003). In Lake Diefenbaker, erosion rates along the river banks are high because of the presence of these weak and highly erodible materials. A study in mid 1960s, after the constructions of the dams, showed that the reservoir widened up to 100 m on each side in some areas (Van Everdingen, 1967). Later on, Yuzyk (1983) provided an overview of earlier work related to sedimentation and erosion at the sediment ranges established in the 1960s, which were the foundation for the monitoring program in the early years of Lake Diefenbaker as the lake filled up and the geomorphic setting shifted from a fluvial to a combination of a fluvial and lacustrine environment. The data from the sediment ranges are available in a series of reports (SWRC, 1968, 1969, 1970, 1971, 1972). Smith and Wigham (1989) provide an overview of earlier work on erosion and sedimentation upstream of and in Lake Diefenbaker. Also, a series of studies took place in the 1980s by Ashmore and Day (1988), about 20 years after the construction of the dams. Their studies showed that the rates and patterns of deposition of sediments from the South Saskatchewan River in the upstream portion of the lake, resuspension of river bed materials, and bluff erosion are significantly changed in Lake Diefenbaker.

In Lake Diefenbaker, field observations indicate high rates of shoreline retreat. Steep, actively retreating cliffs are ubiquitous along the lake shoreline, and there are many instances of, for instance, fences that have collapsed as the shoreline retreats. This pattern of active shoreline retreat is consistent with reports from the early years of the lake describing the need for the range line markers to be moved landward as shoreline erosion caused a number of markers to fall into the lake. In a number of instances, shoreline retreat has resulted in the formation of columnar islands isolated from the shoreline, analogous to sea stacks found in a marine setting. As erosion progresses, these columns ultimately disappear, and there are several instances where it appears that shallows in the lake are all that is left of the pre-lake topography with much higher elevations.

Pomeroy and Shook (2012) found that changes in the rating curves due to bank erosion and deposition on the bed represent a major obstacle for using rating curves to estimate

discharge values in Lake Diefenbaker, especially during extremes. Moreover, WSA (2012) recently provided an overview of the characteristics and the factors determining the current operation of Lake Diefenbaker and identified the lack of data in several categories as a drawback for providing a robust report on the status of the reservoir. Availability of data on the bathymetry and sedimentation rates was repeatedly listed as an information gap in the report (WSA, 2012). The objectives of this study are first, to evaluate rates of erosion and sedimentation in Lake Diefenbaker by comparing the present-day lake bed topography with information collected earlier for the purpose of finding potential areas of shoreline retreat, and second, to extract the elevation data from the Google Maps Elevation API service for these regions in cross sections to establish a baseline for future monitoring and comparison.

The Google Maps Elevation API is a new service from Google that provides elevation data for a location or a cross section (path) in a web browser, which can be a replacement for low-resolution surveying (Google, 2017). The elevation data can be the value at a single location, or an averaged, interpolated value based on four points within a few meters of the location (Google, 2017). The Google Maps Elevation API has been used successfully for optimizing navigation software (Rahaman et al., 2017; Santos et al., 2016), and determining watershed characteristics (Palaka and Sankar, 2014) and environmental studies (Gallus et al., 2017). Although satellite imagery is widely used for monitoring environmental change, we could not find any study that used the Google Maps Elevation API for time-varying conditions such as shoreline retreat. Unlike many Google Maps products, the Google Maps Elevation API only returns the most recent elevation data, and historical records are not accessible yet. Hence, the downloaded data should be treated similar to field observations and kept by the user for future comparisons.

4.3 Methods

The study of sedimentation and erosion rates occurred in four different periods over the last 70 years. There are topographic maps derived from air photos from the 1940s prior to construction of the Gardiner and Qu'Appelle dams (1959 – 1967). After the construction of the dams and filling up of Lake Diefenbaker, the studies started as early as 1968 and continued until 1972. The next studies were in 1985 by the Saskatchewan Watershed

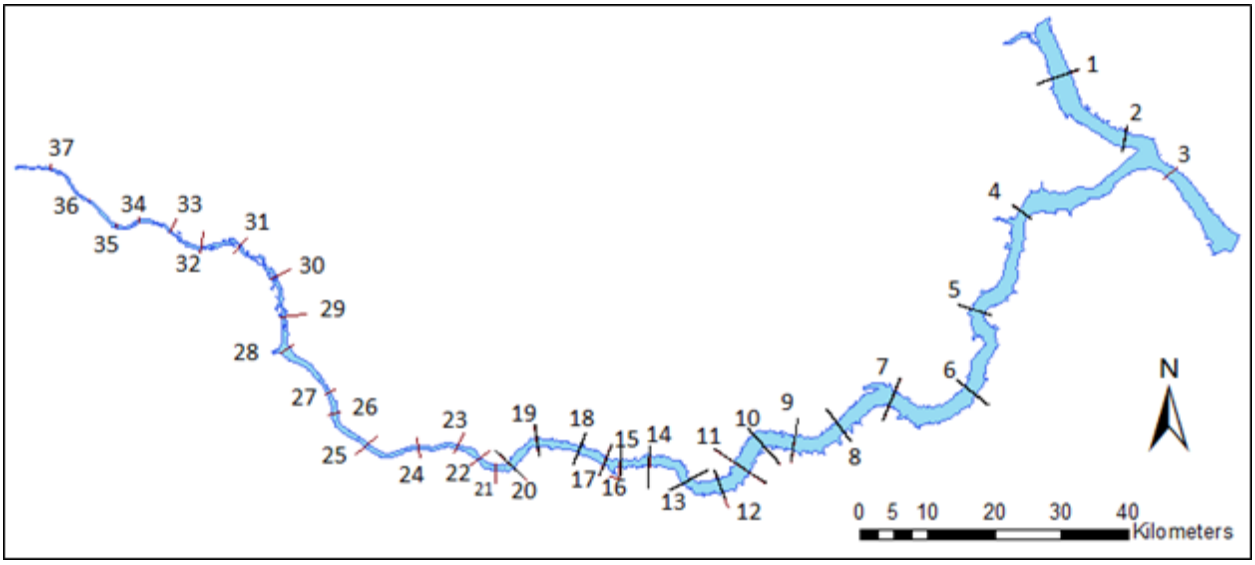

Figure 4.2: 1968–1972 cross section ranges locations for Lake Diefenbaker. The cross sections (ranges) 1–20 were on Lake Diefenbaker and cross sections 21–37 were on the South Saskatchewan River upstream of reservoir

Authority, now Water Security Agency, and the most recent study is by the Global Institute for Water Security at the University of Saskatchewan in 2012 – 2013. The data for these periods are in different formats (aerial maps, printed cross-sectional profiles and digital elevation maps) for different parts of the lake but span the entire lake.

The pre-lake topography for the present study was derived from the 1:50,000 National Topographic System (NTS) maps which were produced by the Canada Surveys and Mapping Branch, Department of Mines and Technical Surveys (1959) based on aerial photos taken in 1944. Individual map sheets were scanned and subsequently georeferenced in ArcGIS. Cross-sectional elevations were derived with a vertical resolution equal to the map's contour interval of 25 ft (7.62 m). The distance between contour lines ranged from 11 to 1300 m.

Preparations for sedimentation studies were carried out before filling of the reservoir by selecting cross sections referred to as "ranges" at 37 locations (20 on Lake Diefenbaker and 17 on the South Saskatchewan River upstream of the reservoir) (Figure 4.2). Following the operation of the reservoir, surveying started at these ranges and continued for 5 years (1968 – 1972). The data were published in a series of reports (SWRC, 1968, 1969, 1970, 1971, 1972). A complete description of site locations, benchmark placements, land surveying, and

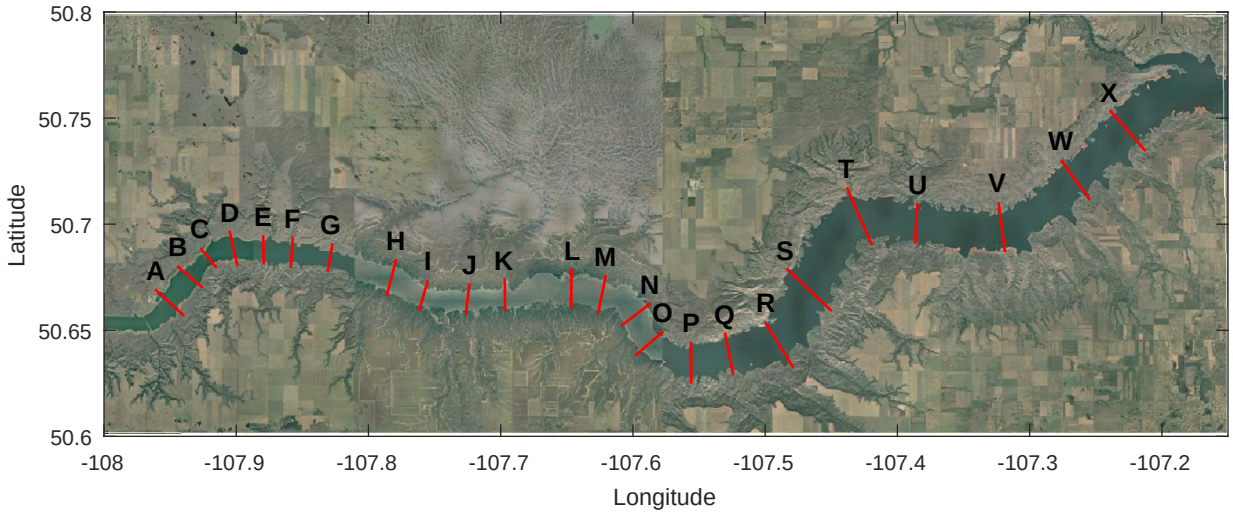

Figure 4.3: Cross section ranges locations used for Google Maps Elevation API for Lake Diefenbaker's upstream. These cross sections are located between ranges 20 and 8 in Figure 4.2. The base map is taken from Google Satellite

underwater echo sound measurements is available in Yuzyk (1983).

The 1985 bathymetry was obtained as ArcGIS shapefiles from the Water Security Agency. No information is available on the methods of data collection. The 1985 bathymetry map was published as a booklet (SPMC, 1986), which was scanned and georeferenced by the Saskatchewan Ministry of Environment (SaskGeomatics Division) in 2005. In 2013, personnel from the Geomatics Division of the Water Security Agency matched up the various map sheets of the GIS vector files to produce a single 1985 bathymetry map. Due to the lack of information on data acquisition and uncertain accuracy of the 1985 bathymetry, no attempt was made to extract cross sections for comparison with data from other years.

In 2012—2013, a new survey of the entire Lake Diefenbaker's bathymetry was conducted by the Global Institute for Water Security at the University of Saskatchewan. Surveying was done by using a BioSonics DT-X echo sounder coupled with a GPS to record the coordinates. After processing the data with the Visual Bottom Typer (VBT) 1.12 software, a bathymetric map was produced using ArcGIS. To extract the cross sections at the ranges used in the previous studies, two approaches were used: using the echo sounder data directly without smoothing, and cross sections drawn from the interpolated bathymetry map in ArcGIS.

Table 4.1: Coordinates for new cross sections locations at Lake Diefenbaker's upstream reach

	Left bank		Right bank	
Cross section	Longitude (West)	Latitude (North)	Longitude (West)	Latitude (North)
A	107° 57' 40.9¨	50° 40' 09.0¨	107° 56' 21.6¨	50° 39' 24.5¨
B	107° 56' 40.9¨	50° 40' 49.0¨	107° 55' 31.0¨	50° 40' 12.1¨
C	107° 55' 37.4¨	50° 41' 19.0¨	107° 54' 52.7¨	50° 40' 45.3¨
D	107° 54' 18.6¨	50° 41' 48.9¨	107° 53' 56.8¨	50° 40' 49.7¨
E	107° 52' 46.7¨	50° 41' 41.3¨	107° 52' 45.2¨	50° 40' 51.5¨
F	107° 51' 25.6¨	50° 41' 38.3¨	107° 51' 31.7¨	50° 40' 45.9¨
G	107° 49' 37.8¨	50° 41' 27.5¨	107° 49' 50.9¨	50° 40' 38.8¨
H	107° 46' 44.6¨	50° 41' 00.5¨	107° 47' 10.1¨	50° 39' 58.1¨
I	107° 45' 18.3¨	50° 40' 24.9¨	107° 45' 42.1¨	50° 39' 33.1¨
J	107° 43' 25.2¨	50° 40' 19.4¨	107° 43' 34.9¨	50° 39' 25.3¨
K	107° 41' 48.8¨	50° 40' 27.9¨	107° 41' 48.3¨	50° 39' 32.0¨
L	107° 38' 47.2¨	50° 40' 44.5¨	107° 38' 48.1¨	50° 39' 37.6¨
M	107° 37' 13.3¨	50° 40' 33.9¨	107° 37' 35.8¨	50° 39' 26.4¨
N	107° 35' 11.0¨	50° 39' 46.0¨	107° 36' 31.3¨	50° 39' 07.9¨
O	107° 34' 36.7¨	50° 38' 58.1¨	107° 35' 52.9¨	50° 38' 17.4¨
P	107° 33' 21.8¨	50° 38' 39.9¨	107° 33' 21.1¨	50° 37' 29.2¨
Q	107° 31' 49.4¨	50° 38' 55.8¨	107° 31' 27.2¨	50° 37' 44.0¨
R	107° 29' 60.0¨	50° 39' 13.5¨	107° 28' 43.2¨	50° 37' 56.1¨
S	107° 29' 02.3¨	50° 40' 44.8¨	107° 26' 58.9¨	50° 39' 32.6¨
T	107° 26' 17.7¨	50° 43' 02.4¨	107° 25' 08.9¨	50° 41' 24.1¨
U	107° 23' 05.4¨	50° 42' 35.8¨	107° 23' 11.9¨	50° 41' 27.0¨
V	107° 19' 24.7¨	50° 42' 37.1¨	107° 19' 07.0¨	50° 41' 12.5¨
W	107° 16' 34.6¨	50° 43' 48.5¨	107° 15' 16.0¨	50° 42' 41.6¨
X	107° 14' 21.4¨	50° 45' 13.2¨	107° 12' 44.1¨	50° 44' 03.9¨

A complete description of data collection and processing procedures is available in Chapter 3.

Elevation data from the Google Maps Elevation API can be downloaded from a web browser by sending a request to the servers through a URL string in the following form:

```
https://maps.googleapis.com/maps/api/elevation/json?parameters
```

The parameter at the end of the URL can be a single or multiple location(s) or a path (cross section) between a series of points in latitude/longitude coordinates. For cross sections, the command returns the elevations and coordinates for the number of points that is requested (up to 500 locations) between the two points. For example, the parameter can take either locations=50.6692,-107.9613 for a single point or path=50.6692,-107.9613—50.6568,-107.9393&samples=500 for a cross section at Lake

Diefenbaker's upstream section and returns the following results (text cleaned).

```
https://maps.googleapis.com/maps/api/elevation/json?locations=50.6692,-107.9613
results :
elevation :  571.6398315429688,
lat :  50.6692,
lng :  -107.9613
resolution :  38.17580795288086
```

The resolution value shows the maximum distance between the source point and the four surrounding points used for interpolation. Further information is available at the Google Maps Elevation API developer's guide website at https://developers.google.com/maps/documentation/elevation/intro.

Based on the information obtained from the historical sedimentation studies, we selected a transect extending 60 km from the upstream portion of Lake Diefenbaker at Highway 4 (at range 20) downstream to range 8 to download the elevation data from Google Maps Elevation API. We chose 24 cross sections for this purpose (Figure 4.3), and requested the elevation data. We used MATLAB to create and post the URLs and to read the responses from its internal web browser. The river banks are considered to be located at the points where the elevation equal to 556.8 m (full supply level). The cross sections were extended 250 m from each bank. The coordinates of the left and right bank benchmarks are available in Table 4.1.

4.4 Results and Discussion

Figures 4.4 and 4.5 show a series of cross sections from upstream at range 24 to downstream at range 15. Cross sections derived from the 1:50,000 topographic maps pre-dating Lake Diefenbaker allow a general comparison of cross-sectional changes, but they do not have sufficient resolution for a detailed comparison. For these maps, contour lines are derived from air photos obtained from the late 1930s to the late 1950s, but uncertainty about the accuracy of the location of each individual contour line and the relatively large contour

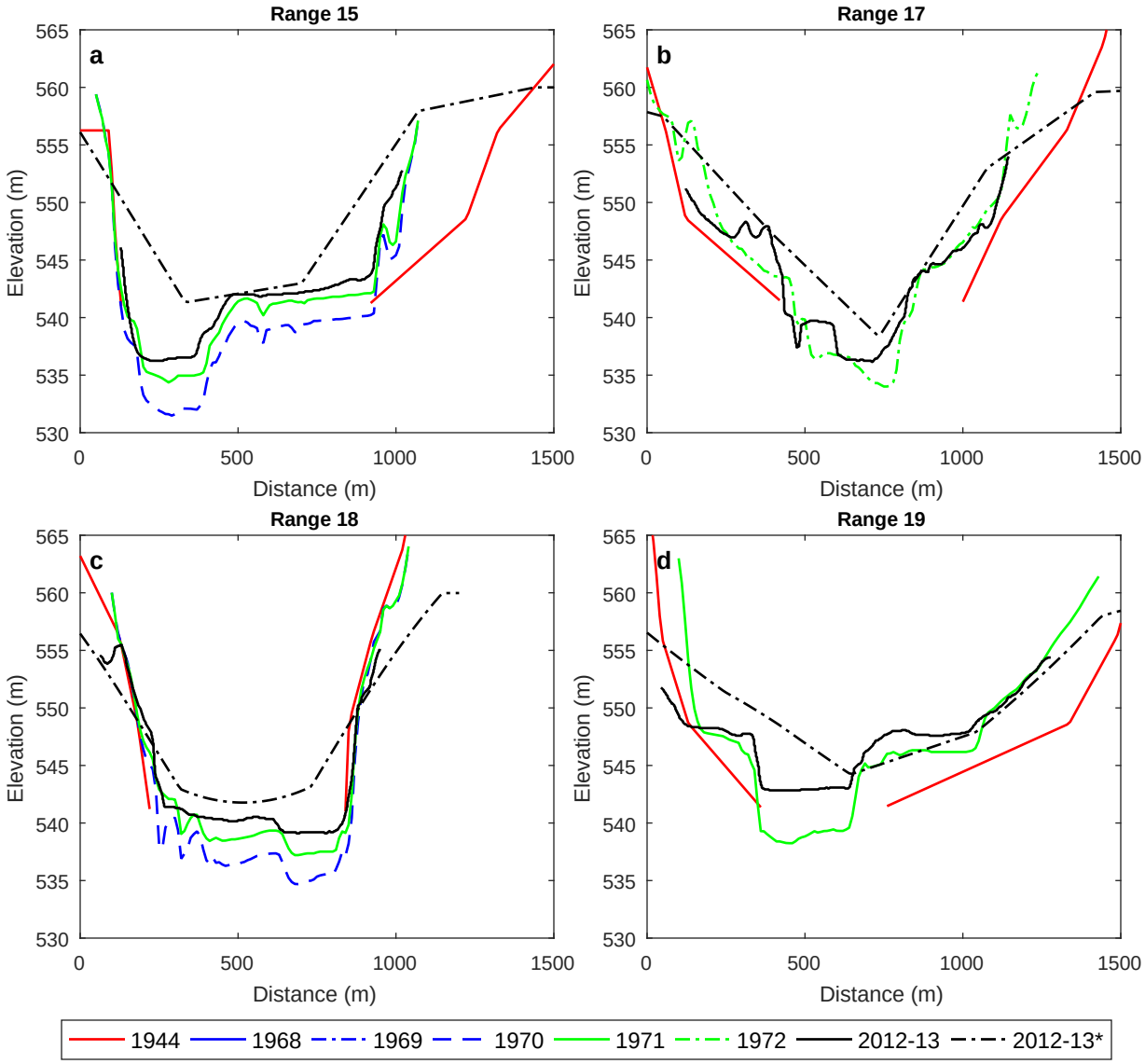

Figure 4.4: Ranges 15, 17, 18 and 19 cross sections for 1944, 1968–1972 and 2012–2013. See Figure 4.2 for locations. (2012–13* are interpolated cross sections). The cross sections (ranges) 1–20 were on Lake Diefenbaker and cross sections 21–37 were on the South Saskatchewan River upstream of reservoir

interval of 25 ft precludes a detailed comparison with other available data (Figures 4.4a to 4.5e). However, they are consistent with the cross sections derived from the subsequent studies in 1968 – 1972 and 2012 – 2013, providing a general measure of shoreline retreat and change in a cross sectional shape.

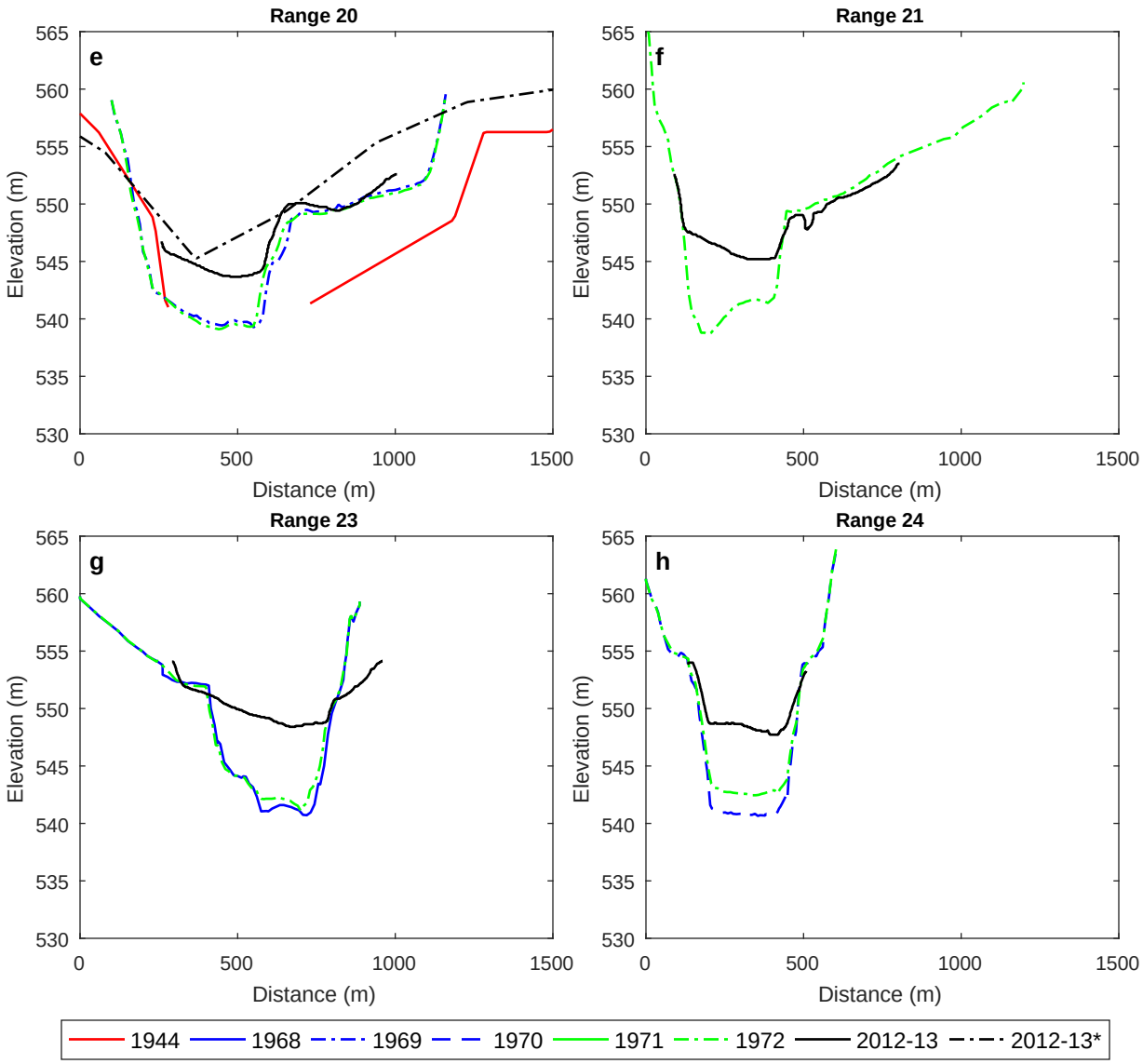

Figure 4.5: Ranges 20, 21, 23 and 24 cross sections for 1944, 1968–1972 and 2012–2013. See Figure 4.2 for locations. (2012–13* are interpolated cross sections)

The 2012 – 2013 cross sections derived from the interpolated bathymetry are generally smooth with little detail, preventing a direct comparison with the cross sections from 1969 to1972 (Figures 4.4a to 4.5e). The 2012 – 2013 cross sections derived directly from the echo sounder data, however, do enable comparison with the 1969 – 1972 data. At the upstream sediment ranges, deposition rates are high. At range 24, on average 7.5 m of sediment was deposited in the deepest, central portion of the channel between 1970 and 2012 – 2013 (Figure 4.5h), resulting in an annual mean deposition rate of 0.18 m year^{-1}. At range 23,

on average 6.8 m of sediment was deposited between 1968 – 1972 and 2012 – 2013 (Figure 4.5g), which amounts to a slightly lower annual mean deposition rate of 0.16 m year^{-1}. At range 21, total deposition in the deepest part of the channel is variable, ranging from 8.5 m on the left side of the channel, to 3.8 m on the right side of the channel, with an average value of 6.2 m (Figure 4.5f). This results in an average deposition rate of 0.16 m year^{-1}. At range 20, total deposition in the deepest part of the channel is 4 m (Figure 4.5e), resulting in an average deposition rate of 0.10 m year^{-1}. At range 19, total deposition is comparable at 4.1 m in the deepest part of the channel (Figure 4.4d), resulting in an average deposition rate of 0.10 m year^{-1}. In contrast to range 20, which shows little deposition on the former floodplain, deposition at range 19 on the former floodplain amounts to an average of 1.75 m (Figure 4.4d), resulting in an average deposition rate of 0.04 m year^{-1}. At range 18, total deposition is much lower than at the ranges further upstream. Total deposition ranges from 1.6 to 2.5 m, with an average of 2.1 m (Figure 4.4c), giving an average deposition rate of 0.05 m year^{-1}. At range 17, deposition rates are variable throughout the cross section (Figure 4.4b). A comparison of the 2012 – 2013 and 1972 cross sections suggests low deposition rates, but the non-uniform pattern of deposition suggests that one of the cross sections, or both, may not be an accurate representation of the bathymetry at the site. The pattern of low deposition rates continues further downstream. At range 15, total deposition ranges from 1.4 m in the deepest part of the channel, resulting in an average deposition rate of 0.03 m year^{-1} to 1.0 m on the former floodplain, resulting in a deposition rate of 0.02 m year^{-1} for the former floodplain and a similar value for the entire cross section (Figure 4.4a). Ranges downstream of range 15 show similarly low to negligible sediment deposition rates.

Overall, the spatial pattern of deposition rates from 1969 – 1972 to 2012 – 2013 is similar to that observed by Yuzyk (1983), who distinguished three reaches. The upstream reach extends from range 38 to range 32. At range 32, the bed elevation is approximately equal to full supply level (556.87 m). In the upstream reach of the inflowing South Saskatchewan River, the lake is more characteristic of a river but is affected by backwater conditions when the lake level is high enough (Yuzyk, 1983). The drawdown reach is located between ranges 32 and 26 and is the section where conditions change from river to reservoir, depending on the water level. Studies of similar reservoirs have indicated that the majority of sediment deposition occurs in this reach (cited in Yuzyk, 1983). Bed elevations in the drawdown reach

Table 4.2: Precision control of Google Maps API data with the Natural Resources Canada control points

No.	Site name	Longitude (West)	Latitude (North)	Elevation (meters)	Google Maps API Elevation (meters)	Difference (meters)
1	94v050	109° 28' 05.9¨	49° 59' 23.1¨	788.53	783.60	4.93
2	94v051	107° 46' 09.3¨	50° 14' 57.9¨	816.54	816.99	0.46
3	94v052	106° 01' 35.6¨	49° 37' 58.2¨	758.63	754.00	4.63
4	94V054	109° 09' 48.5¨	51° 30' 14.3¨	696.47	691.00	5.47
5	94V055	106° 36' 43.4¨	51° 13' 38.2¨	613.85	617.00	3.15
6	94V056	104° 30' 35.0¨	51° 44' 59.2¨	525.07	521.94	3.13
7	94V058	108° 13' 47.4¨	52° 44' 28.2¨	526.54	527.31	0.77
8	88V054	106° 28' 47.1¨	52° 02' 42.9¨	509.38	507.96	1.42
9	90V107	104° 12' 20.3¨	50° 18' 33.9¨	606.46	604.00	2.46
10	90V111	104° 15' 53.0¨	49° 47' 57.8¨	580.34	579.00	1.34

are generally between full supply level (556.87 m) and minimum operating water level (545.59 m), and sediment deposition therefore affects the live storage capacity of the reservoir. The reservoir reach extends from range 26 downstream to range 1 and is the reach where reservoir conditions occur. Bed elevations are below the minimum operating water level, and sediment deposition therefore affects dead storage capacity. Yuzyk (1983) concludes that the drawdown reach has undergone continuous aggradation from 1969 to 1980, with maximum deposition of 1.9 m at range 27, resulting in a deposition rate of 0.17 m year^{-1}, a value similar to those found in the present study further downstream at ranges 24, 23 and 21.

Highway 4 is considered as the upstream end of Lake Diefenbaker in most studies (e.g., Hudson and Vandergucht, 2015; North et al., 2015; Sadeghian et al., 2015) and is also used as the starting point for shoreline retreat monitoring here. Based on the results presented above, the sedimentation and erosion rates become negligible downstream of range 15. However, the shoreline retreat can still occur further downstream. Hence, the monitoring region is from highway 4 (range 20) down to range 8 which is about 60 km in length. To avoid confusion with the ranges from 1968 to 1972, we used the letters of the alphabet for these cross sections, where the first cross section (A) starts from highway 4 and the 24^{th} (X) ends at range 8 (Figure 4.3).

Natural Resources Canada has ten control points in southeastern Saskatchewan as references for location and elevation (Figure 4.6 and Table 4.2) which we have used for controlling the

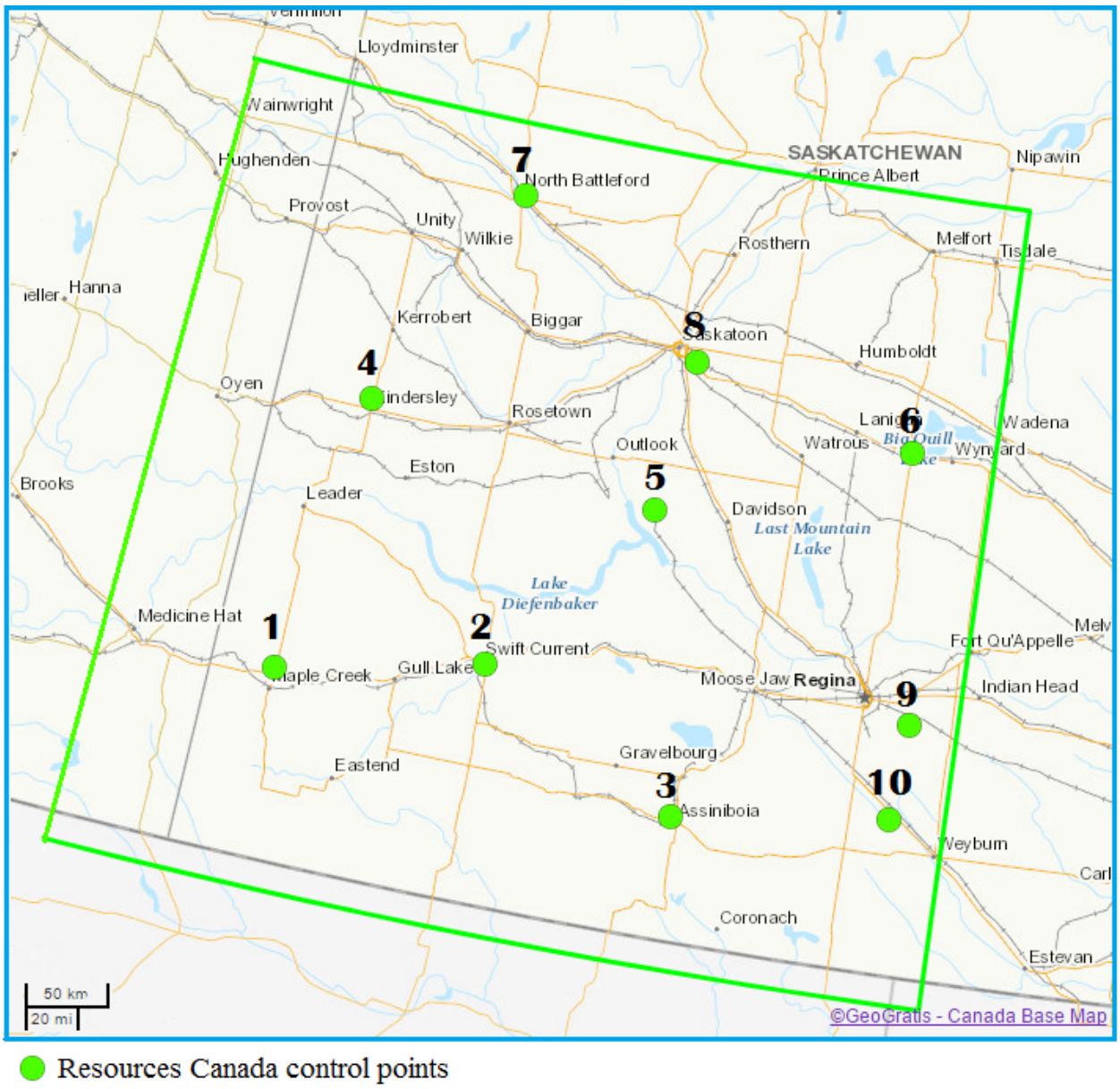

Figure 4.6: Maps of Natural Resources Canada control points used for precision control and comparison with Google Maps Elevation API data. Map obtained from GeoGratis Web Services, Natural Resources Canada

precision of elevation data obtained from the Google Maps Elevation API. The difference in elevation between the two data sources ranged from 0.46 to 5.47 m, with an average difference of 2.78 m. Such a discrepancy is not acceptable in many fine-scale studies, but for a long-term monitoring program the data still can be valuable. Since the construction of the dams, the changes in bottom elevation of the reservoir were up to 15 m in some of the cross

sections shown in Figure 5; hence, an average error of 2.78 m still can detect the changes by erosion and deposition. The Google Maps Elevation API had a spacial resolution of 38.18 m for this region, as the longest distance between the data points. Because several data point are used for interpolations, the estimates of the query points located between these data points are less susceptible to noise in the data compared with a linear function between only two data points. However, the accuracy may still not be comparable with conventional surveying methods.

The cross sections derived from Google Maps Elevation API are shown in Figure 4.7. Every single graph has three parts—the right and left banks which are 250 m each and the portion in the middle which shows the width of the river. In cases where the water level was lower than 556.87 m (full supply), elevation data on river bed (bathymetry) were available, and the cross sections were extended towards the river with the same scale. It is worth noting that the left and the right banks are not connected to each other in these graphs, and each side should be viewed separately.

Cross sections A, B and C are located on a straight segment directed towards the northeast. In cross section A, both sides are almost at the same height and the river has a width of 1,588 m. In the next cross section, the river is 288 m narrower, and the slope almost doubled at the right. Cross section C has a similar shape to the previous one but becomes even narrower to 878 m. In cross section D, the river curves and cross sections D to I are on a bend towards the south with slight changes in their directions. In cross sections D and F, the pattern of bank elevations reverse and the left bank's slopes become steeper. Cross sections E and G are almost equal in all the aspects.

In cross section H, the left bank rises to 600 m and then drops to 590 m in I and J. The river directions becomes straight towards the east in cross sections J, K and L. The elevation in the left bank quickly drops to above 560 m in K and rises again in L. From the M until T, the river has a steep U-shaped bend where the river width also becomes wider. In M and N, the right bank escalates to about 590 m, and in O both left and right banks are in their near maxima. In cross section R, the reservoir width is 2,342 m and the left bank has a very flat slope. The pattern reverses in the next cross section with a flat slope at the right. The reservoir has a maximum width of 2,822 m at T because of the widening at the bends.

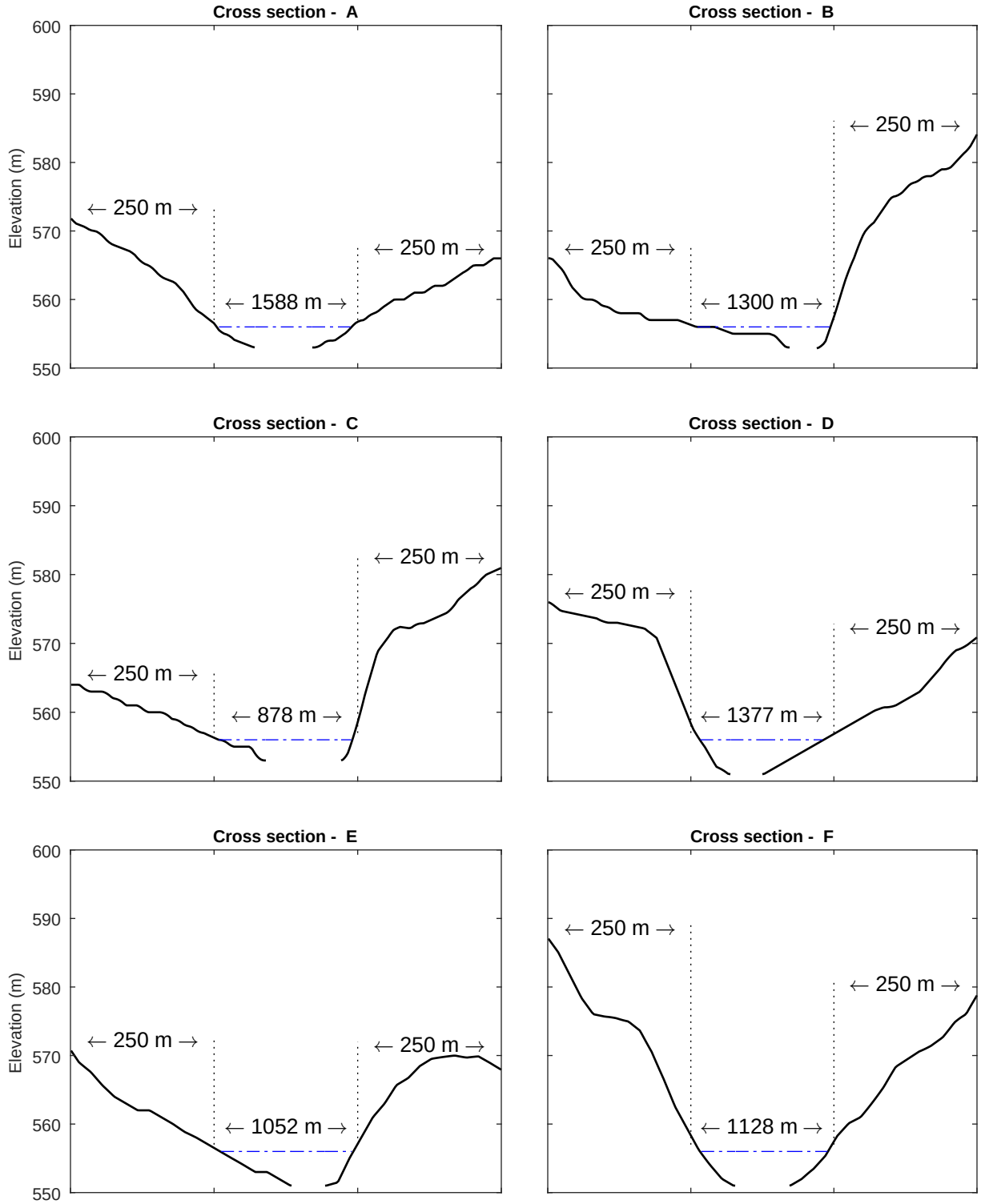
Cross section - A
Elevation (m)
600
590
580
570
560
550
← 250 m →
← 1588 m →
← 250 m →
Cross section - B
← 250 m →
← 1300 m →
← 250 m →
Cross section - C
← 250 m →
← 878 m →
← 250 m →
Cross section - D
← 250 m →
← 1377 m →
← 250 m →
Cross section - E
← 250 m →
← 1052 m →
← 250 m →
Cross section - F
← 250 m →
← 1128 m →
← 250 m →

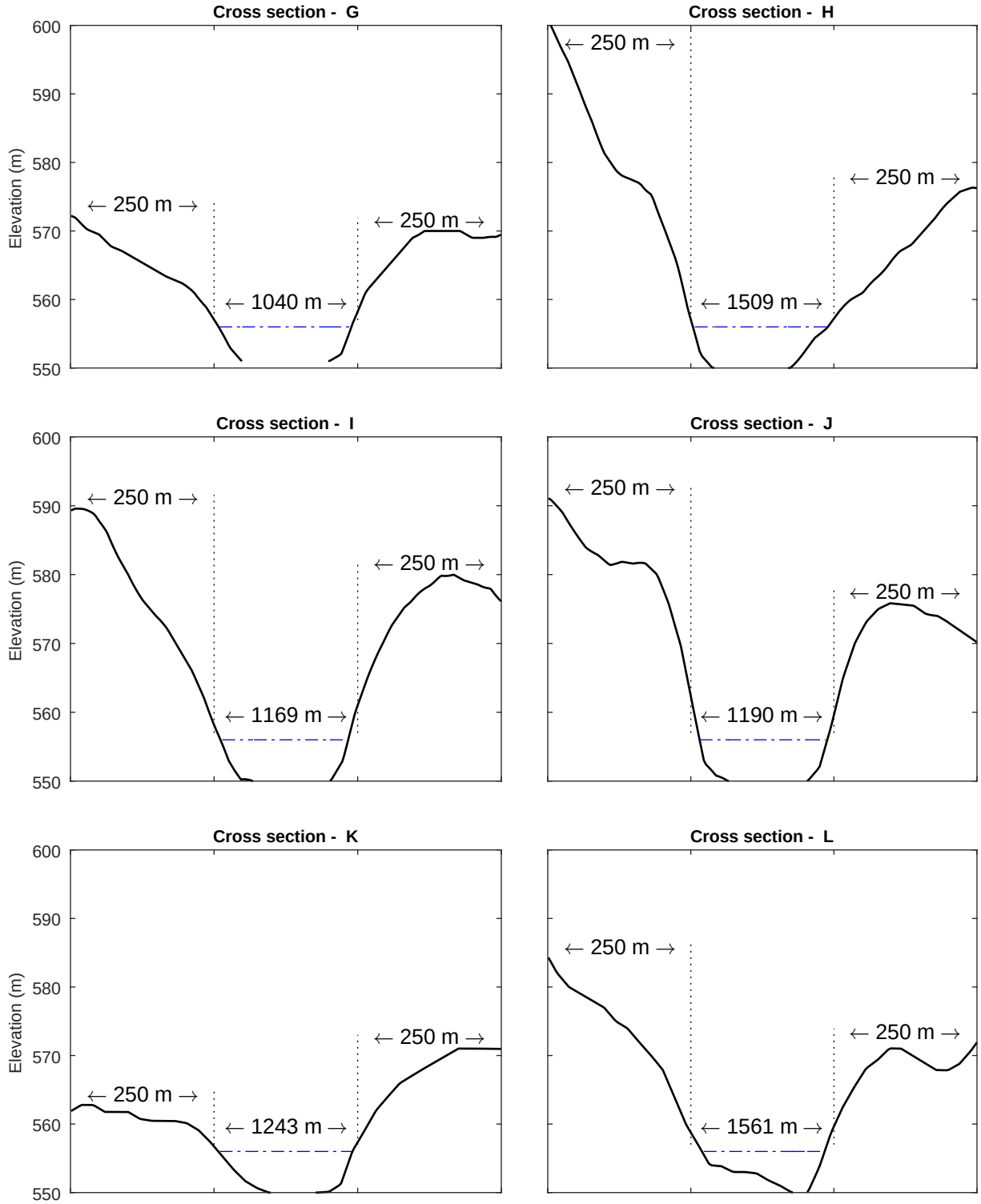
Cross section - G
Elevation (m)
600
590
580
570
560
550
← 250 m →
← 1040 m →
← 250 m →
Cross section - H
← 250 m →
← 1509 m →
← 250 m →
Cross section - I
Elevation (m)
← 250 m →
← 1169 m →
← 250 m →
Cross section - J
← 250 m →
← 1190 m →
← 250 m →
Cross section - K
Elevation (m)
← 250 m →
← 1243 m →
← 250 m →
Cross section - L
← 250 m →
← 1561 m →
← 250 m →

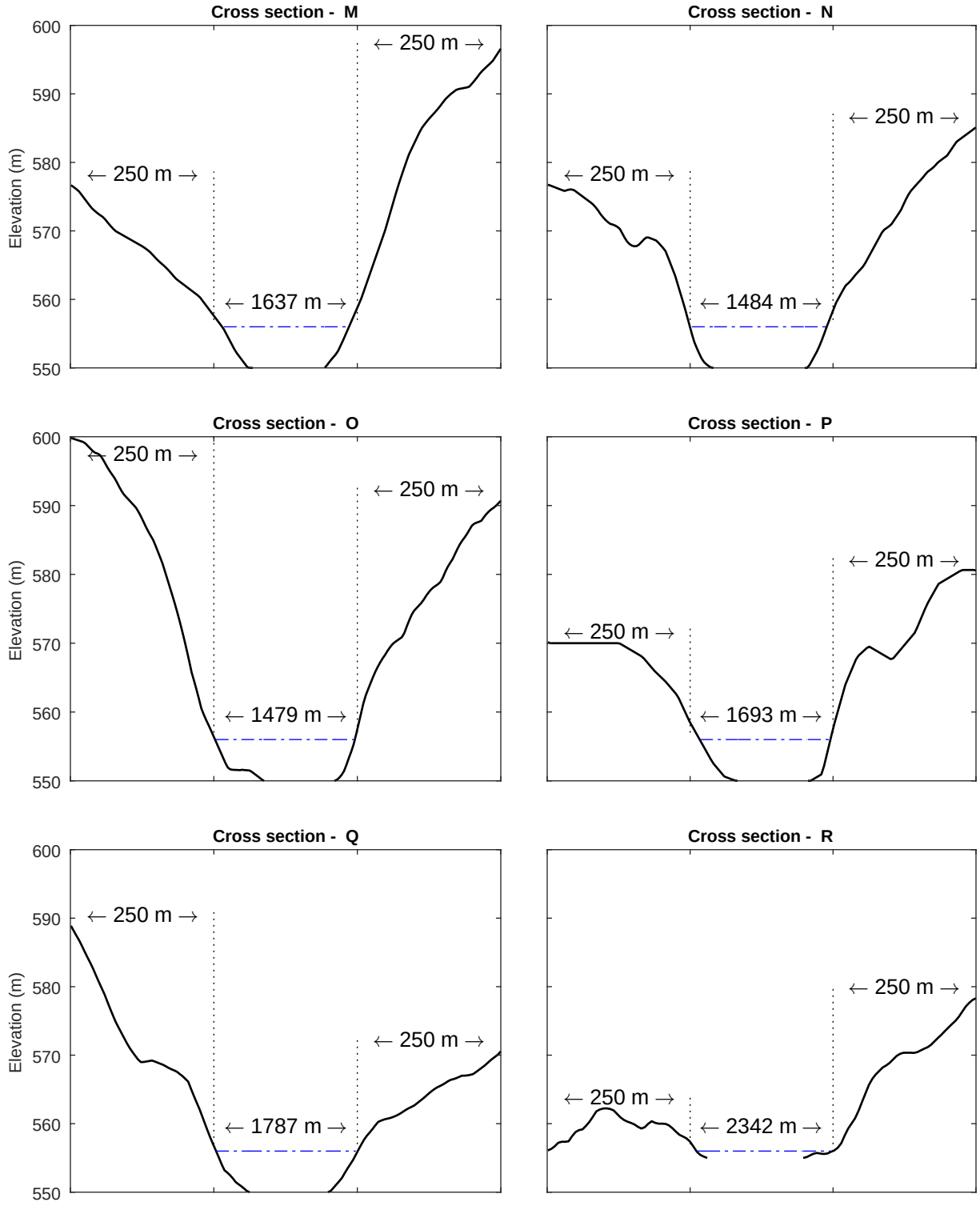
Cross section - M
Elevation (m)
600
590
580
570
560
550
← 250 m →
← 250 m →
← 1637 m →
Cross section - N
← 250 m →
← 250 m →
← 1484 m →
Cross section - O
← 250 m →
← 250 m →
← 1479 m →
Cross section - P
← 250 m →
← 250 m →
← 1693 m →
Cross section - Q
← 250 m →
← 250 m →
← 1787 m →
Cross section - R
← 250 m →
← 250 m →
← 2342 m →

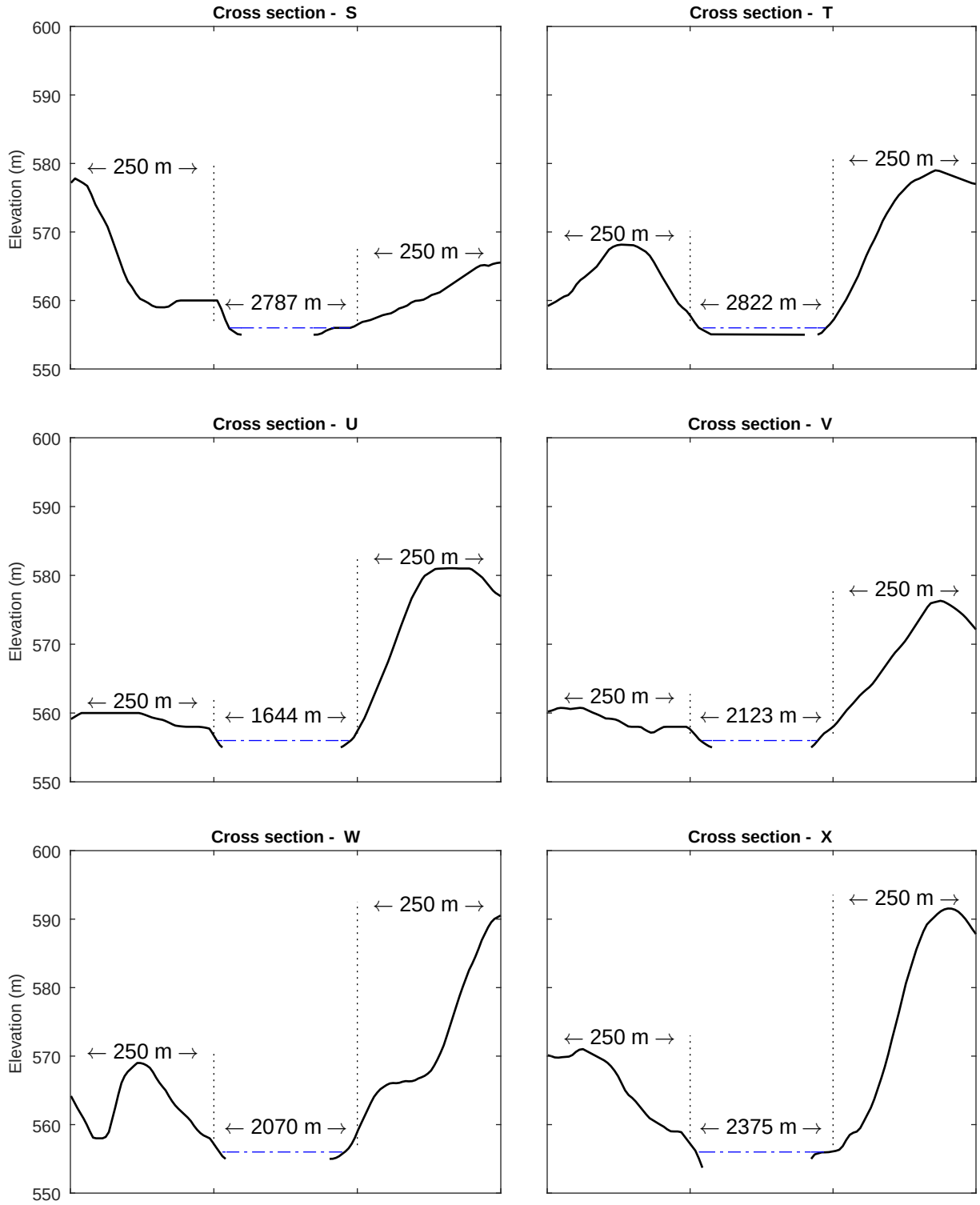

Figure 4.7: Cross sections for locations at Lake Diefenbaker's upstream shown in Figure 4.3

From cross section U, the topography remains almost flat downstream towards cross section X.

Some of the cross sections probably show the changes in shoreline profile better than others. Cross sections located in bends can experience larger shoreline retreat because of the turbulence forces on the banks. Also, cross sections that have a higher gradient can erode faster because of steep slopes at banks, as some of them have an elevation difference as large as 20%.

4.5 Conclusions

Sediment deposited in the lake is derived from two major sources. The South Saskatchewan River transports sediment from upstream regions. The majority of this sediment is deposited in the upstream reach (ranges 38 to 32) and the drawdown reach (ranges 32 to 26). Unfortunately, there is no program to monitor the sediment load so that estimates have to rely on data from the 1960s and 1970s (Ashmore and Day, 1988). A second major source of sediment is shoreline erosion. Studies report retreat rates of 1 to 3 m year^{-1}, but there is little information on the spatial and temporal variability of retreat rates, making estimates of average values uncertain at best. Future estimates of the sediment budget of Lake Diefenbaker would therefore greatly benefit from long-term monitoring programs that address these gaps.

Sedimentation rates studies indicate that erosion and deposition rates become negligible from range 15 to downstream, which is in agreement with the studies by Yuzyk (1983). We chose 24 cross sections between the lake Diefenbaker's most upstream site (highway 4, range 20) and range 8 which is 60 km downstream, and downloaded the elevation data from Google Maps Elevation API.

Some of the Google Maps products (e.g., Google Earth) provide the historical records along the renewed data. Unfortunately, such a service is not yet available for elevation data. Hence, the elevation data must be stored for comparisons with future data. The Google Maps Elevation data is not a replacement for survey maps but can provide valuable

information on shoreline retreats. This service can be used as a low-resolution monitoring tool which is free of charge, fast and easy to access.

Comparing the aerial maps from 1944 with the cross sections of 1968 – 1972 and 2012 – 2013 showed that these maps are consistent with each other. The same strategy can be used for the Google Maps Elevation data where the data will be compared with more precise elevation data in the future. Moreover, these low-resolution cross sections can provide better insights for planning the locations of future surveying activities.

4.6 Acknowledgements

The authors thank Howard Wheater, Canada Excellence Research Chair in Water Security for funding this project, Paul Jones for providing the boat and truck that made the field work possible, and Franny Rawlyk and Bryce Geeraert for assisting with the fieldwork.

References

Ashmore, P. and Day, T. (1988). Spatial and temporal patterns of suspended-sediment yield in the Saskatchewan River basin. *Canadian Journal of Earth Sciences*, 25(9):1450–1463.

Butcher, D., Labadz, J., Potter, A., and White, P. (1992). Assessment of catchment erosion in the southern Pennines, United Kingdom, using reservoir sedimentation monitoring. In Bogen, J., Walling, D. E., and Day, T. J., editors, *Erosion and sediment transport monitoring programmes in river basins*, pages 443–454. International Association of Hydrological Sciences.

Canada Surveys and Mapping Branch, Department of Mines and Technical Surveys (1959). Isle Brochet, Saskatchewan. Canada, National Topographic System Maps, topographic, 1:50,000.

Christiansen, E. A. (1979). The Wisconsinan deglaciation, of southern Saskatchewan and adjacent areas. *Canadian Journal of Earth Sciences*, 16(4):913–938.

Gallus, J., Kirchner, U., Vogt, R., and Benter, T. (2017). Impact of driving style and road grade on gaseous exhaust emissions of passenger vehicles measured by a Portable Emission Measurement System (PEMS). *Transportation Research Part D: Transport and Environment*, 52:215–226.

Google (2017). Google Maps Elevation API developer's guide. Available at: https://developers.google.com/maps/documentation/elevation/intro, Accessed: 26 February 2017.

Graf, W. L., Wohl, E., Sinha, T., and Sabo, J. L. (2010). Sedimentation and sustainability of western American reservoirs. *Water Resources Research*, 46(12).

Hudson, J. J. and Vandergucht, D. M. (2015). Spatial and temporal patterns in physical properties and dissolved oxygen in Lake Diefenbaker, a large reservoir on the Canadian Prairies. *Journal of Great Lakes Research*, 41:22–33.

Juracek, K. E. (2015). The aging of America's reservoirs: in-reservoir and downstream physical changes and habitat implications. *JAWRA Journal of the American Water Resources Association*, 51(1):168–184.

Kemp, G. P., Day, J. W., and Freeman, A. M. (2014). Restoring the sustainability of the Mississippi River Delta. *Ecological Engineering*, 65:131–146.

Klassen, R. W. (1989). Quaternary geology of the southern Canadian Interior Plains. In Fulton, R. J., editor, *Quaternary Geology of Canada and Greenland*, 1, pages 138–174. Geological Survey of Canada.

Meade, R. H. and Moody, J. A. (2010). Causes for the decline of suspended-sediment discharge in the Mississippi River system, 1940–2007. *Hydrological Processes*, 24(1):35–49.

Nelson, N. C., Erwin, S. O., and Schmidt, J. C. (2013). Spatial and temporal patterns in channel change on the Snake River downstream from Jackson Lake dam, Wyoming. *Geomorphology*, 200:132–142.

North, R. L., Johansson, J., Vandergucht, D., Doig, L. E., Liber, K., Lindenschmidt, K.-E., Baulch, H., and Hudson, J. J. (2015). Evidence for internal phosphorus loading in a large prairie reservoir (Lake Diefenbaker, Saskatchewan). *J. Great Lakes Res.*, 41(Supplement 2):91–99.

Palaka, R. and Sankar, G. J. (2014). Study of watershed characteristics using Google Elevation Service. *India Geospatial Digest*, 2:18–26.

Pomeroy, J. and Shook, K. (2012). Review of Lake Diefenbaker operations, 2010–2011. Available at: http://www.usask.ca/hydrology/papers/Pomeroy_Shook_2012.pdf.

Rahaman, M. S., Mei, Y., Hamilton, M., and Salim, F. D. (2017). CAPRA: A contour-based accessible path routing algorithm. *Information Sciences*, 385:157–173.

Sadeghian, A., de Boer, D., Hudson, J. J., Wheater, H., and Lindenschmidt, K.-E. (2015). Lake Diefenbaker temperature model. *Journal of Great Lakes Research*, 41:8–21.

Sadeghian, A., Hudson, J., Wheater, H., and Lindenschmidt, K.-E. (2017). Sediment plume model—a comparison between use of measured turbidity data and satellite images for model calibration. *Environmental Science and Pollution Research*, 24(24):19583–19598.

Santos, D., Pinto, J., Rossetti, R. J., and Oliveira, E. (2016). Modelling altitude information in two-dimensional traffic networks for electric mobility simulation. 1(3):191–198.

Schmid, B., van Everdingen, R., and Maathuis, H. (2003). The impact of the creation of Lake Diefenbaker on water levels in underlying extensive bedrock aquifers; a 40-year history. In *56th Canadian geotechnical conference, 4th joint IAH-CNC/CGS conference and 2003 NAGS conference*.

Smith, C. and Wigham, J. (1989). Erosion and sedimentation in the South Saskatchewan River Basin. Technical report C.9, Study Board for the Canada-Saskatchewan South Saskatchewan River Basin Study.

SPMC (1986). Lake Diefenbaker depth sounding chart. Technical report, Saskatchewan Property Management Corporation, S.D.

SWRC (1968). Delta formation and sedimentation in Lake Diefenbaker. Annual project report, Saskatchewan Water Resources Commission.

SWRC (1969). Delta formation and sedimentation in Lake Diefenbaker. Annual project report, Saskatchewan Water Resources Commission.

SWRC (1970). Delta formation and sedimentation in Lake Diefenbaker. Annual project report, Saskatchewan Water Resources Commission.

SWRC (1971). Delta formation and sedimentation in Lake Diefenbaker. Annual project report, Saskatchewan Water Resources Commission.

SWRC (1972). Delta formation and sedimentation in Lake Diefenbaker. Annual project report, Saskatchewan Water Resources Commission.

Syvitski, J. P., Vörösmarty, C. J., Kettner, A. J., and Green, P. (2005). Impact of humans on the flux of terrestrial sediment to the global coastal ocean. *Science*, 308(5720):376–380.

Van Everdingen, R. (1967). *Diefenbaker Lake: Effects of Bank Erosion on Storage Capacity*. Technical bulletin no. 10. Canada. Department of Energy, Mines and Resources. Inland Waters Branch.

Walling, D. (2006). Human impact on land–ocean sediment transfer by the world's rivers. *Geomorphology*, 79(3):192–216.

WSA (2012). *State of Lake Diefenbaker*. Water Security Agency. Available at: https://www.wsask.ca/Global/Lakes%20and%20Rivers/Dams%20and%20Reservoirs/Operating%20Plans/Developing%20an%20Operating%20Plan%20for%20Lake%20Diefenbaker/State%20of%20Lake%20Diefenbaker%20Report%20-%20October%2019%202012.pdf, Accessed: 21 May 2015.

Yu, Y., Wang, H., Shi, X., Ran, X., Cui, T., Qiao, S., and Liu, Y. (2013). New discharge regime of the Huanghe (Yellow River): causes and implications. *Continental Shelf Research*, 69:62–72.

Yuzyk, T. R. (1983). *Lake Diefenbaker, Saskatchewan: a case study of reservoir sedimentation*. Inland Waters Directorate, Environment Canada.

Chapter 5

Effects of meteorological data: long- and short-term quality controlled measured meteorological data and re-analyzed meteorological data on water temperature calibration

This chapter is submitted to the journal of Hydrologic Engineering. The submission id is: HEENG-3891.

Sadeghian, A., Hudson, J. J., and Lindenschmidt, K. E. Effects of meteorological data: long- and short-term quality controlled measured meteorological data and re-analyzed meteorological data on water temperature calibration.

Contributions of the candidate and co-authors

The candidate's contributions are follows: setting up and calibrating the Lake Diefenbaker temperature model; compiling the Windows based CE-QUAL-W2 (v 3.72) model on the University of Saskatchewan HPC (CentOS release 6.3) to run more model scenarios for calibration; adding an algorithm to the CE-QUAL-W2 model for considering a variable Manning coefficient in the river section of SSR to prevent the model's crash in low flow conditions; sensitivity analysis of the effects of different meteorological climate databases on the accuracy of the Lake Diefenbaker temperature model; wring the thesis manuscript. Karl-Erich Lindenschmidt was the supervisor and designed the whole study, and helped the candidate through the research process and manuscript writing. Jeff Hudson provided the Sonde and Laboratory data for model calibration and by contributed comments.

5.1 Abstract

There are different sources of uncertainty in an environmental modeling exercise. One of the most prominent sources of error and uncertainty is the input data to the models. Data on bathymetry, flow, nutrients and meteorological data are needed for water quality models. In this study, data from three meteorological databases were used to test the performance of the temperature and hydrodynamic models of Lake Diefenbaker: the data from the Environment and Climate Change Canada had long-term quality control (>20 years); the data from the AccuWeather had short-term quality control (<10 years), and the data from the MeteoBlue database were modeled data. The CE-QUAL-W2 hydrodynamic and water quality model was used for this study. The models were calibrated by adjusting two model coefficients controlling the amount of measured solar radiation and wind that reach the surface of the water. Solar radiation and cloud cover control a major proportion of thermal energy that reaches to the surface of the water and wind affects the mixing patterns within the waterbodies. The sensitivity results of 160 Monte-Carlo runs for each database, showed best performances with the AccuWeather data followed by the MeteoBlue data and thereafter by the Environment and Climate Change Canada data respectively.

5.2 Introduction

Meteorological databases are one of the most important components in many environmental studies, particularly in modeling exercises (Hunt et al., 1998; Sheffield et al., 2006). Model outputs can be significantly affected by the quality and spatiotemporal resolution of these datasets (Haberlandt, 2007; Yang et al., 2006). This reliance on meteorological databases has prompted many federal organizations, e.g., Environment and Climate Change Canada (ECCC), the National Oceanic and Atmospheric Administration (NOAA), and the Swedish Meteorological and Hydrological Institute (SMHI), to introduce strict standards on how data are acquired controlled and archived to assure data quality and continuity. Environment and Climate Change Canada has been collecting meteorological data since 1840 and continuously performs quality control investigations to guarantee high quality and accurate data (Environment and Climate Change Canada, 2017). The NOAA Quality Controlled Local Climatological Data (QCLCD) project provides hourly, daily and monthly data for about 1,600 US meteorological stations beginning in 2005 (NOAA, 2017). SMHI

checks to observation values with 6-hour predictions and believes that 90% of the errors are captured at this stage (Vejen et al., 2002). An investigation of 10 meteorological variables in 726 stations in China showed less than 0.05% inconsistency in data, temporally and spatially, for 1951 – 2000 study period (Feng et al., 2004). As a result, the operational costs for station installation and maintenance remain very high.

Less than 1% of the globe is covered with measured meteorological data from sparse weather stations, where the data from each station are useful up to a maximum radius of 3 to 12 km (MeteoBlue, 2016). Also, these weather stations are located unevenly on land surfaces and are unevenly distributed within vast areas, with some areas not having any weather stations at all (Haberlandt, 2007; Tabios and Salas, 1985). A station in close proximity to the study site can provide very high quality data; otherwise, the data should be used with caution. Another problem arises when the stations do not measure all the variables required for the modeling study. In these cases, data for unmeasured variables can be estimated for example, by using empirical equations (Sentelhas et al., 2010). A variable commonly missing in many (e.g., Environment and Climate Change Canada) stations is sky/cloud cover data (Kassianov et al., 2005; Sadeghian et al., 2015).

Cloud cover has a substantial impact on the significance of short- and long-wave solar radiations that reach the land and water surfaces (Cazorla et al., 2008). Solar radiation is a critical component for photosynthesis (Aguilera et al., 1999; Yamashita et al., 2004); hence, also for studying eutrophication (Assemany et al., 2015; Goldman, 1988; Strickland, 1958). There are many well-established methods for calculating direct and indirect solar radiation based on location, time of year, air temperature and air moisture and cloud cover (e.g., Annear and Wells, 2007; De Jong and Stewart, 1993). However, empirical relations to calculate cloud cover are uncertain and can influence model outcomes (Cazorla et al., 2008; Souza-Echer et al., 2006). Hence, generally, all the meteorological variables required for an eutrophication modeling exercise are available, except for cloud cover. A measure for cloud cover would be most beneficial, but is the one parameter that is often missing in a sampling program.

Not only national institutions (e.g., ECCC, SMHI, USGS), but also many large private institutions are involved in measuring meteorological data (Craft, 1999) as well as

small national/private regional institutes that study local climate (Changnon et al., 1990). AccuWeather, with headquarters in the USA, is an excellent example of a database comprised of climate data from numerous sources. These sources range from national organizations such as Environment and Climate Change Canada, Agriculture and Agri-Food Canada, private local institutions as well as AccuWeather meteorological stations. The company provides hourly measurements and forecasted meteorological data with high accuracy for millions of users worldwide (AccuWeather, 2016). Besides direct measurements, some companies forecast and calculate these data using weather models and each company may use different modeling approaches to simulate the data and incorporate land surface characteristics such as topography, ground cover and surface cover. MeteoBlue, located in Switzerland, is a good example. Since 1984, it has provided data on 45 meteorological variables for any location with a resolution of 3 – 30 km.

In this study, we compare the outputs of a water temperature model using meteorological data from three sources of meteorological data: the Environment and Climate Change Canada whose data is highly accurate, AccuWeather which has less than ten years of quality controlled data (for the study area used here), and MeteoBlue whose data stems from model simulations. The primary objective was to quantify the effects of sources of meteorological data on modeled water temperature and ultimately water quality result. Based on these results, we can provide guidelines for modelers and researchers for selecting the most suitable climate database.

5.3 Methods

The study area is Lake Diefenbaker, a vital source of water in Saskatchewan, Canada. It is a reservoir formed on the South Saskatchewan River (SSR) valley by the construction two dams on the arms after the main channel bifurcates near the village of Elbow (Figure 5.1). It has a length of 140 km from the inlet at Saskatchewan Landing until its bifurcation point. Two arms each about 20 km in length, extend to the Gardiner Dam and the Qu'Appelle Dam making the total length of the reservoir to 182 km. The Gardiner Dam arm is the main stream with an outflow capacity of up to 9,700 m^3/s (11 spillway gates that can exit up to 700 m^3/s of water each and 4 withdrawal pipes of 500 m^3/s capacity each) and has a

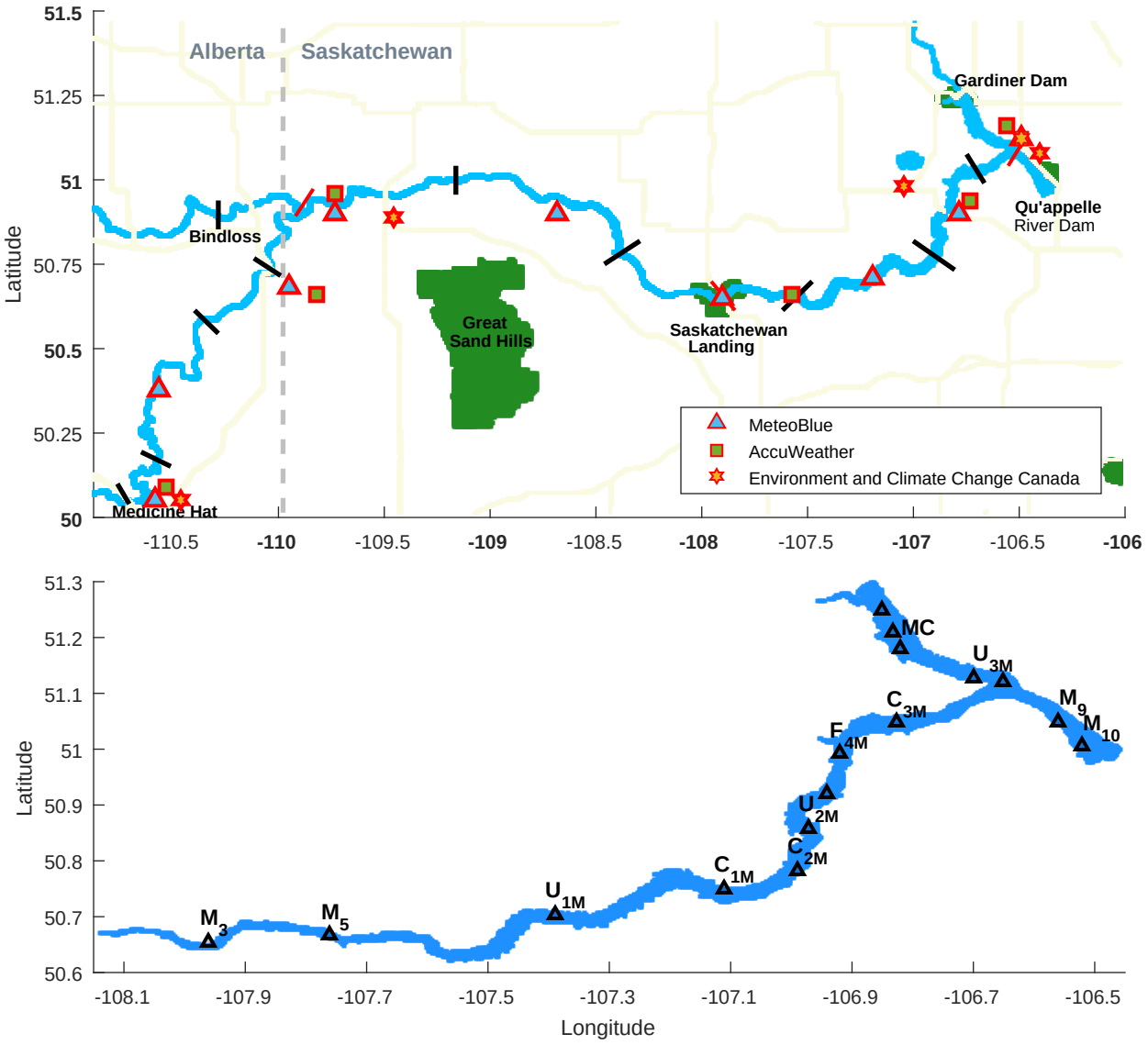

Figure 5.1: Map of South Saskatchewan River SSR, Red Deer River RDRand Lake Diefenbaker. The meteorological stations for the three databases are shown in graph on top. The graph in bottom shows the location of filed observation stations used for model calibration

maximum depth of 60 m. The Qu'Appelle Dam arm has a mean outflow of 1.5 m^3/s and a maximum depth of 22 m.

We used a two-dimensional surface water quality model to evaluate the outcomes of using different meteorological databases. The CE-QUAL-W2 model, developed by the US Army Corps of Engineers and maintained by Portland State University, was selected for this study.

The CE-QUAL-W2 model has over 40 years of development and has been successful used for studying hydrodynamic, temperature, nutrients, and sediment transport characteristics of rivers, lakes and estuaries. The model also has been successfully used on Canadian prairie reservoirs (e.g., Sadeghian et al., 2015; Terry et al., 2017).

This study is an extension of a previous study on which Lake Diefenbaker temperature model was calibrated for the period of 2011 – 2013 (Sadeghian et al., 2015). Based on temperature model calibration and global sensitivity analysis, the results of temperature simulations had the highest sensitivities with the wind sheltering coefficient (WSC) and the shading coefficient (SHADE) which adjust the amount of wind and solar radiation applied on the surface of the water, respectively. The WSC is the percentage of recorded wind speed from a land station near a waterbody that is transferred to the water surface. The wind becomes slower when it passes through barriers such as trees and topographic peaks near the edge of the water, or becomes faster when blowing over a lake with a long fetch. SHADE is the amount of short wave solar radiation that impinges the water surface. Similar to WSC, SHADE is reduced by vegetation and topographic barriers along the shore.

In the previous study (Sadeghian et al., 2015), it was found that the inflow water temperature, which was calculated from the average weekly air temperature, is the primary source of thermal energy to the reservoir. Hence, the model boundaries were extended to Medicine-Hat on the SSR (374 km) and Bindloss on the Red Deer River (218 km) in Alberta, where hydrometric stations are located, and the water temperature is measured (Figure 5.1). The water temperature measurements at the Medicine Hat and Bindloss were used, and the effects of ambient air temperature and solar radiation were considered to adjust the temperate of water that enters into the Lake Diefenbaker.

In the model, the rivers and the reservoir are divided into a total number of nine interconnected waterbodies shown by the black lines in the Figure 5.1. The model reads the meteorological data for each waterbody separately, allowing use of nine meteorological stations along the river and reservoir. These nine waterbodies selected based on changes in topography, morphology and climatology. The state variables for meteorological data are air temperature, dew point temperature, wind speed, wind direction, cloud cover and short-wave solar radiation (Cole and Wells, 2015). Although the model can be used

regardless of the frequencies of the input variables, for accurate results hourly or daily values must be used. We used hourly data for all the meteorological variables and daily flow data at inlet, and the Gardiner and the Qu'Appelle Dams. Model simulations were started 01 April 2011, assuming isothermal conditions to the reservoir after ice melt and spring turnover, until 31 December 2013.

Three meteorological databases (Environment and Climate Change Canada, AccuWeather and MeteoBlue) were used to evaluate the effects of different sources of data on the accuracy of model results. From the data in each meteorological database, we prepared nine meteorological input files for the nine waterbodies in the model. The CE-QUAL-W2 model requires air temperature, dew point temperature, wind speed and direction, and cloud cover data as meteorological input data. Except for cloud cover data in Environment and Climate Change Canada's database, all the other variables were available in hourly resolution for all the databases of the study area. We ran 160 Monte-Carlo runs for each meteorological database for a total of 480 runs on the University of Saskatchewan HPC research clusters. There are a total of 96 nodes that each have 16 processors on the research cluster giving a total of 1,536 processors. To use the computing resources more efficiently, the submitted task should be a multiplication of 16 (number of processors in each node). Hence, 160 runs (10 nodes) were used for each station. The 160 random values were the same in all setups with random selection of two variables, WSC and SHADE uniformity distributed between the defined ranges. The model outputs were compared with the measured temperature profiles at 16 stations along the reservoir (c.f. Sadeghian et al., 2015). The Root Mean Square Error (RMSE) used as the metric for model performance:

$$RMSE = \sqrt{\frac{\sum (O - S)^2}{n}} \tag{5.1}$$

where O is the value of observation in one column, S is the corresponding simulated value and n is the number of samples.

Model temperature simulations were compared with the temperature profiles obtained from a database collected in 2011 – 2013 by the limnology group at Department of Biology at University of Saskatchewan. In total, there are data for 16 locations in Lake Diefenbaker

(Figure 5.1). The complete description of temperature data collection and analysis is available (Hudson and Vandergucht, 2015).

The nine meteorological data files for the waterbodies in the model were prepared based on the description presented below.

5.3.1 Environment and Climate Change Canada Database

Environment and Climate Change Canada has a total of 8,732 meteorological stations, as reported on its website. Of these stations, 1,441 stations are listed more than once mainly because renovated stations are listed with a new station ID; hence, 7,291 stations remain when duplicates are removed (Table 5.1). The number of working stations in 2013 was a small subset of this, about 1,500 stations. Only 59 stations with hourly data intervals are located in Saskatchewan, which is very sparse considering the large size of province (Table 5.1). Fifty nine stations is equivalent to almost one station per 11,035 km^2. However, the quality of the data from these stations is high due to long-term quality control. Another key limitation is lack of cloud cover data. Cloud cover data are critical for calculating short-wave and long-wave solar radiation that reaches the water and land surfaces. The model uses one meteorological station for each waterbody; hence, nine meteorological stations are required. However, there are only four stations within the proximity of the SSR+Lake Diefenbaker region in the Environment and Climate Change Canada database. Thus, these four stations were also used for the remaining waterbodies, according to their proximities.

5.3.2 AccuWeather Database

Different meteorological variables in the AccuWeather database stem from different sources which could be based on a single station or combination of several nearby stations owned by governmental or private agencies or their own stations. If a weather station continues reporting for a long period of time (e.g., 10 years) by which all the metrics can be validated for the time frame that the data is requested, it is designated a “primary” station; otherwise it is called “secondary”. In other words, the secondary stations are meteorological stations that are missing a robust predicting standard to estimate the missing values in case of a device failure. Because all the metrics cannot be validated due to gaps in the data, these

Table 5.1: Total number of stations is listed as 8,732. However, after removing duplicates, 7,291 stations remain. Data derived from downloading the stations information from Environment and Climate Change Canada website on July 24, 2016

Name	Area (km^2)		Number of stations			Active stations in 2013		One station for (km^2)
	Total	Land	Total	Daily	Hourly	Daily	Hourly	
Alberta	661,848	642,317	1,378	1,331	294	262	262	2,526
British Columbia	944,735	925,186	1,653	1,633	249	297	152	6,215
Manitoba	647,797	553,556	512	507	81	95	57	11,365
New Brunswick	72,908	71,450	192	192	33	32	27	2,700
Newfoundland and Labrador	405,212	373,872	280	264	84	69	51	7,945
Northwest Territories	1,346,106	1,183,085	141	130	87	60	63	21,367
Nova Scotia	55,284	53,338	278	260	72	50	43	1,286
Nunavut	2,093,190	1,936,113	176	149	144	78	84	24,919
Ontario	1,076,395	917,741	1,498	1421	256	216	180	5,980
Prince Edward Island	5,660	5,660	43	42	11	17	9	629
Quebec	1,542,056	1,365,128	987	928	209	237	139	11,094
Saskatchewan	651,036	591,670	659	651	85	103	59	11,035
Yukon	482,443	474,391	124	120	37	32	26	18,556
Sum	9,984,670	9,093,507	7,921	7,628	1,642	1,548	1,152	8,667

stations are also referred to as backup stations by AccuWeather. Most of the AccuWeather meteorological stations used in this study were among the secondary stations hence their data did not pass any screening quality control assurance. Among the nine waterbodies in the model, there were only six stations within the proximity of the SSR/Lake Diefenbaker region in AccuWeather's database. The remaining waterbodies used one of these stations according to their proximity.

5.3.3 MeteoBlue Database

MeteoBlue calculates and forecasts meteorological data using its own model based on Nonhydrostatic Meso-Scale Modelling (NMM) technology. Different modeling approaches are used to reflect detailed topography, ground cover and surface cover characteristics. The company has provided data for 45 meteorological parameters with a spatial resolution of 3 – 30 km and a temporal resolution of one hour (hourly data) worldwide since 1984, without any gaps or missing data (MeteoBlue, 2016) (Table 5.2). The reader is referred to "http://content.meteoblue.com/en/verified-quality/verification" for verification and accuracy

Table 5.2: Comparison of measured data from the meteorological stations and MeteoBlue re-analyses data. Source: MeteoBlue (2016)

	MeteoBlue	Measurement
Spatial resolution	3 – 30 km	< 1 km
Worldwide coverage	100%	< 1%
Number of parameters	45	<10
Number of years	30	2 – 30 (with gaps)
Time intervals	hourly, 3 hourly, daily	(hourly), 3 hourly, daily
Completeness (No data)	100%	10 – 99%
Consistency	100%	variable

control information. Since MeteoBlue data are modeled, all the waterbodies were assigned a station in the CE-QUAL-W2 model.

5.4 Results and Discussion

The sensitivity analysis results show that the AccuWeather and the MeteoBlue databases yield much better results than the Environment and Climate Change Canada data (Figures 5.2 and 5.3). Both the WSC and SHADE parameters show sensitivity to the databases which varies for different years. Environment and Climate Change Canada data are of the best quality but yield the least performance results because of greater RMSE values (Figures 5.2 and 5.3). The main reason is that Environment and Climate Change Canada does not have data in close proximity to the study region compared with the other two databases. First, Environment and Climate Change Canada has fewer stations (four), and these stations are several kilometers away from our research sites. Although the topography around Lake Diefenbaker is flat, the distance between the stations and sites can still lead to large errors. Second, all the parameters required for the modeling were not available in the Environment and Climate Change Canada databases. The lack of cloud cover data is the main reason for the larger errors. Solar radiation is the main heat source to the reservoir, and cloud cover controls the amount of shortwave and longwave solar radiation reaching the lake's surface.

Both MeteoBlue and AccuWeather have very good model performances, but with slightly different parameter settings. The WSC has optimum values of 0.9, 1.1 and 1.0 with MeteoBlue and 0.7, 0.9 and 0.9 with AccuWeather for 2011, 2012 and 2013, respectively.

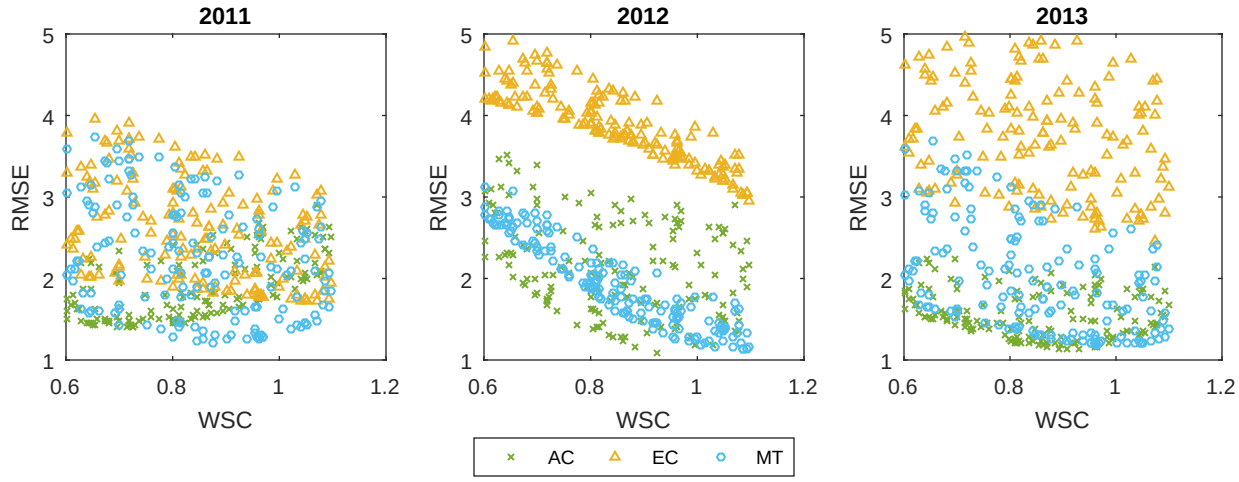

Figure 5.2: Sensitivity analysis of Lake Diefenbaker temperature model performance based on three different meteorological databases. The figure shows effects of wind sheltering coefficient on model performance for all the measurements based on the best run for each meteorological station

The SHADE has optimum performance with 0.6, 0.8 and 0.7 with MeteoBlue and 0.9, 1 and 0.9 for AccuWeather for the same years. It is worth mentioning that a value of one (100%) for these coefficients means that there is no need for adjustment. Thus, AccuWeather data for WSC (wind) provide the best results without any adjustment, while MeteoBlue data require some calibration. For wind speed data, the MeteoBlue performs better.

Errors in model performance with the Environment and Climate Change Canada data decreased when the WSC values are greater than one (Figure 5.2). A value greater than one means the recorded wind speed from the meteorological station needs to be intensified when they are applied to the reservoir. The primary reason is the fetch effect which is a well-understood concept when using land station data on a waterbody (e.g., Condie and Webster, 1997; Gulliver and Stefan, 1986; McJannet et al., 2012). In the other databases, the stations were closer to the reservoir; hence, these effects were less noticed.

In contrast to the WSC, model errors decrease with Environment and Climate Change Canada data when smaller values are used for the SHADE coefficient (Figure 5.3). Small SHADE values indicate that the amount of solar radiation that reaches the surface of water in the river and reservoir should be decreased. As mentioned before, cloud cover data are an important variable which is absent in the Environment and Climate Change Canada

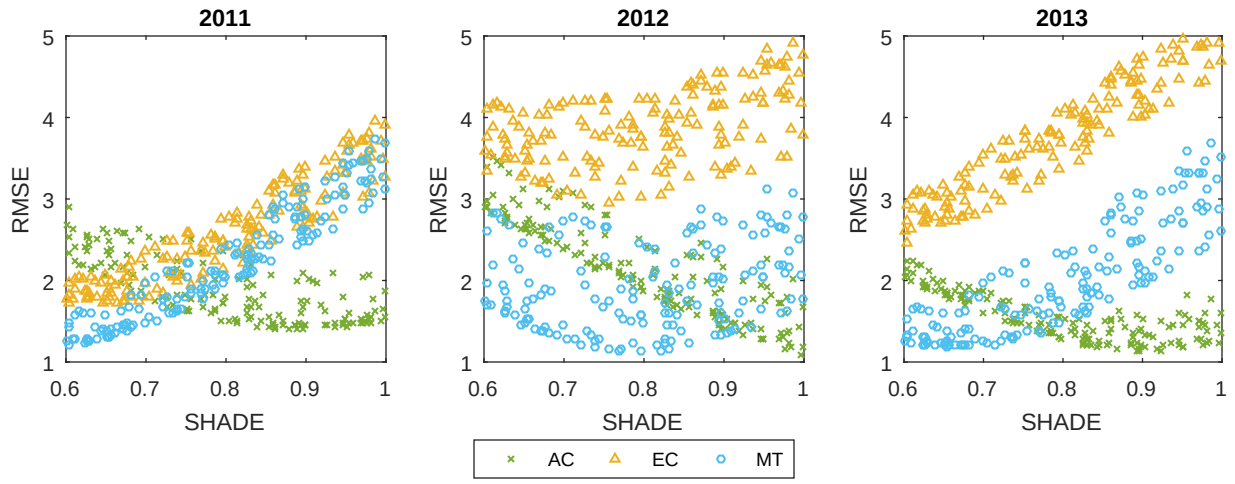

Figure 5.3: Sensitivity analysis of Lake Diefenbaker temperature model performance based on three different meteorological databases. The figure shows effects of solar radiation shading on model performance for all the measurements based on the best run for each meteorological station

database. Therefore, the small SHADE coefficient compensates for cloudy days which are missing from the database.

Model performances with the data from the AccuWeather database are the best with no need for adjustments except for WSC in 2011. Knowing this point is a rewarding achievement for us because we can use the AccuWeather data for historical modeling when there are no data available for model calibration and validation with higher confidence.

Based on RMSE values, the re-analyzed data in the MeteoBlue database may produce slightly better results compared with the actual measured data in the AccuWeather database but with more parameter adjustments. The best results with the MeteoBlue data for WSC are similar to those obtained with the AccuWeather data when the calculated wind speed values are used without any correction. But the model outcomes based on the SHADE coefficient show that the results match better with the observed temperature values when the solar radiation input is used with slight alterations. The reason for this can be uncertainties in cloud cover estimation in the MeteoBlue database while, in AccuWeather database, the cloud cover data are actual measurements.

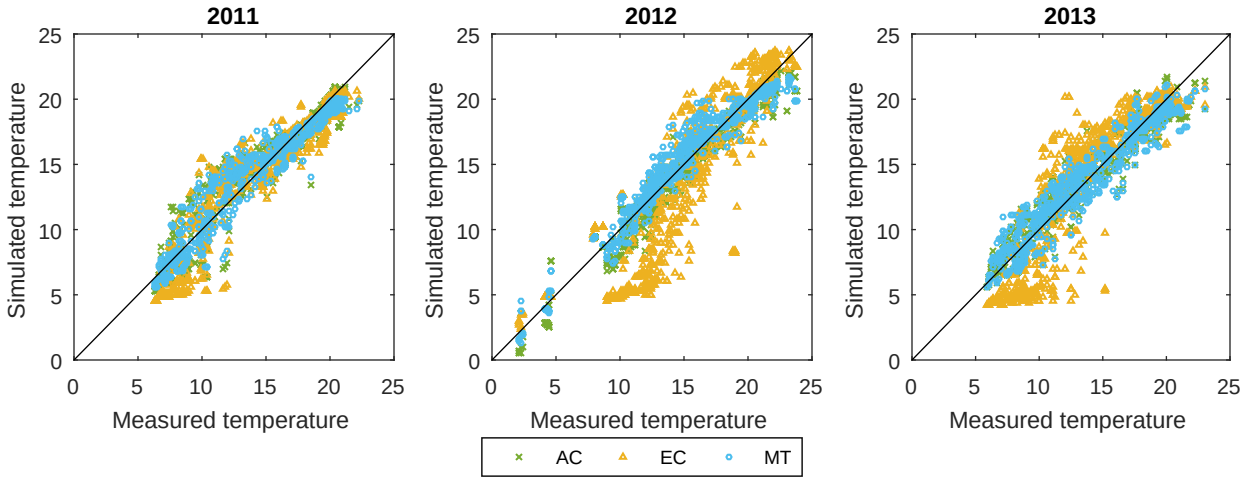

Figure 5.4: Sensitivity analysis of Lake Diefenbaker temperature model performance based on three different meteorological databases. The figure shows the model overall performance for all the measurements based on the best run for each meteorological station

Figure 5.4 shows a scatter plot of all field measurements on the x-axis, and their simulated values on the y-axis for the best model performances based on each database for each year. The recorded water temperature data used for model calibration are from field observations in late spring until early fall. Hence, the measurements seldom approach 0 °C. The majority of observations range between 10 °C and a maximum water temperature of 25 °C in summer. The graphs show that the simulated values from the AccuWeather and MeteoBlue databases plotted against measured values almost overlap each other, whereas the corresponding Environment and Climate Change Canada results show more deviations from the straight line indicating complete agreement between simulated and measured values. These deviations are higher in 2012 followed by 2013, and are also visible in Figures 5.2 and 5.3.

Temperature profiles for the best performances of each database show that the Environment and Climate Change Canada data mainly overestimated temperature at shallower depths (Figure 5.5). The reason can be, again, the absence of cloud cover data which would indicate clear sky for the entire year. The vertical profiles for AccuWeather and MeteoBlue databases almost overlay each other in most locations and most times. Thus, the modeled data from the MeteoBlue database produced results as accurate as those from the AccuWeather database and better than those from the Environment and Climate Change Canada database.

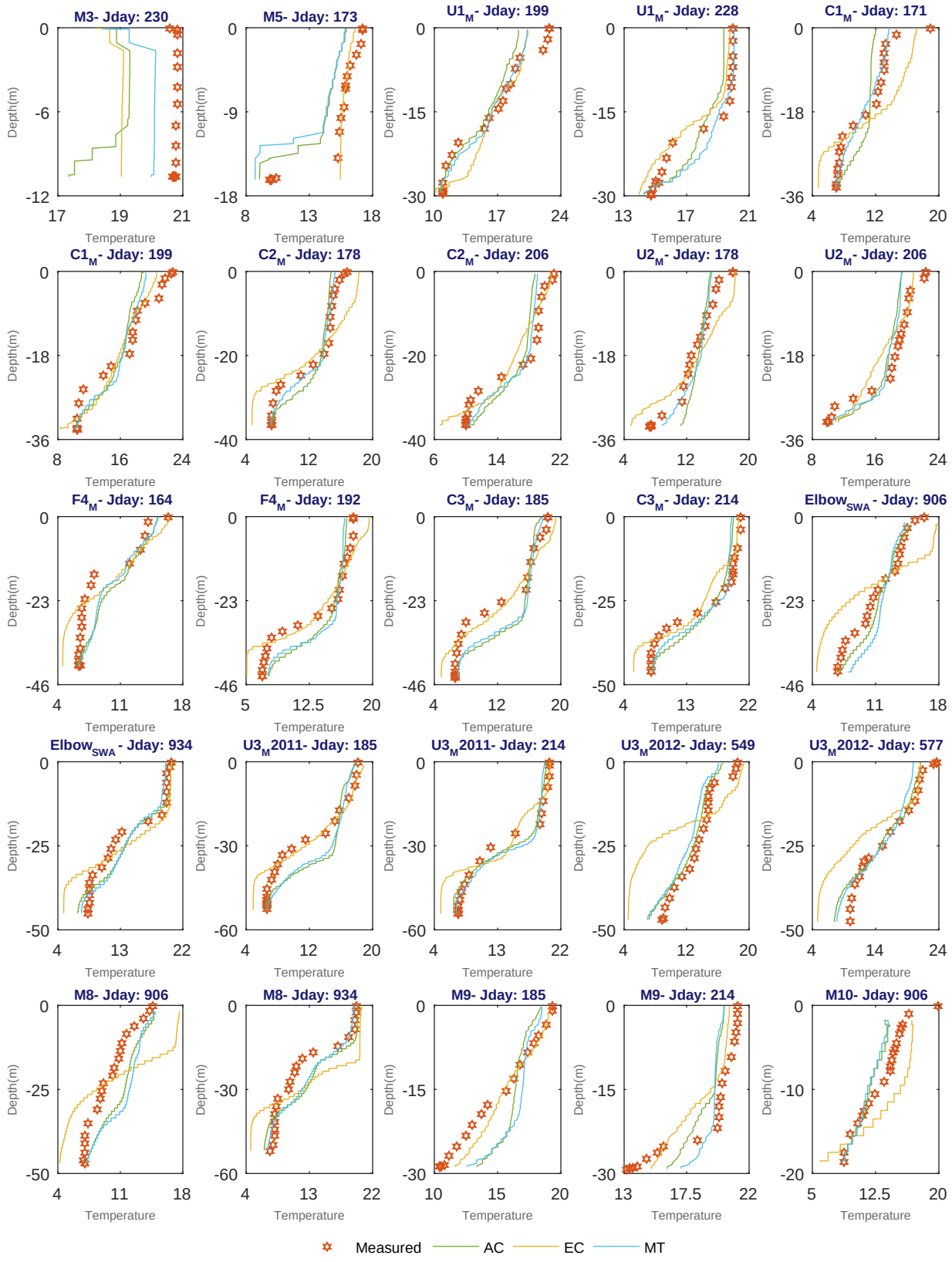

Figure 5.5: Comparing the temperature profiles from the results of different meteorological databases with the measured data. The stations in the top left corner start from upstream towards the dams downstream

An important issue for selecting a database is ease of access to the data. Environment and Climate Change Canada data are available through the Environment and Climate Change Canada website free of charge and are the easiest to obtain. In contrast, there are processing fees for obtaining the data from the other two databases. MeteoBlue provides data free of charge for educational purposes, and we were able to obtain the data in less than 24 hours. AccuWeather data are most expensive and it took almost one month to obtain the data.

In selecting a good climate database, it is important that the database has all the required variables for the specific study. Environment and Climate Change Canada has high quality databases; however, a limited number of meteorological stations and an absence of cloud cover data produced large errors with the CE-QUAL-W2 water quality model. AccuWeather has more stations and variables but the data are expensive and takes weeks to receive. We found the MeteoBlue database the best option because the data produce good results, are free of charge and are readily obtained.

5.5 Conclusions

We used three different climate databases to test the performance of a water quality model: Environment and Climate Change Canada data with long-term quality control standards, AccuWeather data with less than ten years of quality control data and MeteoBlue data which are modeled. We used the climate data from these databases to run the CE-QUAL-W2 water quality model for Lake Diefenbaker in Saskatchewan, Canada. The results show significantly better model performances with the AccuWeather and MeteoBlue data. The main reasons are lack of cloud cover data and the fewer number of stations in Environment and Climate Change Canada databases. Cloud cover influences the heat budget by affecting short- and long-wave solar radiation.

Regarding statistics, MeteoBlue data, which are modeled data produced the smallest error compared with the other databases but required adjustments to some parameters. These results are a validation of the MeteoBlue modeling algorithms as well. Easiness and quick access to the database and support of academic projects by providing free access to those data can be a motivator for considering the MeteoBlue data in many environmental studies

in future.

AccuWeather data are expensive and lengthy to obtain but provide the best results with little need for adjustment of parameters. Considering the length and cost of a study, these fees and time to obtain data can be justifiable in many big research programs. The database can be used for modeling the locations or time frames when observations are not available to calibrate the model parameters. Additionally, AccuWeather data can significantly reduce the field monitoring costs with lower data requirement for model verification.

When selecting a meteorological database, it is important that the database has all the required variables. Environment and Climate Change Canada has high quality databases; however, the lack of cloud cover data produced errors in the CE-QUAL-W2 water quality model. Also, the limited number of meteorological stations is a drawback. Depending on the proximity of study site to available stations in the database and the variables required for the study, the Environment and Climate Change Canada data can be used with confidence or uncertainty.

5.6 Acknowledgements

This work was financially supported by the Canada Excellence Research Chair in Water Security through the Global Institute for Water Security. We thank Environment and Climate Change Canada for providing the meteorological data and the hydrometric data. We are grateful to MeteoBlue for providing the meteorological data. Thanks to the Limnology Laboratory at the University of Saskatchewan for providing the water temperature data. Thanks to the Department of Geography and Planning at the University of Saskatchewan for providing the bathymetry data.

References

AccuWeather (2016). AccuWeather exceeds 9.5 billion requests for global data every day, setting new record in big data demand. Available at: http://www.accuweather.com/en/press/43009943, Accessed: 7 December 2016.

Aguilera, J., Karsten, U., Lippert, H., Vögele, B., Philipp, E., Hanelt, D., and Wiencke, C. (1999). Effects of solar radiation on growth, photosynthesis and respiration of marine macroalgae from the arctic. *Marine Ecology Progress Series*, 191:109–119.

Annear, R. L. and Wells, S. A. (2007). A comparison of five models for estimating clear-sky solar radiation. *Water resources research*, 43(10).

Assemany, P. P., Calijuri, M. L., do Couto, E. d. A., de Souza, M. H. B., Silva, N. C., da Fonseca Santiago, A., and de Siqueira Castro, J. (2015). Algae/bacteria consortium in high rate ponds: influence of solar radiation on the phytoplankton community. *Ecological Engineering*, 77:154–162.

Cazorla, A., Olmo, F., and Alados-Arboledas, L. (2008). Development of a sky imager for cloud cover assessment. *JOSA A*, 25(1):29–39.

Changnon, S. A., Lamb, P. J., and Hubbard, K. G. (1990). Regional climate centers: new institutions for climate services and climate-impact research. *Bulletin of the American Meteorological Society*, 71(4):527–537.

Cole, T. M. and Wells, S. A. (2015). *CE-QUAL-W2: A two-dimensional, laterally averaged, hydrodynamic and water quality model*. Department of Civil and Environmental Engineering, Portland State University, Portland, OR, 3.72 edition.

Condie, S. A. and Webster, I. T. (1997). The influence of wind stress, temperature, and humidity gradients on evaporation from reservoirs. *Water Resources Research*, 33(12):2813–2822.

Craft, E. D. (1999). Private weather organizations and the founding of the United States Weather Bureau. *The Journal of Economic History*, 59(04):1063–1071.

De Jong, R. and Stewart, D. W. (1993). Estimating global solar radiation from common meteorological observations in western Canada. *Canadian Journal of Plant Science*, 73(2):509–518.

Environment and Climate Change Canada (2017). Quality of historical climate data. Available at: http://climate.weather.gc.ca/climate_data/data_quality_e.html, Accessed: 28 February 2017.

Feng, S., Hu, Q., and Qian, W. (2004). Quality control of daily meteorological data in china, 1951–2000: a new dataset. *International Journal of Climatology*, 24(7):853–870.

Goldman, C. R. (1988). Primary productivity, nutrients, and transparency during the early onset of eutrophication in ultra-oligotrophic Lake Tahoe, California-Nevada. *Limnology and Oceanography*, 33(6):1321–1333.

Gulliver, J. S. and Stefan, H. G. (1986). Wind function for a sheltered stream. *Journal of Environmental Engineering*, 112(2):387–399.

Haberlandt, U. (2007). Geostatistical interpolation of hourly precipitation from rain gauges and radar for a large-scale extreme rainfall event. *Journal of Hydrology*, 332(1):144–157.

Hudson, J. J. and Vandergucht, D. M. (2015). Spatial and temporal patterns in physical properties and dissolved oxygen in Lake Diefenbaker, a large reservoir on the Canadian Prairies. *Journal of Great Lakes Research*, 41:22–33.

Hunt, L., Kuchar, L., and Swanton, C. (1998). Estimation of solar radiation for use in crop modelling. *Agricultural and Forest Meteorology*, 91(3):293–300.

Kassianov, E., Long, C. N., and Ovtchinnikov, M. (2005). Cloud sky cover versus cloud fraction: Whole-sky simulations and observations. *Journal of applied meteorology*, 44(1):86–98.

McJannet, D. L., Webster, I. T., and Cook, F. J. (2012). An area-dependent wind function for estimating open water evaporation using land-based meteorological data. *Environmental Modelling & Software*, 31:76–83.

MeteoBlue (2016). Weather simulation data – what's that? Available at: https://content.meteoblue.com/en/products/time-dimensions/history/weather-simulation-data, Accessed: 7 December 2016.

NOAA (2017). Quality controlled local climatological data (qclcd). Available at: https://www.ncdc.noaa.gov/data-access/land-based-station-data/land-based-datasets/quality-controlled-local-climatological-data-qclcd, Accessed: 28 February 2017.

Sadeghian, A., de Boer, D., Hudson, J. J., Wheater, H., and Lindenschmidt, K.-E. (2015). Lake Diefenbaker temperature model. *Journal of Great Lakes Research*, 41:8–21.

Sentelhas, P. C., Gillespie, T. J., and Santos, E. A. (2010). Evaluation of FAO Penman–Monteith and alternative methods for estimating reference evapotranspiration with missing data in Southern Ontario, Canada. *Agricultural Water Management*, 97(5):635–644.

Sheffield, J., Goteti, G., and Wood, E. F. (2006). Development of a 50-year high-resolution global dataset of meteorological forcings for land surface modeling. *Journal of Climate*, 19(13):3088–3111.

Souza-Echer, M., Pereira, E., Bins, L., and Andrade, M. (2006). A simple method for the assessment of the cloud cover state in high-latitude regions by a ground-based digital camera. *Journal of Atmospheric and Oceanic Technology*, 23(3):437–447.

Strickland, J. D. H. (1958). Solar radiation penetrating the ocean. a review of requirements, data and methods of measurement, with particular reference to photosynthetic productivity. *Journal of the Fisheries Board of Canada*, 15(3):453–493.

Tabios, G. Q. and Salas, J. D. (1985). A comparative analysis of techniques for spatial interpolation of precipitation. *JAWRA Journal of the American Water Resources Association*, 21(3):365–380.

Terry, J. A., Sadeghian, A., and Lindenschmidt, K.-E. (2017). Modelling dissolved oxygen/sediment oxygen demand under ice in a shallow eutrophic prairie reservoir. *Water*, 9(2):131.

Vejen, F., Jacobsson, C., Fredriksson, U., Moe, M., Andresen, L., Hellsten, E., Rissanen, P., Pálsdóttir, T., and Arason, T. (2002). Quality control of meteorological observations automatic methods used in the Nordic countries. *Climate Report*, 8.

Yamashita, M., Yoshimura, M., and Nakashizuka, T. (2004). Cloud cover estimation using multitemporal hemisphere imageries. *International Archives of Photogrammetry, Remote Sens. Spat. Inf*, 35:826–829.

Yang, K., Koike, T., and Ye, B. (2006). Improving estimation of hourly, daily, and monthly solar radiation by importing global data sets. *Agricultural and Forest Meteorology*, 137(1):43–55.

Chapter 6

Input data for water quality models: a case study of South Saskatchewan River

An excerpt of this chapter is submitted as a technical note to the journal of Environmental Engineering.

Sadeghian, A., and Lindenschmidt, K. E. Input data for water quality models: a case study of South Saskatchewan River

Contributions of the candidate and co-authors

The candidate's contributions are follows: analyzing and estimating daily water quality input data for the LDF water quality model based on monthly and sparse measured data at SSR upstream. Karl-Erich Lindenschmidt was the supervisor and designed the whole study, and helped the candidate through the research process and manuscript writing. Howard Wheater was the co-supervisor and designed the overall vision of the research at the Global Institute for Water Security (GIWS). He supported the candidate financially as well as provided guidance in research and contributed comments on all the manuscripts.

6.1 Abstract

We developed a fitting approach for constructing daily time series of water quality variables required for comprehensive water quality modeling studies from two databases with monthly water quality data. An average of a first-order and second-order polynomial fitting was used with four components: Julian day to capture the seasonality; the date to incorporate long-term trends and seasonality; discharge to consider daily and seasonal effects of flow; and water temperature to maintain temperature dependence of most water quality components. The first-order polynomial fitting determined the seasonal patterns and the second-order fitting adjusted the small frequency variations. Averaging

the first and second-order polynomial fits provided the best outputs. By using the averaged polynomial fitting method, we constructed a water quality database for the South Saskatchewan River and Red Deer River in Canada for the time frame 2011 – 2014 based on the input requirements of the two-dimensional CE-QUAL-W2 water quality model.

6.2 Introduction

The statistical properties for water quality data are different from those of existing hydrological data due to the smaller number of samples available, both spatially and temporally (Helsel and Cohn, 1988). In climate databases, the data are available with differing frequencies varying from yearly, monthly, daily, hourly to even shorter frequencies; however, for a water quality database, a typical frequency is once per month. Moreover, the spatial distribution of data is more limited for water quality data. The small spatiotemporal resolution of water quality data may not produce correct statistic metrics (Mayer and Butler, 1993), so an expert interpretation of the results is necessary (Arhonditsis and Brett, 2004).

A simple internet search of articles using the phrase "water quality data" revealed that most of the highly cited papers date back to the 1970s, 1980s and early 1990s. Finding techniques to improve the quality of measured water quality data was the primary concern. The main emphasize was on trend analysis (Belle and Hughes, 1984; Hirsch et al., 1982; Hounslow, 1995; Lettenmaier, 1976), and interpolation methods were applied to fill the gaps (Eatherall et al., 1998; Smith et al., 1997).

Many formulas (e.g., Bowie et al., 1985; Chapra, 2008) in today's water quality models (e.g., CE-QUAL-W2, QUAL2K) are also empirical in nature, with many relationships stemming between variables and measured data. Also, many guidelines for field measurements were also developed based on the relationships between different observed water quality variables (e.g., Golterman et al., 1983) to minimize sampling and laboratory analyses costs. At the beginning of the 21^{st} century, the focus of many water quality modeling articles shifted towards uncertainty analyses (e.g., Harmel et al., 2009; Rode and Suhr, 2007; Shrestha and Kazama, 2007). At this time, computers were being applied more and more to numerically

build simplified abstractions of the natural environment (e.g., Abbaspour et al., 2007; Qian and Reckhow, 2007). Papers published in recent years seems to have shifted the research objectives more towards trend analysis techniques again (e.g., Halliday et al., 2012).

There are reasons for these shifts in research objectives at different periods of time. In studies carried out before 2000, the measuring instruments had many limitations, and the accuracy of the measurements was dependent on the users' ability to operate the instrumentations and to interpret the data and identify outliers (e.g., Helsel and Hirsch, 1992; Hounslow, 1995). Also, access to different databases was extremely limited. As a result, researchers endeavored to expand their databases using trend analysis methods. Many advances in sampling and analysis technology occurred in the 2000s, with more accurate and less expensive instruments becoming available and providing efficient laboratory analysis as well as keeping the costs reasonable. Also, there was a marked improvement in computer and software development, enabling models to be developed and extended on personal computers. Since the primary objective of most research studies was to build more accurate models, uncertainty analysis studies received more attention. At this time, the computational cost was the major constraint (Van Griensven et al., 2006), leading to developments of many optimizing techniques (e.g., Karmakar and Mujumdar, 2006; Qin et al., 2007; Rani and Moreira, 2010).

In the past decade, to minimize the costs for sampling labor many hydrometric and meteorological stations were outfitted with automated devices. One effect of reduced operational budget was the closing of many water quality stations, especially stations that sampled water to produce water quality data that required extensive analysis in laboratories. Moreover, even with High-Performance Computing (HPC) systems (e.g., see chapter 7), model performances for many water quality variables are still mediocre at best (Arhonditsis and Brett, 2004). The reason for these poor predictions is that water quality models often use constant input levels for water quality data between each two input timesteps (which are about one month) or calculate a linear interpolation between them. However, the water quality data are very dependent on water flow and temperature, meteorological conditions, and activities such as agriculture, mining, and urban development within the watershed. As a result, it is necessary to often increase the number of temporal observations or rejuvenate water-quality estimation techniques and update adaptive methods taking advantage of more

powerful computers and mathematical toolboxes.

The objective of this study was to lay out a methodology to construct from sparse datasets a daily time series for water-quality variables, required for modeling, decision making and river health assessments. The aim was to show a continuous change between two monthly measurements more realistically instead of using stepwise or linear interpolation usually used in water quality models. To address this objective, two Canadian rivers, the South Saskatchewan River and the Red Deer River, were selected for this study as examples of clear and turbid systems, respectively.

6.3 Methods

The study sites are two important rivers in the South Saskatchewan River Basin: the South Saskatchewan River (SSR) and the Red Deer River (RDR). These two rivers stem from the Rocky Mountains in Alberta, Canada, and merge near the Alberta-Saskatchewan border (Figure 6.1). About 171 km downstream of the confluence they provide 98% of inflow into Lake Diefenbaker, one of the most important sources of water in Saskatchewan. Lake Diefenbaker (with a length of about 182 km) has two primary outflows: one at the Gardiner Dam and the other at the Qu'Appelle River Dam. The majority of the outflow is through four pipes that pass the water into hydroelectric generators at the Gardiner Dam. Then the river flow through the city of Saskatoon and eventually merges with the North Saskatchewan River downstream of the city of Prince Albert. From the confluence, the river has the name of Saskatchewan River and enters the province of Manitoba and finally discharging into Lake Winnipeg. The outflow from the Qu'Appelle River Dam enters into the Qu'Appelle River and eventually merges with the Red River in Manitoba, which also discharges into the Lake Winnipeg. Lake Winnipeg itself drains into Hudson Bay which in turn discharges into the North Atlantic Ocean.

We chose two stations in Alberta, one on the South Saskatchewan River and the other on the Red Deer River, as examples of respective clear and turbid systems for the purpose of building the time series. These stations are located at Medicine Hat for the SSR and Bindloss for the RDR (Figure 6.1). Water quality data for the station at Medicine Hat

Figure 6.1: Map of the South Saskatchewan River and Red Deer River. The hydrometric stations are marked by red triangles on the map

were obtained from Alberta Environment and Sustainable Resource Development and from Environment Canada for the Bindloss station. The station at Medicine Hat has 607 days of measurements for 47 variables from 1970 to 2013; the station at Bindloss has 134 days of measurements for 37 variables from 1992 to 2012. Also, we were able to download the water quality database of South Saskatchewan River Basin from a newly launched Open Data Portal (published 2016–05–02) by Environment and Climate Change Canada. In this database, the water quality data for 93 water quality variables were collected from Federal and Provincial institutions for the period of 2000 – 2016 and combined into a single database; hence, has more consistent data.

To have the best choice of water quality parameters, we looked at the input data requirements for a comprehensive water quality model which would consider most of the parameters required for study of a waterbody. Among different water quality models, CE-QUAL-W2 was selected as an example of a comprehensive model. The CE-QUAL-W2 model has more than 40 years of development with a sophisticated eutrophication algorithm allowing use of many water quality variables. CE-QUAL-W2 is a two-dimensional surface water quality model with many successful applications to lakes, rivers, and estuaries in Canadian prairie reservoirs (Sadeghian et al., 2015; Terry et al., 2017), and globally (e.g., Smith et al., 2014; Torres et al., 2016). The model uses data from several groups of inorganic and organic nutrients, phytoplankton and zooplankton. The CE-QUAL-W2 has 28 state variables, 23 derived water quality variables and 73 water quality fluxes (Cole and Wells, 2015). Most of these variables are included in the monitoring programs and are directly available, but there were some that leave as to be calculated from a series of equations or based on the correlations with other variables.

The temporal resolution of the water quality data in the database was insufficient to be considered as good input for a water quality model. Therefore, we used the strategy by Hirsch et al. (1982) for finding seasonal patterns, slope estimators (long-term trends) and flow adjustment when applying trend analysis to complement a sparse data set with additional values. The first step of Hirsch et al. (1982) was finding seasonal trends and then applying long-term trends to the results and, finally, fine-tuning those values with patterns in discharge values. We combined all of these steps and produced daily time series for the

two selected rivers (SSR and RDR).

To cover the criteria used by Hirsch et al. (1982), we selected four variables to use as a base for finding the trends in the water quality data: date, Julian day (the number of days from the first day of January), discharge (Q) and water temperature. The date was used for capturing the long-term trends (slopes effects) in the water quality data because of climate change, land use change and use of different management practices. The Julian day starts with number one at the first of January each year and ends with 365 (366 in Leap years) and was effective for incorporating seasonal and sine shaped patterns in the water quality data. Daily discharge data were available from the hydrometric stations at the Medicine Hat and Bindloss. Both rivers had similar trends for discharge because both originate from snow melt in the Rocky Mountains. The water flow levels were at minimum (less than 100 m^3/s) in winter and peaked in summer (Figure 6.2). In summer 2013, both rivers experienced the greatest flow over the past 50 years with a peak of about 4,500 m^3/s in the SSR at the Medicine Hat station and close to 1,000 m^3/s in the RDR at the Bindloss station. Because of the high variations in the discharge in the short term and through the year, the discharge was an important component of the fitting method. Water temperature was calculated based on the correlation found between water temperature in the river and weekly average air temperature as described by Sadeghian et al. (2015). Water temperature was added to the calculations because most of the water quality variables are temperature dependent (Ji, 2008).

The time of the study was selected from the beginning of 2011 until the end of 2013 because of the flow characteristics in this period with a wet year in 2011, followed by a dry year in 2012 and the largest flood in the rivers in 2013. Also, there was a series of extensive studies at the Lake Diefenbaker downstream during 2011 – 2013 which the data could be used for.

We used 16 different fitting methods to find a correlation among any of the four variables (date, Julian date, Q, water temperature) and water quality variables in the database. We considered three orders of polynomial, Fourier series, Gaussian series and sine series and two orders of exponentials, and power fitting to determine trends. We found some combinations that had fairly strong correlation but still were not significant enough for building daily time

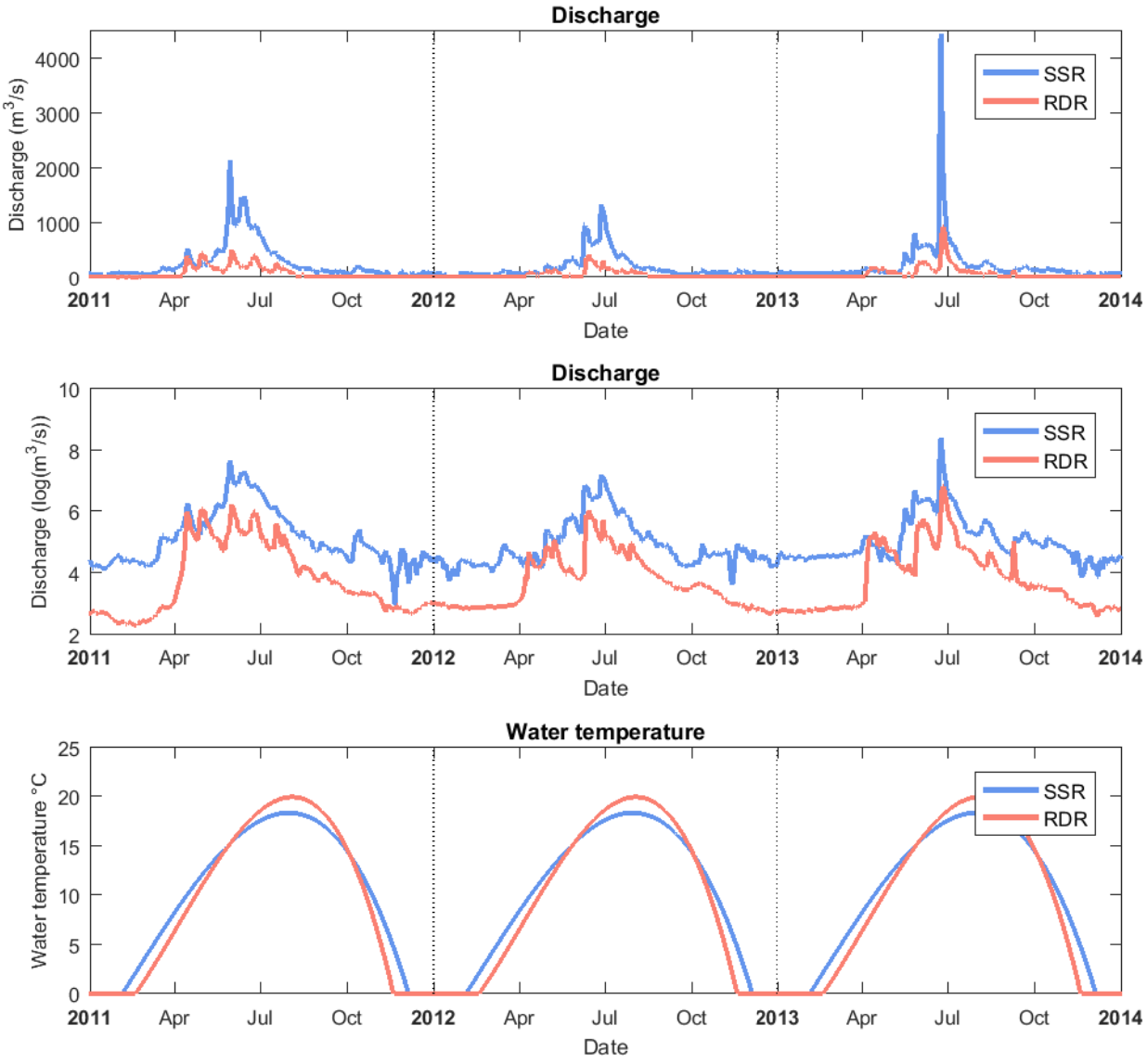

Figure 6.2: Discharge and water temperature data in South Saskatchewan River (SSR) at Medicine Hat station and Red Deer River (RDR) at Bindloss station for 2011 – 2014

series. Therefore, we used all the four variables at the same time in polynomial equations.

A first-order polynomial equation (Equation 6.1) used the water quality variable data (y), four data inputs (x_1 = date, x_2 = Julian day, x_3 = Q, and x_4 = water temperature), and

five coefficients (p_1, p_2, ... ,p_5) that needed to be solved.

$$y = p_1x_1 + p_2x_2 + p_3x_3 + p_4x_4 + p_5 \tag{6.1}$$

We used MATLAB to solve the polynomial equations using the "polyfitn" function (D'Errico, 2016). We found better performance by using logarithmic values of discharge because of the large difference between low flow and high flow conditions. Also, the Julian day was used as the sine of Julian day to avoid sharp changes in water quality variable concentrations at the end of each year (shifting from the value 365 to 1). The first-order polynomial fits well with the trends, however some details were missing in calculations.

We also used a second-order fitting (Equation 6.2) which required the equation for 15 coefficients to be solved by MATLAB.

$$\begin{aligned} y = {} & p_1x_1^2 + p_2x_1x_2 + p_3x_1x_3 + p_4x_1x_4 + p_5x_1 \\ & + p_6x_2^2 + p_7x_2x_3 + p_8x_2x_4 + p_9x_2 \\ & + p_{10}x_3^2 + p_{11}x_3x_4 + p_{12}x_3 \\ & + p_{13}x_4^2 + p_{14}x_4 + p_{15} \end{aligned} \tag{6.2}$$

In contrast to the first-order method, the second-order fitting captured all of the details, but some redundant peaks appeared in the series. To take advantage of the benefits of capturing the correct pattern from the first-order polynomial fitting and the detailed variations from the second-order method, we found that using an average of the first-order and second-order methods provided us with the best overall fittings.

6.4 Results and Discussion

The CE-QUAL-W2 model needs 28 state variables (Table 6.1) for a complete analysis of the system. There were no data available for iron, carbonaceous biochemical oxygen demand (CBOD), particulate silica and zooplankton in the databases, but the remaining 24 variables could be allocated. We started by building the water quality variable time series for the variables that were available directly in the database and then by making the

time series for those variables that were derived based on relationships with the other water quality variables.

Table 6.1: Variables used in CE-QUAL-W2 from model manual (Cole and Wells, 2013)

TDS	Total dissolved solids, mg/l
ISS	inorganic suspended solids, mg/l
PO_4	phosphate$_P$, mg/l as P
NH_4	ammonia$_N$, mg/l as N
NO_3	nitrate$_N$, mg/l as N
DSi	dissolved silica
PSi	particulate silica
Fe	iron, mg/l as Fe total
LDOM	labile dissolved organic matter, mg/l organic matter
RDOM	refractory dissolved organic matter, mg/l organic matter
LPOM	labile particulate organic matter, mg/l organic matter
RPOM	refractory particulate organic matter, mg/l organic matter
CBOD	carbonaceous biological oxygen demand group 1, mg/l O_2
ALG (three groups)	algal group, mg/l organic matter (dry weight)
DO	dissolved oxygen, mg/l O_2
TIC	total inorganic carbon mg/l as C
ALK	alkalinity mg/l as $CaCO_3$
ZOO	zooplankton
$LDOM_P$	Total P in labile dissolved organic matter
$RDOM_P$	Total P in refractory dissolved organic matter
$LPOM_P$	Total P in labile particulate organic matter
$RPOM_P$	Total P in refractory particulate organic matter
$LDOM_N$	Total N in labile dissolved organic matter
$RDOM_N$	Total N in refractory dissolved organic matter
$LPOM_N$	Total N in labile particulate organic matter
$RPOM_N$	Total N in refractory particulate organic matter

The first variable was the specific conductance. Specific conductance has strong linear relationships with total dissolved solids (Thomas, 1986) (Figure 6.3) which is a state variable in the CE-QUAL-W2 model. The polynomial fitting method used in this study showed the trend in the specific conductance very well (Figure 6.4a). The concentrations peaked in winter when the flows were low and decreased in mid-summer when flows were high; hence, dilution due to flow could be a major factor in the specific conductance levels. TDS measurements were available for SSR, but were available only until spring 2012 for RDR. A linear relationship between observed TDS and specific conductivity showed that TDS levels accounted for about 53% of specific conductivity in SSR (Figure 6.3a) and about 60% of that in RDR (Figure 6.3b). The TDS values for the fitting lines in Figure 6.4b were based

on TDS data for the SSR, and specific conductivity fitting line (Figure 6.4a) converted to TDS for the RDR.

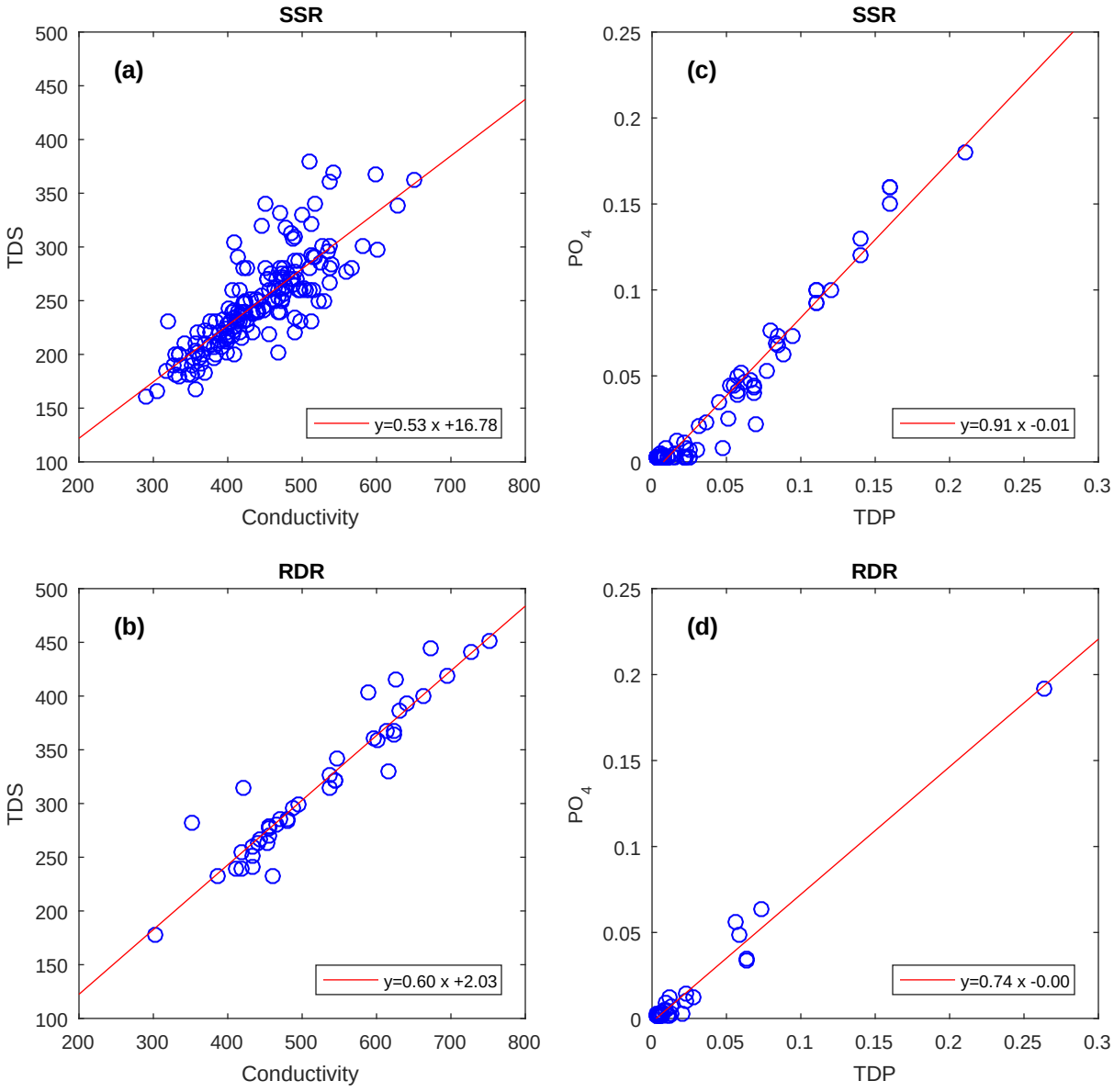

Figure 6.3: Correlations between different water quality variables in the South Saskatchewan River (SSR) at the Medicine Hat station and the Red Deer River (RDR) at the Bindloss station

Total dissolved phosphorus (TDP) is the sum of organic phosphorus compounds which come from algal excretion (Kuenzler, 1970) and inorganic phosphorus (PO_4) which is an

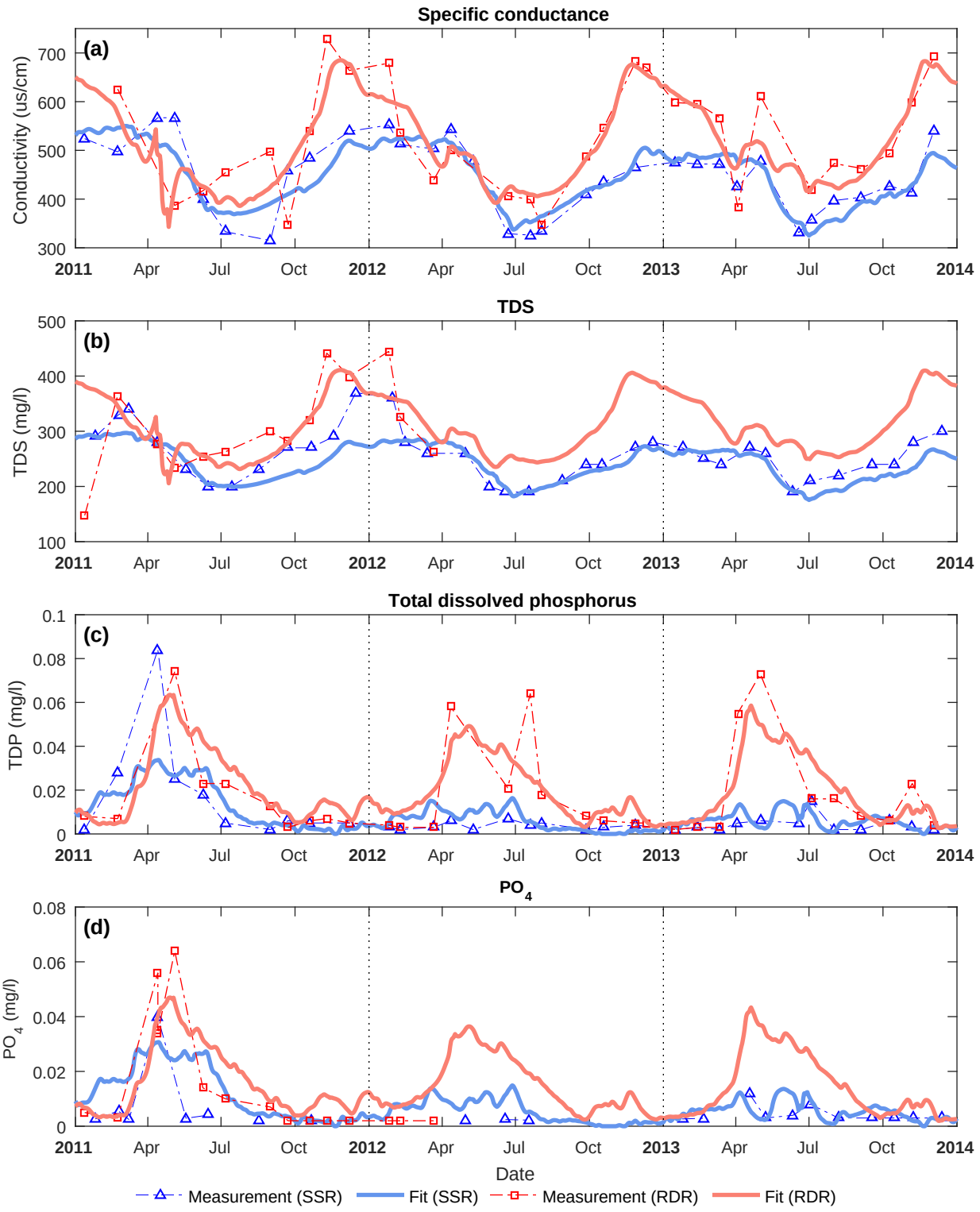

Figure 6.4: Daily time-series for different water quality variables: a) specific conductance, b) total dissolved solids, c) total dissolved phosphorus, d) phosphate. The concentrations of these variables are based on the averaged first-order and second-order polynomial fitting method in the South Saskatchewan River (SSR) at the Medicine Hat station and the Red Deer River (RDR) at the Bindloss station for 2011 – 2014

essential component of algal production (Pote and Daniel, 2000). The polynomial fitting method predicted the TDP concentrations very well for both rivers (Figure 6.4c). Water quality models require the inorganic fraction (PO_4) for simulating algal behaviors. Inorganic phosphorus showed strong linear correlation with TDP in both rivers with PO_4 equal to 91% TDP in SSR (Figure 6.3c), and 74% of that in RDR (Figure 6.3d). The results showed that a larger portion of TDP is available for algal uptake in SSR compared with RDR. Although the RDR has a smaller TDP to PO_4 ratio, the high amount of TDP makes the PO_4 concentrations relatively much higher in RDR (Figure 6.4d). Concentrations in the RDR derived from converting the TDP to PO_4 matched closely with the few observations that were available.

Inorganic phosphorus (PO_4) is the most common limiting nutrient for algal production in freshwaters; hence many restoration programs limit the discharge of this nutrient to freshwaters (Ortolani, 2014). However, because of the strong absorptive characteristics of phosphorus, the potential effects of buried phosphorus in sediment remain for a long time; hence many restoration programs suggest using total phosphorus (TP) instead or in addition to PO_4 for long-term rehabilitation (Havens and Walker Jr, 2002). Our predictions for TP were excellent except for one incident in summer 2012 in the RDR and one in the summer 2013 flood in the SSR (Figure 6.5a).

The CE-QUAL-W2 model uses nitrate (NO_3) plus nitrite (NO_2) as a single state variable (Cole and Wells, 2015). There are strict drinking water guidelines for NO_3 concentrations because of severe health problems associated with elevated levels of NO_3 in drinking water (Metzler and Stoltenberg, 1950). High NO_3 concentrations can promote eutrophication in nitrogen limited waters (McIsaac et al., 2001) and increase phosphorus internal loading from anaerobic sediments (Jensen and Andersen, 1992). The concentrations of NO_3 were higher in the SSR compared with that of the RDR, and both were predicted very well using the polynomial fitting method (Figure 6.5b). The patterns of concentration fluctuations in the SSR were similar to the that for specific conductivity with higher values in winter, but the concentrations in RDR showed a delay when peak concentrations occurred.

Ammonium (NH_4) in addition to NO_3 are the primary sources of inorganic nitrogen to algal photosynthesis for making chlorophyll pigments (Turpin, 1991). A study by McCarthy

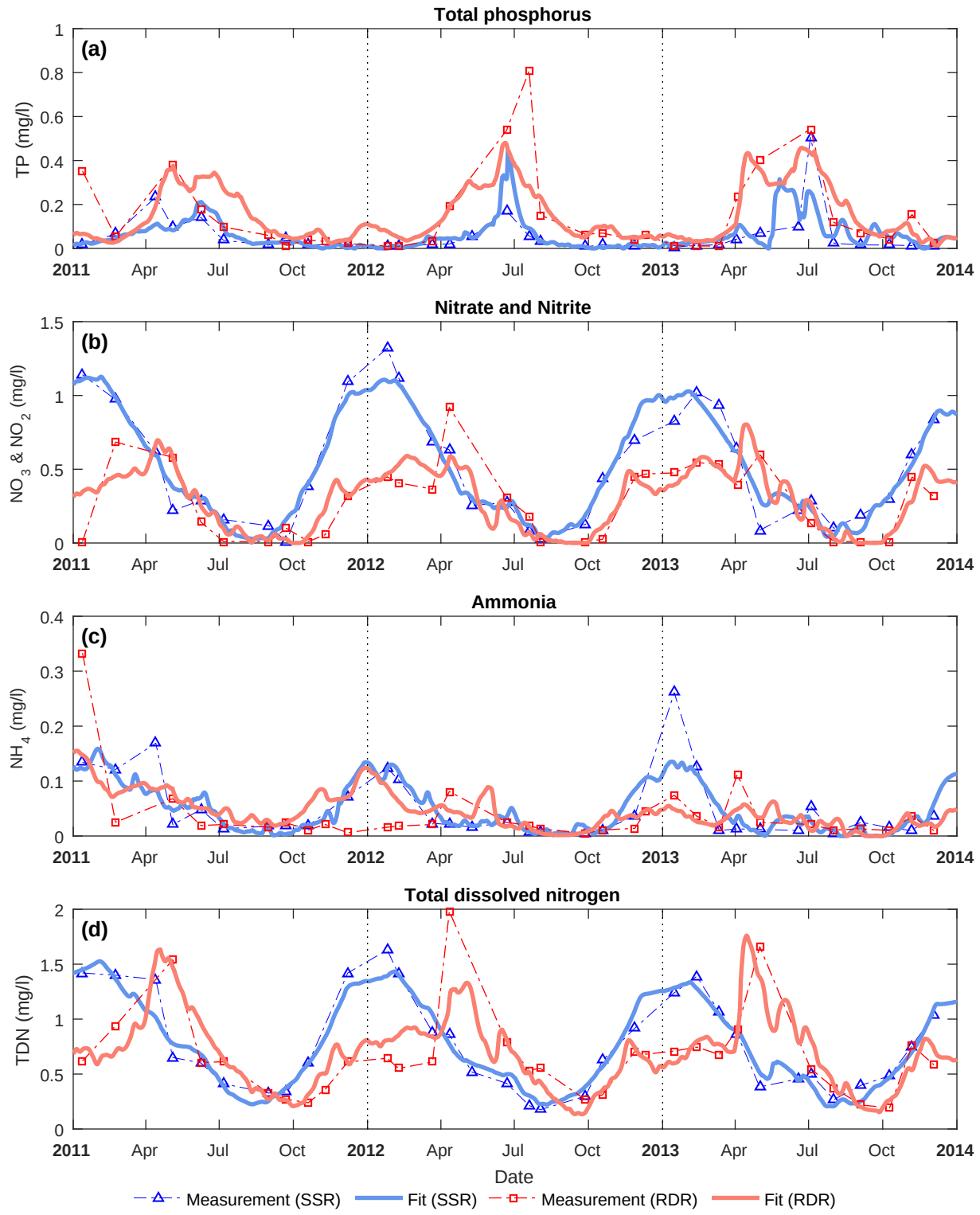

Figure 6.5: Daily time-series for different water quality variables: a) total phosphorous, b) nitrate plus nitrite, c) ammonia, d) total dissolved nitrogen. The concentrations of these variables are based on the averaged first-order and second-order polynomial fitting method in the South Saskatchewan River (SSR) at the Medicine Hat station and the Red Deer River (RDR) at the Bindloss station for 2011 – 2014

et al. (1977) showed that in non-limiting conditions NH_4 is preferred over NO_3 by algae when there is enough NH_4 available. In both the SSR and RDR, the concentrations of NH_4 seldom exceeds over 0.2 mg/l with only one occurrence in each river during 2011 – 2014 study period (Figure 6.5c). The fluctuation pattern and concentrations were very similar in both the SSR and RDR in all years.

To study the effects of the watershed on the quality of water, total dissolved nitrogen (TDN) is a reliable measurement because of it is transported easily by water and shows a quick response to precipitation which is a good indicator of land use and climate changes (Gallo et al., 2015). The fitting method results matched perfectly with the measurements in the SSR, but underestimated a peak in late spring 2012 for the RDR (Figure 6.5d). Particulate nitrogen (PN) has two main contributors: phytoplankton (eutrophic systems) and detritus (oligotrophic systems) (Caperon et al., 1976). The fitting method predicted the patterns well for PN except for the peak in summer 2012 in the RDR (Figure 6.6a).

The inorganic nutrients, especially the nitrogen and phosphorus, become aqueous when they are taken up by phytoplankton; hence many monitoring studies also measure total nitrogen (TN) and total phosphorus to consider the entire pool of nutrients (Guildford and Hecky, 2000). The TN is not a state variable in the CE-QUAL-W2 model, but a number of derived input variables in the model require TN for calculations. Total nitrogen measurements were available for the SSR and the fit line perfectly overlapped the observation values (Figure 6.6b). In the RDR, the measurements were only available until spring 2012, hence the sum of TDN and PN were used for TN calculations.

Algae are a major component of every water quality model and are affected by and as well affect the physical, chemical and biological characteristics of waterbodies. Algae require the physical conditions of thermal energy, light and particular water movement patterns for growth. Also, algae need nutrients mainly inorganic carbon, PO_4, NH_4, NO_3 and dissolved silica. Algae are producers of dissolved oxygen through photosynthesis and an oxygen consumer through respiration and also through decay of excreted organic matter and dead algae (Cole and Wells, 2015). The measurements of algal biomass are usually available in the form of chlorophyll a which needs to be converted into biomass (Wiltshire et al., 1998). Modelers use different approaches by using static or variable stoichiometric ratios

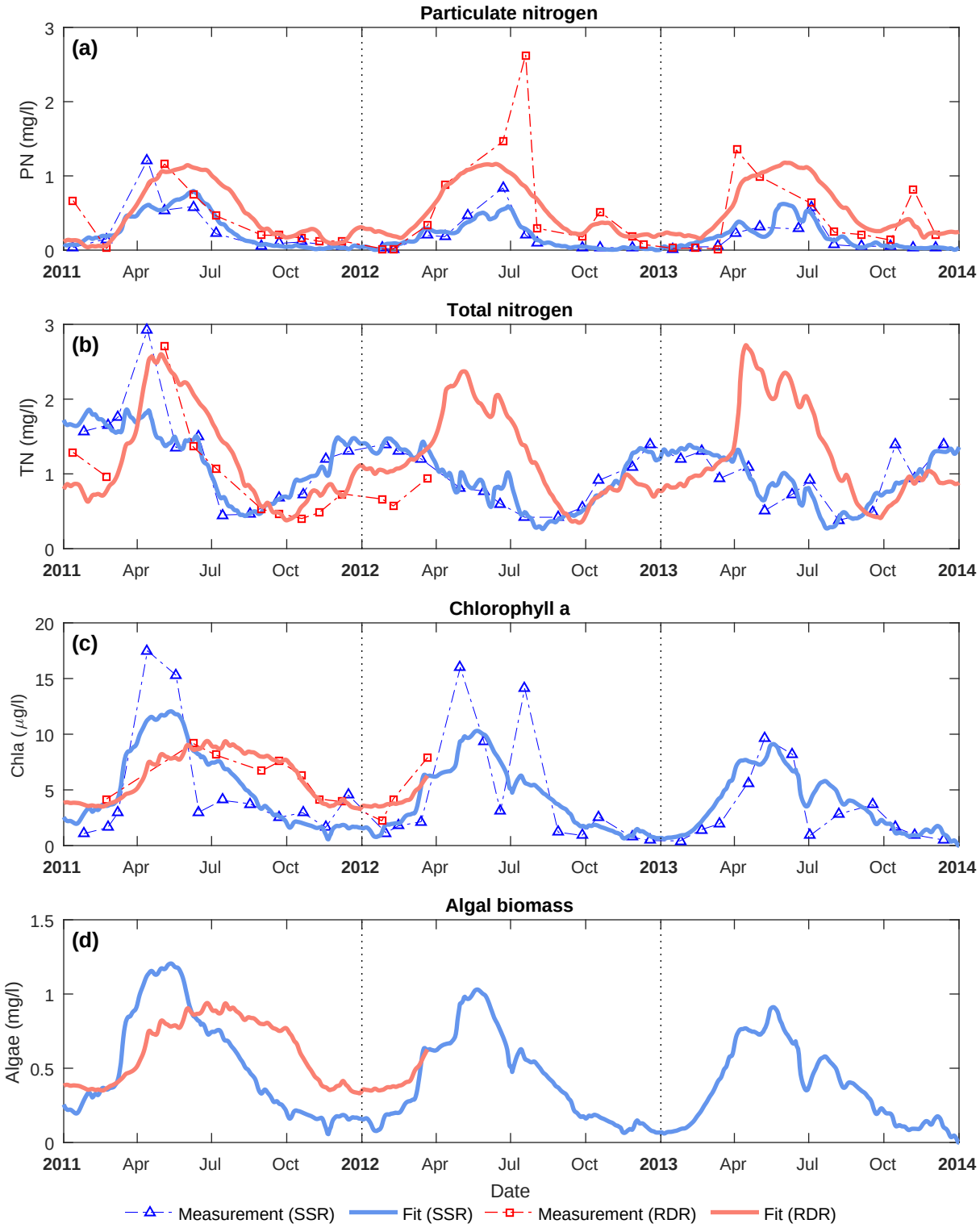

Figure 6.6: Daily time-series for different water quality variables: a) particulate nitrogen, b) total nitrogen, c) chlorophyll a, d) algal biomass. The concentrations of these variables are based on the averaged first-order and second-order polynomial fitting method in the South Saskatchewan River (SSR) at the Medicine Hat station and the Red Deer River (RDR) at the Bindloss station for 2011 – 2014

for converting chlorophyll *a* concentrations into algal biomass (chapter 7). Chlorophyll *a* measurements were available in the SSR for the entire study period but were only available until spring 2012 in RDR. We used algae to chlorophyll *a* conversion ratio of 100 in our calculations for calculating the algal biomass (Figure 6.6c). There are three species of algae that are used more frequently in water quality models: diatom, green algae, and cyanobacteria. Berger and Wells (2005) used species fractions of 60% for diatoms, 30% for greens algae, and 10% for blue-greens algae (cyanobacteria). Because there were no data available on the fractionation of algal species, we only showed the total algal biomass in the results (Figure 6.6d).

The amount of organic compound that passes through a 0.45 μm glass fiber filter is defined as the dissolved organic carbon (DOC) and the amount of residue retained by the filter is the particulate organic carbon (POC) (Evans et al., 2005). The DOC and POC need to be converted to dissolved organic matter (DOM) and particulate organic matter (POM) prior to use in the CE-QUAL-W2 model. Both DOC and POC decrease in winter and increase in summer because of flow and water temperature effects with the concentrations up to three times higher in the RDR than those of the SSR (Figures 6.7a and b). The polynomial fitting worked well with DOC in both rivers, but did not predict a peak of POC in the RDR in mid-summer 2012.

Dissolved organic matter is an oxygen consumer variable in the water quality models and decays to inorganic carbon, PO_4, and NH_4. The organic matter from mortality and excretion of phytoplankton added to DOM concentrations. Similar to DOM, the POM is also an oxygen consumer and also mineralizes into inorganic carbon, PO_4, and NH_4. The main difference is that the POM is only from phytoplankton mortality (no excretion), and a portion of POM deposits into the sediment which may either return to the water column or remain buried permanently. To convert organic carbon into organic matter, the organic carbon needs to be divided by the carbon to biomass ratio (Equations 6.3, 6.4 and 6.5). The carbon to biomass ratio had a value of $\delta c = 0.45$ in our calculations (Figures 6.7c and d).

$$DOM = DOC/\delta \tag{6.3}$$

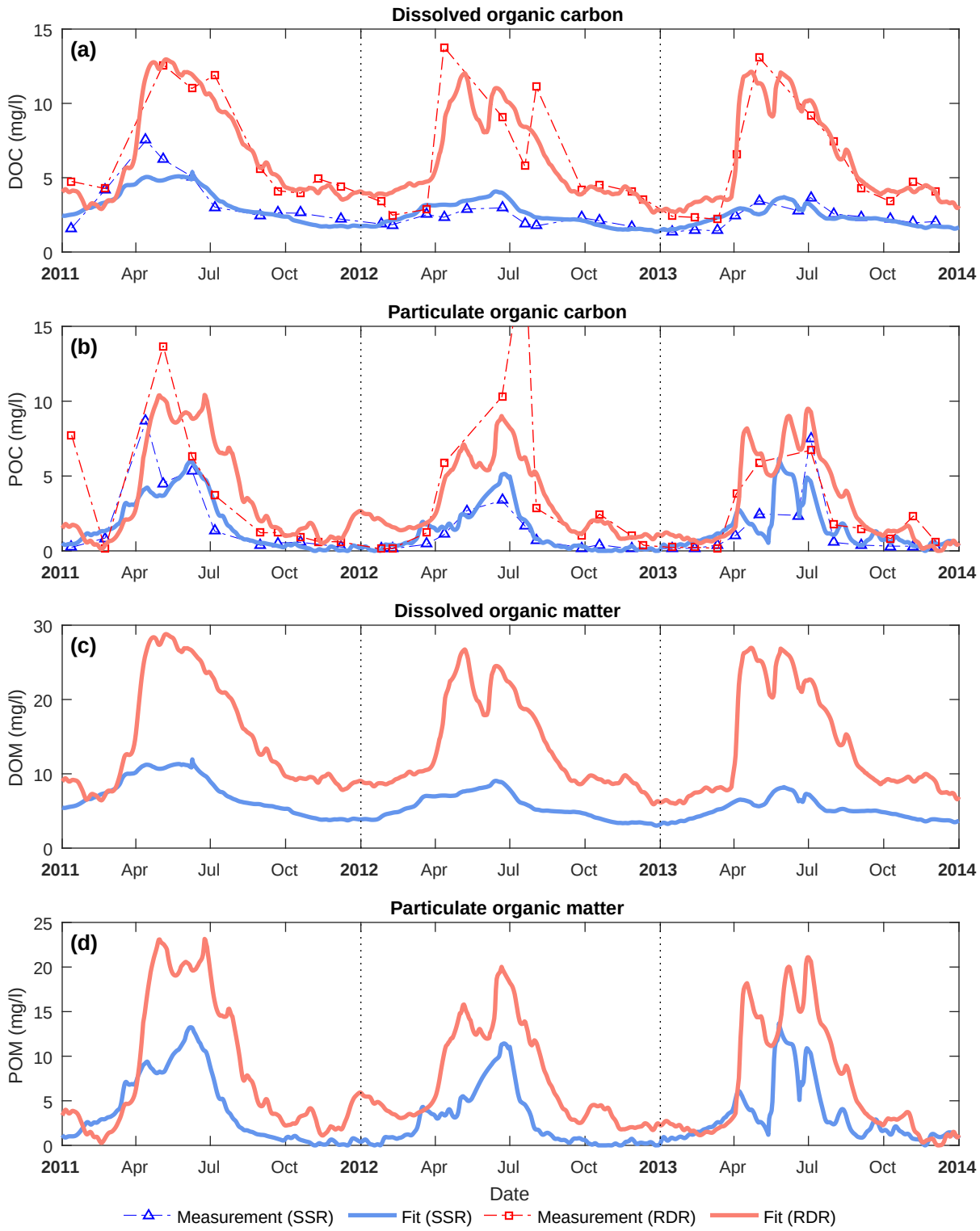

Figure 6.7: Daily time-series for different water quality variables: a) dissolved organic carbon, b) particulate organic carbon, c) dissolved organic matter, d) particulate organic matter. The concentrations of these variables are based on the averaged first-order and second-order polynomial fitting method in the South Saskatchewan River (SSR) at the Medicine Hat station and the Red Deer River (RDR) at the Bindloss station for 2011 – 2014

$$POM = POC/\delta \tag{6.4}$$

Total organic carbon (TOC) is calculated as the sum of DOC and POC (Figure 6.8a). The derived TOC showed much higher levels in the RDR compared with the SSR because of higher DOC and POC concentrations. Similar to DOC and POC, total organic carbon is converted into the organic matter by dividing the organic carbon by the carbon to biomass ratio (Equation 6.5) which had a value of δc = 0.45 in our calculations (Figure 6.8b).

$$TOM = TOC/\delta \tag{6.5}$$

Both the DOM and POM have two forms: labile and refractory. The labile organic matter has a short decay rate of a few days to weeks, while the refractory organic matter has a longer decay rate of up to years (Ji, 2008). Therefore, the labile compounds are removed faster from the water than the refractory portion. For both the SSR and RDR, there were no data available for partitioning between the labile and refractory DOM/POM (LDOM, RDOM, LPOM, and RPOM). Hence, we considered equal fractions of labile and refractory groups and used an $\alpha = 0.50$ in our calculations (Equations 6.6 and 6.8), and therefore only plotted one graph for each of the dissolved and particulate forms (Figures 6.8c and d).

$$LDOM = \alpha \times DOM \tag{6.6}$$

$$RDOM = DOM - LDOM \tag{6.7}$$

$$LPOM = \alpha \times POM \tag{6.8}$$

$$RPOM = POM - LPOM \tag{6.9}$$

The phosphorus portion of the organic matter is used as a state variable in the CE-QUAL-W2 model. As guidelines from Berger and Wells (2005), the phosphorus portion of organic matter is calculated based on equations 6.10, 6.11, 6.12 and 6.13, assuming the phosphorus fraction of algae ($orgp$) to be equal to 0.005. Because there were no fractioning data

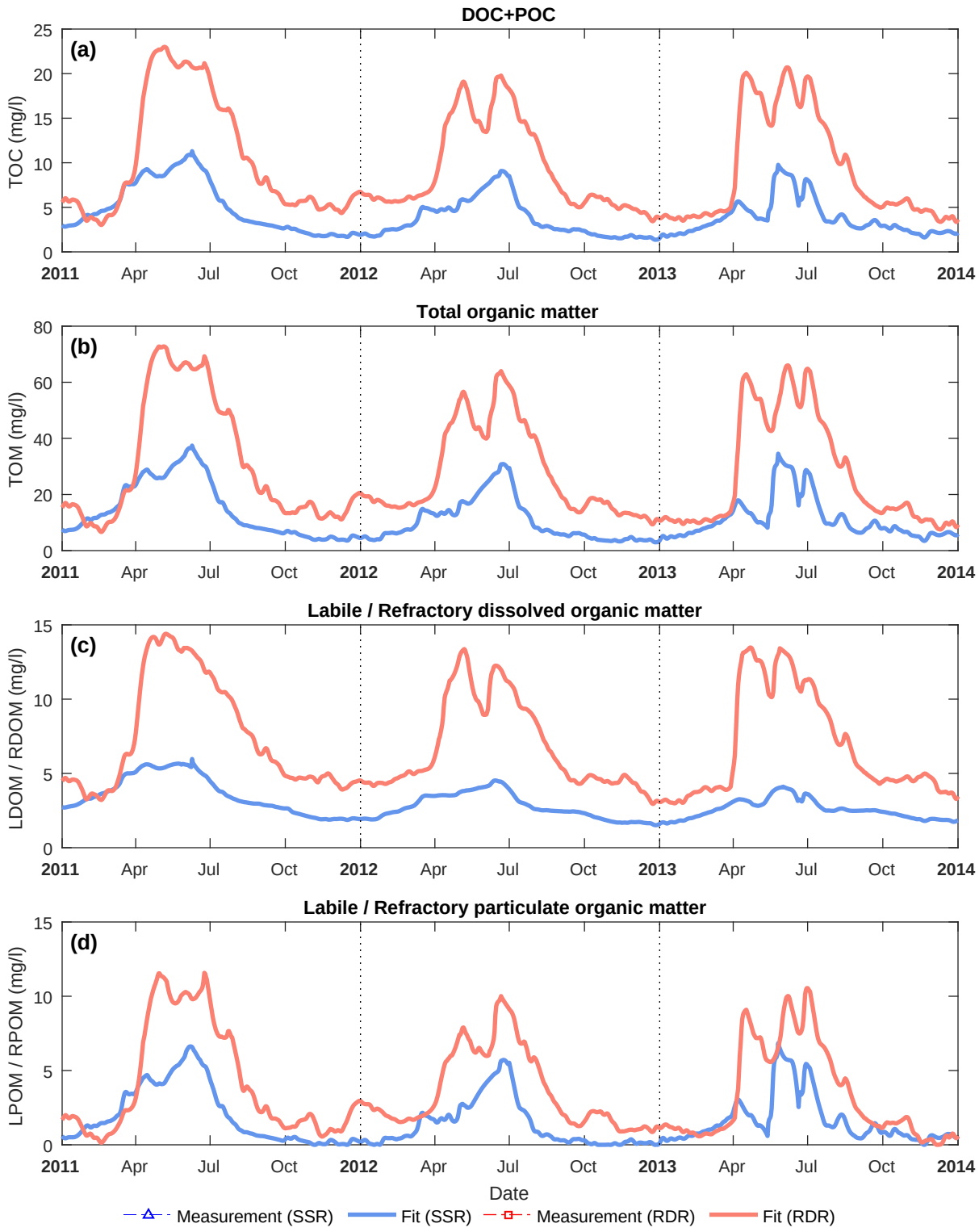

Figure 6.8: Daily time-series for different water quality variables: a) total organic carbon, b) total organic matter, c) labile/refractory dissolved organic matter, d) labile/refractory particulate organic matter. The concentrations of these variables are based on the averaged first-order and second-order polynomial fitting method in the South Saskatchewan River (SSR) at the Medicine Hat station and the Red Deer River (RDR) at the Bindloss station for 2011 – 2014

available for the labile and refractory organic matter, one graph was used for each of the dissolved and particulate forms (Figures 6.9a and b).

$$LDOM_P = (TP - PO_4 - \sum \text{Algae biomass} \times orgp)/TOM \times LDOM \quad (6.10)$$

$$RDOM_P = (TP - PO_4 - \sum \text{Algae biomass} \times orgp)/TOM \times RDOM \quad (6.11)$$

$$LPOM_P = (TP - PO_4 - \sum \text{Algae biomass} \times orgp)/TOM \times LPOM \quad (6.12)$$

$$RPOM_P = (TP - PO_4 - \sum \text{Algae biomass} \times orgp)/TOM \times RPOM \quad (6.13)$$

Similar to phosphorus, the nitrogen portion of the organic matter is also used as a state variable in the CE-QUAl-W2 model. As per guidelines by Berger and Wells (2005), the nitrogen portion of organic matter is calculated based on equations 6.14, 6.15, 6.16 and 6.17, assuming the nitrogen fraction of algae ($orgn$) to be equal to 0.08. Because there were no data available on fractioning between the labile and refractory organic organic matter, similar to phosphorus, only one graph was used for each of the dissolved and particulate forms (Figures 6.9c and d).

$$LDOM_N = (TN - NH_4 - NO_3 - NO_2 - \sum \text{Algae biomass} \times orgn)/TOM \times LDOM \quad (6.14)$$

$$RDOM_N = (TN - NH_4 - NO_3 - NO_2 - \sum \text{Algae biomass} \times orgn)/TOM \times RDOM \quad (6.15)$$

$$LPOM_N = (TN - NH_4 - NO_3 - NO_2 - \sum \text{Algae biomass} \times orgn)/TOM \times LPOM \quad (6.16)$$

$$RPOM_N = (TN - NH_4 - NO_3 - NO_2 - \sum \text{Algae biomass} \times orgn)/TOM \times RPOM \quad (6.17)$$

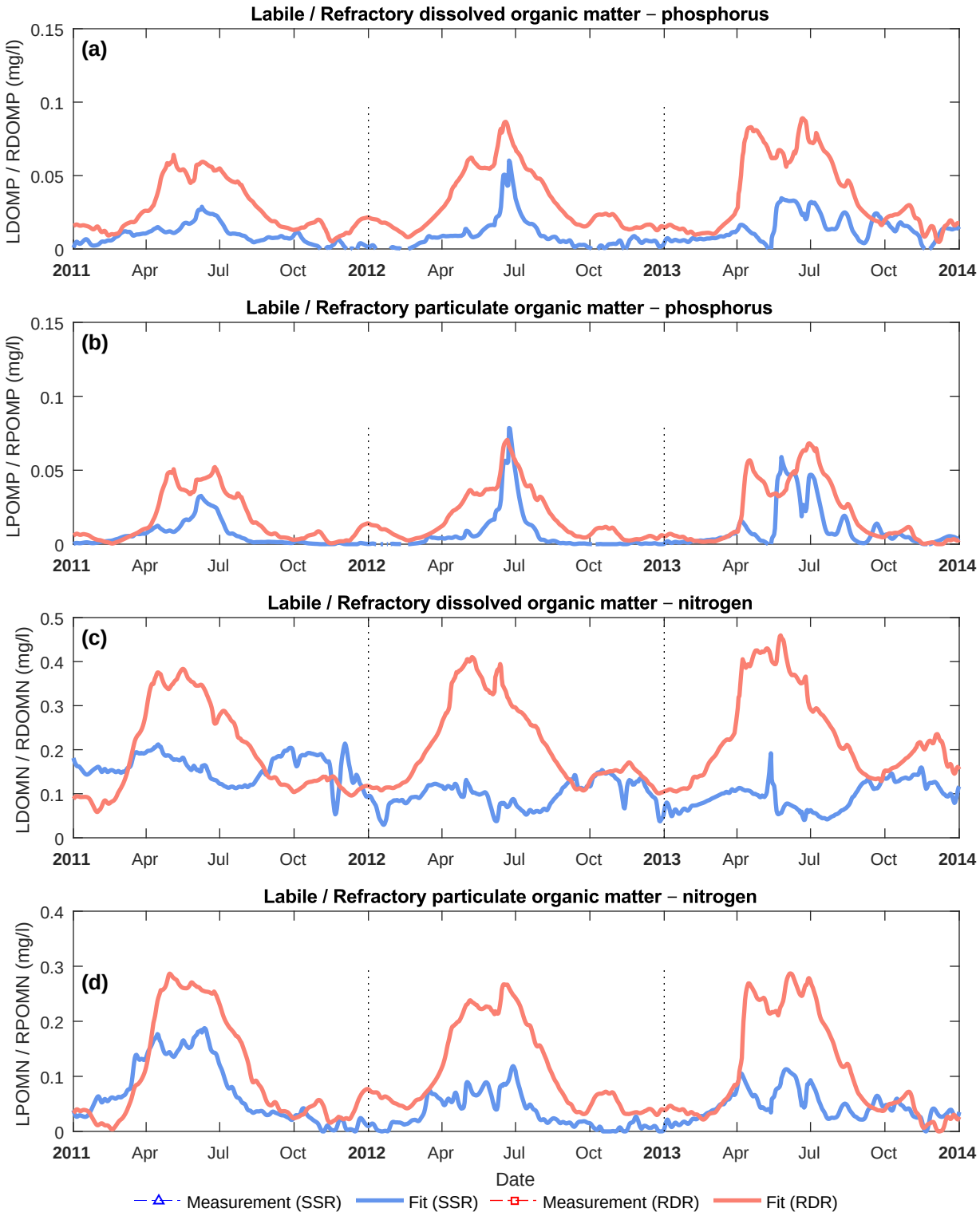

Figure 6.9: Daily time-series for different water quality variables: a) labile/refractory dissolved organic matter - phosphorus, b) labile/refractory particulate organic matter - phosphorus, c) labile/refractory dissolved organic matter - nitrogen, d) labile/refractory particulate organic matter - nitrogen. The concentrations of these variables are based on the averaged first-order and second-order polynomial fitting method in the South Saskatchewan River (SSR) at the Medicine Hat station and the Red Deer River (RDR) at the Bindloss station for 2011 – 2014

The non-filterable residue is the weighing of the residue left on a 0.45 μm glass fiber filter after filtering water, and is the standard method for measuring total suspended solids (TSS) concentration (Zhang and Zhu, 2006). In contrast with the specific conductance, the TSS concentrations were at a minimum in winter and a maximum in summer which shows their dependence on flow and erosion characteristics (Figure 6.10a). The flow in the SSR is several times higher than that of the RDR, but the TSS concentrations were almost double in the RDR. The main reason for that was the higher erosion rates in the RDR because of the steep river bed slope. There was a peak in TSS in June 2012 in the RDR that the polynomial fitting method did not predict well. June 2012 was the same time that the method failed to predict a peak in TP, PN and POC. If the reason was poor sampling of these variables, then it was captured by the fitting method; but, if the measurements were correct, then there would be questions regarding the accuracy of measurements in summer 2013 when the largest recorded flow in the both rivers occurred in 50 years. Inorganic suspended solids (ISS) is a state variable in the CE-QUAL-W2 model and is calculated as the total suspended solids minus the particulate organic matter (Figure 6.10b).

Dissolved oxygen (DO) has interactions with many water quality variables in water and represents the physical, chemical and biological characteristics of a waterbody very well (Sánchez et al., 2007). Dissolved oxygen is a water quality index in many regions (e.g., Boyacioglu, 2007; Cude, 2001; Kannel et al., 2007). Dissolved oxygen measurements were available for all the 2011 – 2014 study period in the SSR, but were available only until April 2012 in the RDR (Figure 6.10c). The DO results from the fitting method were among the best predictions among all the variables.

Dissolved silica is an essential nutrient for the growth of diatoms which considered a favorable form of algae. Dissolved silica is used for the development of the diatom skeleton (Cole and Wells, 2015). In silica limiting conditions, the diatom is succeeded by green algae and cyanobacteria which are less desirable (Koszelnik and Tomaszek, 2008). There were no measurements available for dissolved silica in the RDR, so only the values for the SSR were used in the fitting method. The measurements showed that dissolved silica had two peaks every year. The largest peak occurred in winter and was depleted by the end of spring. Another peak occurred in early summer after high summer flows (Figure 6.10d).

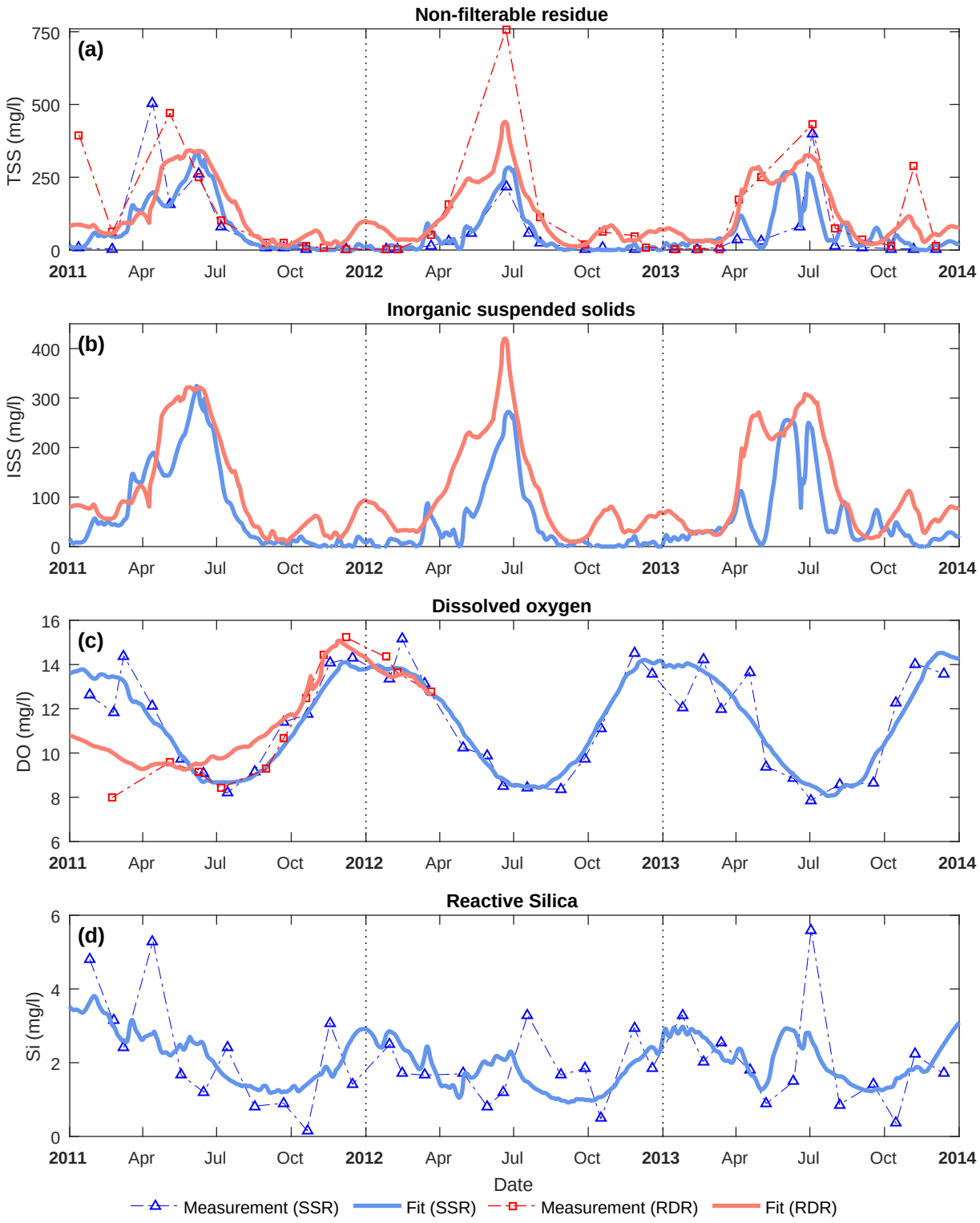

Figure 6.10: Daily time-series for different water quality variables: a) total suspended solids, b) Inorganic suspended solids, c) Dissolved oxygen, d) reactive silica. The concentrations of these variables are based on the averaged first-order and second-order polynomial fitting method in the South Saskatchewan River (SSR) at the Medicine Hat station and the Red Deer River (RDR) at the Bindloss station for 2011 – 2014

Alkalinity buffers the pH of water and can decrease the effects of toxins on aquatic organisms (Laurén and McDonald, 1986). In water quality models, alkalinity and total inorganic carbon (TIC) are used for prediction of the pH of water which in turn affects the chemical and biological reaction rates (Cole and Wells, 2015). The predictions for both alkalinity and pH closely were matched measured values (Figures 6.11a and b). Alkalinity was almost double in the RDR, but the pH levels were similar in the two rivers; hence the TIC should also show different patterns for the two rivers.

Total inorganic carbon (TIC) is a state variable in the CE-QUAL-W2 model. As mentioned above, TIC and alkalinity are used by the model for pH calculations. There were no measurements available for TIC in the SSR and the RDR. We used the "pH-CO_2" subroutine from the CE-QUAL-W2 model (Cole and Wells, 2015), which was based on the equations from Stumm and Morgan (1981), for back calculating the TIC values. The FORTRAN code for the "pH-CO_2" subroutine is available in the Appendix IV. Derived TIC values showed opposite patterns in the SSR and the RDR (Figure 6.11c). The main reason for this could be higher TOC and alkalinity levels in the RDR.

6.5 Conclusions

We developed a fitting approach for constructing a daily water quality database for the CE-QUAL-W2 water quality model from monthly measurements in the South Saskatchewan River (SSR) and the Red Deer River (RDR) which thoroughly covered the criteria used by Hirsch et al. (1982). The polynomial fitting method used four components: Julian day to capture seasonality, the date to incorporate long-term trends and seasonality, discharge to consider daily and seasonal effects of flow, and water temperature to maintain the temperature dependency of most water quality variables. Averaging the first and second-order polynomial fits provided the best outputs. The first-order polynomial fitting determines the seasonal patterns and the second-order fitting adjusts the small frequency variations to ensure no over-smoothing. Also, we were able to do mathematical operations on the water quality variables (e.g., TOC = DOC + POC) which previously was not possible because of different sampling dates.

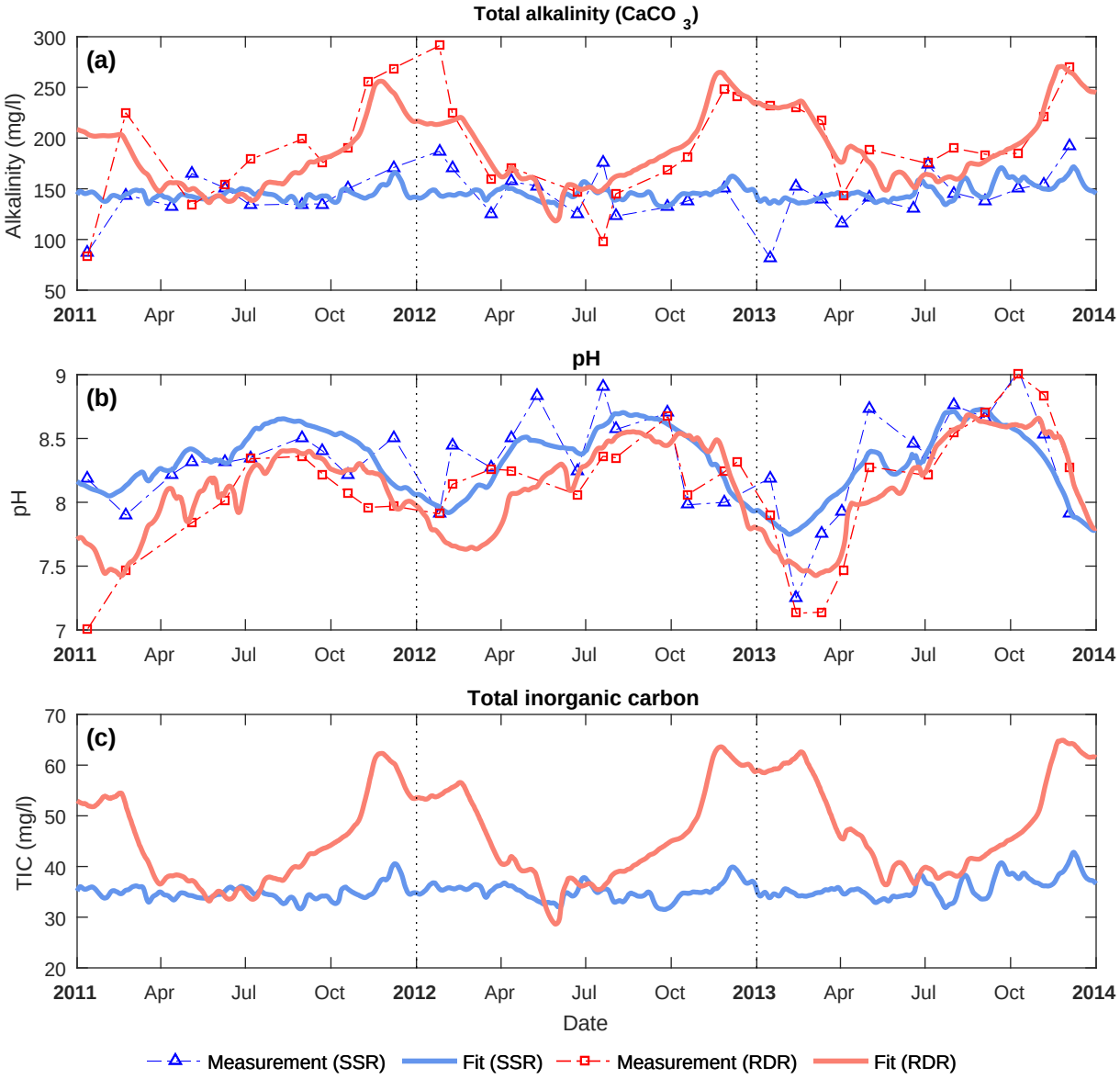

Figure 6.11: Daily time-series for different water quality variables: a) total alkalinity, b) pH, c) total inorganic carbon. The concentrations of these variables are based on the averaged first-order and second-order polynomial fitting method in the South Saskatchewan River (SSR) at the Medicine Hat station and the Red Deer River (RDR) at the Bindloss station for 2011 – 2014

The predictions were very good for both rivers, and we were able to capture the trends in almost all the variables. The results showed that the predictions were better for dissolved constituents compared to those for the particulate constituents. The main reason is that the dissolved substances are in solution and are distributed within the water column, whereas particulate forms are suspended in the water and may settle out on the river bed. Hence,

the particulate materials are more sensitive to when the measurements are made because they are deposited to the river bed when the flow velocity becomes slow.

The patterns of the concentrations were also easier to understand in the fitted lines. In general, the dissolved variables had their maximum in winter, while the particulate variables had their peaks in summer consequence to the peaks in flow intensity. There was a peak in the summer 2012 in the RDR that the polynomial fitting method did not predict well for some particulate water quality variables: Total suspended solids, total phosphorus, particulate nitrogen and particulate organic carbon. If the reason was an incorrect measurement, then it was captured by the fitting method, but if the measurements were correct then there would be questions regarding the accuracy of measurements in summer 2013 which were for the largest recorded flow in the rivers since 50 years ago.

Regarding the derived data, we had greater confidence in the data from the SSR compared to data from the RDR. The reason is that a larger number of measurements were available for the SSR and the fact that the RDR has data only until 2012 for some variables. Although the discharge in the RDR was several times smaller than that of the SSR, the dissolved and particulate constitutions showed several times larger concentrations. Hence, the nutrient contribution of both rivers could be significant to the water quality of downstream waterbodies.

6.6 Acknowledgements

This work was financially supported by the Canada Excellence Research Chair in Water Security through the Global Institute for Water Security. We thank Environment and Climate Change Canada, and Alberta Environment and Sustainable Resource Development for providing the hydrometric and water quality data.

References

Abbaspour, K. C., Yang, J., Maximov, I., Siber, R., Bogner, K., Mieleitner, J., Zobrist, J., and Srinivasan, R. (2007). Modelling hydrology and water quality in the pre-alpine/alpine Thur watershed using SWAT. *Journal of hydrology*, 333(2):413–430.

Arhonditsis, G. B. and Brett, M. T. (2004). Evaluation of the current state of mechanistic aquatic biogeochemical modeling. *Marine Ecology Progress Series*, 271:13–26.

Belle, G. and Hughes, J. P. (1984). Nonparametric tests for trend in water quality. *Water resources research*, 20(1):127–136.

Berger, C. and Wells, S. (2005). Lake Whatcom Water Quality Model. Technical Report EWR-03-05, Maseeh College of Engineering and Computer Science, Department of Civil and Environmental Engineering, Portland State University, Portland, Oregon.

Bowie, G. L., Mills, W. B., Porcella, D. B., Campbell, C. L., Pagenkopf, J. R., Rupp, G. L., Johnson, K. M., Chan, P., Gherini, S. A., Chamberlin, C. E., et al. (1985). Rates, constants, and kinetics formulations in surface water quality modeling. *EPA*, 600:3–85.

Boyacioglu, H. (2007). Development of a water quality index based on a European classification scheme. *Water Sa*, 33(1):101–106.

Caperon, J., Harvey, W. A., and Steinhilper, F. A. (1976). Particulate organic carbon, nitrogen, and chlorophyll as measures of phytoplankton and detritus standing crops in Kaneohe Bay, Oahu, Hawaiian Islands. *Pacific Science*.

Chapra, S. C. (2008). *Surface water-quality modeling*. Waveland press.

Cole, T. M. and Wells, S. A. (2013). *CE-QUAL-W2: A two-dimensional, laterally averaged, hydrodynamic and water quality model*. Department of Civil and Environmental Engineering, Portland State University, Portland, OR, 3.71 edition.

Cole, T. M. and Wells, S. A. (2015). *CE-QUAL-W2: A two-dimensional, laterally averaged, hydrodynamic and water quality model*. Department of Civil and Environmental Engineering, Portland State University, Portland, OR, 3.72 edition.

Cude, C. G. (2001). Oregon water quality index a tool for evaluating water quality management effectiveness. *JAWRA Journal of the American Water Resources Association*, 37(1):125–137.

D'Errico, J. (2016). Polyfitn function. *Mathworks Central Repository*. Available at: http://www.mathworks.com/matlabcentral/fileexchange/34765-polyfitn, Accessed: 7 march 2017.

Eatherall, A., Boorman, D., Williams, R., and Kowe, R. (1998). Modelling in-stream water quality in LOIS. *Science of the total environment*, 210:499–517.

Evans, C., Monteith, D., and Cooper, D. (2005). Long-term increases in surface water dissolved organic carbon: observations, possible causes and environmental impacts. *Environmental Pollution*, 137(1):55–71.

Gallo, E. L., Meixner, T., Aoubid, H., Lohse, K. A., and Brooks, P. D. (2015). Combined impact of catchment size, land cover, and precipitation on streamflow and total dissolved nitrogen: A global comparative analysis. *Global Biogeochemical Cycles*, 29(7):1109–1121.

Golterman, H. L., Sly, P. G., and Thomas, R. L. (1983). Study of the relationship between water quality and sediment transport: a guide for the collection and interpretation of sediment quality data.

Guildford, S. J. and Hecky, R. E. (2000). Total nitrogen, total phosphorus, and nutrient limitation in lakes and oceans: Is there a common relationship? *Limnology and Oceanography*, 45(6):1213–1223.

Halliday, S. J., Wade, A. J., Skeffington, R. A., Neal, C., Reynolds, B., Rowland, P., Neal, M., and Norris, D. (2012). An analysis of long-term trends, seasonality and short-term dynamics in water quality data from Plynlimon, Wales. *Science of the Total Environment*, 434:186–200.

Harmel, R., Smith, D., King, K., and Slade, R. (2009). Estimating storm discharge and water quality data uncertainty: A software tool for monitoring and modeling applications. *Environmental Modelling & Software*, 24(7):832–842.

Havens, K. E. and Walker Jr, W. W. (2002). Development of a total phosphorus concentration goal in the TMDL process for Lake Okeechobee, Florida (USA). *Lake and Reservoir Management*, 18(3):227–238.

Helsel, D. R. and Cohn, T. A. (1988). Estimation of descriptive statistics for multiply censored water quality data. *Water Resources Research*, 24(12):1997–2004.

Helsel, D. R. and Hirsch, R. M. (1992). *Statistical methods in water resources*, volume 49. Elsevier.

Hirsch, R. M., Slack, J. R., and Smith, R. A. (1982). Techniques of trend analysis for monthly water quality data. *Water resources research*, 18(1):107–121.

Hounslow, A. (1995). *Water quality data: analysis and interpretation*. CRC press.

Jensen, H. S. and Andersen, F. O. (1992). Importance of temperature, nitrate, and pH for phosphate release from aerobic sediments of four shallow, eutrophic lakes. *Limnology and Oceanography*, 37(3):577–589.

Ji, Z.-G. (2008). *Hydrodynamics and water quality: modeling rivers, lakes, and estuaries*. John Wiley & Sons.

Kannel, P. R., Lee, S., Lee, Y.-S., Kanel, S. R., and Khan, S. P. (2007). Application of water quality indices and dissolved oxygen as indicators for river water classification and urban impact assessment. *Environmental Monitoring and Assessment*, 132(1):93–110.

Karmakar, S. and Mujumdar, P. (2006). Grey fuzzy optimization model for water quality management of a river system. *Advances in Water Resources*, 29(7):1088–1105.

Koszelnik, P. and Tomaszek, J. A. (2008). Dissolved silica retention and its impact on eutrophication in a complex of mountain reservoirs. *Water, air, and soil pollution*, 189(1-4):189–198.

Kuenzler, E. J. (1970). Dissolved organic phosphorus excretion by marine phytoplankton. *Journal of Phycology*, 6(1):7–13.

Laurén, D. J. and McDonald, D. (1986). Influence of water hardness, pH, and alkalinity on the mechanisms of copper toxicity in juvenile rainbow trout, Salmo gairdneri. *Canadian Journal of Fisheries and Aquatic Sciences*, 43(8):1488–1496.

Lettenmaier, D. P. (1976). Detection of trends in water quality data from records with dependent observations. *Water Resources Research*, 12(5):1037–1046.

Mayer, D. and Butler, D. (1993). Statistical validation. *Ecological modelling*, 68(1-2):21–32.

McCarthy, J. J., Taylor, W. R., and Taft, J. L. (1977). Nitrogenous nutrition of the plankton in the Chesapeake Bay. 1. nutrient availability and phytoplankton preferences. *Limnol. Oceanogr*, 22(6):996–1011.

McIsaac, G. F., David, M. B., Gertner, G. Z., and Goolsby, D. A. (2001). Eutrophication: Nitrate flux in the Mississippi river. *Nature*, 414(6860):166–167.

Metzler, D. F. and Stoltenberg, H. A. (1950). The public health significance of high nitrate waters as a cause of infant cyanosis and methods of control. *Transactions of the Kansas Academy of Science (1903-)*, 53(2):194–211.

Ortolani, V. (2014). Land use and its effects on water quality using the BASINS model. *Environmental earth sciences*, 71(5):2059–2063.

Pote, D. and Daniel, T. (2000). Analyzing for total phosphorus and total dissolved phosphorus in water samples. *Methods of Phosphorus Analysis for Soils, Sediments, Residuals, and Water*, pages 94–97.

Qian, S. S. and Reckhow, K. H. (2007). Combining model results and monitoring data for water quality assessment. *Environmental science & technology*, 41(14):5008–5013.

Qin, X.-S., Huang, G. H., Zeng, G.-M., Chakma, A., and Huang, Y. (2007). An interval-parameter fuzzy nonlinear optimization model for stream water quality management under uncertainty. *European journal of operational research*, 180(3):1331–1357.

Rani, D. and Moreira, M. M. (2010). Simulation–optimization modeling: a survey and potential application in reservoir systems operation. *Water resources management*, 24(6):1107–1138.

Rode, M. and Suhr, U. (2007). Uncertainties in selected river water quality data. *Hydrology and Earth System Sciences Discussions*, 11(2):863–874.

Sadeghian, A., de Boer, D., Hudson, J. J., Wheater, H., and Lindenschmidt, K.-E. (2015). Lake Diefenbaker temperature model. *Journal of Great Lakes Research*, 41:8–21.

Sánchez, E., Colmenarejo, M. F., Vicente, J., Rubio, A., García, M. G., Travieso, L., and Borja, R. (2007). Use of the water quality index and dissolved oxygen deficit as simple indicators of watersheds pollution. *Ecological Indicators*, 7(2):315–328.

Shrestha, S. and Kazama, F. (2007). Assessment of surface water quality using multivariate statistical techniques: A case study of the Fuji river basin, Japan. *Environmental Modelling & Software*, 22(4):464–475.

Smith, E. A., Kiesling, R. L., Galloway, J. M., and Ziegeweid, J. R. (2014). Water quality and algal community dynamics of three deep water lakes in Minnesota utilizing CE-QUAL-W2 models. Technical report, US Geological Survey.

Smith, R. A., Schwarz, G. E., and Alexander, R. B. (1997). Regional interpretation of water-quality monitoring data. *Water resources research*, 33(12):2781–2798.

Stumm, W. and Morgan, J. J. (1981). *Aquatic chemistry*. Wiley.

Terry, J. A., Sadeghian, A., and Lindenschmidt, K.-E. (2017). Modelling dissolved oxygen/sediment oxygen demand under ice in a shallow eutrophic prairie reservoir. *Water*, 9(2):131.

Thomas, A. (1986). Specific conductance as an indicator of total dissolved solids in cold, dilute waters. *Hydrological Sciences Journal*, 31(1):81–92.

Torres, E., Galván, L., Cánovas, C. R., Soria-Píriz, S., Arbat-Bofill, M., Nardi, A., Papaspyrou, S., and Ayora, C. (2016). Oxycline formation induced by Fe (II) oxidation in a water reservoir affected by acid mine drainage modeled using a 2D hydrodynamic and water quality model—CE-QUAL-W2. *Science of the Total Environment*, 562:1–12.

Turpin, D. H. (1991). Effects of inorganic N availability on algal photosynthesis and carbon metabolism. *Journal of Phycology*, 27(1):14–20.

Van Griensven, A., Meixner, T., Grunwald, S., Bishop, T., Diluzio, M., and Srinivasan, R. (2006). A global sensitivity analysis tool for the parameters of multi-variable catchment models. *Journal of hydrology*, 324(1):10–23.

Wiltshire, K. H., Harsdorf, S., Smidt, B., Blöcker, G., Reuter, R., and Schroeder, F. (1998). The determination of algal biomass (as chlorophyll) in suspended matter from the Elbe estuary and the German Bight: A comparison of high-performance liquid chromatography, delayed fluorescence and prompt fluorescence methods. *Journal of Experimental Marine Biology and Ecology*, 222(1):113–131.

Zhang, Z. and Zhu, J. (2006). Characteristics of solids, BOD 5 and VFAs in liquid swine manure treated by short-term low-intensity aeration for long-term storage. *Bioresource technology*, 97(1):140–149.

Chapter 7

Water quality modeling of Lake Diefenbaker by using variable chlorophyll a/algal biomass ratio

This chapter is submitted to the journal of Environmental Modelling & Software. The submission id is: ENVSOFT–2017–582

Sadeghian, A., Chapra, S., Hudson, J. J., Wheater, H., and Lindenschmidt, K. E. Improving in-lake water quality modeling using variable chlorophyll a/algal biomass ratios.

Contributions of the candidate and co-authors

The candidate's contributions are follows: setting up and calibrating the Lake Diefenbaker water quality model; adding an algorithm to the CE-QUAL-W2 model for considering variable chlorophyll a/algal biomass ratio in algae simulations for better predictions of chlorophyll a concentrations; wring the manuscript. Karl-Erich Lindenschmidt was the supervisor and designed the whole study, and helped the candidate through the research process and manuscript writing. Howard Wheater was the co-supervisor and designed the overall vision of the research at the Global Institute for Water Security (GIWS). He supported the candidate financially as well as provided guidance in research and contributed comments on the manuscripts. Steven Chapra helped in applying the variable chlorophyll a/algal biomass ratio for the chlorophyll a calculation and by contributing comments.

7.1 Abstract

A water quality model of Lake Diefenbaker, a prairie reservoir in Saskatchewan, Canada was developed for which variable chlorophyll a/algal biomass ratios in simulations of algae concentrations were used. CE-QUAL-W2, a two-dimensional laterally averaged water quality model was implemented for this application. A top-down approach was considered by first developing a large, complex model and gradually simplifying it. The model with

variable chlorophyll a/algal biomass ratio was the simplified model which could be used to reproduce measurements for several water quality variables during the time frame 2011 – 2013. With some modifications to the source code of the CE-QUAL-W2 model, the chlorophyll a/algal biomass ratio parameter was designed to change based on the nutrient and light limiting conditions in the water column. A minimum of either nitrogen or phosphorus limitation was applied as the nutrient limiting rate and then the light limiting effects were incorporated into the calculations of the chlorophyll a/algal biomass ratio. Comparing the simulation results of the model with the variable chlorophyll a/algal ratio with those derived by using a static chlorophyll a/algal ratio showed 50% smaller errors in simulating algae concentrations. The main reason was that the chlorophyll a/algal ratio was not held constant during simulations, because, in reality, it changes dynamically through time and space based on light and nutrient availability in Lake Diefenbaker.

7.2 Introduction

Within a waterbody, the physical, chemical and biological variables can change in a short period of time (e.g., in hours) (Chapra, 2008). Examples are diurnal changes in dissolved oxygen, carbon dioxide (CO_2), and temperature (Yates et al., 2007). At the boundaries (e.g., inlets), these variations are even faster. For instance, suspended solids concentration is heavily dependent on flow rates. Based on the flow characteristics, suspended solids can settle to the bottom sediments or remain suspended within the water current. At high velocities, erosion and sediment resuspension add to suspended solids concentrations. Hence, when studying waterbodies with dynamic flow characteristics and changing water quality variables, short-term variations need to be considered to fully evaluate the system.

Generally, the temporal sampling frequencies and spatial distribution of stations in water quality databases are not satisfactory enough to carry out an accurate evaluation of the environment on which responsible agencies can make management decisions. Also, there are many external factors that must be taken into consideration because of their influence on the outcomes on management decisions. These factors include effects of climate change (Gosling and Arnell, 2016), land use changes (El-Khoury et al., 2015), increasing populations (Vörösmarty et al., 2000), industrial development (Aulakh et al., 2009), mining

activities (Schmidt et al., 2012), wastewater treatment plant affluents (Bunzel et al., 2013), agricultural tillage practices (Kachi et al., 2016) and fish, poultry and livestock farming (Herbst et al., 2012). The biggest problem with these activities is their contribution to both point source and nonpoint source contamination (e.g., pesticides) and nutrients (mainly phosphorus and nitrogen) discharged into waterbodies (Chislock et al., 2013; Wu and Chen, 2013). Water quality models are useful tools to compensate these limitations in water quality data and to consider effects of different sources of uncertainties.

Water quality models are used to address characteristics of the waterscape including complex geomorphology (Missaghi and Hondzo, 2010), complicated boundary conditions (Jin et al., 2007), and multidimensional internal processes (Kopmann and Markofsky, 2000). A typical water quality model might use hourly climate data, daily flow data and monthly chemical and biological data (James, 2016; Leon et al., 2011). A water quality model is often expected to produce high-resolution results (e.g., hourly) by using monthly input data (Hughes and Slaughter, 2016). Model results may be improved by using more complex processes (inclusion of fluxes and derived nutrient constituents) but at the cost of higher uncertainty levels due to over-parameterization (Freni et al., 2011). As a result, some modelers are tempted to move towards more complex models with higher dimensions [e.g., two and three-dimensional (2D and 3D)], while others believe that it is the quality of the observations and correctness of model theories that determine model accuracy, not model complexity (Reckhow, 1999).

Algal concentrations are representative of the health of aquatic systems, hence they are a component of any water quality models. Algae have many interactions with the inorganic and organic pools of nutrients in water. Therefore, the quality of the input data is critical for obtaining a correct algae simulation. As a result of low quality input data, most water quality models simulate algal behavior only moderately well, and poorly in most cases (Arhonditsis et al., 2006). In addition to the quality of input data, the other primary reason leading to poor algal results is using fixed growth, mortality, respiration, excretion, and settling rates for algae in models. In reality, algae adjust these ratios based on nutrient and light availability and temperature conditions (Ji, 2008). Algal biomass measurements are difficult to make so limnologists prefer measuring chlorophyll a concentrations (Ji, 2008). Since water quality models simulate algae as biomass, algae is converted to chlorophyll a

Table 7.1: Distance between different sections in SSR / RDR / LDF. For locations see Figure 7.1

From	To	Mileage (km)
Bindloss	Confluence	47
Medicine Hat	Confluence	203
Medicine Hat	Highway 4	374
Bindloss	Highway 4	218
Confluence	Highway 4	171
Highway 4	Gardiner Dam	161
Elbow	Qu'Appelle River Dam	19
Gardiner Dam	Saskatoon	120

by multiplying it with a chlorophyll a/algal biomass ratio. The chlorophyll a/algal biomass ratio is held constant during simulations, while, in reality, it changes dynamically through time and space based on light and nutrient availability (Chapra, 2008).

This study implemented a water quality modeling exercise on a prairie reservoir in Saskatchewan, Canada, where the measurements confirmed that algae adjust their chlorophyll a/algal biomass ratios based on phosphorus availability (Abirhire et al., 2015). Lake Diefenbaker is a strategic reservoir formed by the construction of two earth-filled dams (the Gardiner Dam and the Qu'Appelle River Dam) on the South Saskatchewan River (SSR) (Figure 7.1). The reservoir is 181 km long with increasing depth from 8 m at its upstream boundary, to 60 m at the Gardiner Dam (Sadeghian et al., 2015). Most of the inflowing water (∼98%) is from the SSR which merged with the Red Deer River (RDR) near the Alberta-Saskatchewan border (∼331 km upstream of the dams). The data on inflow to and outflow from Lake Diefenbaker is highly uncertain and the quality of the water quality data is limited. The closest hydrometric stations for water flow rates and sampling stations for water quality data are at Medicine Hat and Bindloss stations, 203 km and 47 km upstream of the SSR-RDR confluence (374 km and 218 km to reservoir), respectively (Table 7.1). The outflow from the reservoir was not measured directly at the Gardiner Dam but at the nearest station 120 km downstream of the dam in the city of Saskatoon. The closest meteorological stations are several kilometers away from the reservoir, and there were no buoy stations on this large strategic waterbody.

In this study, we endeavored to develop a water quality model for Lake Diefenbaker that could be used to support decision-making based on the limited water quality field

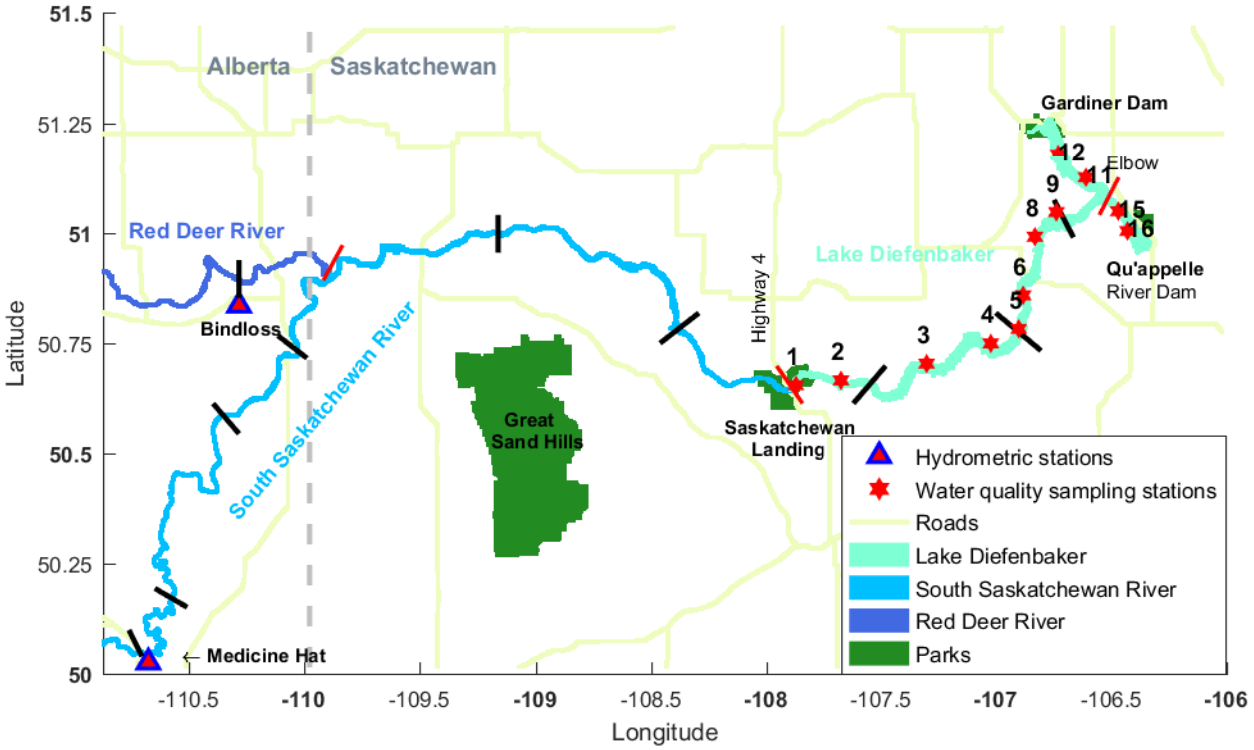

Figure 7.1: South Saskatchewan River (SSR) and Lake Diefenbaker (LDF), Alberta and Saskatchewan, Canada. The segmentations show different waterbodies (black lines) and branches (red lines) used by the CE-QUAL-W2 model. Blue triangles with red filling show locations of observation stations

measurements and highly uncertain boundary conditions of the reservoir. The general study objectives were to:

1. Evaluate measurement and observation requirements for a water quality model.
2. Address limitations and challenges for model calibration.
3. Present some techniques to improve the accuracy of model output (e.g., variable chlorophyll a/algal biomass ratio).

Specific objectives for the Lake Diefenbaker system were to:

1. Understand the physical, chemical and biological characteristics of the reservoir.
2. Estimate the rates of physical, chemical and biological changes in different parts of the reservoir.

3. Provide a predictive framework for applying available climate change and land use change scenarios.

7.3 Methods

The South Saskatchewan River is a long river (1,392 km) (Sheelanere et al., 2013) flowing through the Canadian provinces of Alberta and Saskatchewan. Merging with the SSR near the Alberta-Saskatchewan border, the Red Deer River (RDR) has turbid water due to the river's steep slope and prairie land setting. The average SSR flow is about 4.5 times larger than that of the RDR flow based on 50 years of daily data. Approximately 171 kilometers downstream of the SSR-RDR confluence is the inlet to Lake Diefenbaker at Highway 4 (Figure 7.1). The Lake Diefenbaker bifurcates near the village of Elbow due to the construction of the Gardiner and Qu'Appelle River dams in the 1960s. Most of the inflow (∼98%) comes from the SSR, and the main outflow (∼98%) flows north through the Gardiner Dam. Details on the physical characteristics of Lake Diefenbaker are available in Sadeghian et al. (2015). The hydrometric station for water flow rates and water quality sampling for SSR is at Medicine Hat, 374 km upstream of the reservoir, and for RDR is at Bindloss, 218 km upstream of the reservoir (203 km and 47 km upstream of the SSR-RDR confluence), respectively (Table 7.1). The outflow from the reservoir is used from the hydrometric station at city of Saskatoon, 120 km downstream of the Gardiner Dam.

There are some preliminary guidelines to estimate and interpolate the flow and climate data at the reservoir (Pomeroy and Shook, 2012). However, the same routing methods could not be used to estimate the nutrient input data for Lake Diefenbaker because comparable guidelines for predicting the chemical and biological constituents had not been developed by biologists and engineers. The reason is that many factors such as sedimentation, erosion, retention, point source (e.g., waste water treatment plants) and nonpoint source loadings (e.g., agriculture field surface runoff and groundwater infusion) could significantly change nutrient concentrations in the inflow to Lake Diefenbaker via the SSR. We found the best approach to estimate the state variable concentrations at the Lake Diefenbaker inlet was to first build the daily water quality database by correlating the water quality variables with the date, Julian day, discharge and water temperature (see Chapter 6) at the hydrometric stations. Then a simple model, which was calibrated with measurements at the most

upstream stations on Lake Diefenbaker, was employed to transfer these values to the Lake Diefenbaker inlet.

The current study required a model that can be implemented for both the river and reservoir systems. The length of the whole system from the hydrometric station on the South Saskatchewan River near Medicine Hat to the dams plus the distance from the Bindloss station at Red Deer River to the confluence is 602 km. Because the reservoir has a maximum depth of 60 m, a two-dimensional model was required to adequately simulate the hydrodynamics as well as resolve the longitudinal and vertical water quality gradients (lateral values are averaged). A third lateral dimension was not necessary because of the narrow width of the river and reservoir. We selected the CE-QUAL-W2 model which could be used to perform both hydrodynamic and water quality simulations in both the riverine (SSR and RDR) and the lacustrine (Lake Diefenbaker) parts of the system.

The CE-QUAL-W2 model is a 2D laterally averaged water quality model over 40 years in development. The US Army Corps of Engineers launched the model in 1975 (Edinger and Buchak, 1975). Developments continued by Edinger and Buchak for about ten years (Buchak and Edinger, 1984; Edinger and Buchak, 1978), and, in 1984, the model was handed over to a team led by Tom Cole. During the next 20 years, major refinement of both the hydrodynamic and water quality components were incorporated (Cole and Buchak, 1995; Cole and Wells, 2003a,b, 2006). After 30 years of progress, the US Corps of Engineers stopped model development, and the model was handed over to Portland State University. Model development is still continuing with an emphasis on computational efficiency, easier application through a graphical user interface and more efficient and accurate numerical schemes (Cole and Wells, 2008, 2013, 2015a,b).

The CE-QUAL-W2 model could be used to simulate all the major constituents and processes required for our research objectives including water temperature, hydrodynamics, dissolved/particulate solids, dissolved oxygen, nutrients, organic matter and algae. In addition, it had an up-to-date user manual and an active user forum. Finally, the source code was freely available with clear comments, allowing extension and application of new formulations and algorithms.

Model development for Lake Diefenbaker was carried out in several stages. We started by building a segmentation network of the SSR (Medicine Hat to Saskatchewan Landing) and Lake Diefenbaker (Saskatchewan Landing to dams), so the river was directly coupled with the reservoir. The benefits of such a system were numerous. Based on the water level of the reservoir and river discharge, flow at the upstream end of the reservoir can back up into the river. Because of these reverse flow effects in the reservoir, particularly at its upper end, the nutrients and flow characteristics were more accurately captured than with separate river and lake systems. Another benefit was that this combination reduced the need for data processing and transfer to the lake model. The main drawback was the computational cost. The calculation time for a combined river/reservoir system increased dramatically. The main reason was that the timestep requirement for the river is more stringent than for the reservoir. Much smaller timesteps were used for the reservoir than would be required if the model for the lake was ran independently of that for the river. Based on our access to the high-performance cluster (HPC) system of University of Saskatchewan, we found that the computational burden was justifiable at the first stage for calculating water quality state variables at the reservoir inlet. The CE-QUAL-W2 model is designed for WINDOWS platforms, so in order to run the model on the Linux HPC, the code was adapted and compiled for the CentOS (Linux) platform. The instructions on how to compile and run the code on Linux servers were added to the model user forum (http://w2forum.cee.pdx.edu/?q=node/500).

Although the model became more complex, nine inter-connected waterbodies, as delineated by black lines in Figure 7.1, were considered in the model. The reason for having several waterbodies permitted the use of different climate data stations, different water quality parameters and constants and different slopes for the river sections. Each waterbody had one main branch to which additional branches could be added. The additional branches were required to define a different slope or to connect a stream to the main river stem. One extra branch connected the RDR to the SSR, the second branch changes the river slope to almost zero when the river enters the reservoir at Saskatchewan Landing (see Figure 7.1), and the last branch was the Qu'Appelle arm at the downstream end. The model has 827 segments ranging in length from 200 m to 1200 m and has 60 Cartesian vertical layers, each one meter in thickness.

We considered algae, total dissolved solids (TDS), inorganic suspended solids (ISS), phosphate (PO_4), ammonium (NH_4), nitrate (NO_3), labile dissolved organic matter (LDOM), refractory dissolved organic matter (RDOM), labile particulate organic matter (LPOM), refractory particulate organic matter (RPOM), dissolved oxygen, dissolved silica and total inorganic carbon (TIC) in our simulations. We also used derived constituents in our outputs where we had measurements available: including dissolved organic carbon (DOC), particulate organic carbon (POC), dissolved organic nitrogen (DON), particulate organic nitrogen (PON), total nitrogen (TN), dissolved organic phosphorus (DOP), particulate organic phosphorus (POP), total phosphorus (TP), chlorophyll *a*, and total suspended solids (TSS). We calibrated the model based on measurements at the most upstream station (# 1 in Figure 7.1) by using the same methodology employed in the hydrodynamic model of Sadeghian et al. (2015). We used the model results to prepare the input data at the Lake Diefenbaker inlet.

To reduce computational expenditure, we excluded the riverine SSR-RDR sections and reduced the segmentation from 827 to 302 segments, keeping the vertical layers intact (Figure 7.2). The computation time decreased from 18 hours when the whole system (602 km) was considered to only 3 hours for each run on a desktop computer (Intel Core i7-3770S / 8 MB cache 3.4 GHz 5.0 GT/ 12 GB DDR3). Then, we calibrated the model using the same methodology.

By combining some segments, the number of segments in the *Lite* model was reduced to 87 segments of length 800 m – 4,000 m (Figure 7.2), and the layers were reduced to 21 ascending from 1 m at the water surface to 4.5 m toward the reservoir bed (Figure 7.3). More details on the *Lite* model preparation are provided in Table V.1. The computational time for the *Lite* model was less than five minutes.

The motive for development of the *Lite* model was that, in many cases, a fast and straightforward setup is more desirable. For example, during the 2013 Calgary flooding, a flood plume moved rapidly towards Lake Diefenbaker. When using the model as a predictive tool, reduced simulation times become invaluable. Another use of the *Lite* model is to test and verify new model formulations. For example, in this study, we have examined the effects of variable algal stoichiometry on the accuracy of chlorophyll *a* concentration calculations

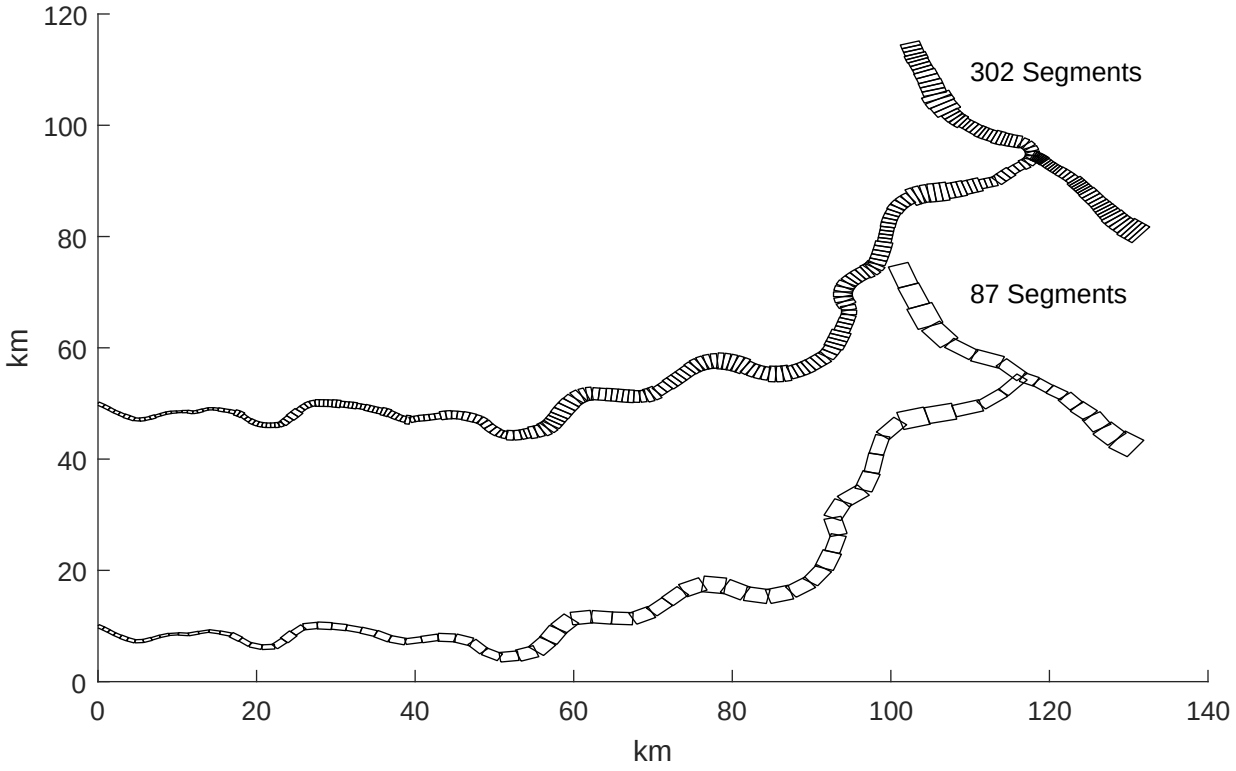

Figure 7.2: LDF model segmentation for the normal (fine) and *Lite* (coarse) models in CE-QUAL-W2

based on the formulations provided by Chapra (2008). We still have small layers within the euphotic zone, but the layering did not have any effect on the accuracy of the results.

7.4 Results

The CE-QUAL-W2 model has a complete set of output generation tools. It can print the outputs for almost every single component of the model for any longitudinal, vertical and temporal point. We prepared detailed plots for our visual calibration and also produced small files with outputs only for the measurement locations and times that were significantly smaller and faster for Monte-Carlo calibrations.

The model calibration was dependent on the parameters used in the model. For example, the light extinction coefficient is a function of algae, zooplankton, macrophyte and suspended solids (both inorganic and organic). In our model, we did not consider macrophytes and

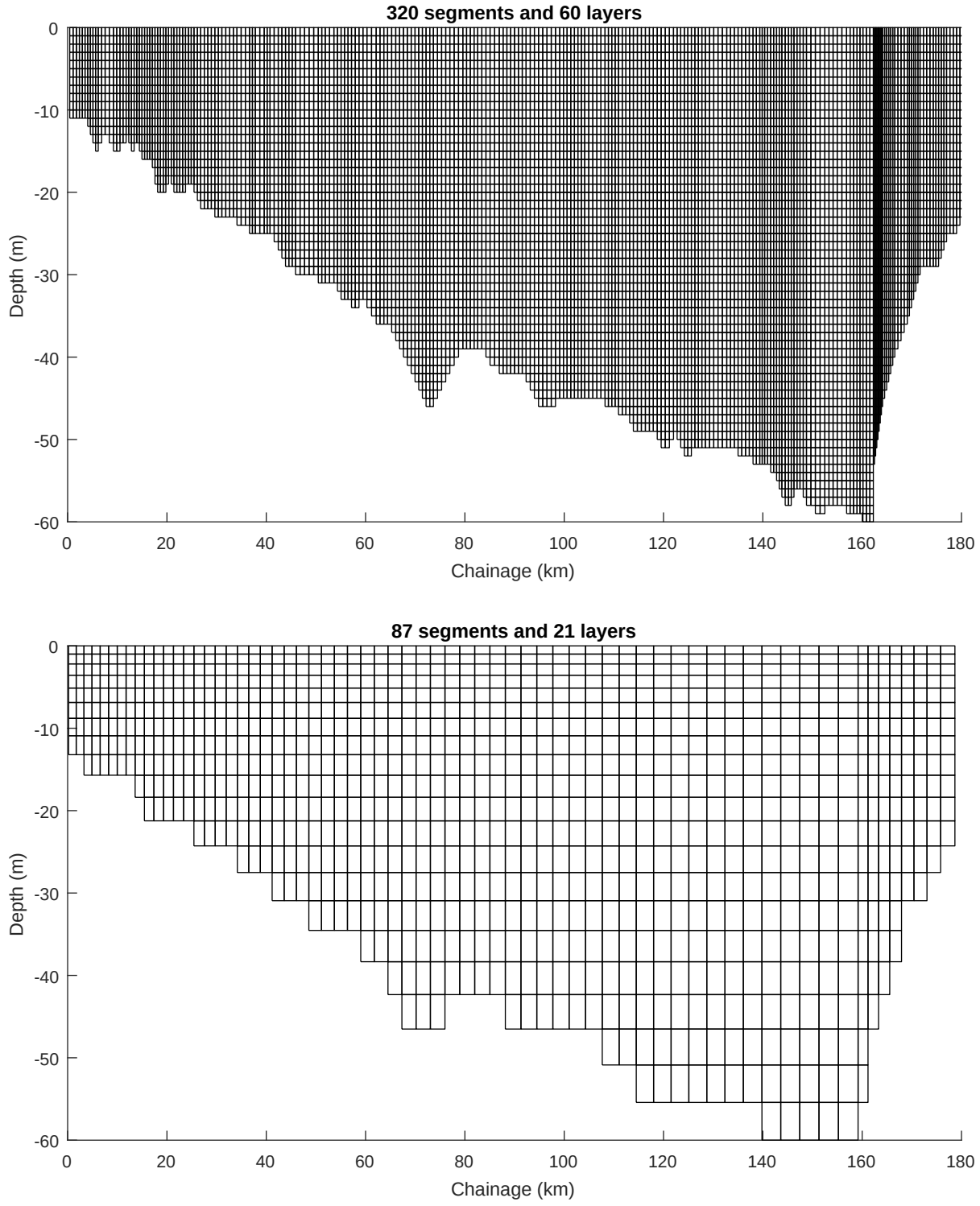

Figure 7.3: Lake Diefenbaker segmentation and layering for the normal (fine) and *Lite* (coarse) models

zooplankton. The influences of macrophytes was found to be negligible, whereas that of zooplankton was not. We compensated for the influence of zooplankton by using higher extinction values for algae and suspended solids.

Model calibration was done by comparing the simulated values for different water quality variables from the model with the measured values from the field works and laboratory analyses. The averaged root mean squared error ($\overline{RMSE}$) (Eq. 7.1) was used as the objective function for measuring the model performance statistically.

$$\overline{RMSE} = \frac{\sqrt{\frac{\sum (O-S)^2}{n}}}{\overline{O}} \tag{7.1}$$

where O are the observed and S are the simulated values. n is the number of samples and $\overline{O}$ is the average of observed values. The use of $\overline{RMSE}$ is preferred to the RMSE to normalize the error associated with different water quality variables. The optimum values of the parameters determined through the calibration are provided in Table V.1.

Water temperature and flow were the dominant factors influencing model calibration. Calibration of the thermal and hydrodynamic regimes are discussed in detail in Chapter 3. The next most influential variable was dissolved oxygen. Dissolved oxygen is an important water quality component, which can provide insight about the quality of water in the absence of other variables (Ji, 2008). Oxygen is necessary for the most of chemical and biological processes in the water (Figure 7.4). Due to the interdependence of nutrients, we first calibrated the DO, PO_4, NH_4, NO_3 and organic matter together to estimate the model coefficients. Then, the remaining parameters (TDS, ISS, DOC, POC, PON, TN and TP) were calibrated.

Based on our model setup, atmospheric aeration, algal photosynthesis and oxygen in inflow water were the sources of dissolved oxygen to the reservoir. Algal respiration, excretion and mortality, organic matter decay, nitrification and sediment oxygen demand were the consumers of oxygen. Similar to water temperature, DO measurements were based on Sonde-probes, yielding a higher number of measurements than those made in the laboratory. Therefore, the calibration was easier for DO and made with less uncertainty. The averaged

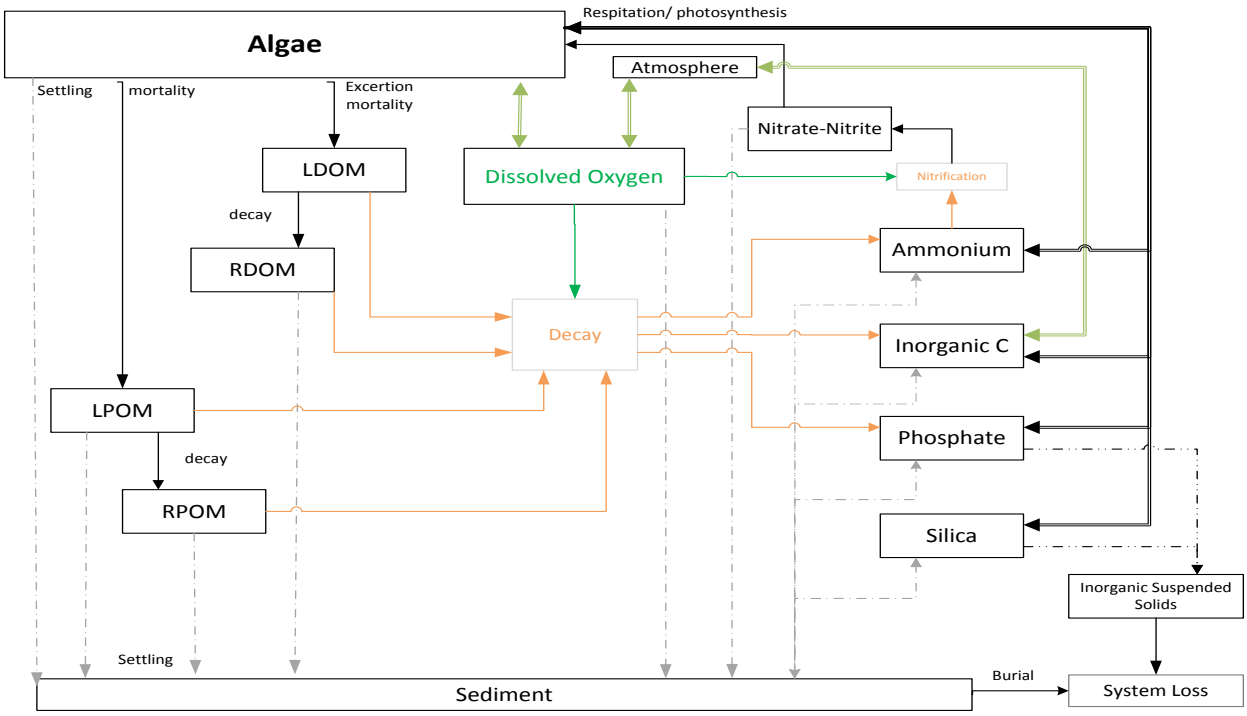

Figure 7.4: Simplified flow diagram of the components and interactions within the the CE-QUAL-W2 model based on CE-QUAL-W2 manual, (Cole and Wells, 2013). LDOM, RDOM, LPOM, RPOM are labile/refractory dissolved/particulate organic matter

root mean squared error ($\overline{RMSE}$) for dissolved oxygen based on 5,000 field measurements (one-meter vertical resolution) at 14 stations on 79 different days from 2011 to 2013 was 0.19 (Figure 7.5).

Inorganic nutrients used directly as inputs to the model were PO_4, NH_4, NO_3 and dissolved silica, and the organic components were algae biomass and organic matter concentration. There were also a few variables considered as derived variables. The main reason for using the derived variables was the availability of measured data. These variables included particulate organic carbon (POC), particulate organic nitrogen (PON), total nitrogen (TN) and total phosphorus (TP). Table V.2 contains equations for calculating the derived variables and their explanations.

Biological components of the CE-QUAL-W2 model are phytoplankton (algae), epiphyte/periphyton, macrophytes, and zooplankton (animals). Epiphyte and macrophytes are more related to the riverine and shallow waterbodies, and algae is more prevailed in

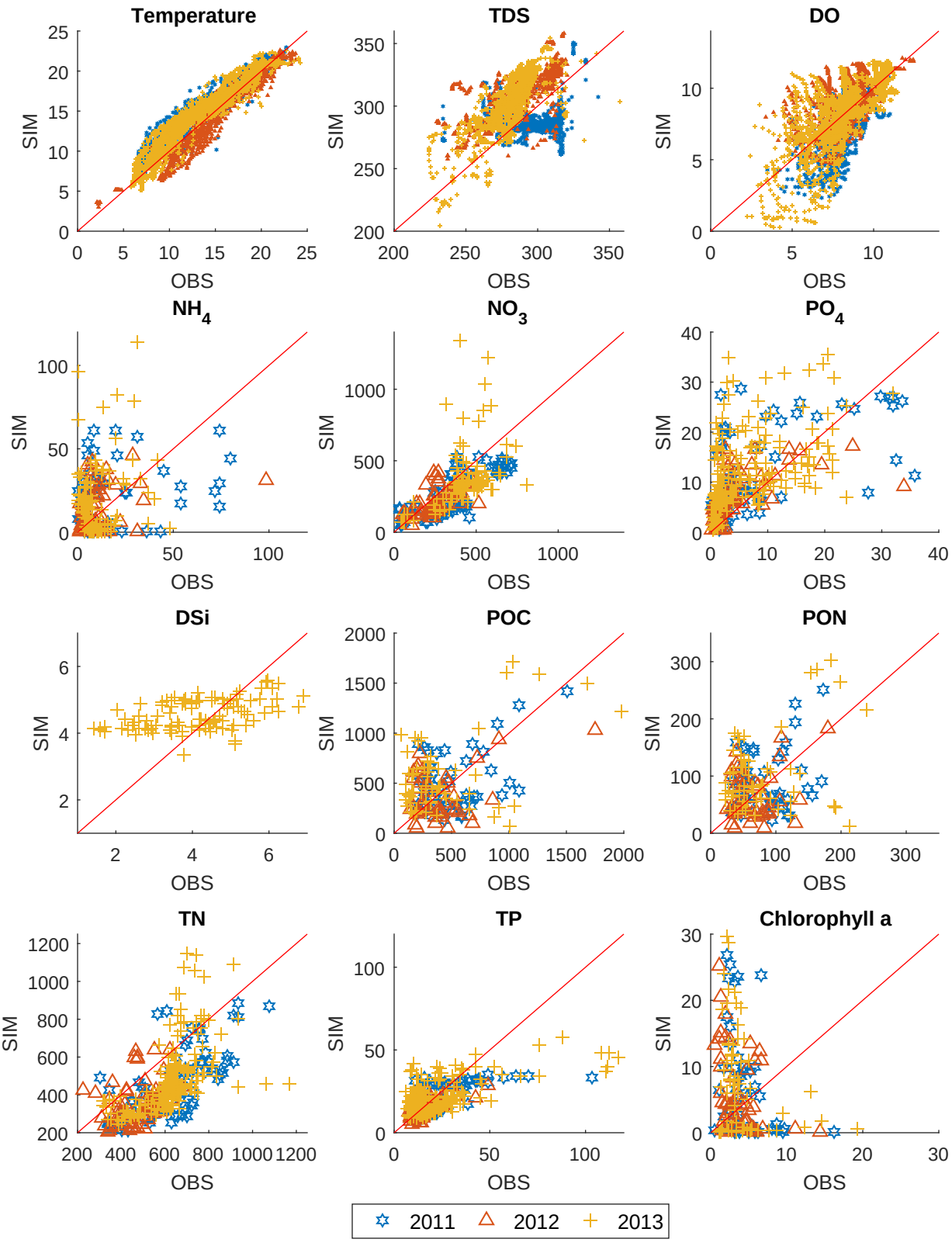

Figure 7.5: Model performance for the *Lite* model based on fixed ACHLA. OBS stands for observation values and SIM for simulated values

Table 7.2: Statistics for model performance in normal and *Lite* models

Model variable	$\overline{RMSE}$			Number of samples
	Normal	*Lite*		
	Fixed	Fixed ACHLA	Variable	
Chlorophyll a	2.28	2.22	1.15	159
DO	0.19	0.17	0.17	5135
*D*Si	0.47	0.29	0.29	98
NH_4	1.77	1.81	1.73	242
NO_3	0.49	0.45	0.48	239
PO_4	1.51	1.24	2.33	335
POC	1.67	0.77	0.75	156
PON	1.74	0.80	0.79	157
TDS	0.09	0.09	0.09	5186
TN	0.40	0.39	0.35	338
TP	0.75	0.67	0.75	337
Temperature	0.12	0.12	0.12	5186

lakes and reservoirs. In this study, data on zooplankton were not available, and the reservoir environment of Lake Diefenbaker led us to use algae as the sole biological component. The use of algae is challenging for the development of water quality models because it interacts with almost every single variable within the model (Figure 7.4). Other problems associated with the use of algae are the limited number of observations and that the measurements are mainly in the form of chlorophyll *a* concentrations which need to be converted to algal biomass.

To make the comparisons, either the chlorophyll *a* concentrations from measurements or the algal biomasses concentrations from simulations need to be converted to the other form. Algae biomass is multiplied by Algae/chlorophyll *a* ratio (ACHLA) to obtain chlorophyll *a* concentrations. ACHLA is a fixed value in the model; however, in a natural setting, this rate is not constant and changes based on light and nutrient availability. Chlorophyll *a* simulations were almost the poorest among all the variables (Table 7.2). Therefore, as a novel aspect of this study, with some modifications to the source code, the ACHLA parameter was designed to change based on the limiting conditions of water (Eq. 7.2 and 7.3). Equation 7.2 is based on the formulation suggested by Chapra (2008) and was successfully adopted in the 1D, steady state water quality model QUAL2K.

$$Chla/C = 6.4 + 45\Phi_n(1 - \Phi_L) \text{ (Chapra, 2008)} \tag{7.2}$$

$$ACHLA = \frac{1}{Chla/C} \text{ (Cole and Wells, 2015a)} \tag{7.3}$$

where $Chla$ is chlorophyll a, Φ_n is nutrient limiting factor ($0 \leq \Phi_n \leq 1$), and Φ_L is light limiting factor ($0 \leq \Phi_L \leq 1$).

The CE-QUAL-W2 model already calculates the limiting factor for algae production for nutrients (Eq. 7.4) and light (Eq. 7.5); therefore, only the conversion from Algal biomass to chlorophyll a needs to be adjusted.

$$\Phi_n = \frac{N}{N_{HS} + N} \text{ (Monod, 1949)} \tag{7.4}$$

$$\Phi_L = \frac{I}{I_k} exp(1 - \frac{I}{I_k}) \text{ (Steele, 1962)} \tag{7.5}$$

where N is nutrient concentration, N_{HS} is algal half saturation for nutrient limited growth, I is light intensity, and I_k is light saturation intensity at maximum photosynthetic rate.

A minimum of either nitrogen or phosphorus limitation was applied as the nutrient limiting rate and then the light limiting effects were incorporated into the calculations of the Chla:C ratio. Based on model results, ACHLA had a range of 20 to 130 (mg algae/mg chlorophyll a) for Lake Diefenbaker during 2011 – 2013 (Figure 7.6). The minimum ACHLA rate was at the upstream end of the lake in winter when light is most limiting. In terms of model performance, the $\overline{RMSE}$ value for chlorophyll a decreased from 2.28 to 1.15 (Table 7.2) (Figure 7.7), which is almost half of the $\overline{RMSE}$ value when we used a constant ACHLA.

TDS was treated as a conservative variable inside the model. TDS influences the movement of water by changing density and also affects pH. The measured TDS was considered as 65% of recorded electrical conductivity compared with the model simulations. Since the TDS is non-conservative, its concentration is mainly dependent on the correct inflow concentrations and accurate hydrodynamics. Interestingly, TDS simulations produced the lowest errors

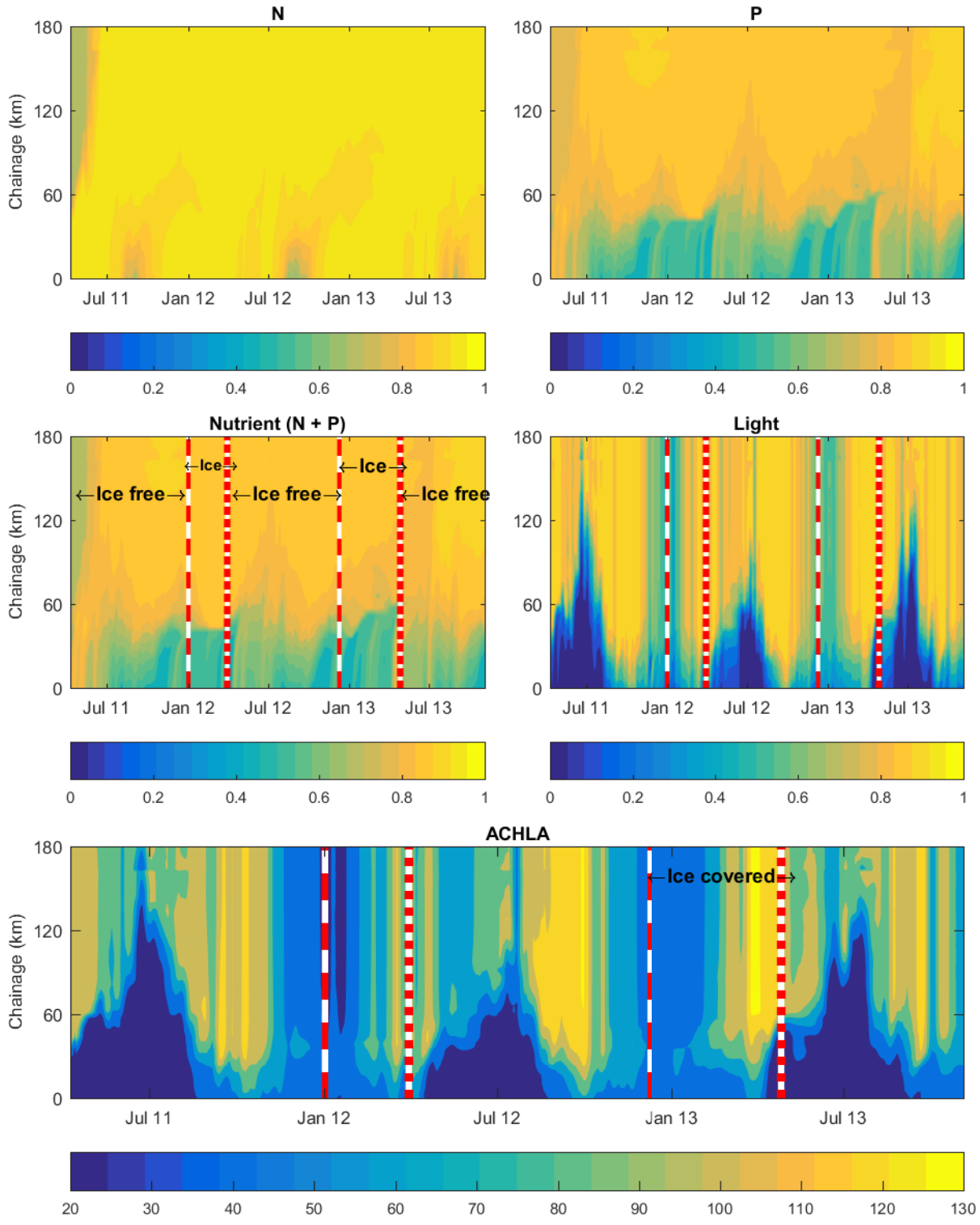

Figure 7.6: Top and left: nitrogen limiting for algal growth. Top and right: phosphorus limiting. Middle and left: nutrients (nitrogen and phosphorus) limiting. Middle and right: light limiting. Bottom: ACHLA values based on limiting conditions. All the sub-plots show the values at the depth of 2 m from the surface

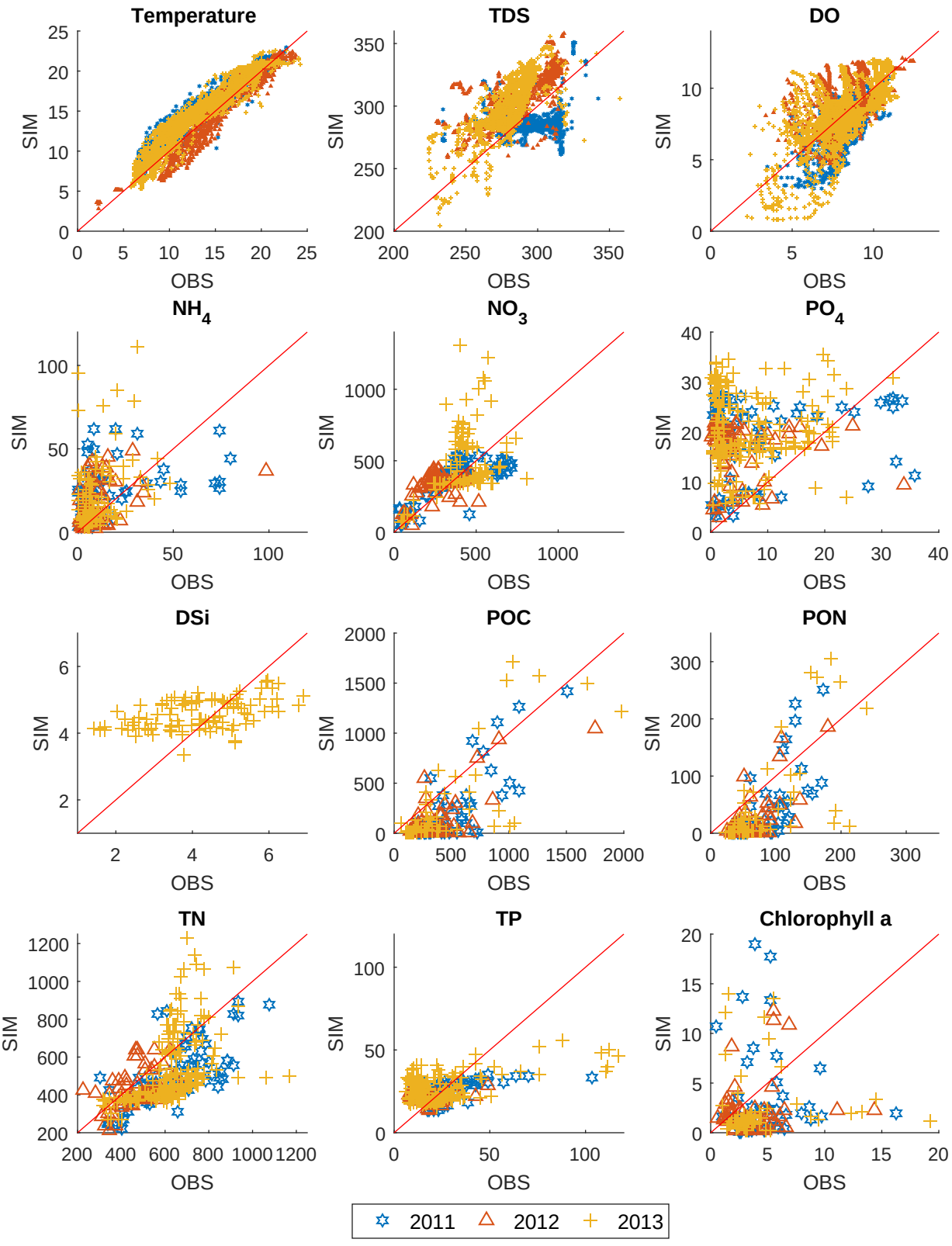

Figure 7.7: Model performance for the *Lite* model based on variable ACHLA. OBS stands for observation values and SIM for simulated values

among all the variables used for calibration (Table 7.2).

7.5 Discussion

Temperature, light, dissolved oxygen and nutrient availability (both inorganic and organic) determine the rates of chemical and biological reactions in water. Dissolved oxygen concentration is simple to calibrate but difficult to validate because many components interact with oxygen (Figure 7.4), with many parameters contributing to oxygen production and consumption. Additionally, incorrect model parameters can produce accurate results. For example, the decay of ammonium uses about four times more oxygen compared to organic matter decay. Although a decay rate of 0.1 day^{-1} for ammonium has the same mathematical effect on oxygen consumption as a decay rate of 0.4 day^{-1} for organic matter, the results on the nutrient pool are significantly different. To avoid an incorrect setup, DO, organic matter, PO_4, NH_4 and NO_3 were calibrated simultaneously (Figure 7.5). Due to a high number of observations for DO, the model results for DO have small uncertainties. Correctly predicting dissolved oxygen is a crucial part of water quality modeling because oxygen plays a vital role in the lives of aquatic organisms.

The model results showed that oxygen depletion occurred more in areas with higher ammonium concentrations. The ammonium stems from both the inflow (SSR) and organic matter decay. In lower dark layers of the lake, where algal activities are minimal due to poor light conditions, the oxygen depletion is higher (low photosynthesis). At these depths, nitrification is the primary oxygen consumer because three molecules of oxygen are required to convert two molecules of ammonium to two molecules of nitrite and another molecule of oxygen is required to convert those nitrite to nitrate (Eq. 7.6).

$$\begin{aligned} 2NH_4 + 3O_2 &= 2H_2O + 4H + 2NO_2 \\ 2NO_2 + O_2 &= 2NO_3 \end{aligned} \tag{7.6}$$

Ammonium and nitrate are not taken up by algae equally. Some algae groups may prefer ammonium over nitrate (Cole and Wells, 2015a), and the preference may change through the life of algae. For example, at early stages, algae may prefer ammonium but resort to nitrate as they mature (Aquarium-fertilizer, 2012). The Lake Diefenbaker model was

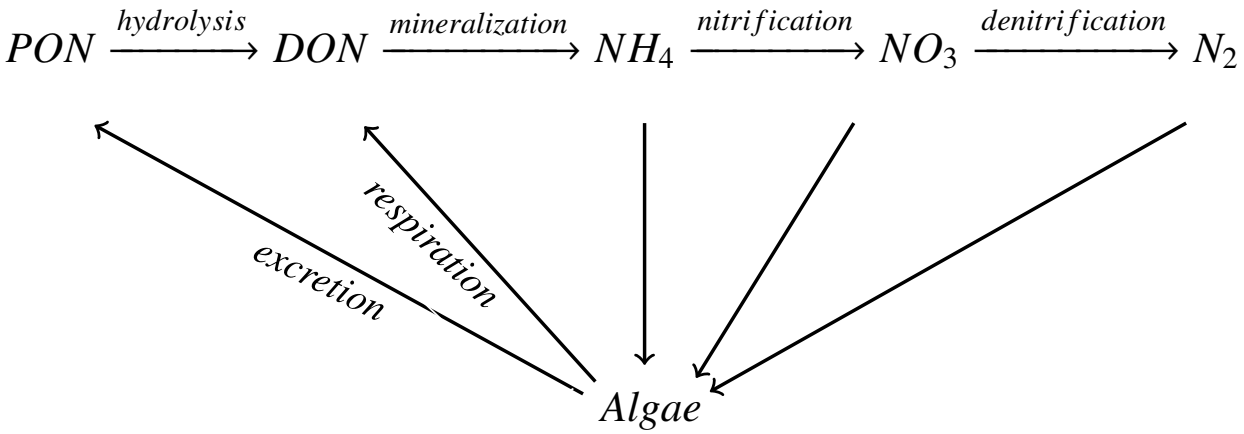

Figure 7.8: Simplified nitrogen cycle in water

not sensitive to the coefficient for algal nitrogen uptake preference (ANEQN) (between ammonium and nitrate). Because nitrate and phosphate were consumed by algae, oxygen depletion occurred more at the water surface. The decay of organic matter accompanied by formation and release of nitrate and phosphate from sediment was also an oxygen depleting process near the bed of the reservoir.

Both the dissolved and particulate forms of organic matter were considered in the model setup. Each group, was divided to two categories: liable (short decay time, e.g., days) and refractory (longer decay time, e.g., weeks to months). The main sources of organic matter into the system are the incoming concentrations by SSR inflow (external source) and algal production (in-lake process). The organic matter mineralizes to form inorganic nutrients and some of which deposit in the sediment (Figure 7.4). Algal mortality contributes to particulate organic matter, and algal excretion to both dissolved and particulate organic matter. An example of a simplified cycle of nitrogen, as a calibration variable in this model, is presented in Figure 7.8. Algae contribute to both the particulate and dissolved organic nitrogen through mortality, excretion and respiration. A portion of the particulate form goes into sediment (Figure 7.4) and a portion mineralizes into a dissolved form.

Since algae are a good representative of the health of aquatic system, they are a component of any water quality model. Algae have many interactions with inorganic and organic pools of nutrients in water. Looking into the example of the nitrogen cycle (Figure 7.8), algae interacts with five different forms of nitrogen. Therefore, quality of input data is critical

for obtaining a correct algae simulation. As a result of low quality input data, most water quality models simulate algae behavior only moderately well, or even poorly in many cases (Arhonditsis et al., 2006). In addition to the quality of input data, the other primary reason for getting poor algal results is using fixed growth, mortality, respiration, excretion, and settling ratios for algae in models.

The measurements at Lake Diefenbaker confirmed that algae adjust their Chla:C ratios based on P availability (Abirhire et al., 2015). The upstream part of the reservoir is turbid, so the algae have lower ACHLA values due to low light conditions (see Eq. 7.2). In other words, equal amounts of measured chlorophyll a in both the upstream and downstream ends of reservoir means that less algae biomass will be found at the downstream end. In the model used in this study, we used a variable Chla:C ratio for converting the simulated algal biomass into chlorophyll a concentrations. By doing so, simulation errors ($\overline{RMSE}$) decreased by 50%, meaning better performance and predictive capability of the model.

Depending on the objectives of the study, the grid discretization may be made coarser or finer. For example, for the variable stoichiometry, the study required the correct nutrient, temperature and light values at the euphotic zone. The *Lite* model has longer longitudinal segments and thicker vertical layers. However, the layers become thicker with depth (Figure 7.3). As a result, the euphotic zone for algae production remains almost unchanged, and the thicker layers at the bottom did not significantly affect the results. By increasing the longitudinal and vertical spacing, we were able to run this *Lite* model about 40 times faster without sacrificing accuracy. It is worth mentioning that the grid discretization should be made according to the study objectives. For example, for a study with the objective of locating the thermocline depth at the Coteau Creek arm (recreational beach near the Gardiner dam) on the 5^{th} of August, a model with fine vertical grids would be required.

7.6 Conclusion

We developed a 2D laterally averaged water quality model of Lake Diefenbaker by using the CE-QUAL-W2 model. We considered a top-down approach by first developing a large, complex model and gradually simplifying it. We first began building a riverine plus

reservoir model (827 segments and 60 vertical layers) and then making the model smaller by eliminating the riverine sections and considering only Lake Diefenbaker (302 segments) and further simplifying the model by making the segments longer and vertical layer heights thicker (87 segments and 21 vertical layers). Depending on the study objective and available input data, these models can be used to launch future climate and land use change scenarios.

We considered DO, PO_4, NH_4, NO_3, LDOM, RDOM, LPOM, RPOM, algae, TDS and TSS in the model. We also applied Chapra's (2008) proposed method for calculating chlorophyll *a* concentrations based on nutrient and light availability. By using a variable stoichiometry, we were able to calculate chlorophyll *a* more accurately compared with using a fixed chlorophyll *a*/algal biomass ratio in Lake Diefenbaker.

Although we were able to calibrate these models successfully, excessive computational resources and time were used for calculations and interpretations of the results. The majority of these efforts could have been avoided if better field measurements had been available for this reservoir. Regarding the input data, we recommend that a fixed sampling station be installed at the upstream end of the reservoir to measure daily/hourly flow and weekly/monthly water chemistry data.

7.7 Acknowledgements

This work was financially supported by the Canada Excellence Research Chair in Water Security through the Global Institute for Water Security. We thank Environment Canada, the Saskatchewan Water Security Agency and Alberta Environment for providing the hydrometric and water quality data. We are grateful to MeteoBlue for providing the meteorological data. Thanks to the Limnology Laboratory at the University of Saskatchewan for providing the water turbidity and temperature data. Thanks also to the Department of Geography and Planning at the University of Saskatchewan for providing the bathymetry data.

References

Abirhire, O., North, R. L., Hunter, K., Vandergucht, D. M., Sereda, J., and Hudson, J. J. (2015). Environmental factors influencing phytoplankton communities in Lake Diefenbaker, Saskatchewan, Canada. *Journal of Great Lakes Research*, 41:118–128.

Aquarium-fertilizer (2012). Nitrate (NO_3) and phosphate (PO_4) don't cause algae. Ammonia does. Available at: http://aquarium-fertilizer.com/nitrate-no3-and-phosphate-po4-dont-cause-algae-ammonia-does, Accessed: 27 September 2016.

Arhonditsis, G. B., Adams-VanHarn, B. A., Nielsen, L., Stow, C. A., and Reckhow, K. H. (2006). Evaluation of the current state of mechanistic aquatic biogeochemical modeling: citation analysis and future perspectives. *Environmental science & technology*, 40(21):6547–6554.

Aulakh, M. S., Khurana, M. P. S., and Singh, D. (2009). Water pollution related to agricultural, industrial, and urban activities, and its effects on the food chain: Case studies from Punjab. *Journal of New Seeds*, 10(2):112–137.

Buchak, E. M. and Edinger, J. E. (1984). Generalized, longitudinal-vertical hydrodynamics and transport: Development, programming, and applications. Technical report, prepared for US Army Corps of Engineers Waterways Experiment Station, Vicksburg, MS.

Bunzel, K., Kattwinkel, M., and Liess, M. (2013). Effects of organic pollutants from wastewater treatment plants on aquatic invertebrate communities. *Water Research*, 47(2):597–606.

Chapra, S. C. (2008). *Surface water-quality modeling*. Waveland press.

Chislock, M. F., Doster, E., Zitomer, R. A., and Wilson, A. (2013). Eutrophication: causes, consequences, and controls in aquatic ecosystems. *Nature Education Knowledge*, 4(4):10.

Cole, T. M. and Buchak, E. (1995). *CE-QUAL-W2: A two-dimensional, laterally averaged, hydrodynamic and water quality model*. US Army Engineer Waterways Experiment Station, Vicksburg, MS, 2.0 edition.

Cole, T. M. and Wells, S. A. (2003a). *CE-QUAL-W2: A two-dimensional, laterally averaged, hydrodynamic and water quality model*. US Army Engineer Waterways Experiment Station, Vicksburg, MS, 3.1 edition.

Cole, T. M. and Wells, S. A. (2003b). *CE-QUAL-W2: A two-dimensional, laterally averaged, hydrodynamic and water quality model*. US Army Engineer Waterways Experiment Station, Vicksburg, MS, 3.2 edition.

Cole, T. M. and Wells, S. A. (2006). *CE-QUAL-W2: A two-dimensional, laterally averaged, hydrodynamic and water quality model*. US Army Engineer Waterways Experiment Station, Vicksburg, MS, 3.5 edition.

Cole, T. M. and Wells, S. A. (2008). *CE-QUAL-W2: A two-dimensional, laterally averaged, hydrodynamic and water quality model*. Department of Civil and Environmental Engineering, Portland State University, Portland, OR, 3.6 edition.

Cole, T. M. and Wells, S. A. (2013). *CE-QUAL-W2: A two-dimensional, laterally averaged, hydrodynamic and water quality model*. Department of Civil and Environmental Engineering, Portland State University, Portland, OR, 3.71 edition.

Cole, T. M. and Wells, S. A. (2015a). *CE-QUAL-W2: A two-dimensional, laterally averaged, hydrodynamic and water quality model*. Department of Civil and Environmental Engineering, Portland State University, Portland, OR, 3.72 edition.

Cole, T. M. and Wells, S. A. (2015b). *CE-QUAL-W2: A two-dimensional, laterally averaged, hydrodynamic and water quality model*. Department of Civil and Environmental Engineering, Portland State University, Portland, OR, 4.0 edition.

Edinger, J. and Buchak, E. (1975). *A hydrodynamic, two-dimensional reservoir model: The computational basis*. US Army Engineer Division, Ohio River. Cincinnati, OH.

Edinger, J. and Buchak, E. (1978). Reservoir longitudinal and vertical implicit hydrodynamics. In *Proc. Int. Conf. on environmental effects of hydraulic engineering works, American society of civil engineers, Knoxville, TN*.

El-Khoury, A., Seidou, O., Lapen, D., Que, Z., Mohammadian, M., Sunohara, M., and Bahram, D. (2015). Combined impacts of future climate and land use changes on discharge, nitrogen and phosphorus loads for a Canadian river basin. *Journal of environmental management*, 151:76–86.

Freni, G., Mannina, G., and Viviani, G. (2011). Assessment of the integrated urban water quality model complexity through identifiability analysis. *Water Research*, 45(1):37–50.

Gosling, S. N. and Arnell, N. W. (2016). A global assessment of the impact of climate change on water scarcity. *Climatic Change*, 134(3):371–385.

Herbst, D. B., Bogan, M. T., Roll, S. K., and Safford, H. D. (2012). Effects of livestock exclusion on in-stream habitat and benthic invertebrate assemblages in montane streams. *Freshwater biology*, 57(1):204–217.

Hughes, D. and Slaughter, A. (2016). Disaggregating the components of a monthly water resources system model to daily values for use with a water quality model. *Environmental Modelling & Software*, 80:122–131.

James, R. T. (2016). Recalibration of the Lake Okeechobee Water Quality Model (LOWQM) to extreme hydro-meteorological events. *Ecological Modelling*, 325:71–83.

Ji, Z.-G. (2008). *Hydrodynamics and water quality: modeling rivers, lakes, and estuaries*. John Wiley & Sons.

Jin, K.-R., Ji, Z.-G., and James, R. T. (2007). Three-dimensional water quality and SAV modeling of a large shallow lake. *Journal of Great Lakes Research*, 33(1):28–45.

Kachi, N., Kachi, S., Bousnoubra, H., et al. (2016). Effects of irrigated agriculture on water and soil quality (case perimeter Guelma, Algeria). *Soil & Water Res*, 11:97–104.

Kopmann, R. and Markofsky, M. (2000). Three-dimensional water quality modelling with TELEMAC-3D. *Hydrological Processes*, 14(13):2279–2292.

Leon, L. F., Smith, R. E., Hipsey, M. R., Bocaniov, S. A., Higgins, S. N., Hecky, R. E., Antenucci, J. P., Imberger, J. A., and Guildford, S. J. (2011). Application of a 3D hydrodynamic–biological model for seasonal and spatial dynamics of water quality and phytoplankton in Lake Erie. *Journal of Great Lakes Research*, 37(1):41–53.

Missaghi, S. and Hondzo, M. (2010). Evaluation and application of a three-dimensional water quality model in a shallow lake with complex morphometry. *Ecological Modelling*, 221(11):1512–1525.

Monod, J. (1949). The growth of bacterial cultures. *Annual Reviews in Microbiology*, 3(1):371–394.

Pomeroy, J. and Shook, K. (2012). Review of Lake Diefenbaker operations, 2010–2011. Available at: http://www.usask.ca/hydrology/papers/Pomeroy_Shook_2012.pdf.

Reckhow, K. H. (1999). Water quality prediction and probability network models. *Canadian Journal of Fisheries and Aquatic Sciences*, 56(7):1150–1158.

Sadeghian, A., de Boer, D., Hudson, J. J., Wheater, H., and Lindenschmidt, K.-E. (2015). Lake Diefenbaker temperature model. *Journal of Great Lakes Research*, 41:8–21.

Schmidt, T. S., Clements, W. H., Wanty, R. B., Verplanck, P. L., Church, S. E., San Juan, C. A., Fey, D. L., Rockwell, B. W., DeWitt, E. H., and Klein, T. L. (2012). Geologic processes influence the effects of mining on aquatic ecosystems. *Ecological Applications*, 22(3):870–879.

Sheelanere, P., Noble, B. F., and Patrick, R. J. (2013). Institutional requirements for watershed cumulative effects assessment and management: Lessons from a Canadian trans-boundary watershed. *Land Use Policy*, 30(1):67–75.

Steele, J. H. (1962). Environmental control of photosynthesis in the sea. *Limnology and oceanography*, 7(2):137–150.

Vörösmarty, C. J., Green, P., Salisbury, J., and Lammers, R. B. (2000). Global water resources: vulnerability from climate change and population growth. *Science*, 289(5477):284–288.

Wu, Y. and Chen, J. (2013). Investigating the effects of point source and nonpoint source pollution on the water quality of the East River (Dongjiang) in South China. *Ecological Indicators*, 32:294–304.

Yates, K. K., Dufore, C., Smiley, N., Jackson, C., and Halley, R. B. (2007). Diurnal variation of oxygen and carbonate system parameters in Tampa Bay and Florida Bay. *Marine Chemistry*, 104(1):110–124.

Chapter 8

Sediment plume model - a comparison between use of measured turbidity data and satellite images for model calibration

This chapter is a published paper in the journal of Environmental Science and Pollution Research.

Sadeghian, A., Hudson, J. J., Wheater, H., and Lindenschmidt, K. E. (2017). Sediment plume model - a method for tracking the transport of suspended solids during an extreme flood event. *Journal of Environmental Science and Pollution Research*, 24(24):19583–19598. DOI: 10.1007/s11356-017-9616-y

The document has been reformatted from the original version for inclusion in the thesis, and no content has changed from the published version. The permission to use the manuscript in this thesis from the publisher (SPRINGER) is included in Appendix VI.

Contributions of the candidate and co-authors

The candidate's contributions are follows: setting up and calibrating the Lake Diefenbaker sediment model; wring the manuscript. Karl-Erich Lindenschmidt was the supervisor and designed the whole study, and helped the candidate through the research process and manuscript writing. Howard Wheater was the co-supervisor and designed the overall vision of the research at the Global Institute for Water Security (GIWS). He supported the candidate financially as well as provided guidance in research and contributed comments on all the manuscripts. Jeff Hudson provided the Sonde and Laboratory data for model calibration and by contributed comments.

8.1 Abstract

In this study, we built a two-dimensional sediment transport model of Lake Diefenbaker, Saskatchewan, Canada. It was calibrated by using measured turbidity data from stations along the reservoir and satellite images based on a flood event in 2013. In June 2013, there was heavy rainfall for two consecutive days on the frozen and snow-covered ground in the higher elevations of western Alberta, Canada. The runoff from the rainfall and the melted snow caused one of the largest recorded inflows to the headwaters of the South Saskatchewan River and Lake Diefenbaker downstream. An estimated discharge peak of over 5,200 m^3/s arrived at the reservoir inlet with a thick sediment front within a few days. The sediment plume moved quickly through the entire reservoir and remained visible from satellite images for over two weeks along most of the reservoir, leading to concerns regarding water quality. The aim of this study is to compare, quantitatively and qualitatively, the efficacy of using turbidity data and satellite images for sediment transport model calibration and to determine how accurately a sediment transport model can simulate sediment transport based on each of them. Both turbidity data and satellite images were very useful for calibrating the sediment transport model quantitatively and qualitatively. Model predictions and turbidity measurements show that the flood water and suspended sediments entered upstream fairly well mixed and moved downstream as overflow with a sharp gradient at the plume front. The model results suggest that the settling and resuspension rates of sediment are directly proportional to flow characteristics and that the use of constant coefficients leads to model underestimation or overestimation unless more data on sediment formation become available. Hence, this study reiterates the significance of the availability of data on sediment distribution and characteristics for building a robust and reliable sediment transport model.

8.2 Introduction

We are facing more demands and competition for the use of water resources every day and, at the same time, are confronted with greater uncertainties when attempting to predict future conditions (Wheater and Gober, 2013). Uncertainties can be especially numerous when trying to accurately predict floods (Horritt, 2006; Pappenberger et al., 2006), while they are becoming more frequent due to climate change (Bolstad, 2016; Wheater and Evans,

2009). Flood peaks lead to high erosion rates and, consequently, high suspended sediments and turbidity in surface waters (Grove et al., 2013). Suspended sediments (SS) contribute to the turbidity of the water and change density and nutrient availability, as well as attenuating the effects of sunlight which protects pathogens from UV radiation (Ji, 2008). Suspended solids are also an important carrier of pollutants to lakes and reservoirs (Kroon et al., 2012). Contaminants adsorb to SS surfaces and can be transported hundreds of kilometers with the water flow (Surbeck et al., 2006). Phosphorous, which is the main limiting nutrient for eutrophication in freshwaters, also bonds strongly with SS and is transported when there are high erosion rates which can cause water quality problems. Extensive sediment deposition and siltation leads to expensive maintenance costs and may impede or hinder navigation (Liu et al., 2011). Extensive siltation in a reservoir can decrease the operational lifespan of the waterbody and become an ecological problem itself (Valero-Garces et al., 1999). Also, accumulated loads of sediment behind the dams can increase dam instability because of the excessive forces applied to the dam walls by the sediment loads (Mama and Okafor, 2011). Hence, more money and resources are expended to mitigate the impacts of climate change and research new approaches for adaptation (Derworiz, 2016).

Floods can bring significant amounts of suspended solids to lakes and at the same time change the mixing patterns in lakes by turbulence currents. The effects of vertical mixing are dependent on the direction of water exchange in lakes. Depending on the inflow water density gradient (a function of water temperature and dissolved and suspended solids), the incoming flow could enter the reservoir in three different ways (Romero and Imberger, 2003). Warmer river waters usually have a lower density than the lake's water and enter along the top of the lake's water as overflow (Ji, 2008). The heavier river waters which are mainly due to cold and sediment-laden flood waters enter along the lakebed as underflow or density currents (Fink et al., 2016). At the point where the density of the underflow become lower than the density of the water at the lakebed, the flow spreads into the upper layers as interflow until the mixing balances the density gradient (Alavian et al., 1992).

The intrusion of the nutrient-rich hypolimnion water with the oxygen-rich epilimnion water can increase the productivity, while the reverse would reduce the oxygen deficiency and even leads to hypolimnetic oxygen saturation (Wüest et al., 1988). Large quantities of suspended solids can influence the water quality by changing the sediment-water interactions

and the ecological balance (Walling, 1977). In an incident in August 2002, the channel walls in the Mulde River, Germany, broke during a severe flood and the nutrient rich water drained into nearby stratified pit lakes (Klemm et al., 2005). The flood caused oxygen depletion in the epilimnion and the occurrence of algal blooms in these oligotrophic to mesotrophic lakes, which was of concern regarding the water supply (Boehrer et al., 2005).

The floods are also essential for renewal of water in deep layers of lakes and reservoir and can even reduce eutrophication (Fink et al., 2016). Springtime flood water has a higher density than lake surface water because of lower water temperatures and higher concentrations of suspended solids, hence transport the oxygen-rich water along lake's bottom (Fink et al., 2016). In a study of the Rhine River/Lake Constance, Germany, it was found that the spring-time underflow floods renew about 27% of the hypolimnion water with oxygen-rich water every year which is essential to maintain higher quality of the water in deep areas (Fink et al., 2016). In Lake Burragorang, Australia, winter flood completely replace the anoxic hypolimnion with the underflow (Romero and Imberger, 2003). A study on Lake Rotoiti, New Zealand, found that, depending on the timing and flow characteristics, the density-driven underflow has both positive and adverse effects on the ecological dynamics, nutrient loading, dissolved oxygen concentration and eutrophication on this lake (Vincent et al., 1991).

Even the best-controlled floods can be subject to the above mentioned potential environmental and ecological impacts by transported suspended solids. At such time, key questions and concerns require accurate and quick answers, such as, the amount of sediment and pollutants transported through flooding, the effect of the sediment plume (e.g., contamination), bacterial counts, safety of recreational beaches, and the need for drinking water advisories.

Answering these questions is not easy and becomes even more complicated as we go forward in an uncertain future. Water quality models are useful tools for studying the physical, chemical and biological processes and mechanisms in rivers and lakes (Sadeghian et al., 2014). Modeling SS transport can provide valuable information on contaminant transport characteristics and rates (Langeveld et al., 2005). In this study, we built and calibrated a sediment transport model based on the largest recorded flood for Lake Diefenbaker (LDF),

since its impoundment in 1967, in the prairie province of Saskatchewan, Canada.

The primary factors affecting the characteristics of a reservoir include climate, soil mineralogical composition, vegetation, land use and management practices in the watershed (Wetzel, 2001). Also, the topography of the region regarding the solar radiation shading and the wind speed sheltering are important (Huber et al., 2008). The heat exchange at the surface by solar radiation and the wind forces on the surface provide a significant proportion of energy for mixing in the lakes (Wüest et al., 1988). In Lake Diefenbaker, the energy from the inflow also has considerable effects on the mixing and horizontal water movements (Sadeghian et al., 2015).

In June 2013, there was heavy rainfall for two consecutive days on the frozen and snow-covered ground in the higher elevations of western Alberta, Canada (Sutherland, 2016). The runoff from the rainfall and melted snow caused one of the largest recorded inflows to the headwaters of the South Saskatchewan River (SSR) and caused heavy damage to population centers, particularly High River and Calgary, and devastation in the surrounding areas (De Vynck and Polson, 2013; Welsch and De Vynck, 2013). The gauges recorded discharge with peaks of 4,500 m^3/s at the Medicine Hat station (SSR) and 950 m^3/s at the Bindloss station (Red Deer River (RDR)), which merge at the Alberta-Saskatchewan border, 171 km from the Lake Diefenbaker inlet. Lake Diefenbaker, located downstream, was formed by the construction of the Gardiner Dam and the Qu'Appelle River Dam in the 1960s (Figure 8.1). Similar to many reservoirs, Lake Diefenbaker also functions as a flood mitigation reservoir. The 2013 Alberta flood brought highly turbid water into the reservoir (Hudson and Vandergucht, 2015), where the sediment settling and resuspension rates were unknown, leading to concerns regarding water quality.

We used measured turbidity data collected from stations along the reservoir over the course of two months (June and July 2013) to validate the sediment model quantitatively. In a sediment transport model, the use of suspended solids (SS) concentrations is preferred over turbidity because it is a state variable in the model, while the turbidity needs to be converted to SS for comparisons. However, a fundamental limitation with SS is maintaining a consistent sampling program of sediment with a temporal frequency that is adequate to capture the variations between seasons and events such as floods (Stroud et al., 2009). The

Figure 8.1: Lake Diefenbaker (LDF), Saskatchewan, Canada. The reservoir is divided into four sections (waterbodies) which allow use of four different meteorological stations along the reservoir. Solid red lines show locations of waterbodies in the model. The dotted red line at the Elbow shows the location at which the Qu'Appelle River Dam branch merges to the main channel in the model. Red circles show locations of stations with turbidity data measurements.

acquisition of data, from which decisions are often based is frequently inadequate, and this may lead to underestimation or overestimation and, ultimately, to poor management and policy decisions (Littlewood, 1992). Therefore, a practical alternative is using turbidity measurements (Gippel, 1995). Sonde-based turbidity measurements correlate the light scattering in water with SS concentrations, and are easier, faster and less expensive to operate compared with suspended solids sampling. Hence, sondes provide SS readings at finer temporal and spatial scales. The results will be very close to the direct measurements when the sensors are calibrated properly, according to particle size variations (Gippel, 1995).

In addition, we used MODIS satellite images to qualitatively calibrate the model based on near-surface suspended solids and to track the sediment plume front. Use of satellite images is not a new technique in studying near surface conditions in waterbodies. They

are being used in two primary fields: phytoplankton dominated systems, which are based on absorption of light at the water surface, and inorganic sediments systems, which are based on scattering of light at the water surface (Budd and Warrington, 2004; Myint and Walker, 2002). The focus of this study is the second category. Turbid waters exhibit strong relationships between sediment concentrations and reflected bands because the SS properties, such as particle size distribution, exert considerable control over the reflectance and scattering (Binding et al., 2005). One of the most comprehensive studies on freshwater, in this context, is the study of sediment transport and resuspension in Lake Michigan, which was accompanied by an extensive data collection project entitled "Episodic Events Great Lakes Experiment (EEGLE)" (Cardenas et al., 2005; Eadie et al., 2002; Lee et al., 2007, 2005; Stroud et al., 2009). Sakmont Engineering (1987) was one of the first groups who looked at satellite images of the South Saskatchewan River Basin and suggested incorporation of NOAA-VHRR and LANDSAT images for consistent data with reasonable resolutions. For Lake Diefenbaker, the first use of satellite images was in estimating chlorophyll *a* concentrations using MODIS and LANDSAT data (Giesy et al., 2009), with further work completed by Hecker et al. (2012) and Yip (2015).

Lake Diefenbaker is a long (180 km) and narrow reservoir where the width increases from about 800 m upstream to about 4,000 m downstream. MODIS data with the finest resolution (i.e. 250 m) would have three pixels for the upstream part and about 16 pixels downstream. The chlorophyll *a* concentrations are generally higher downstream, and the upstream area is more light limited because of higher SS concentrations (Dubourg et al., 2015). Therefore, studies based on the use of satellite images were mainly concentrated on estimating chlorophyll *a* concentrations downstream. We could not find any study that correlates SS or turbidity data with reflectance bands from satellite images for Lake Diefenbaker.

A recent research study by Akomeah et al. (2015) conducted a modeling study of the nutrient-algal dynamics of the upper South Saskatchewan River; due to the high importance of this waterbody to the province of Saskatchewan, we are presenting an extension to that study by looking at the sediment transport characteristics using recorded satellite images, onsite turbidity measurements and numerical modeling. In this paper, we successfully demonstrate a sediment transport modeling for the largest recorded discharge to Lake

Diefenbaker, an important drinking water source, with the objective of reproducing the measured turbidity data quantitatively and reproducing the movement of the sediment plume front qualitatively. A novelty of this work is incorporating space-borne remote sensing data to calibrate the sediment plume progression through the reservoir. The model itself has a sensitivity analysis component for finding the most important parameters that influence the accuracy of the results.

8.3 Methods

8.3.1 Study site

The study covers the two month period of June and July 2013 and the study area is Lake Diefenbaker (LDF). Lake Diefenbaker is one of the most strategic sources of water in the prairie province of Saskatchewan, Canada. The reservoir is 182 km long, with about 98% of its inflow coming from the headwaters of the Rocky Mountains in Alberta. The average annual inflow to the reservoir is 170 m^3/s of which 95% is released from the dams to downstream rivers. The South Saskatchewan River (SSR) and Red Deer River (RDR) merge about 171 km from the Lake Diefenbaker inlet. The closest stations to the reservoir that measure the discharge and suspended solids are the Medicine Hat station, 203 km upstream of the confluence for the SSR, and the Bindloss station, 47 km upstream of the confluence for the RDR. The SSR has a 50-year average flow of 550 m^3/s for June and 271 m^3/s for July, with a minimum flow of 8.5 m^3/s in November 1984 and a maximum of 4,440 m^3/s in June 2013. The RDR has a 50-year average flow of 135 m^3/s and 122 m^3/s for June and July respectively, with a minimum flow of 2.2 m^3/s in November 1982 and a maximum of 984 m^3/s in June 2005. The second and third largest recorded flows for the RDR are 932 m^3/s and 928 m^3/s in June 2013. Figure 8.2 shows the inflow and outflow to and from Lake Diefenbaker based on the routed discharges of the SSR and RDR, according to the methodology described in Hudson and Vandergucht (2015).

The air temperature ranged between 5 °C and 35 °C with mostly clear skies in June and July 2013 (Figure 8.3). The wind had a maximum velocity of about 11 m/s and was faster than 6 m/s for 10% of the time during this period, which could cause fairly strong mixing up to several meters below the surface. The heat budget for water temperature

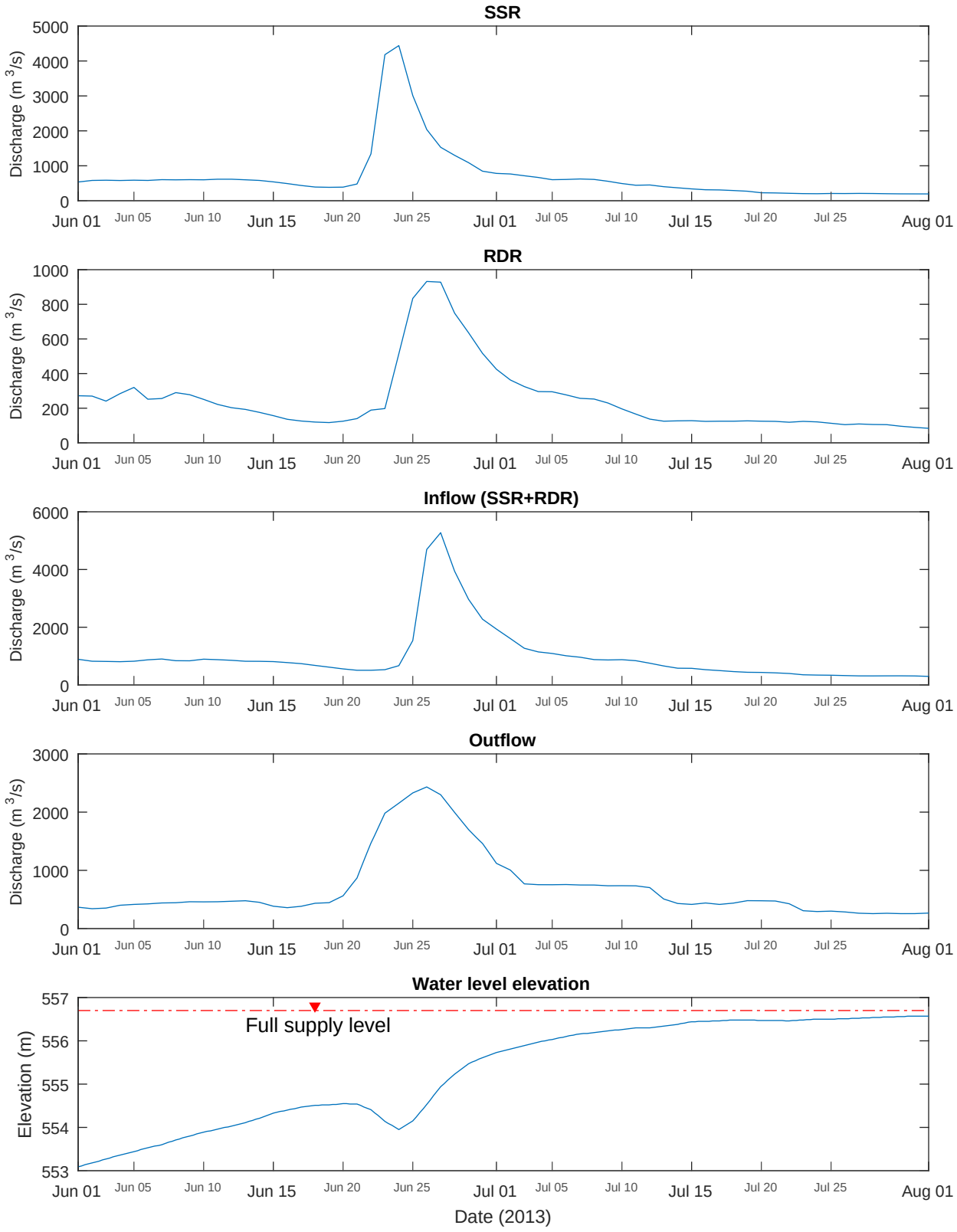

Figure 8.2: Discharge values at South Saskatchewan River (SSR), Red Deer River (RDR), inflow to Lake Diefenbaker (LDF), outflow from LDF and water level elevation at the Gardiner Dam. The SSR and RDR merge 171 km upstream of the LDF inlet.

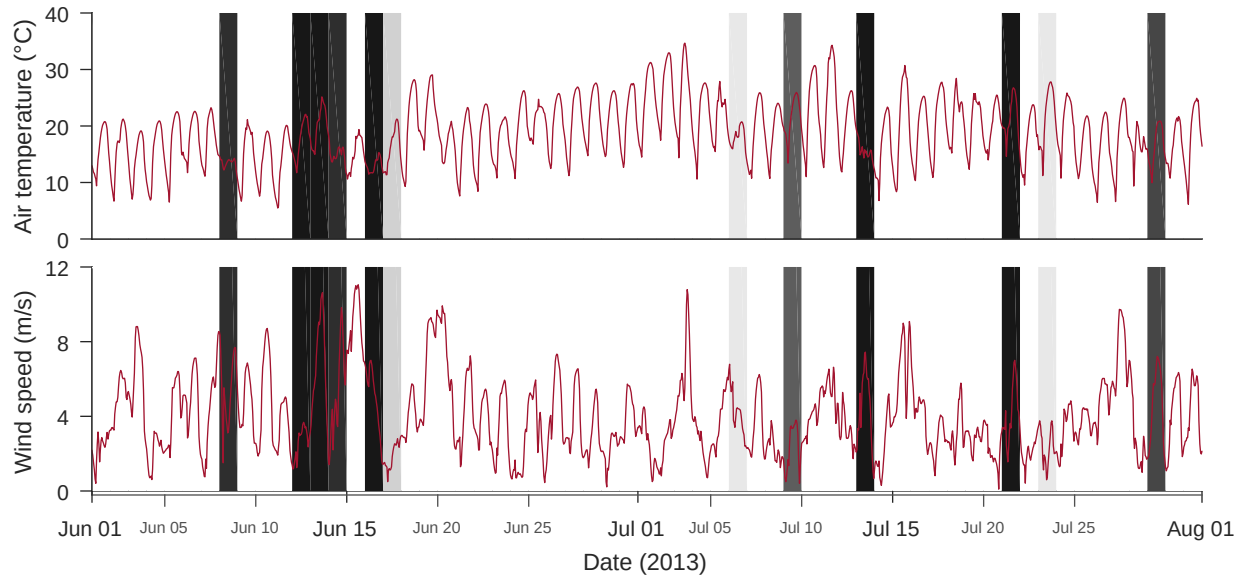

Figure 8.3: Recorded air temperature (top) and wind speed (bottom) at the Elbow station. The vertical strips show cloud amount with darker bands meaning more clouds.

in Lake Diefenbaker has two main sources: heat from inflow water, which is transported longitudinally by advection, and energy at the surface from solar radiation, which is distributed vertically by wind forces (Sadeghian et al., 2015). Modeling studies by Sadeghian et al. (2015) show that, at the time when the flood peak arrived at the reservoir, there was a fairly distinct stratification, with the thermocline about 20 m from the surface (Figure 8.4).

8.3.2 Measurements

The turbidity measurements were collected using YSI 6600 v2 multi-parameter sonde for 12 locations along the reservoir (Figure 8.1), with two or three vertical profiles for each station during the study period in June and July 2013 (Figure 8.5). The upstream stations had turbidity values several orders of magnitude higher than the downstream stations. The values obtained prior to the flooding (June 5^{th}) almost doubled after the flood peak arrived at the reservoir (July 4^{th}). Further downstream, the turbidity increased up to 20 times after the flood peak. The reservoir bifurcates near the village of Elbow into two 20 km arms. For the stations along these two arms (MC, M_8 , M_9 and M_{10}), maximum turbidity values rarely get close to 4 NTU even after the flood.

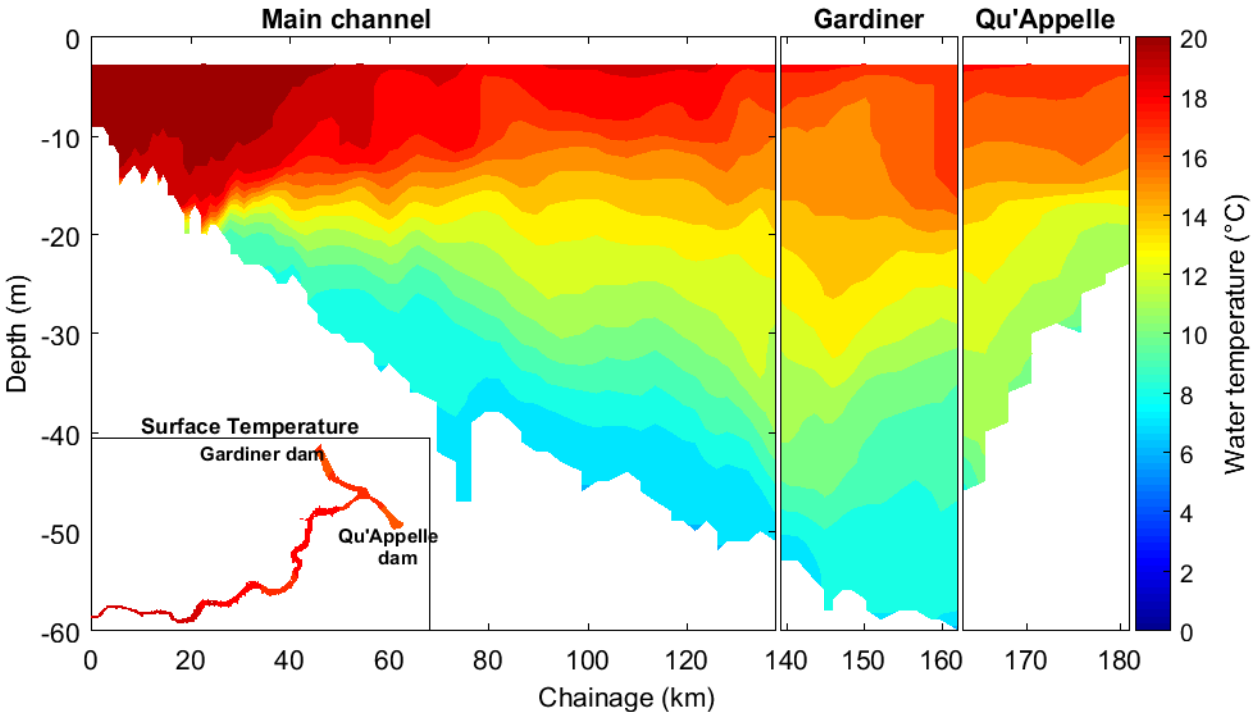

Figure 8.4: Water temperature on July 1^{st}, 2013 in Lake Diefenbaker when the flood peak arrived at the reservoir.

Satellite images were acquired using MODIS (Terra/MODIS 2013/155–243, Bands 1–4–3 (true color), Pixel sizes: 250 m) for this period. In total, there were 16 images that were available for June and July without having a cloud cover over the reservoir. For the missing days, we linearly interpolated between two available maps. Each pixel (i.e. 250 m) in the image, consists of values for three color bands (RGB). For example, the RGB values for a pixel upstream for the 4^{th} of June is [102, 89, 55] and for the 7^{th} is [104, 94, 64]. In order to reproduce the images for the missing days, the 5^{th} and 6^{th}, we interpolated for each of the RGB values separately. In Figure 8.6, the days that have data are shown in green and the days that are estimated based on linear interpolation are shown in red. Each image has 400,000 pixels of which 10,555 are for Lake Diefenbaker amounting to about 2.5% water and the most of the reminder are land surfaces. The arrows in each image show the estimated sediment front for each day.

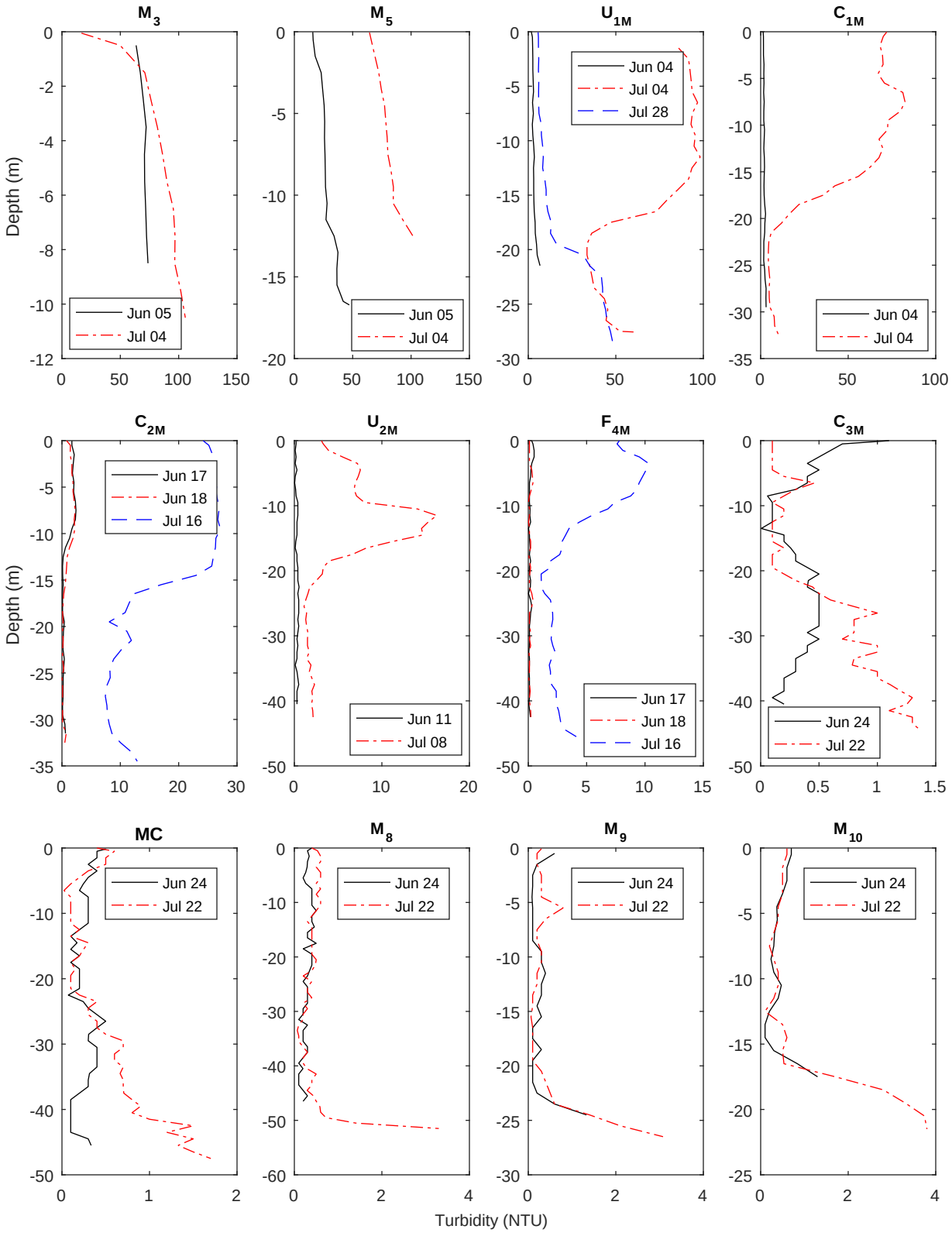

Figure 8.5: Vertical turbidity profiles collected at 12 stations along Lake Diefenbaker in June and July 2013.

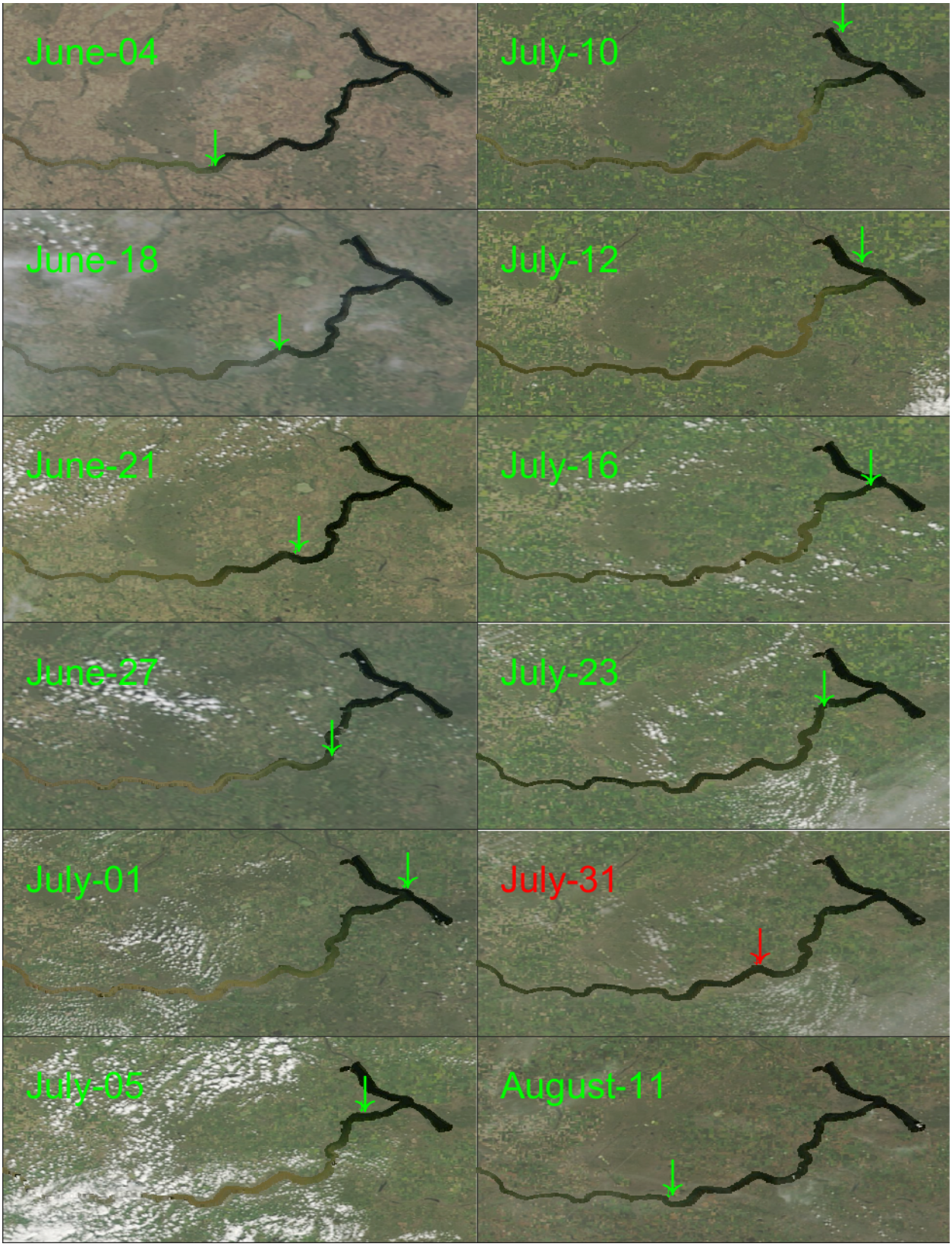

Figure 8.6: Satellite images obtained from MODIS for Lake Diefenbaker during the 2013 flood event. Land areas around Lake Diefenbaker blurred by 70% to better show the reservoir area. The images with green marker and date are real satellite images. The image with red marker (July 31^{st}) is interpolated.

8.3.3 Model

We used the laterally averaged water quality model, CE-QUAL-W2 for this study. This model was initiated in 1975 by the US Army Corps of Engineers, was then developed for about ten years by Edinger and Buchak (Buchak and Edinger, 1984; Edinger and Buchak, 1975, 1978), and then for more than 20 years by Cole (Cole and Buchak, 1995; Cole and Wells, 2003a,b, 2006). Further development is now being continued at Portland State University by Wells and his team (Cole and Wells, 2008, 2013, 2015a,b).

CE-QUAL-W2 is capable of performing both hydrodynamic and water quality simulations for both rivers and reservoirs. CE-QUAL-W2 was previously calibrated for temperature and hydrodynamics of Lake Diefenbaker for the 2011 – 2013 period (Sadeghian et al., 2015). Also, a sensitivity analysis for choosing the best meteorological stations from three available databases (Environment Canada, AccuWeather and MeteoBlue) was carried out for 2011 – 2013 using this model (Chapter 6). The model can simulate several groups of suspended solids for consideration of the effects of different sediment sizes and compositions. The model uses adoptive timesteps by calculating the Courant number for each step, with a maximum allowed timestep of 360 seconds for model stability. Inputs to the model are hourly meteorological data and daily flow and TSS data.

The model setup consists of 300 longitudinal segments, in Cartesian coordinates, ranging from 300 m to 950 m in length, and 60 uniform vertical layers with a thickness of one meter each. Also, the reservoir is divided into four waterbodies, connected to each other as shown in Figure 8.1. The inclusion of several waterbodies enables the use of different climate data stations for a large domain, as well as the implementation of different rates and constants for geomorphologically different river and lake sections. Each waterbody has one main branch, to which several side branches can be connected. The additional branches define a slope or connect a stream to the main river. For example, one extra branch connects the Qu'Appelle arm to the main stream at the downstream region of the reservoir.

We started the model simulations at the beginning of April 2013, as we could assume an isothermal condition for the whole reservoir just after the snow cover melted on the reservoir's surface. The model has a warm up period of about two weeks, so the effects of

initial conditions had completely disappeared for the study period in June and July. Also, all the suspended solids transported to the reservoir by flood were assumed to be inorganic. Therefore, other modules (e.g. eutrophication) in the model were kept inactive to save computational expenditure. Data from sediment traps were not available to correlate the turbidity measurements with the corresponding total suspended solids (TSS) concentrations. Although there are many studies available that provide guidelines for converting the turbidity measurements into TSS concentrations, we were hesitant in using these resources. The main reason was the data ownership and license limitations that prevented us from working directly on the data. Hence, to avoid estimation errors and provide a clear path for applying corrections in future studies the turbidity data (NTU) was considered to be equal to TSS (1 NTU = 1 mg/l). For the same reason, only one class of sediment was considered in the model.

To save computational time, we routed discharge and estimated the TSS value for the upstream portion of LDF instead of running the model for the whole SSR+LDF domain (see Chapter 7 for more details). The discharge was routed based on available guidelines (Hudson and Vandergucht, 2015). Also, a first order polynomial fitting ($R^2 = 0.86$) between TSS and discharge at the lake's inflow provided a means of extending the TSS measurements to Lake Diefenbaker's upstream stations. A good relationship was also obtained between the TSS concentrations of the LDF upstream stations and the discharge and TSS values along the SSR and RDR (Figure 8.7). We cannot accurately detect how much TSS the SSR and RDR each contribute to LDF because of the distance between observation stations and the reservoir's inlet. The first observation station is about 171 km downstream of the SSR and RDR confluence, but based on the derived equation, about 80% – 96% of the TSS settled on arrival at LDF under normal flow conditions. However, in the 2013 flood, 77% of the sediment had already deposited.

The primary factors that influence the suspended solids concentration in Lake Diefenbaker are the inflow, lake hydrodynamics, sediment concentrations at the inflow (advection), erosion, and sediment resuspension of bed material. Two adjustable model parameters (constant) control the concentration simulations: the suspended solids settling rate (SSS) and the critical shear stress for sediment resuspension ($\boldsymbol{\tau}_{cr}$). The SSS removes suspended solids from the water column and deposits them along the river bottom, while the $\boldsymbol{\tau}_{cr}$ resuspends them back from the bottom sediment to the water column. The SSS also serves

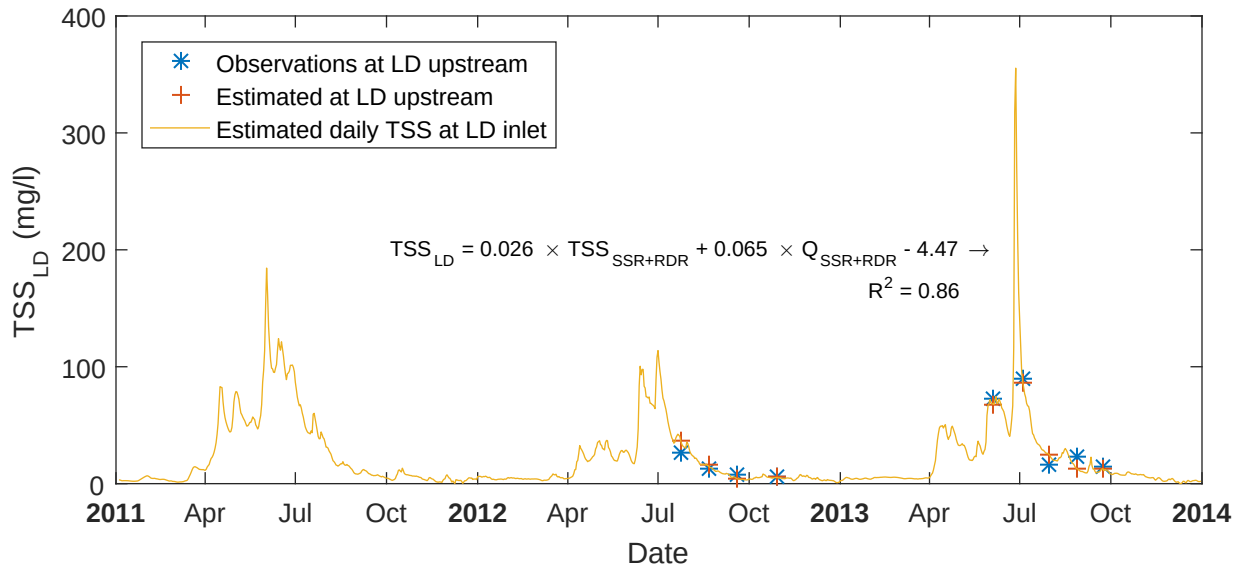

Figure 8.7: Estimating the TSS concentration at LDF upstream based on C_{IN} and discharge.

a critical role in removing particulate phosphorus adsorbed on the SS surfaces; $\boldsymbol{\tau}_{cr}$ in return, influences resuspension of nutrients bonded to sediments. The calibrating parameter SSS has a fixed rate expressed as m/day regardless of flow characteristics. Shear stress at the water-sediment surface is calculated in each timestep based on the near bed turbulences induced by the flow and wind effects, but the $\boldsymbol{\tau}_{cr}$ has a fixed value for each TSS group during simulations.

In total, 1,000 Monte-Carlo runs were carried out with uniform distribution for the two calibrating parameters (SSS and $\boldsymbol{\tau}_{cr}$) using the University of Saskatchewan High-performance computing (HPC) platforms. TSS was the primary state variable in our simulations for this study. The settling rate (SSS) and the critical shear stress for sediment resuspension were used to calibrate TSS concentrations by giving the lowest discrepancy with measured turbidity data. Calibrations and sensitivity analysis were performed by optimizing the objective function, Root Mean Square Error (RMSE):

$$RMSE = \sqrt{\frac{\sum (O - S)^2}{n}} \tag{8.1}$$

where O is the observed values, S is the simulated values and n is the total number of observations.

Calibration of the model, based on the lowest deviation between simulations and measurements within a Monte-Carlo environment, has already been described in depth for the Lake Diefenbaker temperature model (Sadeghian et al., 2015). For each Monte-Carlo run, we calculated the RMSE based on Equation 8.1. To calculate the RMSE for the entire reservoir, all the turbidity measurements from all different depths and locations were sorted in one column and compared with the simulated values at the same place and depth. To calculate the RMSE values for each segment (observation station), only values of that portion filtered to a similar time and depth were considered.

8.4 Results

Initial processing of the satellite images revealed that the upper portion of Lake Diefenbaker (up to station M_5) was visibly turbid even before the flood because of high flows in June (Figures 8.2 and 8.6). The plume gradually moved through the reservoir and reached the Riverhurst area by June 27^{th}, just before the arrival of flood waters. On July 1^{st}, after the flood water arrived at the reservoir, there was a jump in the plume-front's location to Elbow. By July 5^{th} the plume disappeared and again extended up to the Gardiner Dam on July 10^{th}. Then, it took about one month for the plume to disappear completely from the satellite images.

The turbidity measurements also confirm the trends in water clarity visible from satellite images. Before the flood waters entered the reservoir, the vertical profile of turbidity, especially upstream, had higher concentrations near the bed. The vertical profiles for the first two stations (M_3 and M_5) show higher concentrations near the bed, which could be due to sediment resuspension from high discharge values. However, this trend reversed, excluding upstream, once the peak discharge passed through the reservoir, with more cloudy water near the surface (Figure 8.5). The values obtained prior to the flooding (June 5^{th}) almost doubled after the flood peak arrived at the reservoir (July 4^{th}). Further downstream (U_{1M} to F_{4M}), with increasing reservoir depth, sharp changes in the concentrations are

visible at depths around 20 m from the surface. The turbidity measurements recorded immediately after the flooding show up to 20 times increase in turbidity values above the first 20 m from the water surface (on the top of the thermocline). The reason could be that, in shallower upstream areas (about 10 m deep), advection and resuspension are the main sources of sediment, while further downstream it is only advection. These regions had clear water before the flood and the sediment plume increased the turbidity of the water here. The reason for higher turbidities in only the first 20 meters could be due to the summer stratification and also be an indication of overflow conditions. The reservoir bifurcates near the village of Elbow into two 20 km arms. For the stations along these two arms (MC, M_8 , M_9 and M_{10}) and the C_{3M} station (before branching), maximum turbidity values rarely get close to 4 NTU even after the flood. It is likely that all the SS settled down when it passed through the curvy and indented channel of the reservoir. Resuspension became negligible in deep areas, and also because there was overflow conditions.

Among the 27 turbidity measurements (Figure 8.5), two thirds had concentrations of less than 15 NTU, which indicated almost clear water. Most of these samples were collected from downstream areas where most of the turbulence energy of the water had dampened. The simulations on these days/stations produced smaller RMSE errors when compared with the other remaining days/stations. Also, the model results were more satisfactory with settling rates (SSS) greater than 2 m/day for suspended solids at these low turbidity events (Figure 8.8). The days/locations that had higher turbidities were sensitive to the values of calibrating parameters. Therefore, the results for turbidity observations with a maximum recorded turbidity of over 15 NTU will be discussed in more detail.

Overall, the Monte-Carlo simulation results show high sensitivity to SSS values, but no detectable trend was found with τ_{cr} (Figure 8.8). A general trend for SSS is that the best results upstream were derived with small values, as we go downstream the results get better with larger settling rates. On one occasion, U_{1M} on July 4^{th}, there are two optimum values for the SSS coefficient. The main reason is the vertical profile of turbidity at this day/location (Figure 8.5). There was high turbidity that arrived at the top of the thermocline, while the area below was still clear because of pre-flood clear water conditions. The two optimum values are for two different simulated vertical profiles of which one of them is a false optimum value. This equifinality occurs when the model

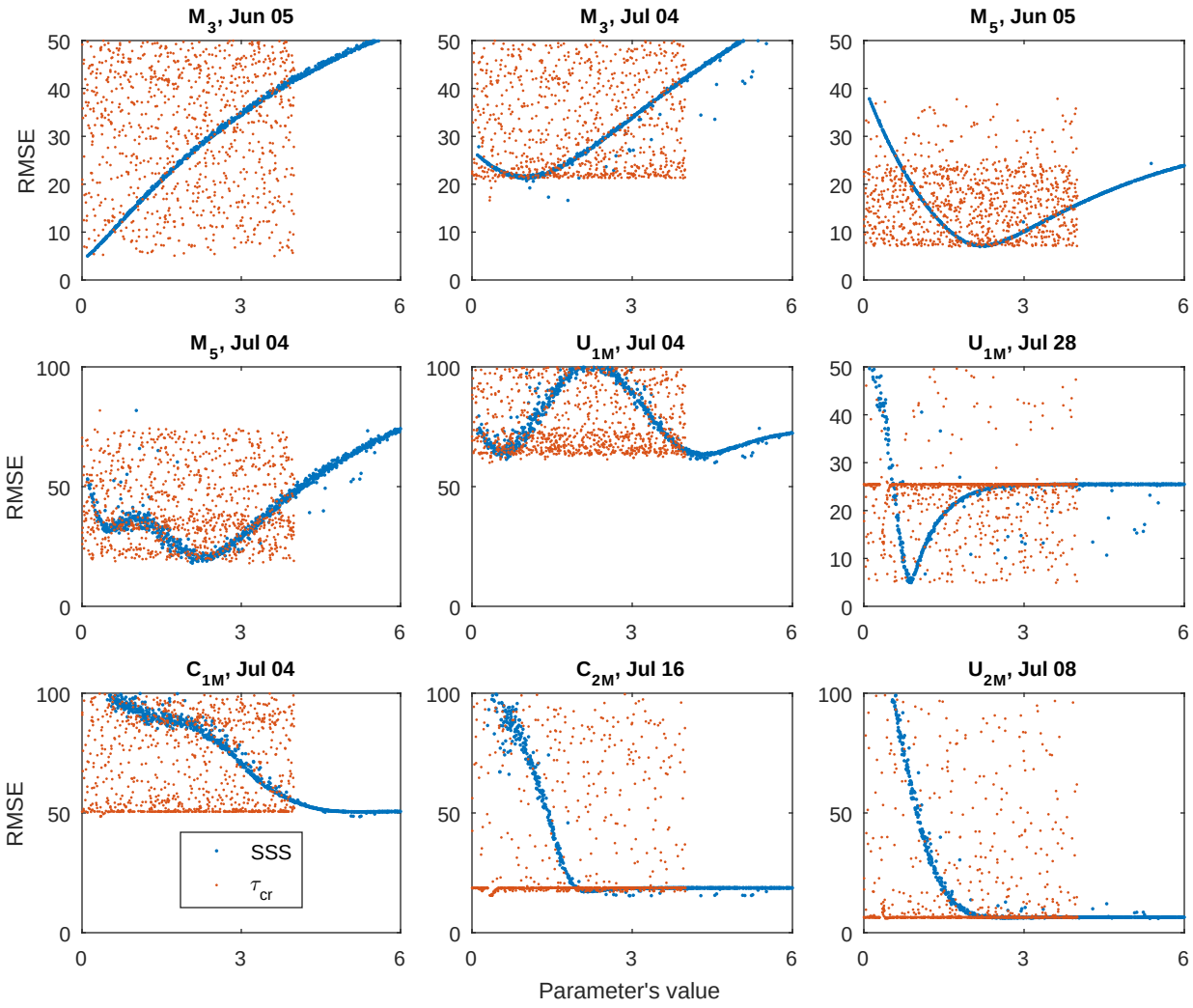

Figure 8.8: Sensitivity analysis for parameters SSS (m/day) and τ_{cr} (dynes/cm^2) for observations with TSS values larger than 15 mg/l. SSS ranged between zero and 6. τ_{cr} ranged between zero and 4

predicts large concentrations below the thermocline and small values on the top (inverse profile). The sum of underestimation at the top of the thermocline (negative values) and overprediction below the thermocline (positive values) gives small RMSE values which are not correct. According to the RMSE values, the best results were obtained when SSS increased from 1 m/day to 5 m/day from upstream to downstream in the reservoir.

We chose four different ranges for SSS to look at the results in more detail (Figure 8.9). The bands show the ranges that the model calculated for TSS for days/locations by SSS values in the specified ranges. SSS values in the range between zero and 0.5 m/day produce

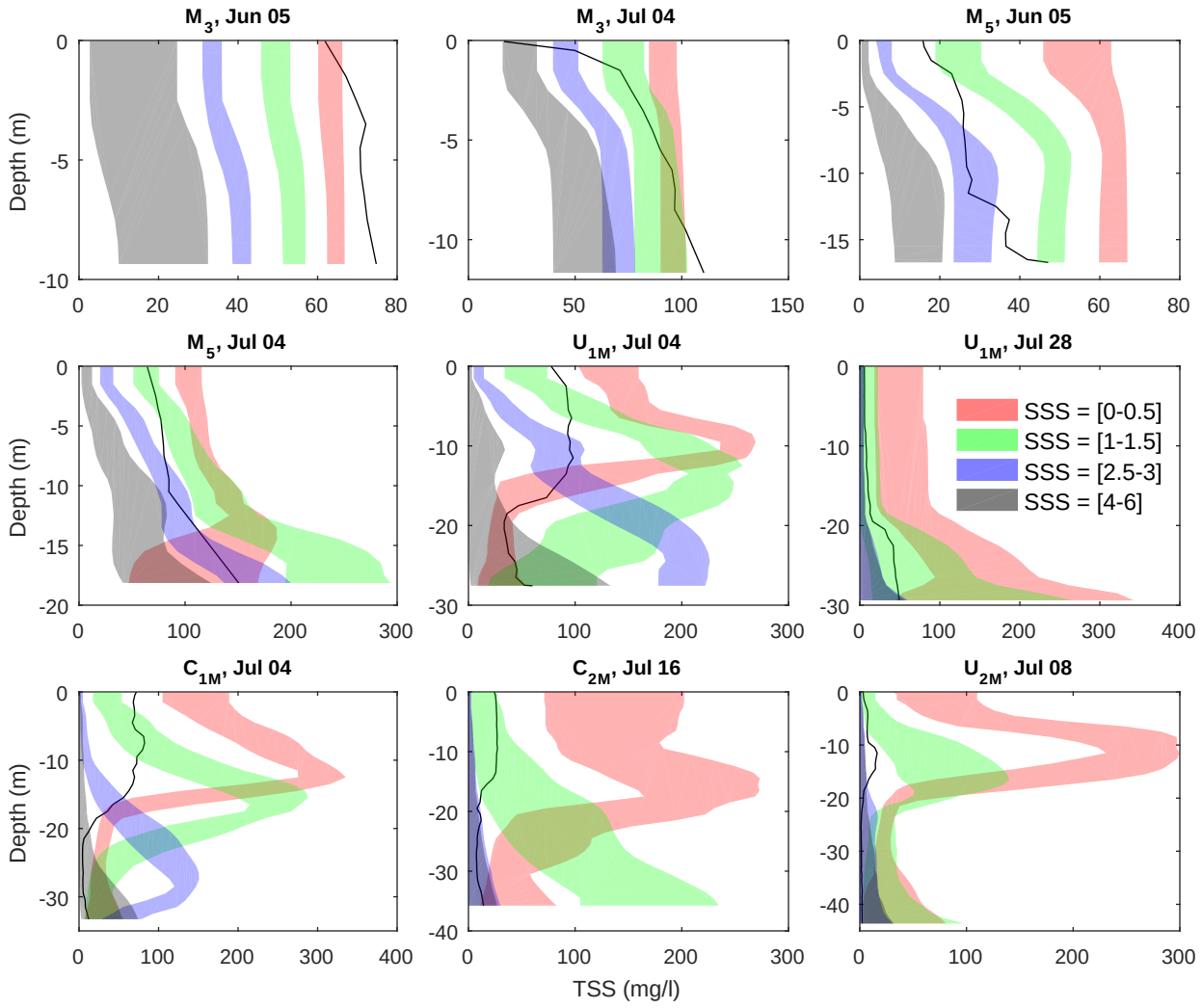

Figure 8.9: Simulated TSS ranges for different SSS (m/day) values. The bands show the ranges that the model calculated the TSS concentrations by using the SSS values in the specified ranges for different days/locations. Small SSS over-predict TSS at downstream several order of magnitudes

the best match with the observed turbidity data for station M_3 upstream. The same range over-predicts the TSS by about four times at M_5 and about 15 times at U_{2M}. The range between 1 and 1.5 underestimates the TSS at M_3 before the flood, but works well for the period of the time after the flood. However, it still overestimates at stations more downstream. Larger SSS values underestimate TSS upstream, but are better matched with observations downstream.

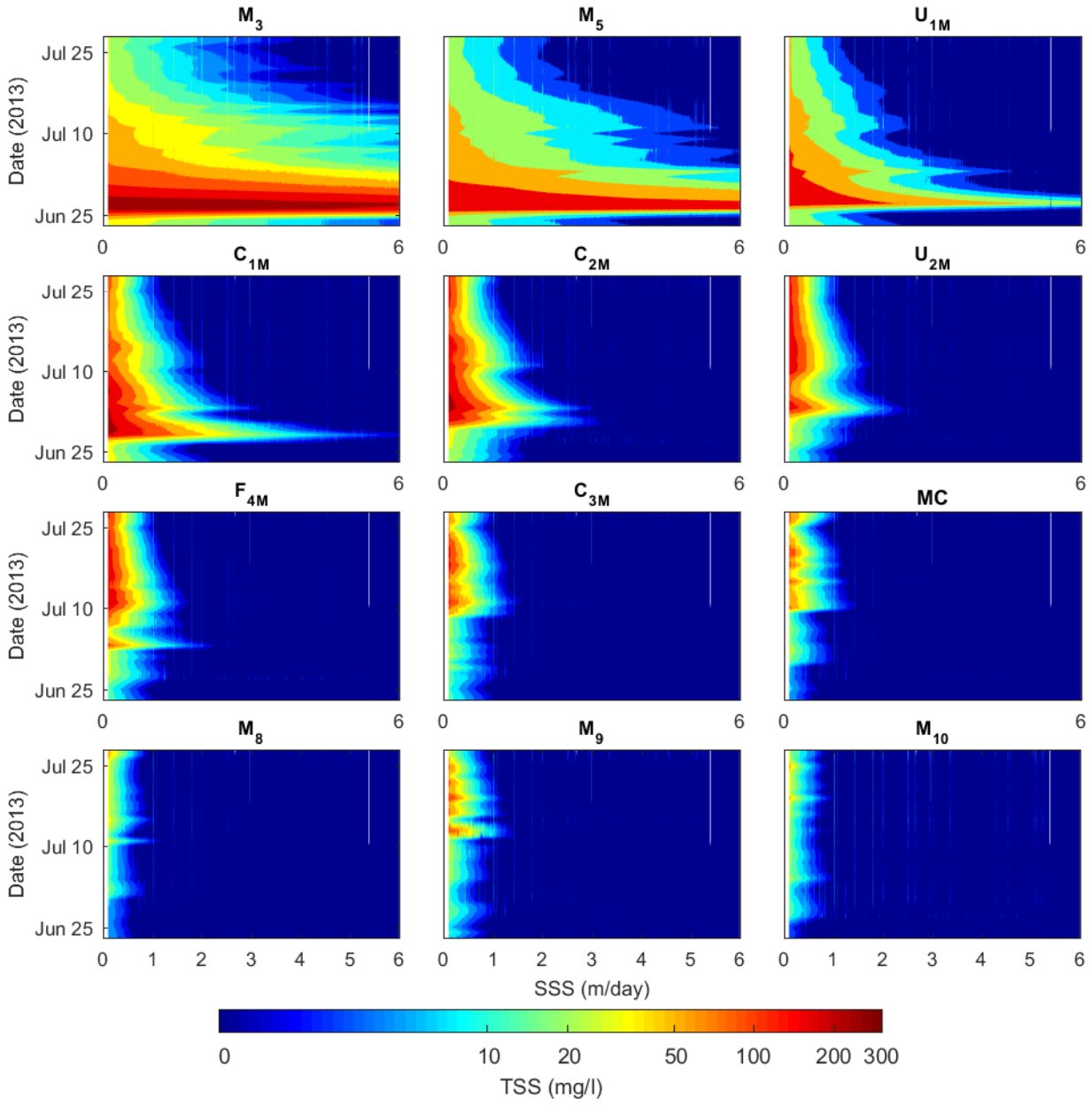

Figure 8.10: Simulated TSS values at the water surface for different SSS (m/day) values. The color-bar is in logarithmic scale to capture trends in both upstream with large TSS concentrations and downstream with small concentrations

Comparing model results at the surface with sediment movement detected in satellite images shows that the value of 6 m/day was a large upper band for SSS (Figure 8.10). Almost all the sediment was removed from the top layer by ten days after the incident, while the images recorded that the surface water upstream was turbid until the end of July. At the same time, SSS values smaller than 1 m/day produced very large concentrations (TSS over

100 mg/l) downstream, which are not correct. No observation or satellite image confirms such high turbid conditions downstream.

8.5 Discussion

In 2013, the Alberta flood had a peak flow of 5,200 m^3/s with a maximum TSS concentration of 1,500 mg/l at the SSR-RDR confluence (171 km upstream of LDF). Dam operation authorities released the water from the Gardiner Dam at a rate of 2,000 m^3/s for three consecutive days (Saskatoon City News, 2013). Due to the high inflow and outflow, the sediment plume traveled through the reservoir very quickly. Saskatchewan's Water Security Agency reduced the dam's outflow to 1,000 m^3/s on the third day when the inflow decreased to less than 2,000 m^3/s. As a result, the sediment plume began settling gradually. Based on our modeling results, the inflow water from the South Saskatchewan River had a temperature close to the temperature of the water at the surface of Lake Diefenbaker. Although most of the flow waters stemmed from snowmelt, warm days with extensive sunshine hours ($\sim$17 hours in June) had brought enough thermal energy to the river. Hence, water entered the lake above the colder and heavier lower layers because of density gradients. However, the large inflow (5,200 m^3/s) to the reservoir and the large outflow through the spillways at the Gardiner Dam (2,000 m^3/s) induced high velocity water in transit with large turbulent mixing especially at the upstream sections. Also, during the flood of June, the water level in Lake Diefenbaker raised about 3 meters (Figure 8.2). According to the recorded water level elevations, there was a rapid drawdown of about one meter before the flood arrival in June 25^{th} because of the opening of the spillway gates at the Gardiner Dam. According to the model results, the inflow water from SSR thoroughly mixed with the upstream reservoir water and then traveled along the top of thermocline due to density gradients. Hence, the elevated water level added to the epilimnion thickness.

We used two different sources to calibrate the sediment transport model: comparing the movement of the plume through the reservoir with the acquired satellite images and comparing the observed turbidity measurements with TSS. These comparisons had an interesting result in that the coefficients for the best performance based on satellite images

were very close to those based on turbidity measurements.

The turbidity measurements recorded immediately after the flooding show the peaks occurred in the first 20 m from the water surface (on the top of the thermocline), which was also confirmed by the model results. Therefore, the satellite images of the surface of the water are an accurate representation of the sediment plume movements. The satellite images show consistent movement of the turbid front of water through Lake Diefenbaker in June. On July 1^{st}, the flood waters arrived at the reservoir, and the movement was faster than in June for a few days, but the plume disappeared in the image recorded on July 5^{th}. On the image recorded on July 10^{th}, the plume moved forward again. Unfortunately, there is no turbidity measurement between these two dates in the downstream portion, but the changes in the flow intensities can verify this back and forth movement. As mentioned above, there was a huge inflow into the reservoir and large outflows from the dam, which both decreased considerably from the third day after the arrival of the flood waters. The rapid change in flow intensities could create backflow conditions with hypolimnetic mixing. Also, there were huge wind velocities on the 4^{th} of July, which could have further increased the hypolimnetic mixing there.

C-QUAL-W2 was able to track the changes in turbidity only moderately well when fixed coefficients were considered for sediment settling. We can not clearly say that it was a limitation with the model or with the data. A limitation of the CE-QUAL-W2, and, indeed, many water quality models, is the use of fixed rates for the parameters in simulations of the state variables. These rates are used in many equations related to transport, hydrodynamics or water quality. For example, using fixed daily rates for sediment settling produces overestimations and underestimations, depending on flow conditions. Hence, it may be difficult, if not impossible, to obtain simulations that coincide exactly with the values obtained through sampling due to uncertainties inherent in measurement errors, spatiotemporal limits, and calculation limits. However, the model does extend our understanding of the overall responses of the system to different scenarios, particularly extremes.

In water quality modeling of lakes and reservoirs, the simulation errors can be reduced if the input data at the boundaries are well monitored (Romero and Imberger, 2003). For

having a correct image of the sediment transport by rivers, regular sampling programs are required (Walling, 1977). Sediment rating curves can work as a replacement for sampling programs in case of financial austerity, missed events such as floods, and gaps of past sediment transport time series (Walling, 1977). Turbidity measurements can also be used instead of directly measuring suspended solid concentrations. The turbidity measurements are highly affected by the particle size distribution of the suspended solids in water; hence, an adequate number of sampling is required when using the turbidity measurements with confidence, especially during flood events (Lenzi and Marchi, 2000).

A large proportion of sediment transported in rivers is in the form of suspended solids; hence, sediment rating curves which relate the suspended solids concentrations to the discharge values are commonly used for quantifying the amount of sediment transport in rivers and reservoirs (Asselman, 2000). Although suspended solids make a large proportion of the total sediment load, the percentage is very variable along the river with greater variations at the headwaters and more consistent rates downstream (Lenzi and Marchi, 2000). These changes can produce errors of up to 50% in estimating the sediment transport in rivers (Walling, 1977). To reduce the uncertainties in determining the suspended solids concentrations and to have information on the characteristics of the sediment transport, different sediment rating curves are needed at various locations along rivers and reservoirs. The slopes of these rating curves provide information on the erosion and sedimentation rates in rivers, but not for all events. A study of the sediment rating curves of the Rhine River, Germany (Asselman, 2000) found that the descending slopes of rating curves along the river do not influence the sediment transport rates. Due to data ownership limitations, the aim of this study was not to make a sediment rating curve based on the turbidity measurements, and the measured turbidity data was only used for the purpose of sediment model validation.

Accurate estimation of suspended solids concentrations with correct size distribution is essential at boundaries (Lee et al., 2007). Lack of input data could also be considered a limitation or even an opportunity for planning future studies. For example, we could potentially extract more information from the satellite images if there was a study looking into the relationship between the different bands in reflectance images and characteristics of suspended sediments such as particle size distribution and mineralogy. Having access to such a table would provide data at the inlet as input TSS and through the reservoir

for calibration purposes. Also, it could reduce the need for using a variable settling coefficient inside the model, if we had a measure of sediment size distribution from linking the turbidity data to the corresponding TSS concentration by using sediment traps. The South Saskatchewan River (SSR) and Red Deer River (RDR) have considerable differences in the characteristics of the turbidity; the SSR has very clear water while the RDR has turbid water due to steep riverbed slopes. These two rivers merge in Saskatchewan only a few kilometer from the border of Alberta. In Saskatchewan, the general quality of water in the SSR was considered as "good" by the Saskatchewan Water Security Agency (WSA, 2012), hence fewer resources and water quality parameters were required for monitoring the quality of the water. The availability of water with an acceptable quality and less disturbance of the water resources by industrial activities and urbanization led to a very limited historical database of the water quality variables for the South Saskatchewan River and Lake Diefenbaker. One important factor which is missing in the model is river bank erosion, which is a very important source of sediment in Lake Diefenbaker (Ashmore and Day, 1988). Bank erosion is different from sediment resuspension in bed material and could be imported into the model as TSS concentrations distributed over the upstream portion.

By using the turbidity as the only available data, a pronounced hurdle in the modeling was defining the suspended solids settling rates. This parameter has a fixed value of m/day, which is very restrictive, since, in actuality, the settling rates are extremely dependent on flow characteristics. In the example of LDF (Figures 8.8, 8.9 and 8.10), it can be clearly seen that larger settling rates are required as the reservoir becomes deeper and, consequently, the flow becomes slower. Comparing the TSS concentration at the LDF inflow with the discharge and TSS at the SSR/RDR indicates that the TSS is more dependent on the flow than on the upstream concentration. Therefore, the current version of the CE-QUAL-W2 should only be used for sediment transport calculations of short time periods or for the systems with more uniform flow rates, unless the concentrations for different sediment classes are available. The model needs a more flexible sediment-settling coefficient that can differentiate between different sections of the river and reservoir.

The sensitivity results based on the Monte-Carlo runs also demonstrate the need for using a dynamic SSS coefficient for an accurate sediment transport model (Figure 8.8). RMSE values are higher upstream because TSS concentrations are larger at the reservoir inlet.

Based on the available field measurements, the upstream concentrations are up to several times higher than those downstream. It is worth mentioning that the settling rates along the upstream areas are not actual sedimentation rates. The main reasons are that the model did not include the bank erosions rates, and only used one group of suspended solids in the simulations. In reality, bank erosion can contribute a significant portion to the sediment load. Also, the composition of the lake-bed sediment and consequently the resuspension rates are different at different locations along the reservoir. Hence, the lower settling rates upstream are sedimentation rates reduced somewhat from the actual values to compensate for the simplifications in model setup. According to the RMSE values, the best results were obtained when SSS increased from 1 to 5 m/day from upstream to downstream in the reservoir. Based on our modeling results, the settling in the reservoir occurs more quickly than it does in the river because the flow velocity is smaller and the wind effects are dampened in the deeper layers. The settling rates increase even more downstream towards the dams. Also, because of suspended solids settling along the lake-bed, the density gradient decreases down to the point that becomes smaller than the lake-bed water density. At this stage the sediment-laden water starts mixing with less turbid water at mid-layers and a larger proportion of the turbulent energy is used for mixing water vertically and laterally. As the head of the plume moves forward longitudinally, the laterally mixed waters have higher settling capacities.

Based on RMSE values, the results were not sensitive to τ_{cr} values (Figures 8.8). However, this does not mean that the model also was not sensitive to this coefficient or the resuspension was not an important process. The reason is the over-predicting of the TSS by about two times at M_5 and about 15 times at U_{2M} when small values for SSS were selected in the model (Figure 8.9). In that case, the values downstream were several times larger than the incoming TSS at the inlet, meaning the extra TSS concentrations were from resuspension. The reason could be that the resuspended material was also affected by settling rates again, and that would be why the SSS was more identifiable.

8.6 Conclusion

A water quality model was developed for Lake Diefenbaker to determine suspended solids transport and the rates of settling and resuspension through the reservoir. The length of the study was the two months of June and July 2013 when a flood occurred in the head waters of the South Saskatchewan River. The flood created the largest inflow to the reservoir since its construction in 1967, with flood waves carrying high loads of suspended sediments. We calibrated the model based on measured turbidity data from 12 stations along Lake Diefenbaker collected during June and July 2013 and images obtained from cloud-free MODIS satellite imagery. We defined only one group of TSS because data on sediment texture (fine, medium and coarse) were not available. TSS was modeled as a tracer, and its movement through the reservoir was traced starting at the upstream portion of Lake Diefenbaker, with the sediment plume gradually becoming less concentrated by sedimentation and dilution as it moved through the reservoir. This setup allowed us to develop a dispersion and diffusion transport model of Lake Diefenbaker using the two-dimensional hydrodynamic and water quality model CE-QUAL-W2. The model was capable of tracing the flood's sediment plume movements through the reservoir. This has resulted in a better understanding of the settling and resuspension rates of the suspended sediments in the reservoir which will support decision making.

The model results and turbidity measurements confirm that the inflow to the reservoir entered as an overflow and moved above the thermocline. Suspended solids were also transported by advection through the epilimnion, which was about 20 m at that time. As a result, the vertical alignment of suspended solids reversed with higher concentrations at the upper layers after the flooding. It took only a couple days for the plume to scatter throughout the reservoir, but took almost one month to disappear completely.

Satellite images were used to estimate the sediment's settling and resuspension rates by comparing the suspended solids transport with the sediment plume qualitatively. The turbidity in the upstream river is high, and it may be useful to apply wavelength studies to find correlations with TSS values. The narrow range of a few hundred meters is still a barrier, but improvements may become possible with higher resolution satellite data in the future. Although a relationship between the reflectance bands from satellite images and the

sediment concentrations was not available, the visible sediment plume movement provided good estimates of sediment transport in Lake Diefenbaker. The rates found confirmed those derived from the Monte-Carlo results. This is a remarkable outcome considering that, in many cases, field measurements may not be available, however other data sources may be successfully drawn upon to aid in calibration of such an event.

With the assumption of one single grain size, a limitation of the model was the lack of definition of the suspended solids settling rate in the CE-QUAL-W2 model. This parameter has a fixed value, which is restrictive, since settling rates are extremely dependent on flow characteristics. However, good results were obtained by increasing settling rates in areas where the reservoir becomes deeper, and flow currents become slower. Therefore, the current version of the CE-QUAL-W2 model may be more suited for sediment transport calculations of shorter time periods and for systems with a uniform flow distribution. The model needs a more flexible sediment-settling coefficient that at least differentiates between different sections of the river and reservoir.

More insight and confidence in the model could be obtained if several different data sources became available for model calibration. Finding correlations between reflectance bands from satellite images and sediment concentrations would considerably improve the quality of results. Also, finding the rates between the turbidity and corresponding TSS concentrations is essential for model validations. Input of suspended sediment distribution with a classification for different (fine, medium and coarse) sizes is crucial. Finally, river bank erosion effects need to be considered in model calibrations.

8.7 Acknowledgements

This work was financially supported by the Canada Excellence Research Chair in Water Security through the Global Institute for Water Security. We thank Environment Canada, the Saskatchewan Water Security Agency and Alberta Environment for providing the hydrometric and water quality data. We are grateful to MeteoBlue for providing the meteorological data. Thanks to the Limnology Laboratory at the University of Saskatchewan for providing the water turbidity and temperature data. Thanks also to the

Department of Geography and Planning at the University of Saskatchewan for providing the bathymetry data.

References

Akomeah, E., Chun, K. P., and Lindenschmidt, K.-E. (2015). Dynamic water quality modelling and uncertainty analysis of phytoplankton and nutrient cycles for the upper South Saskatchewan River. *Environmental Science and Pollution Research*, 22(22):18239–18251.

Alavian, V., Jirka, G. H., Denton, R. A., Johnson, M. C., and Stefan, H. G. (1992). Density currents entering lakes and reservoirs. *Journal of Hydraulic Engineering*, 118(11):1464–1489.

Ashmore, P. and Day, T. (1988). Spatial and temporal patterns of suspended-sediment yield in the Saskatchewan River basin. *Canadian Journal of Earth Sciences*, 25(9):1450–1463.

Asselman, N. (2000). Fitting and interpretation of sediment rating curves. *Journal of Hydrology*, 234(3):228–248.

Binding, C., Bowers, D., and Mitchelson-Jacob, E. (2005). Estimating suspended sediment concentrations from ocean colour measurements in moderately turbid waters; the impact of variable particle scattering properties. *Remote sensing of Environment*, 94(3):373–383.

Boehrer, B., Schultze, M., Ockenfeld, K., and Geller, W. (2005). Path of the 2002 Mulde flood through lake Goitsche, Germany. *Internationale Vereinigung fur Theoretische und Angewandte Limnologie Verhandlungen*, 29(1):369–372.

Bolstad, E. (2016). Extreme floods may be the new normal. Available at: http://www.scientificamerican.com/article/extreme-floods-may-be-the-new-normal/, Accessed: 3 October 2016.

Buchak, E. M. and Edinger, J. E. (1984). Generalized, longitudinal-vertical hydrodynamics and transport: Development, programming, and applications. Technical report, prepared for US Army Corps of Engineers Waterways Experiment Station, Vicksburg, MS.

Budd, J. W. and Warrington, D. S. (2004). Satellite-based sediment and chlorophyll a estimates for Lake Superior. *Journal of Great Lakes Research*, 30:459–466.

Cardenas, M. P., Schwab, D. J., Eadie, B. J., Hawley, N., and Lesht, B. M. (2005). Sediment transport model validation in Lake Michigan. *Journal of Great Lakes Research*, 31(4):373–385.

Cole, T. M. and Buchak, E. (1995). *CE-QUAL-W2: A two-dimensional, laterally averaged, hydrodynamic and water quality model*. US Army Engineer Waterways Experiment Station, Vicksburg, MS, 2.0 edition.

Cole, T. M. and Wells, S. A. (2003a). *CE-QUAL-W2: A two-dimensional, laterally averaged, hydrodynamic and water quality model*. US Army Engineer Waterways Experiment Station, Vicksburg, MS, 3.1 edition.

Cole, T. M. and Wells, S. A. (2003b). *CE-QUAL-W2: A two-dimensional, laterally averaged, hydrodynamic and water quality model*. US Army Engineer Waterways Experiment Station, Vicksburg, MS, 3.2 edition.

Cole, T. M. and Wells, S. A. (2006). *CE-QUAL-W2: A two-dimensional, laterally averaged, hydrodynamic and water quality model*. US Army Engineer Waterways Experiment Station, Vicksburg, MS, 3.5 edition.

Cole, T. M. and Wells, S. A. (2008). *CE-QUAL-W2: A two-dimensional, laterally averaged, hydrodynamic and water quality model*. Department of Civil and Environmental Engineering, Portland State University, Portland, OR, 3.6 edition.

Cole, T. M. and Wells, S. A. (2013). *CE-QUAL-W2: A two-dimensional, laterally averaged, hydrodynamic and water quality model*. Department of Civil and Environmental Engineering, Portland State University, Portland, OR, 3.71 edition.

Cole, T. M. and Wells, S. A. (2015a). *CE-QUAL-W2: A two-dimensional, laterally averaged, hydrodynamic and water quality model*. Department of Civil and Environmental Engineering, Portland State University, Portland, OR, 3.72 edition.

Cole, T. M. and Wells, S. A. (2015b). *CE-QUAL-W2: A two-dimensional, laterally averaged, hydrodynamic and water quality model*. Department of Civil and Environmental Engineering, Portland State University, Portland, OR, 4.0 edition.

De Vynck, G. and Polson, J. (2013). Suncor among Calgary offices closed amid severe Alberta floods. Available at: http://business.financialpost.com/news/suncor-among-calgary-offices-closed-amid-severe-alberta-floods, Accessed: 3 October 2016.

Derworiz, C. (2016). Southern Alberta flood leads to "argest university-led water project in the world". Available at: http://calgaryherald.com/news/national/southern-alberta-flood-leads-to-largest-university-led-water-project-in-the-world, Accessed: 3 October 2016.

Dubourg, P., North, R. L., Hunter, K., Vandergucht, D. M., Abirhire, O., Silsbe, G. M., Guildford, S. J., and Hudson, J. J. (2015). Light and nutrient co-limitation of phytoplankton communities in a large reservoir: Lake Diefenbaker, Saskatchewan, Canada. *Journal of Great Lakes Research*, 41:129–143.

Eadie, B. J., Schwab, D. J., Johengen, T. H., Lavrentyev, P. J., Miller, G. S., Holland, R. E., Leshkevich, G. A., Lansing, M. B., Morehead, N. R., Robbins, J. A., et al. (2002). Particle transport, nutrient cycling, and algal community structure associated with a major winter-spring sediment resuspension event in southern Lake Michigan. *Journal of Great Lakes Research*, 28(3):324–337.

Edinger, J. and Buchak, E. (1975). *A hydrodynamic, two-dimensional reservoir model: The computational basis*. US Army Engineer Division, Ohio River. Cincinnati, OH.

Edinger, J. and Buchak, E. (1978). Reservoir longitudinal and vertical implicit hydrodynamics. In *Proc. Int. Conf. on environmental effects of hydraulic engineering works, American society of civil engineers, Knoxville, TN*.

Fink, G., Wessels, M., and Wüest, A. (2016). Flood frequency matters: Why climate change degrades deep-water quality of peri-alpine lakes. *Journal of Hydrology*, 540:457–468.

Giesy, J. P., Li, P. D. S., and Khim, J. S. (2009). Water quality analysis report. Technical report, Toxicology Centre, University of Saskatchewan.

Gippel, C. J. (1995). Potential of turbidity monitoring for measuring the transport of suspended solids in streams. *Hydrological processes*, 9(1):83–97.

Grove, J. R., Croke, J., and Thompson, C. (2013). Quantifying different riverbank erosion processes during an extreme flood event. *Earth Surface Processes and Landforms*, 38(12):1393–1406.

Hecker, M., Khim, J. S., Giesy, J. P., Li, S.-Q., and Ryu, J.-H. (2012). Seasonal dynamics of nutrient loading and chlorophyll a in a northern prairies reservoir, Saskatchewan, Canada. *Journal of Water Resource and Protection*, 4(04):180.

Horritt, M. (2006). A methodology for the validation of uncertain flood inundation models. *Journal of Hydrology*, 326(1):153–165.

Huber, A., Ivey, G. N., Wake, G., and Oldham, C. E. (2008). Near-surface wind-induced mixing in a Mine Lake. *Journal of Hydraulic Engineering*, 134(10):1464–1472.

Hudson, J. J. and Vandergucht, D. M. (2015). Spatial and temporal patterns in physical properties and dissolved oxygen in Lake Diefenbaker, a large reservoir on the Canadian Prairies. *Journal of Great Lakes Research*, 41:22–33.

Ji, Z.-G. (2008). *Hydrodynamics and water quality: modeling rivers, lakes, and estuaries*. John Wiley & Sons.

Klemm, W., Greif, A., Broekaert, J. A., Siemens, V., Junge, F. W., Van der Veen, A., Schultze, M., and Duffek, A. (2005). A study on arsenic and the heavy metals in the Mulde river system. *CLEAN–Soil, Air, Water*, 33(5):475–491.

Kroon, F. J., Kuhnert, P. M., Henderson, B. L., Wilkinson, S. N., Kinsey-Henderson, A., Abbott, B., Brodie, J. E., and Turner, R. D. (2012). River loads of suspended solids, nitrogen, phosphorus and herbicides delivered to the Great Barrier Reef lagoon. *Marine pollution bulletin*, 65(4):167–181.

Langeveld, J., Veldkamp, R., and Clemens, F. (2005). Suspended solids transport: an analysis based on turbidity measurements and event based fully calibrated hydrodynamic models. *Water Science and Technology*, 52(3):93–101.

Lee, C., Schwab, D. J., Beletsky, D., Stroud, J., and Lesht, B. (2007). Numerical modeling of mixed sediment resuspension, transport, and deposition during the March 1998 episodic events in southern Lake Michigan. *Journal of Geophysical Research: Oceans*, 112(C2).

Lee, C., Schwab, D. J., and Hawley, N. (2005). Sensitivity analysis of sediment resuspension parameters in coastal area of southern Lake Michigan. *Journal of Geophysical Research: Oceans*, 110(C3).

Lenzi, M. A. and Marchi, L. (2000). Suspended sediment load during floods in a small stream of the Dolomites (northeastern Italy). *Catena*, 39(4):267–282.

Littlewood, I. G. (1992). *Estimating contaminant loads in rivers: a review*. Institute of Hydrology Hydrology (Centre for Ecology & Hydrology), Crowmarsh Gifford, Wallingford, Oxfordshire, OX1O 8BB.

Liu, G., Zhu, J., Wang, Y., Wu, H., and Wu, J. (2011). Tripod measured residual currents and sediment flux: Impacts on the silting of the Deepwater Navigation Channel in the Changjiang Estuary. *Estuarine, Coastal and Shelf Science*, 93(3):192–201.

Mama, C. and Okafor, F. (2011). Siltation in reservoirs. *Nigerian Journal of Technology*, 30(1):85–90.

Myint, S. and Walker, N. (2002). Quantification of surface suspended sediments along a river dominated coast with NOAA AVHRR and SeaWiFS measurements: Louisiana, USA. *International Journal of Remote Sensing*, 23(16):3229–3249.

Pappenberger, F., Matgen, P., Beven, K. J., Henry, J.-B., Pfister, L., and Fraipont, P. (2006). Influence of uncertain boundary conditions and model structure on flood inundation predictions. *Advances in Water Resources*, 29(10):1430–1449.

Romero, J. R. and Imberger, J. (2003). Effect of a flood underflow on reservoir water quality: Data and three-dimensional modeling. *Archiv für Hydrobiologie*, 157(1):1–25.

Sadeghian, A., de Boer, D., Hudson, J. J., Wheater, H., and Lindenschmidt, K.-E. (2015). Lake Diefenbaker temperature model. *Journal of Great Lakes Research*, 41:8–21.

Sadeghian, A., Hudson, J., Wheater, H., and Lindenschmidt, K. (2014). Water quality modeling of Lake Diefenbaker. *Water news. Can Water Res Assoc*, 33(2):17–20.

Sakmont Engineering (1987). A satellite imagery survey of land use in the effective drainage area of the South Saskatchewan River Basin. technical report d.2. Technical report, Consulting Hydraulic Engineers. Saskatoon, Saskatchewan.

Saskatoon City News (2013). 2013 high river flow updates. Available at: www.saskatooncitynews.ca, Accessed: 28 June 2013.

Stroud, J. R., Lesht, B. M., Schwab, D. J., Beletsky, D., and Stein, M. L. (2009). Assimilation of satellite images into a sediment transport model of Lake Michigan. *Water resources research*, 45(2).

Surbeck, C. Q., Jiang, S. C., Ahn, J. H., and Grant, S. B. (2006). Flow fingerprinting fecal pollution and suspended solids in stormwater runoff from an urban coastal watershed. *Environmental science & technology*, 40(14):4435–4441.

Sutherland, S. (2016). Three years later: What caused the 2013 Alberta floods? Available at: https://www.theweathernetwork.com/news/articles/why-was-southern-alberta-so-vulnerable-to-flooding-in-2013/29800, Accessed: 3 October 2016.

Valero-Garces, B. L., Navas, A., Machin, J., and Walling, D. (1999). Sediment sources and siltation in mountain reservoirs: a case study from the central spanish pyrenees. *Geomorphology*, 28(1):23–41.

Vincent, W. F., Gibbs, M. M., and Spigel, R. H. (1991). Eutrophication processes regulated by a plunging river inflow. *Hydrobiologia*, 226(1):51–63.

Walling, D. (1977). Limitations of the rating curve technique for estimating suspended sediment loads, with particular reference to British rivers. *Erosion and solid matter transport in inland waters*, pages 34–48. IAHS Publication 122.

Welsch, E. and De Vynck, G. (2013). Alberta floods spread as water subsides in Calgary. Available at: http://www.bloomberg.com/news/articles/2013-06-24/alberta-floods-spread-as-water-subsides-in-oil-hub-of-calgary, Accessed: 3 October 2016.

Wetzel, R. G. (2001). *Limnology: lake and river ecosystems*. Gulf Professional Publishing, 3rd edition.

Wheater, H. and Evans, E. (2009). Land use, water management and future flood risk. *Land Use Policy*, 26:S251–S264.

Wheater, H. and Gober, P. (2013). Water security in the Canadian Prairies: science and management challenges. *Philosophical Transactions of the Royal Society of London A: Mathematical, Physical and Engineering Sciences*, 371(2002):20120409.

WSA (2012). *State of Lake Diefenbaker*. Water Security Agency. Available at: https://www.wsask.ca/Global/Lakes%20and%20Rivers/Dams%20and%20Reservoirs/Operating%20Plans/Developing%20an%20Operating%20Plan%20for%20Lake%20Diefenbaker/State%20of%20Lake%20Diefenbaker%20Report%20-%20October%2019%202012.pdf, Accessed: 21 May 2015.

Wüest, A., Imboden, D., and Schurter, M. (1988). Origin and size of hypolimnic mixing in Urnersee, the southern basin of Vierwaldstättersee (Lake Lucerne). *Schweizerische Zeitschrift für Hydrology*, 50(1):40–70.

Yip, H. (2015). An assessment of present and historical (1984–2012) Lake Diefenbaker water clarity and chlorophyll-a concentration using Landsat imagery. Master's thesis, University of Saskatchewan.

Chapter 9

Synthesis, conclusions and future works

9.1 Overviews

In previous chapters, different stages of water quality modeling of Lake Diefenbaker were discussed. Both the model development and reservoir's status were of concern in this study. In Chapter 1, we presented an overview of the study area, Lake Diefenbaker, and briefly described the modeling stages. In Chapter 3, the temperature and hydrodynamic processes in Lake Diefenbaker were discussed. Also, the historical study of sedimentation rates in the reservoir was presented. A method for better and faster calibration by using combined global/local optimization techniques was used, and, finally, snow cover effects on the ice surface were included in the calculations. In Chapters 4, 5 and 6, the effects of bathymetry, meteorological data and inflow water quality data were presented. I estimated the water quality variables required for the modeling based on the date, Julian day, discharge and water temperature. Three meteorological databases, Environment Canada, AccuWeather and MeteoBlue, were used and results were compared to find the most suitable database for Lake Diefenbaker. In Chapter 7, the complete water quality model of Lake Diefenbaker was built and presented. I also built a *Lite* model, being able to reproduce accurate results in a short time, useful for management purposes. Also, a method for better calculation of chlorophyll *a* concentrations was employed. Finally, in Chapter 8, the sediment transport model for Lake Diefenbaker was built and presented based on the 2013 Calgary flood. The model was calibrated based on the MODIS satellite images and on-site turbidity measurements and provided information on the transport characteristics of suspended solids in Lake Diefenbaker.

The South Saskatchewan River (SSR) is a long river (1,392 km) (Sheelanere et al., 2013) flowing through the provinces of Alberta (AB) and Saskatchewan (SK) in Canada. Near the AB-SK border (∼331 km upstream of dams), the Red Deer River (RDR) merges with the SSR. Much of the Saskatchewan River Basin (SRB) lies within the Canadian Prairie

region, which experiences many weather extremes and a wide range in weather variability during the year. Examples are the wide yearly range in air temperature (-40 to +40 °C) as well as extreme dry and wet conditions (the 1999 – 2004 drought period and 2011 and 2013 large-scale flooding). Eighty percent of the Saskatchewan River's runoff stems from its headwaters in the Rocky Mountains. Eighty percent of Canada's agricultural land lies within the Prairies, with 82% of Canada's irrigated agriculture in the river basin (c.f. Wheater and Gober, 2013; Wheater, 2015). Approximately 171 kilometers downstream of the SSR and RDR confluence is the inlet to Lake Diefenbaker (LDF) at Highway 4.

Lake Diefenbaker is one of the most important sources of water in Saskatchewan, with most of its inflow stems from the upper SSR (WSA, 2012). The lake is a strategic reservoir formed by the construction of two earth-filled dams (the Gardiner Dam and the Qu'Appelle River Dam) in the SSR valley. The reservoir is 181 km long, with increasing depth from 8 m at its upstream to 60 m at the Gardiner Dam (Sadeghian et al., 2015). Most of the inflow (∼98%) comes from the SSR, and the main outflow (∼98%) is through the Gardiner Dam. The reservoir provides water storage capacity for irrigation, drinking water, recreation, eco-services, hydropower generation, fish farming, and waste receptacles. It also plays a key role in flood mitigation.

Lake Diefenbaker receives high loads of phosphorus from the SSR, with 1,533 and 616 tons per year in 2011 and 2012, respectively (North et al., 2015). The phosphorus load is primarily in particulate form (North et al., 2015; Saskatchewan Environment and Public Safety, 1988) and not readily available for immediate uptake by aquatic organisms such as algae. As a result, the reservoir acts as a sink for phosphorus (P), retaining 86% and 84% of the incoming phosphorus in the years 2011 and 2012, respectively (North et al., 2015). During low hypolimnetic oxygen conditions in summer, there is a high potential for the phosphorus to be released from the bottom sediments in a more accessible dissolved form (North et al., 2015). The release rate of P can be greatly affected by temperature. Algal blooms, an indicator of eutrophication, have already been observed in some parts of the reservoir in late summer and early fall (Abirhire et al., 2015; Giesy et al., 2009; WSA, 2012).

According to recent Regional Climate Model (RCM) studies on future climate change impacts (Khaliq et al., 2015; Mearns et al., 2012), the South Saskatchewan River Basin

(SSRB) is expected to become warmer, based on average air temperature. These future differences in air temperature will affect the timing and intensity of precipitation; evaporation and ice melting; and the frequency of droughts and floods (Gober and Wheater, 2014). These changes could alter the lake's heat balance and, consequently, affects thermally dependent components such as the dissolved oxygen concentration and lake productivity (Hudson and Vandergucht, 2015; Jankowski et al., 2006; Peeters et al., 2002). For many species, these changes could be devastating as their reproduction and migration are based on water temperature (Ji, 2008). More frequent extreme events are also consequences of climate change and land management practices (Wheater and Evans, 2009). Higher flood peaks lead to higher erosion rates and consequently higher suspended sediments and turbidity. High turbidity cancels the effects of sunlight in killing pathogens and creates expensive maintenance costs and navigation problems due to sediment deposition and siltation (Ji, 2008).

Concerns about climate change, water security and environmental sustainability have enhanced the motivation to use a numerical model for studying the behaviors of Lake Diefenbaker. Water quality modeling has significantly evolved during the past several years. For example, these models have more dimensions (2D and 3D) with greater capabilities in prediction and analysis and integration with watershed models (Hellweger, 2015). Models exist for many different processes and with a wide range of complexities. Based on the study's objectives, the physical and chemical characteristics of the lake and available data, the CE-QUAL-W2 hydrodynamic and water quality model was deemed the best model for Lake Diefenbaker. The CE-QUAL-W2 is a 2D laterally averaged water quality model over 40 years in development. CE-QUAL-W2 can simulate water temperature, hydrodynamics, dissolved and particulate suspended solids, dissolved oxygen, nutrients, organic matter and algae, enabling us to fulfill all our research objectives. Due to several decades of model development, it has an up-to-date user manual and an active user forum. The best feature is that the source code is freely available with clear comments allowing the extension and application of new formulations and algorithms.

The hydrological, morphological and ecological variations of the reservoir were successfully captured in the model, an important objective of the simulations to better understand the complexity of the system, as well as the key factors that lead to changes in the lake's

aquatic ecosystem.

9.2 Conclusions

9.2.1 Bathymetry

Prior to the operation of Lake Diefenbaker, sedimentation studies were planned and a series of cross sections, referred to as ranges, were established at different locations along the lake for this purpose (Figure 4.2). The range "cross sections" begin with # 1 at Gardiner dam and ascend upstream to # 21 at Highway 4. Profiling of the land portion of each range down to the waterline was done using the surveyor's chain and level method. The underwater portion of each range was measured from a boat using an echo sounder. In 2012 and 2013, field data were re-collected using a *BioSonics DT-X* surface unit launched on a boat and the *BioSonics Acquisition* software. Fieldwork was done by simultaneously recording latitudes and longitudes from a GPS and depth data from the echo sounder. The 2012 – 2013 cross sections were then obtained from the interpolated bathymetry.

The results showed that sedimentation rates from the late 1960s-early 1970s to 2012 – 2013 decreased rapidly from 0.18 m year^{-1} m at range 24 to 0.02 m year^{-1} at range 15 to lower, negligible values downstream. This pattern of rapid decrease of the sedimentation rate downstream in the lake is consistent with observations of sedimentation rates in the early years of the lake as reported by Yuzyk (1983). Field observations indicate high rates of shoreline retreat. Steep, actively retreating cliffs are ubiquitous along the lake's shoreline, and there are many instances of fences that have collapsed as the shoreline retreated. This pattern of active shoreline retreat is consistent with reports from the early years of the lake describing the need for the range line markers to be moved landward as shoreline erosion had caused a number of markers to fall into the lake. In a number of instances, shoreline retreat has resulted in the formation of columnar islands isolated from the shoreline, analogous to sea stacks found in a marine setting. As erosion progresses, these columns ultimately disappear, and there are several places where it appears that shallows in the lake are all that remain of the pre-lake topography with much higher elevations. Sediment deposited in the lake is derived from two major sources. The South Saskatchewan River transports sediment from upstream regions. The majority of this sediment is deposited in the upstream

reach (ranges 38 to 32) and the drawdown reach (ranges 32 to 26). Unfortunately, there is no program to monitor the sediment load so that estimates have to rely on data from the 1960s and 1970s (Ashmore and Day, 1988). A second major source of sediment is shoreline erosion. Studies report retreat rates of 1 to 3 m year^{-1}, but there is little information on spatial and temporal variability of retreat rates, making estimates of average values uncertain at best. Future estimates of the sediment budget of Lake Diefenbaker would therefore greatly benefit from long-term monitoring programs that address these gaps.

9.2.2 Temperature and hydrodynamics

A two-dimensional laterally-averaged numerical model was applied to Lake Diefenbaker for the period 2011 – 2012 to study the changes in the lake's thermal structure. The model successfully simulated the basic features of the thermal structure of the lake, including spring isothermal conditions, summer stratification and the overturn in late fall, as well as water temperature in both the epilimnion and hypolimnion. A novel contribution of this work was the application of a lake temperature model to explore the impact of an inflowing tributary on the heat budget of a reservoir. The 2011 – 2012 simulations showed that the higher flows and warmer temperatures of the SSR in late spring and early summer, along with the short residence time of Lake Diefenbaker, caused the stratification to occur earlier in this season. The lower discharge of the inflow in the fall does not significantly change the timing of the fall turnover.

The Monte-Carlo sensitivity analysis demonstrated the high sensitivity of the wind sheltering and shading coefficients. The light extinction coefficient and inflow water temperature were rather insensitive to changes within the defined ranges in calibration parameter values. Differences in results from using models with either 126 or 187 segments were minimal; however, the model with coarser grids (126 segments) showed less sensitivity to the WSC and SHADE parameters on model variables. The PSO+LM optimization method was able to find the best parameter settings after 41 iterations (on average), significantly reducing calculation times. Using continuous versus non-continuous simulations for the 2011 – 2012 period did not have any effect on results.

A hydrodynamic model may forecast algal bloom formations without having data on nutrients and oxygen concentrations. The model recognized several areas that were sensitive to strong winds (e.g., chainage 90 and 130 km in Figure 3.8). In these areas, strong winds can bring nutrient-rich sediment to the water column. Secondly, areas with low flow and high temperature were identified, particularly in the Qu'Appelle River arm.

Since the construction of Lake Diefenbaker, many studies have been carried out in different fields of research, but there has never been a study quantifying the effects of different heat sources to the heat budget. The current temperature model can provide a comprehensive synopsis for researchers and water managers to assist in determining and forecasting changes associated with different management practices in the SSR basin and the reservoir. It could also provide the Saskatchewan Water Security Agency (SWSA), the main water management agency in Saskatchewan, with valuable information to guide future flow management practices.

9.2.3 Meteorological data

We used three different climate databases to test the performance of a water quality model: Environment Canada data with long-term quality control standards, AccuWeather data with less than ten years of quality control data and MeteoBlue data, which were modeled. We used the climate data from these databases to run the CE-QUAL-W2 water quality model for Lake Diefenbaker in Saskatchewan, Canada. The results show significantly better model performances with the AccuWeather and MeteoBlue data. The main reasons are lack of cloudiness data and the fewer number of stations in EC databases. Cloudiness influences the heat budget by affecting short wave and longwave solar radiation. When selecting a good meteorological database, it is important that the database has all the required parameters. Environment Canada has high quality databases; however, the lack of cloud data produces large errors in water quality models. AccuWeather has more stations and parameters, but it is expensive and its data require lengthy delivery time. I found MeteoBlue to be the best option as the data produces good results, are free and are rapidly delivered.

9.2.4 Water quality data

I developed the best fitting approach for constructing a daily water quality database for a water quality model. A polynomial fitting used four components: Julian day to capture the seasonality; the date to incorporate long-term trends and seasonality; discharge to consider daily and seasonal effects of flow; and water temperature to maintain temperature dependence of most water quality components. Averaging the first and second order polynomial fits provided the best outputs. The first order polynomial fitting determines the seasonal patterns and the second order fitting adjusts for small frequency variations. Regarding the derived data, the confidence in the data in SSR is higher compared with those in RDR because of the larger number of samples for the SSR and the fact that the RDR has data only until 2012. The recorded data show that, because of smaller discharges and more turbid waters in the RDR than the SSR, the dissolved constitutions (e.g., TDS, DOM) are approximately at the same ranges, but the particulate constitutions (e.g., ISS, POM) are several times larger in the RDR.

9.2.5 Water quality modeling

The gaps between the biologists and modelers are much bigger compared with other fields of water resources engineering like hydrology and hydraulics. Many findings in limnology are not presented in the recent water-quality models (Hellweger, 2015). A very simple example is algae, crucial components of almost all water quality models. Algae concentrations are linked to biological, chemical and physical characteristics of the waterbody including carbon, phosphorous, nitrogen, silica, organic matter, dissolved oxygen, zooplankton, sediments and temperature (Sadeghian et al., 2014).

Below is the chemical equation for photosynthesis in algae (c.f. Ji, 2008):

$$106CO_2 + 16NO_3 + HPO_4 + 122H_2O + 18H \rightarrow C_{106}H_{263}O_{110}N_{16}P + 138O_2 \tag{9.1}$$

The weight ratios of carbon, phosphorous and nitrogen are:

$$C : P = \frac{106 \times 12}{1 \times 31} = 41 \tag{9.2}$$

$$N : P = \frac{16 \times 4}{1 \times 31} = 7.2 \tag{9.3}$$

Based on equation 9.3, if N:P becomes smaller than 7.2 there is a nitrogen limitation, and values above that show phosphorus limiting environments for algal growth. Ji (2008) found ranges different in practice with N:P ratios above 20 as P limited and below ten as N limited. Furthermore, many water quality models consider fixed ratios for these limiting nutrients, while, in reality, algae adjust their uptakes, and there can be multiple nutrient limitation conditions at the same time (Flynn, 2005). Lake Diefenbaker is an excellent example where the measurements show that algae adjust their C:P ratios based on P availability (Abirhire et al., 2015).

It is also common to show algae biomass (expressed as carbon per unit volume) as chlorophyll *a* in chlorophyll *a*/algal biomass ratios (Ji, 2008). In most water quality models Chla:C is fixed during simulations, while algae have very dynamic behaviors (Hellweger, 2015), and the ratios vary 10-fold based on light and nutrient conditions (Chapra, 2008; Flynn, 2005).

Improper representations of algal uptake and composition can be one of the reasons for moderately good or even poor performance of water quality models (Hellweger, 2015; Robson, 2014). Another source of error is using fixed rates for algae growth, mortality, respiration, excretion, and settling in different years in continuous simulations (Cole and Wells, 2013). One solution is using different algal groups in the models to cover all different characteristics of the algae behavior. However, the interpretation of results needs more expertise, time and field measurements.

I developed the 2D laterally averaged water quality model of Lake Diefenbaker using the CE-QUAL-W2 model. I considered a top-down approach by first developing a large, complex model and gradually simplifying it. I first began building the whole SSR+RDR+LDF model (827 segments and 60 vertical layers) and simplifying it to a LDF sole model (87 segments and 21 vertical layers). Depending on the study objective and available data, these models

can be used to launch future climate and land use change scenarios.

I considered DO, PO_4, NH_4, NO_3, LDOM, RDOM, LPOM, RPOM, algae, TDS and TSS in the model. I also applied Chapra's (2008) proposed method for calculating Chla concentrations based on nutrient and light availability. By using a variable stoichiometry, I was able to calculate Chla more accurately compared with using a fixed rate in Lake Diefenbaker.

9.2.6 Sediment transport

A water quality model was developed for Lake Diefenbaker to determine suspended solids transport and the rates of settling and resuspension through the reservoir. The length of the study was the two months of June and July 2013 when a flood occurred in the head waters of the South Saskatchewan River. The flood created the largest inflow to the reservoir since its construction in 1967, with flood waves carrying high loads of suspended sediments. I calibrated the model based on measured turbidity data from 12 stations along the Lake Diefenbaker collected during June and July 2013 and images obtained from cloud-free MODIS satellite imagery. I defined only one group of TSS because data on sediment texture (fine, medium and coarse) were not available. TSS was modeled as a tracer, and its movement through the reservoir was traced starting at the upstream portion of Lake Diefenbaker, with the sediment plume gradually becoming less concentrated by sedimentation and dilution as it moved through the reservoir. This setup allowed me to develop a dispersion and diffusion transport model of Lake Diefenbaker using the two-dimensional hydrodynamic and water quality model CE-QUAL-W2. The model was capable of tracing the flood's sediment plume movements through the reservoir. This has resulted in a better understanding of the settling and resuspension rates of the suspended sediments in the reservoir which will support decision making.

9.3 Future research

Water quality modeling practices have the ultimate objective of providing decision support for the protection and enhancement of ambient water quality. The outcomes of this study will help to support research in environmental water issues in Saskatchewan, Canada and,

ultimately worldwide.

This study can be extended by testing scenarios on land use and climate change to determine key factors that lead to accelerated eutrophication of Lake Diefenbaker. To provide a complete picture of future situations, the new boundary conditions will need to be defined. Hence, simulations using statistically downscaled meteorological data for climate change scenarios and extrapolated patterns of nutrient export mimicking land-use change scenarios will need to complement this modeling work.

The original ice algorithm yielded extremely poor ice thickness, formation and breakup simulations. The modified ice code calculated these terms with improved accuracy, albeit empirically. A physically-based model that considers snow cover, snow compaction, snow melting, refreezing and other parameters may be more suitable and will be a focus of future work.

The high sensitivity of model results to wind speed measurements and the effect of wind on mixing and occurrences of upwelling have highlighted the need for onsite measurements of wind for accurate calibration. The installation of a data-collecting buoy on the surface of Lake Diefenbaker is highly recommended.

Although I was able to calibrate these models successfully, too many computational resources and too much time were used for calculations and interpretations of the results. The majority of these efforts could have been avoided if better field measurements had been available for this reservoir. Regarding the input data, I recommend that a fixed sampling station be installed at the upstream end of the reservoir to measure daily/hourly flow and weekly/monthly water chemistry data.

Sediment models also need more work, as there are many crucial parameters missing in these models. For instance, CE-QUAL-W2 considers a fixed sediment oxygen demand (SOD) rate during the whole simulation time. Inside the model, SOD decay is dependent on temperature fluctuations, but the DO availability near the bed is not included in calculations. In a recent study carried out on the Buffalo Pond Lake, we showed the effects of variable SOD on the accuracy of dissolved oxygen simulations in winter (Terry

et al., 2017). Ji (2008) calls for a complete sediment model that includes full sediment diagenesis processes and fluxes. Diagenesis occurs when the sediment particulate organic matter undergoes decomposition and mineralization (converting to dissolved inorganic nutrient) and sediment flux occurs when the dissolved inorganic nutrients return to the water column and become available for plants and algae uptake (Ji, 2008). A recent version of CE-QUAL-W2 (Version 4.0) incorporates the sediment diagenesis model *Oil Sands Pit Lake Model (OSPLM)* to the main code, which is a big achievement.

The main limitation of CE-QUAL-W2 for studying sediment transport is the lack of definition of the suspended solids settling rate in the model. This parameter has a fixed value, which is restrictive since settling rates are extremely dependent on flow characteristics. However, good results were obtained by increasing settling rates in areas where the reservoir becomes deeper and the flow currents become slower. Therefore, the current version of the CE-QUAL-W2 model may be more suited for sediment transport calculations of shorter time periods and for systems with a uniform flow distribution. The model needs a more flexible sediment-settling coefficient that at least differentiates between different sections of the river and reservoir.

References

Abirhire, O., North, R. L., Hunter, K., Vandergucht, D. M., Sereda, J., and Hudson, J. J. (2015). Environmental factors influencing phytoplankton communities in Lake Diefenbaker, Saskatchewan, Canada. *Journal of Great Lakes Research*, 41:118–128.

Ashmore, P. and Day, T. (1988). Spatial and temporal patterns of suspended-sediment yield in the Saskatchewan River basin. *Canadian Journal of Earth Sciences*, 25(9):1450–1463.

Chapra, S. C. (2008). *Surface water-quality modeling*. Waveland press.

Cole, T. M. and Wells, S. A. (2013). *CE-QUAL-W2: A two-dimensional, laterally averaged, hydrodynamic and water quality model*. Department of Civil and Environmental Engineering, Portland State University, Portland, OR, 3.71 edition.

Flynn, K. (2005). Castles built on sand: dysfunctionality in plankton models and the inadequacy of dialogue between biologists and modellers. *Journal of Plankton Research*, 27(12):1205–1210.

Giesy, J. P., Li, P. D. S., and Khim, J. S. (2009). Water quality analysis report. Technical report, Toxicology Centre, University of Saskatchewan.

Gober, P. and Wheater, H. (2014). Socio-hydrology and the science–policy interface: a case study of the Saskatchewan River basin. *Hydrology and Earth System Sciences*, 18(4):1413–1422.

Hellweger, F. L. (2015). 100 years since streeter and phelps: it is time to update the biology in our water quality models. *Environmental science & technology*, 49(11):6372–6373.

Hudson, J. J. and Vandergucht, D. M. (2015). Spatial and temporal patterns in physical properties and dissolved oxygen in Lake Diefenbaker, a large reservoir on the Canadian Prairies. *Journal of Great Lakes Research*, 41:22–33.

Jankowski, T., Livingstone, D. M., Bührer, H., Forster, R., and Niederhauser, P. (2006). Consequences of the 2003 european heat wave for lake temperature profiles, thermal stability, and hypolimnetic oxygen depletion: Implications for a warmer world. *Limnology and Oceanography*, 51(2):815–819.

Ji, Z.-G. (2008). *Hydrodynamics and water quality: modeling rivers, lakes, and estuaries*. John Wiley & Sons.

Khaliq, M., Sushama, L., Monette, A., and Wheater, H. (2015). Seasonal and extreme precipitation characteristics for the watersheds of the Canadian Prairie provinces as simulated by the NARCCAP multi-RCM ensemble. *Climate Dynamics*, 44(1-2):255–277.

Mearns, L. O., Arritt, R., Biner, S., Bukovsky, M. S., McGinnis, S., Sain, S., Caya, D., Correia Jr, J., Flory, D., Gutowski, W., et al. (2012). The North American regional climate change assessment program: overview of phase I results. *Bulletin of the American Meteorological Society*, 93(9):1337–1362.

North, R. L., Johansson, J., Vandergucht, D., Doig, L. E., Liber, K., Lindenschmidt, K.-E., Baulch, H., and Hudson, J. J. (2015). Evidence for internal phosphorus loading in a large prairie reservoir (Lake Diefenbaker, Saskatchewan). *J. Great Lakes Res.*, 41(Supplement 2):91–99.

Peeters, F., Livingstone, D. M., Goudsmit, G.-H., Kipfer, R., and Forster, R. (2002). Modeling 50 years of historical temperature profiles in a large central European lake. *Limnology and Oceanography*, 47(1):186–197.

Robson, B. J. (2014). State of the art in modelling of phosphorus in aquatic systems: review, criticisms and commentary. *Environmental Modelling & Software*, 61:339–359.

Sadeghian, A., de Boer, D., Hudson, J. J., Wheater, H., and Lindenschmidt, K.-E. (2015). Lake Diefenbaker temperature model. *Journal of Great Lakes Research*, 41:8–21.

Sadeghian, A., Hudson, J., Wheater, H., and Lindenschmidt, K. (2014). Water quality modeling of Lake Diefenbaker. *Water news. Can Water Res Assoc*, 33(2):17–20.

Saskatchewan Environment and Public Safety (1988). *Lake Diefenbaker and upper South Saskatchewan River: water quality study 1984 – 85.* Water Quality Branch and Environment Canada, Inland Waters Directorate, Water Quality Branch. Available at: http:/library2.usask.ca/gp/sk/en/scanned/lake.diefenbaker.water.study.1988.pdf.

Sheelanere, P., Noble, B. F., and Patrick, R. J. (2013). Institutional requirements for watershed cumulative effects assessment and management: Lessons from a Canadian trans-boundary watershed. *Land Use Policy*, 30(1):67–75.

Terry, J. A., Sadeghian, A., and Lindenschmidt, K.-E. (2017). Modelling dissolved oxygen/sediment oxygen demand under ice in a shallow eutrophic prairie reservoir. *Water*, 9(2):131.

Wheater, H. and Evans, E. (2009). Land use, water management and future flood risk. *Land Use Policy*, 26:S251–S264.

Wheater, H. and Gober, P. (2013). Water security in the Canadian Prairies: science and management challenges. *Philosophical Transactions of the Royal Society of London A: Mathematical, Physical and Engineering Sciences*, 371(2002):20120409.

Wheater, H. S. (2015). Water security-science and management challenges. *Proceedings of the International Association of Hydrological Sciences*, 366:23.

WSA (2012). *Area and capacity curves for Lake Diefenbaker*. Number Plan No. J5-1(33). Water Security Agency.

Yuzyk, T. R. (1983). *Lake Diefenbaker, Saskatchewan: a case study of reservoir sedimentation*. Inland Waters Directorate, Environment Canada.

Appendix I

Modelling Scenarios to Estimate the Potential Impact of Hydrological Standards on Nutrient Retention in the Tobacco Creek Watershed, Manitoba, Canada

This chapter is a published paper in the journal of Water Resources Management.

Weber, D., **Sadeghian, A.**, Luo, B., Waiser, M., Lindenschmidt, K.E. (2017). Modelling scenarios to estimate the potential impact of drainage standards on nutrient retention in a Canadian prairie watershed. *Journal of Water Resources Management*, 31 (4), 1305-1321, DOI: 10.1007/s11269-017-1578-9

The document has been reformatted from the original version for inclusion in the thesis, and no content has changed from the published version. The permission to use the manuscript in this thesis from the publisher (SPRINGER) is included in Appendix VI.

Contributions of the candidate and co-authors

The candidate's contributions are follows: setting up and calibrating the water quality model; wring parts of the manuscript. The first author conducted the analyses and manuscript writing. The last three authors helped through the research process and manuscript writing.

Contribution of this chapter to the overall study

The overall objective of this Ph.D. research was to conduct the water quality modeling of Lake Diefenbaker. Lake Diefenbaker is a large and complex waterbody which requires extensive computational resources and expertise for performing the simulations. Hence, before building the model of Lake Diefenbaker, two small sites, in the region, were selected

for constructing the test model. These sites were the Blackstrap Lake in Saskatchewan and the Brown drain within the Tobacco Creek watershed in Manitoba. The results of the Blackstrap Lake model are presented in Chapter 3, and the results of the Tobacco Creek model are presented here. This study helped to better understand the model performance and calibration for water quality and nutrients variables.

I Abstract

Nutrient loading from agricultural drainage systems into downstream aquatic ecosystems, like Lake Winnipeg in the prairie province of Manitoba, Canada, represents a major challenge for water quality management. In order to improve water quality in downstream waterbodies, the Manitoba government is currently investigating the relationship between hydrological standard of agricultural drainage network and nutrient retention in the drainage systems. Briefly, oversized drains have more capacity to transport nutrients, which can increase nutrient loading to downstream waterbodies, especially during rainfall events. Currently, the hydrological standards of agricultural drainage design in Manitoba were mainly developed according to cost-benefit analysis without considering nutrient retention. The purpose of this study was to use computer modelling techniques to simulate the impact of drain size (based on different hydrological standards) on nutrient retention within an agricultural drainage network. The site chosen was the Tobacco Creek Watershed, an agricultural area which drains into the Red River, and thence into Lake Winnipeg. Suspended sediment, nutrient and flow data, from several locations along the Brown drain within this watershed, were used to calibrate a water quality model. Scenarios were then simulated with the model to estimate how different drain sizes affect nutrient transport and retention. Sampling took place during the spring and summer of 2013 starting with freshet and ending when the drains dried up near mid-summer. Study results indicated that the amount of nutrients transported was generally greater during freshet and summer rain storms. Occasionally, however, nutrients in summer discharge exceeded those transported during freshet. The water quality model was applied to the Brown drain to investigate the effects of different drain sizes for rainfall amounts under 2, 5, 10, 15, and 20 year return periods. Generally the results indicate that as the return periods became larger (in larger channels) lower nutrients concentrations were predicted downstream (higher decay

rates). On average, the model predicted a 15%–20% decline in nutrient concentration with a 20-year return channel design compared to a 2-year return. The research from this study may provide an impetus to the policy-making process of drainage design.

II Introduction

Lake Winnipeg in Manitoba, Canada, experiences severe water quality problems which threaten both aquatic and terrestrial life. Due to excessive nutrient loading (phosphorus (P) and nitrogen (N)), cyanobacterial blooms have been increasing in frequency, duration, and intensity in the Lake over the past 30 years (LWSB, 2006). A long term study conducted from 1994 to 2001 estimated that Lake Winnipeg received approximately 63,207 t/year of total nitrogen (TN) and 5838 t/year of total phosphorous (TP). Almost half of the TN (46%) and three quarters of the TP (73%) originated from the Red River Valley drainage basin (Bourne et al., 2002).

To improve lake health, the Manitoba government has recommended Lake Winnipeg should return to its pre-1970's nutrient levels. Such a return would require a 13% reduction in N and 10% in P concentrations (LWSB, 2006). Consequently, an action plan was created, targeting different provincial areas, in an attempt to lessen the excess nutrient load to the lake. As part of this plan, the Lake Winnipeg Stewardship Board requested a review of agricultural land drainage networks in watersheds around the province (LWSB, 2006). Upon completion, the review recommended more research to investigate non-point source pollution from agricultural sources. As the review pointed out, such research would necessarily have to balance three important hydrological concerns: flood damage, water quality, and nutrient retention (LWSB, 2009).

Ditches throughout small agricultural watersheds in the Red River Valley ensure quick water drainage to avoid damage to infrastructure and crops during flood events. Water from agricultural drainage network contains significant nutrient concentrations; nutrients which end up in the Red River and in turn Lake Winnipeg. Unfortunately, the current agricultural drainage design standard in Manitoba does not take into consideration nutrient retention. Instead, drains within the landscape empty runoff quickly, thereby minimizing

crop losses from inundation and maximizing long term agriculture yields. As a result of higher flow capacities and a quicker water conveyance, nutrients in some drainage networks are not retained to any great degree. To address this problem, the action plan suggested that some research should focus on the influence of drain size on water velocity and nutrient loading. Tobacco Creek is one of many waterways in the Red River Valley whose waters eventually drain into Lake Winnipeg. This small watershed with its extensive network of drainage ditches was therefore considered an ideal choice for a study to evaluate the effect of differing drain sizes on nutrient retention and loading.

Within the Tobacco Creek watershed numerous long term studies have detailed land and water use practices (Glozier et al., 2006; Hope et al., 2002; Tiessen et al., 2010). Most of these studies, however, focus on the Tobacco Creek watershed headwaters, particularly the South Tobacco Creek sub-watershed with fewer in the downstream section of the Tobacco Creek watershed. A drain (The Brown drain) located in this downstream section was chosen as a study site for a number of reasons. Firstly it is a more encapsulated tributary and not influenced by the Tobacco Creek headwaters. As well, this particular drain was representative of many similar drains within the Red River Valley. And finally it was thought that focusing on smaller, localized tributaries would give a better understanding of nutrients that originate and are transported within the basin. To this end, computer modelling was applied to better address the effect of resizing drains on nutrient retention and transport. It was hoped that the results of this modeling exercise could be used to recommend which drain sizes might work best to improve nutrient retention in drained lands.

III Study Site

Tobacco Creek (outlet coordinates at the Morris River near Rosenort, Manitoba: 49°.44' N and 97°.44' W) is located within the Red River Basin in southern Manitoba, about 150 km southwest of Winnipeg. Watershed headwaters lie on the outer edge of the Manitoba Escarpment, which is the boundary of the ancient glacial Lake Agassiz. The Escarpment forms a 60 m drop in elevation over a distance of 3 km and the entire watershed branches out to cover 74 km^2 of land. Further downstream, Tobacco Creek drains into the Morris River, a tributary of the Red River, which then flows into Lake Winnipeg. Soils here are

predominantly clay loams formed on moderate to strong calcareous glacial till, overlaying shale bedrock (AAFC, 2013). Land use in the area is mainly agricultural, with 71% under annual cropping and 6% under permanent forage (Hope et al., 2002). Average annual precipitation amounts to approximately 550 mm and the average temperature is 2.75 °C. There are quantitative precipitation and temperature differences between the upper escarpment and lowlands of about 90 mm and 1.1 °C, respectively (Hope et al., 2002).

This research focuses on two study areas within the downstream, lowland catchment (Fig. I.1), an area encompassing about 1000 km^2. In the first study area, four sites along the main channel of Tobacco Creek (Sites 4, 5, 6, and 7 in Fig. I.1) were sampled. The second study area, the main focus of this paper, was located at a small, local drain north of the main creek called Brown drain. Here, two sites (17 (upstream) and 11 (downstream)) were sampled. Site 5 is located just downstream of where the Brown drain flows into Tobacco Creek. Although only results from the Brown drain will be presented here, patterns at both drains were similar. For comparison purposes, data for the Main drain is located in the supplementary materials. The catchment area of the Main drain is significantly larger than the Brown drain and has more headwater influence. Water flows in the Brown drain for only a few months following the snow melt and is usually dry by the fall.

IV Methods and Data

IV.1 Water Sampling

Water sampling was carried out from the end of April to September of 2013 at all 6 sites mentioned above. Grab samples were collected from the water surface at the middle of the creek channel and subsequently analysed by the Department of Fisheries and Oceans (DFO) laboratories in Winnipeg for nitrate (NO_3), nitrite (NO_2), ammonium (NH_4^+), suspended nitrogen (SUSPN), total dissolved nitrogen (TDN), soluble reactive phosphorous (SRP), suspended phosphorous (SUSPP), total dissolved phosphorous (TDP), dissolved organic carbon (DOC), and total dissolved solids (TSS) according to Stainton, Capel and Armstrong (1977). Water discharge was calculated from water levels recorded over the summer months. Samples were collected almost daily from the end of April to May, and

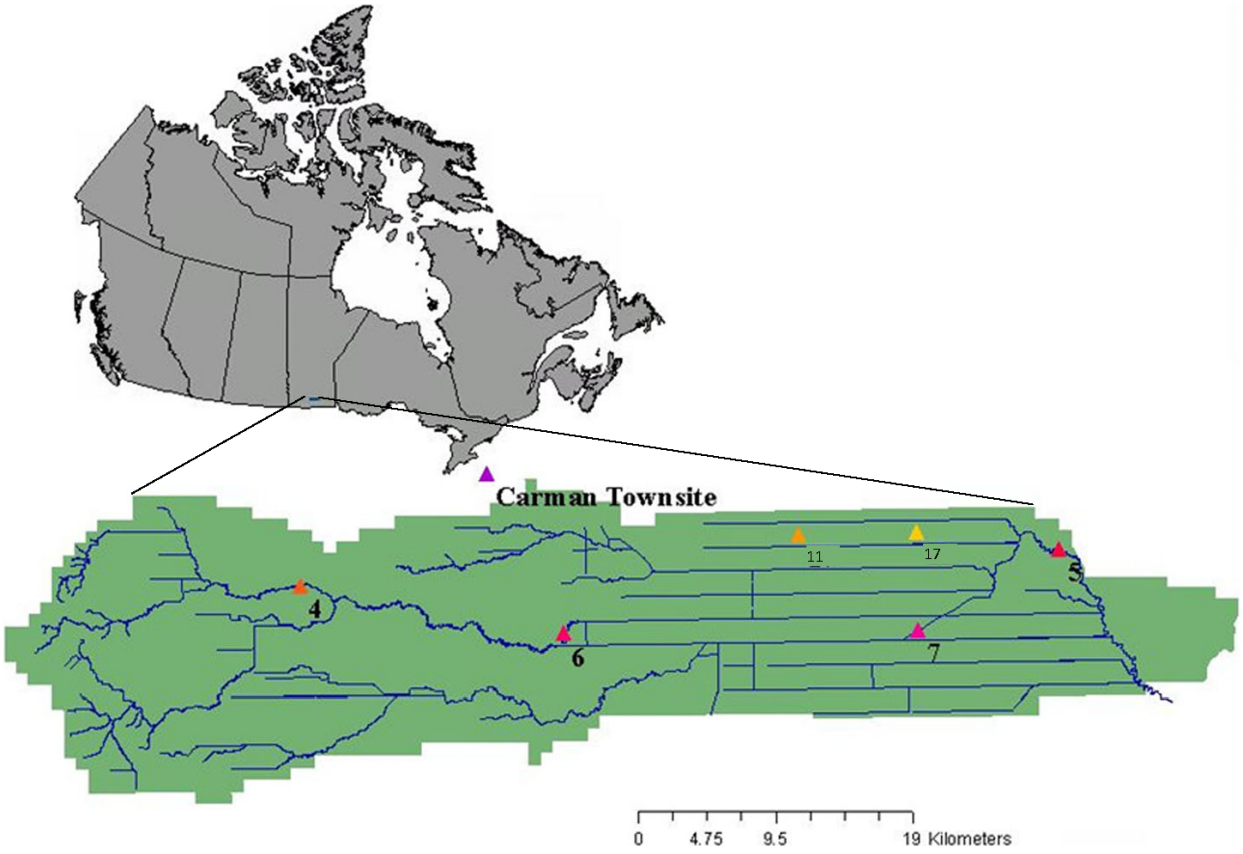

Figure I.1: The Tobacco creek watershed is located in southern Manitoba. the brown drain is at sites 17 and 11 while the main drain is sites 4, 6. 7, and 5

then weekly for the remaining months.

IV.2 Modelling

For the modeling exercise, the Brown drain was selected as a typical drain in the Tobacco Creek watershed, and used as a representative of the entire drainage network here. The model selected was CE-QUAL-W2, a 2D (longitudinal and vertical) water quality and hydrodynamic model for rivers, estuaries, lakes and other aquatic ecosystems (Cole and Wells, 2013; Sadeghian et al., 2015). This model can be used to model basic eutrophication processes including temperature-nutrient-algae and organic matter relationships. For the Tobacco Creek study, however, inflow discharge and nutrient inputs were used in the model to calculate the change in concentration during channel travel time. The key input data for modeling the Brown drain were: bathymetry, discharge rates, nutrients loads,

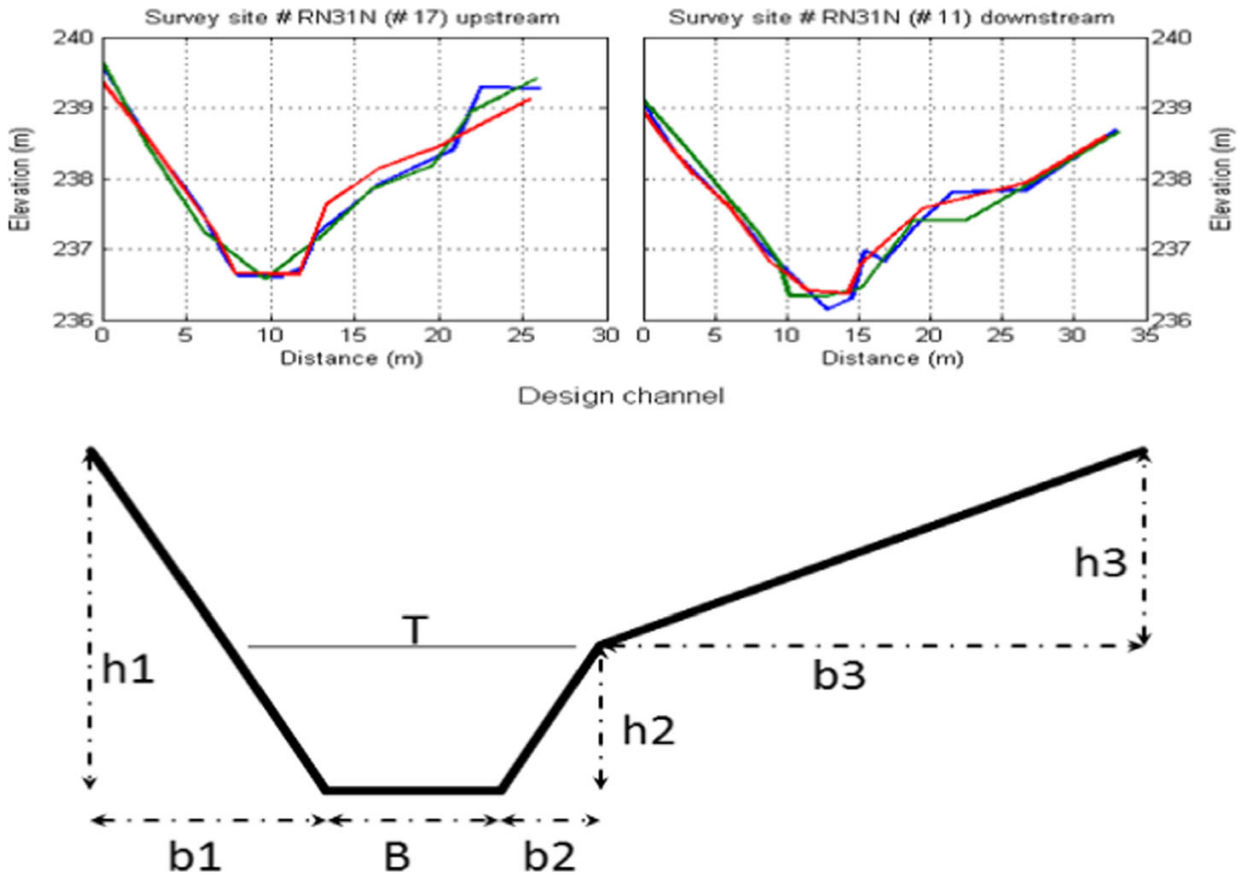

Figure I.2: Channel geometry of the Brown drain in tobacco creek

and meteorological data. Meteorological data was collected from a station at the town of Carman (Carman University of Manitoba Climate Station) located northwest of the creek. Nutrient concentrations used were based on 2013 field measurements from Sites 11 and 17 and included nitrate and nitrite (NO_3 and NO_2), ammonium (NH_4) inorganic dissolved phosphorous (PO_4) and total nitrogen and phosphorous in labile dissolved organic matter ($LDOM_N$ and $LDOM_P$).

For bathymetry calculations, the channel profile of Brown drain was extracted from previous work (Petzold, 2012). The design channel was defined as a trapezoid with uneven banks (Fig. I.2). At Site 17 the channel was 27 m wide while at Site 11 it was 34 m. The difference in bed elevation between the 2 cross sections was 30 cm in 8 km (5 miles) giving a slope of 0.0037%.

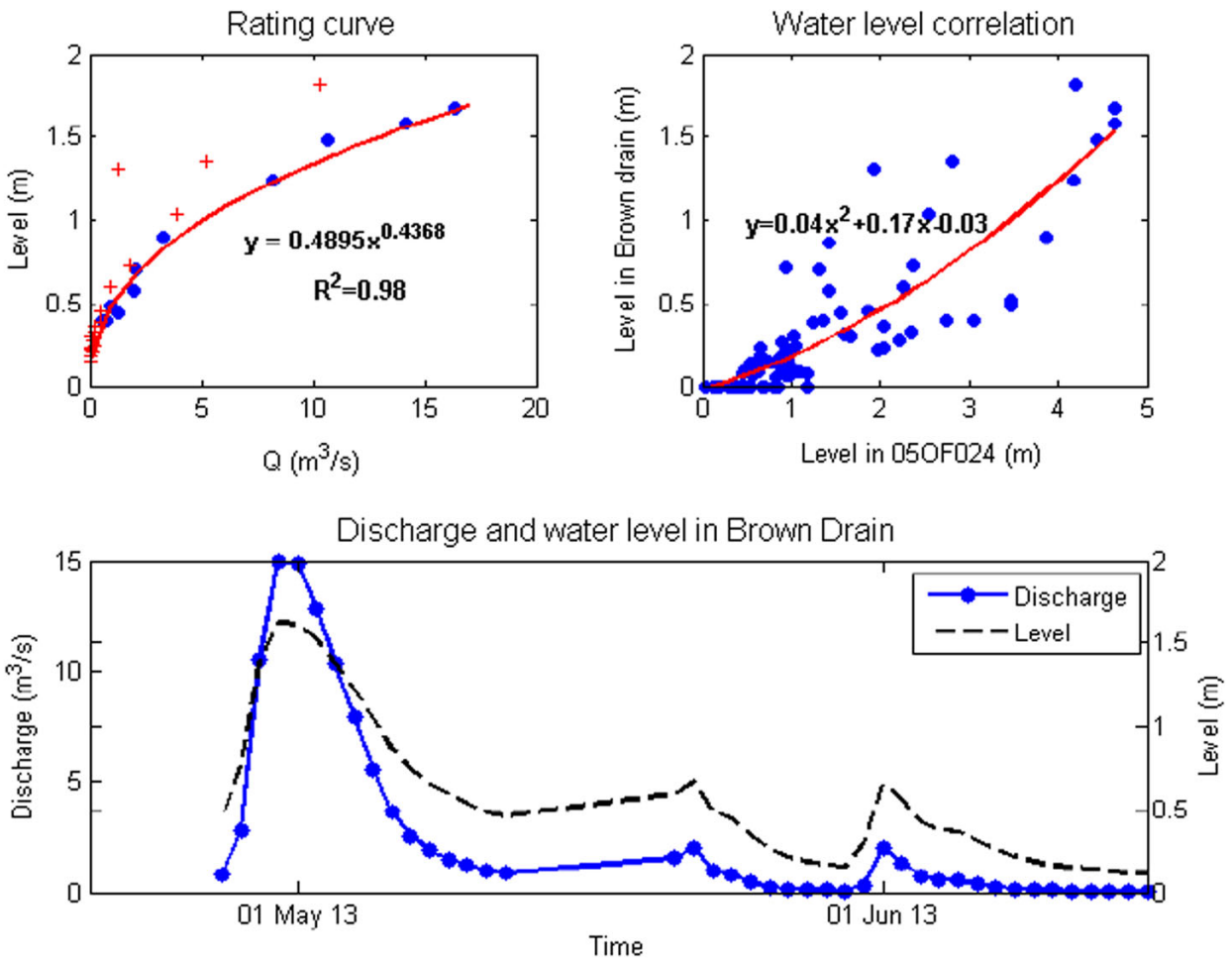

Figure I.3: Flow and water level in the Brown drain during the year 2013. outliers in the data are marked with a red cross

Because there was no hydrometric station on the Brown drain for measuring flow rates they had to be estimated for the modelling scenario. Water level and velocity data from 2013 were used to create a rating curve (Fig. I.3). This curve was subsequently used to determine a correlation between channel water levels and the flow recorded at the Rosenort hydrometric station (# 05OF024 on Little Morris River near Rosenort located at Site 5 sampling station). Discharges for the rating curve were calculated by using the water velocity and channel wetted area ($Q = V \times A$). Equations for calculating discharge and channel geometries are summarized in Tables I.1 and I.2 respectively. To remove outliers in the data, Manning coefficients were calculated and coefficients larger than 0.045 were removed from rating curve calculations.

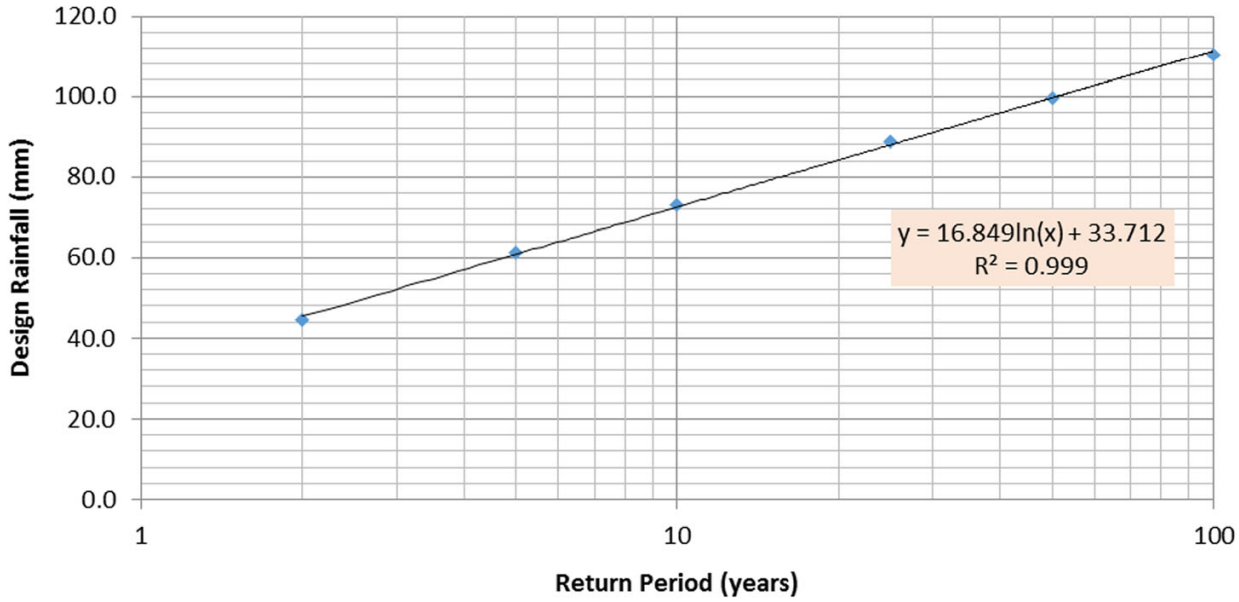

Figure I.4: St. Adolphe design storms (environment Canada, 1967 – 2000)

IV.3 New Channel Design

In order to examine the effects of channel size on nutrient retention, five different scenarios for rainfalls with 2, 5, 10, 15 and 20 year return periods were chosen. Design rainfalls were based on 12-h rainfall amounts obtained from the St. Adolphe, Manitoba design storms [design rainfall (mm) = 16.849 × ln(return period in years) + 33.712, see Fig. I.4]. By using the same channel slope, bed elevation, side slope and Manning coefficient, the bottom width for new channels was determined. A minimum bottom width of one meter was considered to avoid narrow channels. Values for bank slopes and widths are the same as those in Table I.1. The new bottom width values for both upstream and downstream are given in Tables I.3 and I.4 respectively. New channel profiles are shown in Fig. I.5.

CE-QUAL-W2 has the ability to work with different discharge types. The watershed has 48% of the water entering the Brown drain as direct inflow from upstream and the remaining 52% entering the channel along the length as a distributed tributary. A spillway was defined as the transfer of water based on the water elevation and channels rating curves (Fig. I.6).

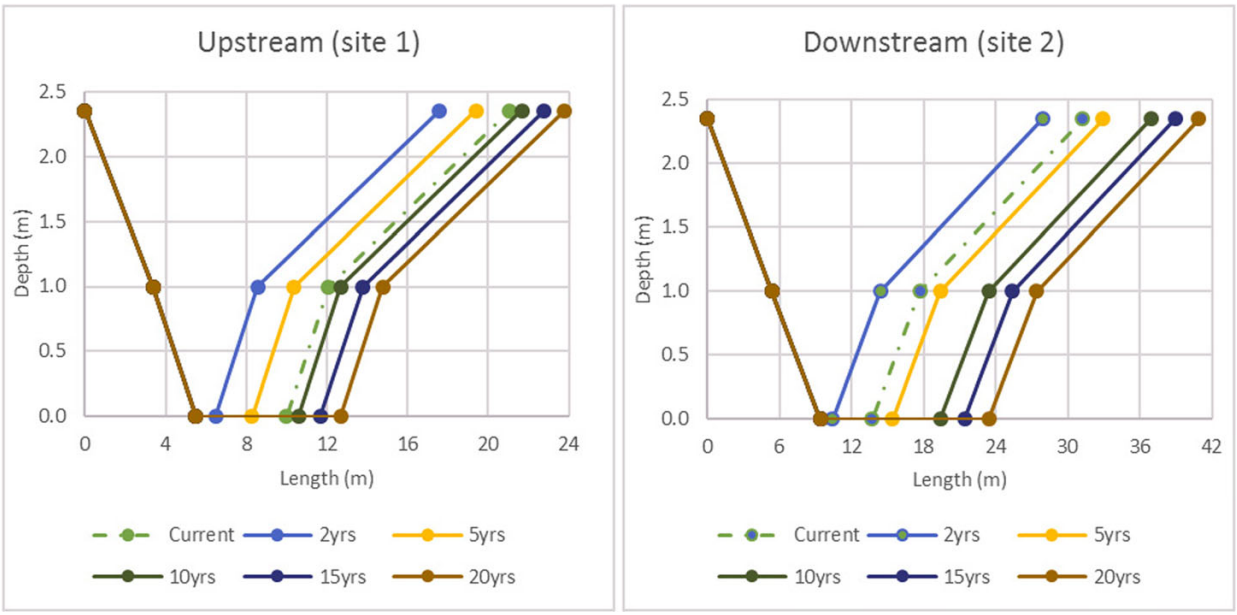

Figure I.5: Channel profiles for different return period rainfalls

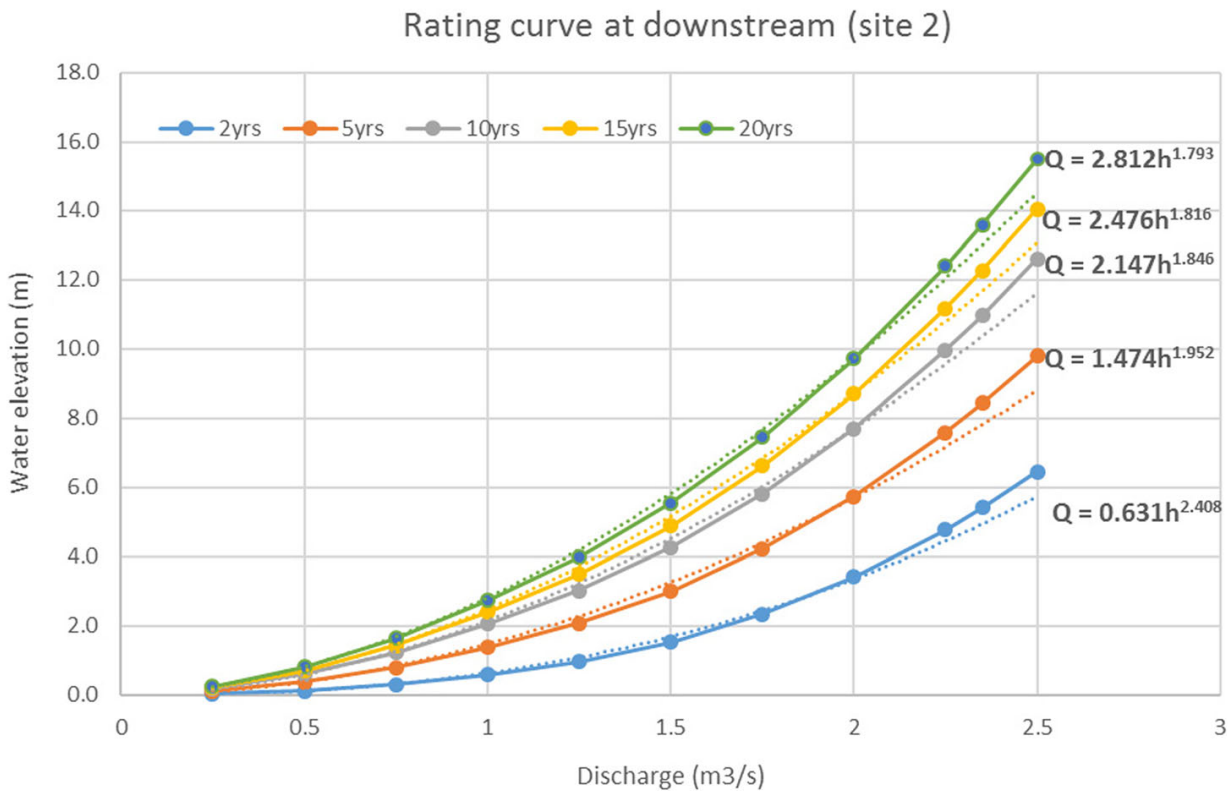

Figure I.6: Rating curve for outflowing water at downstream

Table I.1: Flow calculation table

$Z = \frac{b}{h}$	Side slope on bank
$T = B + h \times Z_L + h \times Z_R$	Top width
$A = \frac{B+T}{2} \times h$	Wetted area of trapezoid
$P = B + h\sqrt{1 + Z_L^2} + h\sqrt{1 + Z_R^2}$	Wetted perimeter of trapezoid
$R = \frac{A}{P}$	Hydraulic radius
$Q = A \times V$	Discharge
$n = \frac{R^{2/3}\sqrt{S}}{V}$	Manning coefficient

B Bottom width, b bank width, h bank height, V velocity (m/s), S channel slope, Z_L left bank slope, Z_R Right bank slope

Table I.2: Brown drain channel geometries at upstream and downstream

	h1 (m)	h2 (m)	h3 (m)	b1 (m)	b2 (m	b3 (m)	Z1	Z2	Z3
Upstream	2.35	1	1.35	5.88	1.67	9	2.5	1.67	6.67
Downstream	2.35	1	1.35	9.4	4	13.5	4	4	10

V Results and Discussion

V.1 Nitrogen (N)

N concentrations (all species) varied both temporally and spatially in 2013 (Fig. I.7). Highest concentrations were observed at both sites 11 and 17 during freshet and the two large rainfall events in late spring and early summer (Figs. 7 and 8). For example, TDN concentrations peaked at 4.5 mg/L during spring melt at upstream Site 17, while those during the two rainfall events at this site were greater than 3.5 mg/L (Figs. I.7 and I.8). Such high TDN concentrations indicate that the water is hypersaturated with N (concentrations >3.0 mg/L – CCME 2005). Although N concentrations were somewhat lower at the downstream Site 11, a similar pattern was noted with peaks appearing during freshet and the major rainfalls of spring and early summer. The majority of TDN at both sites was in the form of nitrate.

A number of factors including topography, snow depth, ground frost, rainfall, air temperature and antecedent moisture can affect water flow path and N deposition (Oczkowski et al., 2006). The high freshet export of N noted in this study is not unusual. In an American study, for example, approximately one-half of the annual dissolved inorganic N watershed load was exported during the high discharge associated with spring freshet (Oczkowski

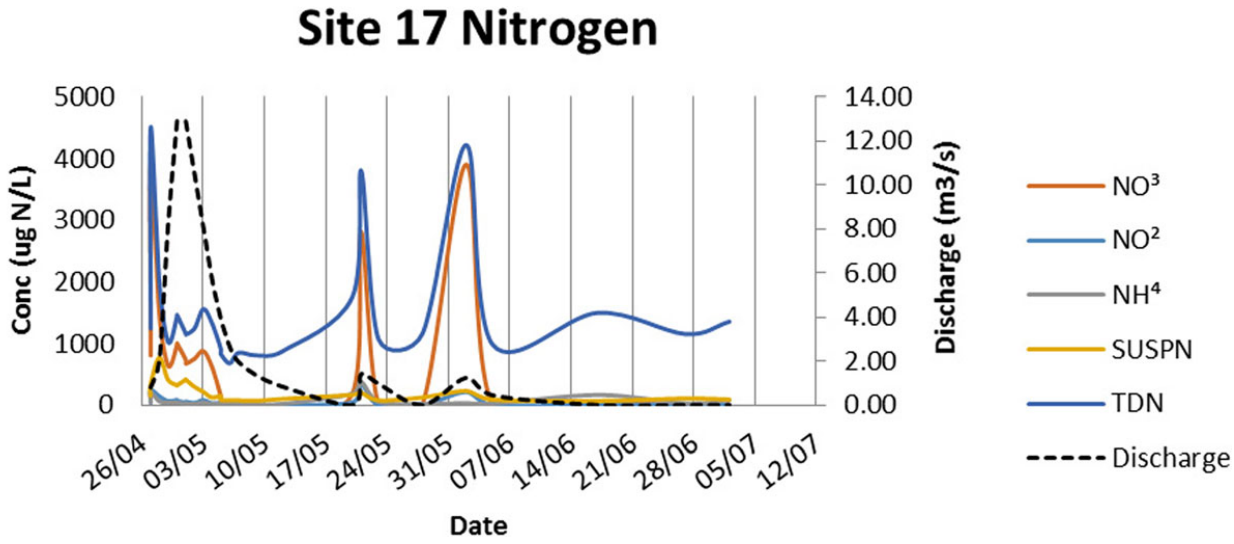

Figure I.7: Nitrogen concentrations at Site 17 in the Brown drain during the year 2013

Table I.3: Design discharge at upstream site under various return periods

Return Period (years)	Design Rainfall Amount (mm)	Runoff (mm)	Design Discharge (cms)	Channel Bottom Width (m)	Discharge (cms)
2	44.4	18.12	2.46	1	3.22
5	61.2	31.39	4.26	2.8	4.27
10	73.2	41.56	5.64	5.1	5.67
15	79.3	46.89	6.36	6.2	6.37
20	84.2	51.23	6.95	7.2	7.00

et al., 2006). Another observation from the Brown drain was that most of the N during high discharge events was NO_3. Although the reasons for such high NO_3 concentrations are unclear, a number of other studies have reported that flow through shallow soils during storm events and snowmelt may result in the flushing of NO_3 (accumulated from nitrification over the winter) into receiving water bodies, thereby increasing NO_3 (Burns and Kendall, 2002).

V.2 Phosphorus (P)

For the most part, SRP and TDP concentrations tracked each other throughout most of the study period at both study sites in the Brown drain (Figs. I.9 and I.10). Concentrations were always much lower than either TDP or SRP at both sites. Similar to TDN concentrations,

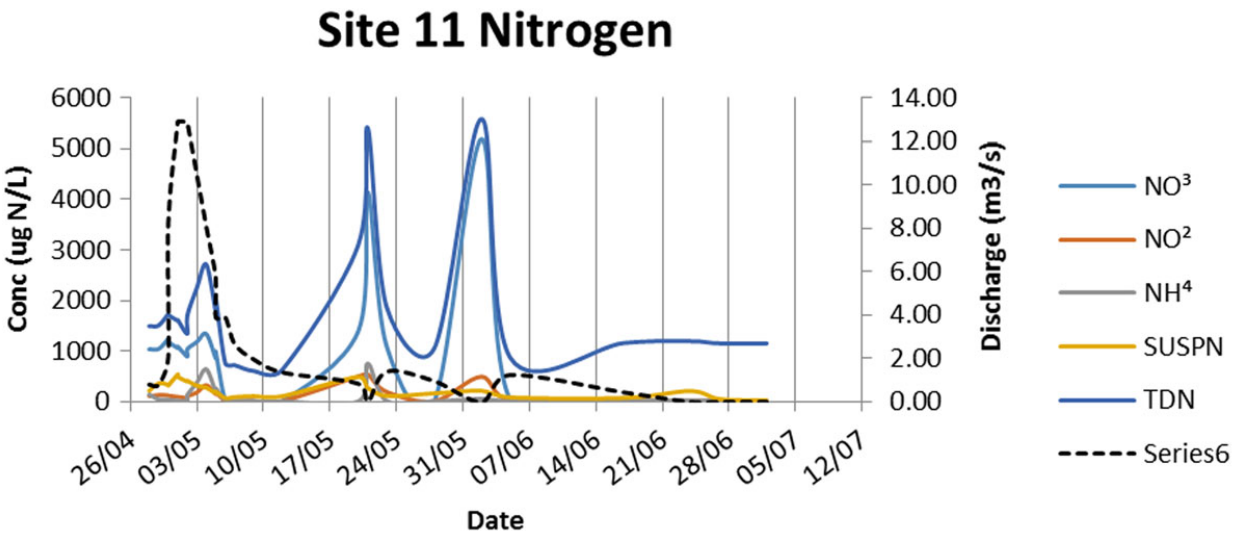

Figure I.8: Nitrogen concentrations at Site 17 in the Brown drain during the year 2013

the largest peaks in TDP coincided with spring snowmelt with observed concentrations at Sites 11 and 17 greater than 1.4 and 0.5 mg/L, respectively (Figs. I.9 and I.10). Peaks at both sites were also noted during the two major rainfalls. According to the Canadian Council of the Ministers of the Environment (CCME), Water Quality Guidelines, P concentration in the Brown drain at most sampling times far exceeded the concentration set for hypereutrophic aquatic ecosystems (> 100 μg/L - CCME 2005).

The high TDP concentrations observed during freshet and rainfall events may be due to a number of factors. Phosphorus generally adsorbs to soil organic matter and within that matrix its solubility and mobility are generally low. During prairie spring, snow meltwater generally travels over frozen ground, carrying soil (and adsorbed P with it). The frozen ground during the freshet has low permeability causing most of the nutrients to be transported via the high overland runoff (Han et al., 2010). On the prairies, repeated freeze-thaw cycles have weakened the cohesive abilities of soil over time. Increased soil erosion occurring as a result of this process and the flat prairie landscape aids in the movement of P into receiving water bodies. Exacerbating this process are the lack of buffer strips surrounding prairie streams as well as the disappearance of wetlands (as land was cleared for agriculture) which might otherwise trap eroding soil. The land use changes since settlement have been substantial with 70% of wetlands across the Canadian Prairies being

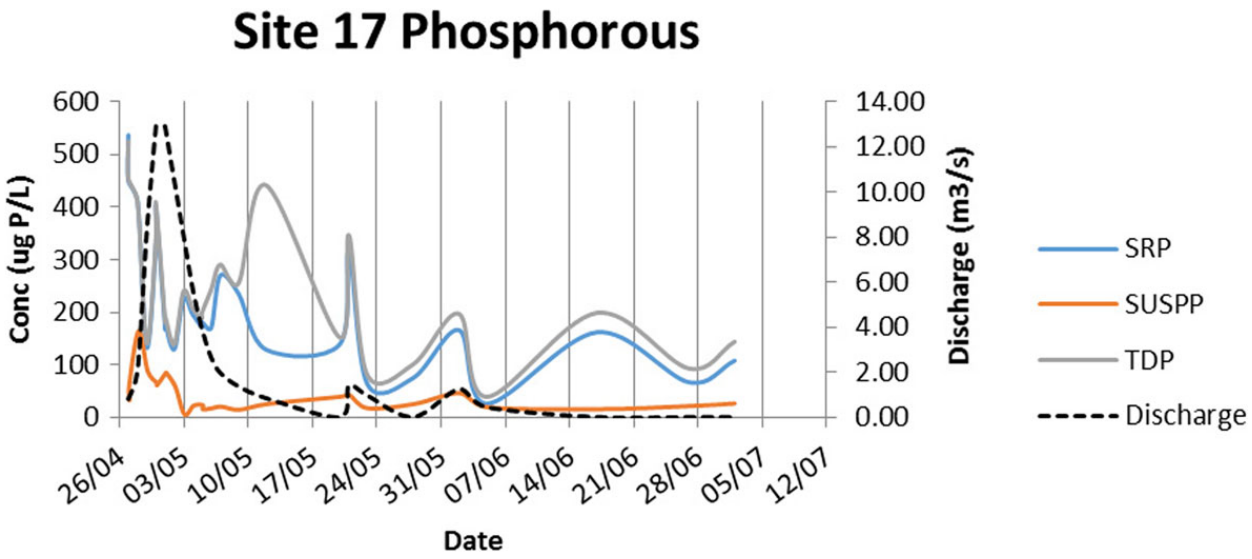

Figure I.9: Phosphorus concentrations at Site 17 in the Brown drain during the year 2013

filled or drained (Dumanski et al., 2015).

In cold weather ecosystems, like the Canadian prairies, spring freshet is generally associated with high P loads to receiving water bodies. And such loading was certainly observed in this study. In temperate climatic zones, however, higher P input is more often associated with runoff from intense rainfall events (Jensen et al., 2011). It is interesting that in the Tobacco Creek watershed study high P inputs from intense rainfall events were also seen. A number of prairie studies have documented that TP concentrations correlate strongly with stream flow. In fact, much of the annual TP load, (75–90% of which is sediment bound), may be associated with large storm events (Long et al., 2014). The fact that the frequency of multi-day rain events have increased by 50% in this climatic zone hint at the possibility of concomitantly increasing stream P loads (Dumanski et al., 2015).

V.3 Total Suspended Solids (TSS) and Dissolved Organic Carbon (DOC)

At the Brown drain, highest TSS values (> 100 mg/L) were recorded after freshet at both sites (Figs. I.11 and I.12). Smaller peaks at both sites were associated with the two rainfall events. Similar observations were made at the Main drain except that the largest peaks

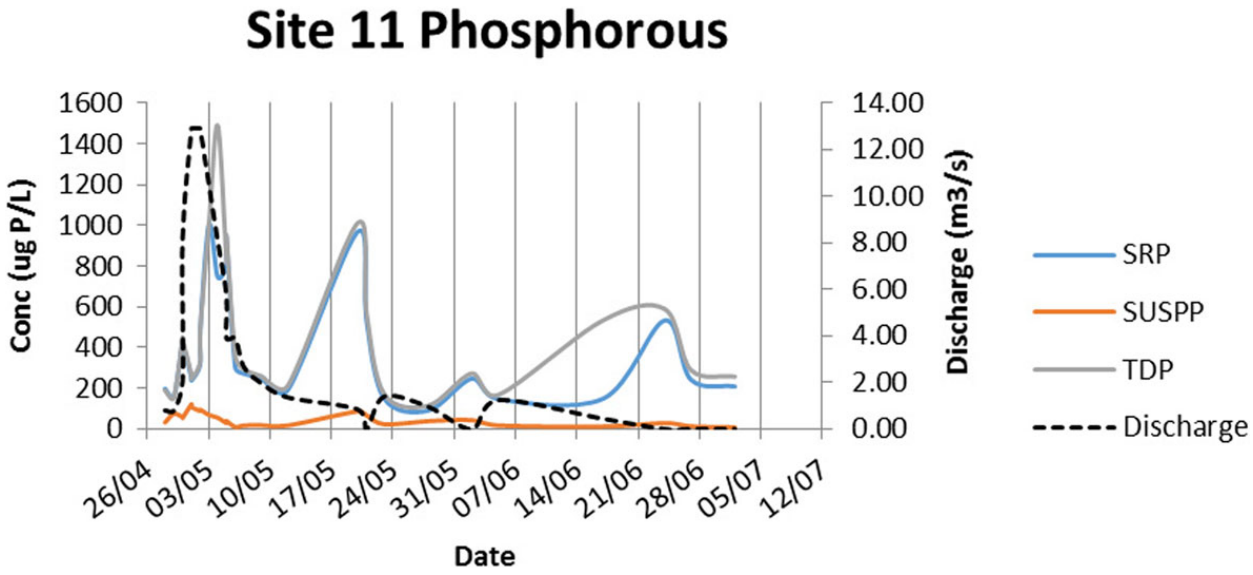

Figure I.10: Phosphorus concentrations at Site 11 in the Brown drain during the year 2013

Table I.4: Design discharge at downstream site under various return periods

Return Period (years)	Design Rainfall Amount (mm)	Runoff (mm)	Design Discharge (cms)	Channel Bottom Width (m)	Discharge (cms)
2	44.4	18.12	4.7	1	5.40
5	61.2	31.39	8.14	6	8.43
10	73.2	41.56	10.79	10	10.97
15	79.3	46.89	12.17	12	12.27
20	84.2	51.23	13.29	14	13.58

were associated with the May rainfall event.

During the study, DOC concentrations at both Brown drain sites gradually increased with two exceptions (Figs. I.11 and I.12). After the two rain events, although DOC concentrations appeared to decline, this change was likely due to dilution as the creek stage rose. The gradual increase in DOC concentration may reflect a concentration effect associated with decreased water volume in the drain (cf Waiser, 2006).

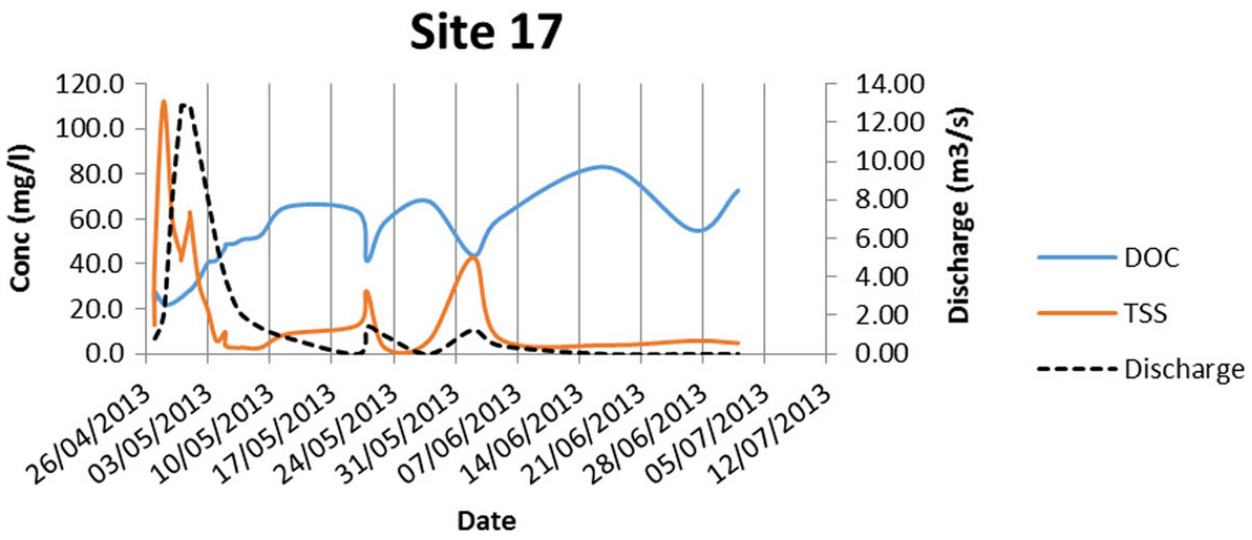

Figure I.11: DOC, TSS, and discharge at site 17 of the Brown drain during the year 2013

V.4 Total Sediment Load

Total sediment loads estimated using concentrations and calculated flows indicated that loads were greatest during spring freshet. Estimated loads at sites 11 and 17, for example, were 100 and 120 mg/L, respectively (Figs. I.13 and I.14). Smaller peaks were recorded at Site 11 after the May rain event (60 mg/L) and Site 17 after the June rain (40 mg/L). Such large loads are consistent with what is known regarding consolidation drainage. Such drainage is known to increase sediment and contaminant influx into basins lower in the catchment due to increased drainage areas and numbers of drained wetlands (often tilled) within the upper catchment (Anteau, 2012).

V.5 Modelling Results

Inputs for discharge, inflow water temperature, meteorological data and nutrients data were required by the water quality model to obtain the nutrient retention results. Existing inflow values were inputted into the model and the outflow downstream was calculated by the model itself. The model used spillway coefficients and channel slopes to calculate discharged water. As well, nutrient concentrations including PO_4, NH_4, NO_3, NO_2, $LDOM_P$ and $LDOM_N$ for the Brown drain and discharge values shown in Fig. I.3 were used in preparing the model. The model simulation was run for two months (late April until mid-June) as

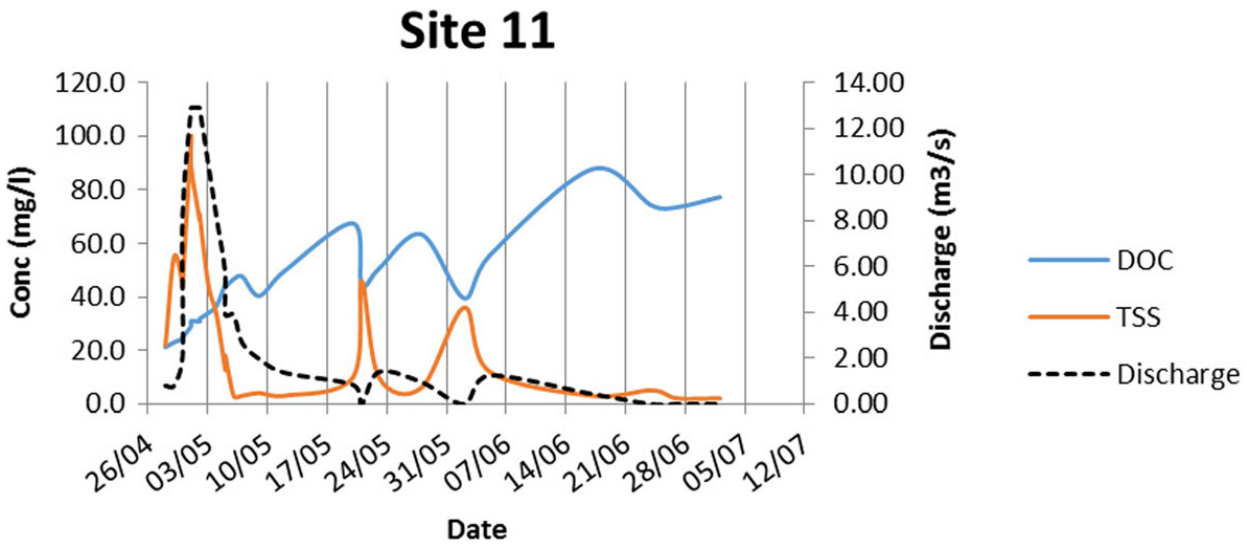

Figure I.12: DOC, TSS, and discharge at site 11 of the Brown drain during the year 2013

this is when the water normally flows in the channel.

The simulated nutrient concentrations were compared with the measured values for model calibrations. Several parameters including decay rates, settling velocities, oxygen demand, and turbulence coefficients affected model performance. A sensitivity analysis was subsequently carried out from which 12 of the most sensitive parameters in the model output were selected for model calibration (Table I.5). These parameters were changed until the lowest discrepancy was achieved between the simulated and measured values. The model results from this exercise matched fairly well with measurements for simulated components (Fig. I.15).

The calibrated model was then used for implementing new rainstorm drain designs under different return periods (2, 5, 10, 15 and 20 years). To this end, design rainfall hyetographs were derived by using Alternating Block Method based on corresponding IDF values at the St. Adolphe, Manitoba weather station. Cross-sections for each return period are given in Tables I.3 and I.4, and Fig. I.5. Modeling time was 72 h during the period when the drain was at its highest flow (Julian days 119–122).

One drawback of the model simulations was the low diversity of available nutrient and water quality data. For example, data for algal biomass (as Chlorophyll a) and the various carbon

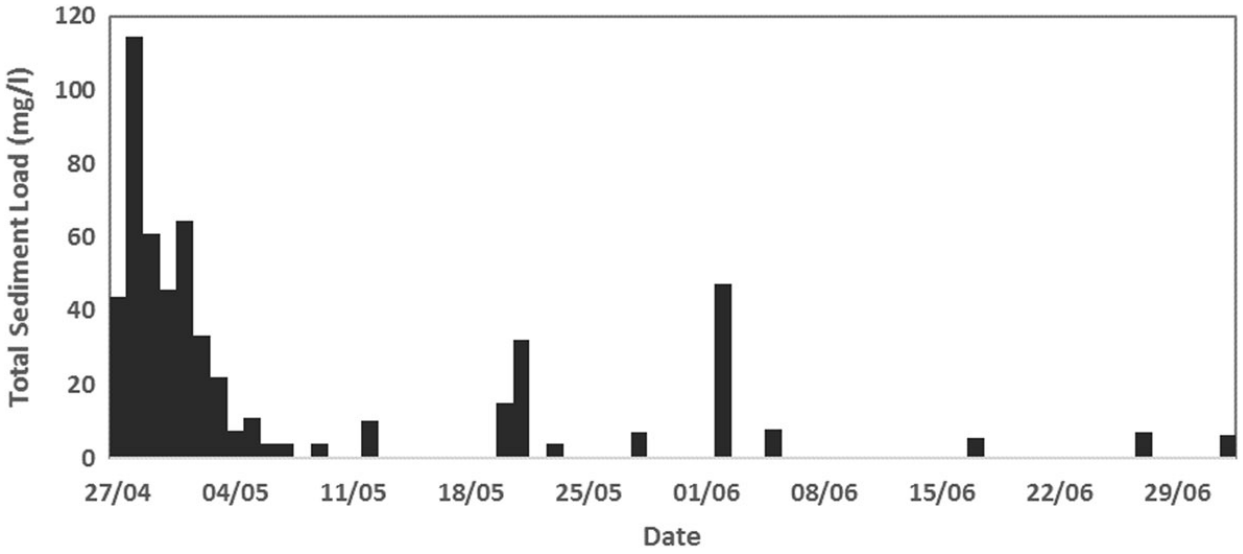

Figure I.13: Total sediment load at site 17 in the Brown drain

species were not collected and therefore could not be added to the model. In an effort to get accurate results for the Brown drain, nutrient data from Spokane River, a tributary of Columbia River, WA, USA, was used for comparison. This river has been extensively monitored and is used as an example for river modeling in the CE-QUAL-W2 software package. Although the data is from 2011, it can be used to visualize how different drain sizes might affect additional model parameters.

The accumulated model values indicated that there were many similar trends in the Brown drain and Spokane River data. Additionally, the model not only worked well with the Spokane River nutrient data, it delivered accurate approximations of system behaviors for nutrients not available in the Brown drain model.

According to the model, N components behaved differently depending on the channel size and return period. For example, if the return period was altered yet channel size remained the same, there was no effect of return period on NH_4 or NO_3 concentrations. When the channel size was altered, however, large difference in concentrations for NH_4 (about 27%) and NO_3 (15%) between the 2 and 20 year channels was evident. N values in the upstream section were about 80% and 69% of the downstream values in the 2 and 20 year channels, respectively. P results were similar. If the channel size remained the same and the return

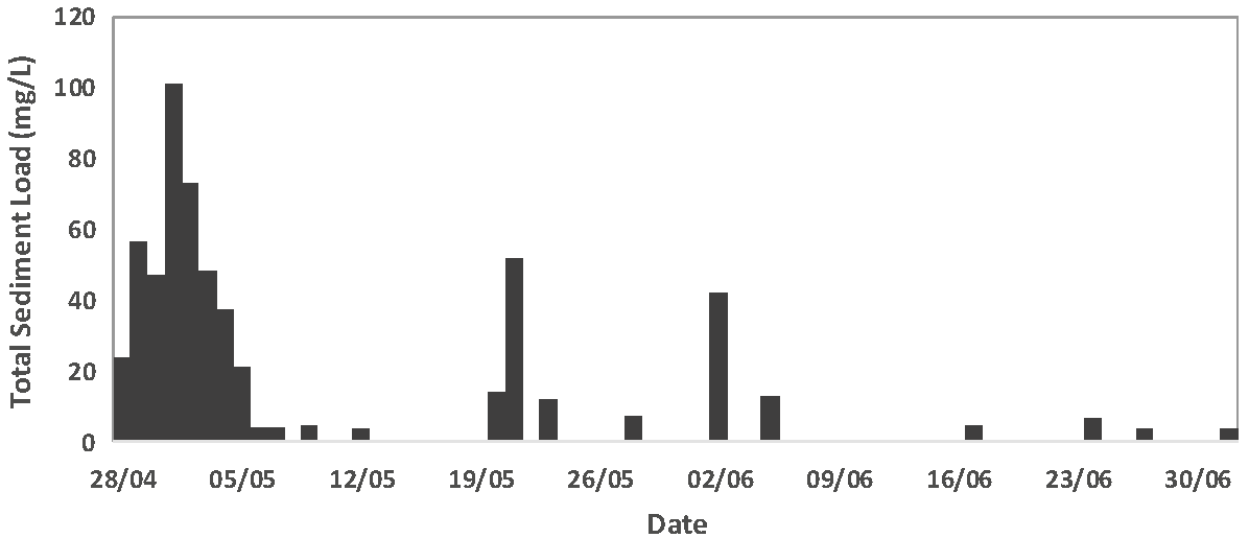

Figure I.14: Total sediment load at site 11 in the Brown drain

period was varied, no difference in PO_4 concentrations were observed. Changing the drain size and return period did make a difference. For example, PO_4 concentration was up to 40% less for the 20 year return period as compared to the 2 year. TP concentrations were about 77% and 67% of input values at the upstream site for 2 and 20 year channels.

Although Chlorophyll *a* was not sampled in Tobacco Creek, based on model results for the Spokane River nutrient data, Chlorophyll *a* concentrations were up to 16% smaller in the 20 year channel compared with the 2 year channel. Almost all carbon components including CO_2, CO_3, HCO_3, CBOD, DOC, POC and TOC had similar behaviors. All were about 16% (on average) smaller in the 20 year channel than the 2 year channel. Total inorganic suspended solids had 67% and 52% of inflow concentrations downstream in 2 and 20 year channels respectively. Total suspended solids concentrations had 18% difference between 2 and 20 year channels.

V.6 Discussion

One of the most important results of this study was that the largest nutrient loads to streams in the basin coincided with three major hydrological events; spring freshet and two summer rainfall events. Although increased nutrient loads during freshet were likely due to high overland runoff on frozen ground with low permeability (Han et al., 2010), our

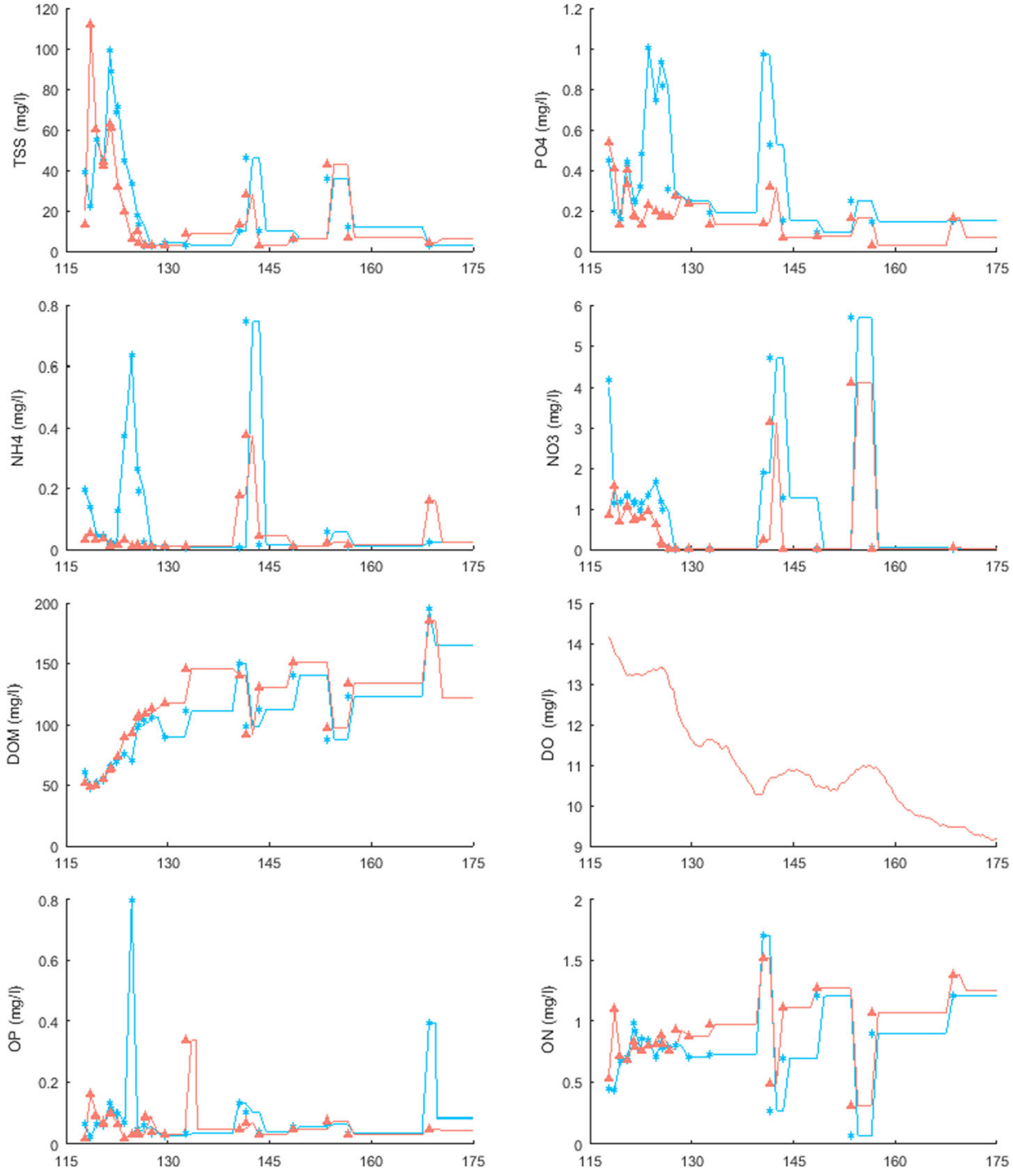

Figure I.15: Simulated and observed nutrient concentrations

study indicated that nutrient losses were apparently just as high when the soil was not frozen. These results are similar to those reported in a 2006 Environment Canada (EC) study (Glozier et al., 2006). In the EC study, although spring fertilizer use of N and P increased by 17% between 1991 and 2000, the correlation between land use and nutrient concentrations was not strong (Glozier et al., 2006). Instead, hydrological events as opposed to crop type and fertilizer use, appeared to trigger the increased nutrient loads to streams in this basin. The EC study also indicated that even though much lower flows originated from summer rainfall events compared to spring freshet, summer sediment transport was still comparable and sometimes even larger than spring freshet (Glozier et al., 2006). Hydrological studies across the prairies have documented similar results to those presented here. For example, studies on the Seine, LaSalle and Little Morris Rivers in the Lake Winnipeg Basin, Manitoba, Canada indicated that hydrologic patterns and nutrient loading in all three prairie rivers were dominated by the snowmelt period. Snowmelt contributed 34–94% of the total annual river volume, 40–97% of the total annual TP load, and 54–97% of the total annual TN load (Chambers et al., 2012). As in this Tobacco Creek watershed, dissolved P and N dominated the total nutrient pool throughout snowmelt. The authors cited factors including flat topography, frozen soils and stream banks, and gradual snow cover melt as contributing to this domination. Another example would be the Red River watershed, also within the Lake Winnipeg Basin. Here, higher discharge from snowmelt and spring runoff during the month of April contributes twice the N loading of all other months (Stewardship, 2011).

The prairies will be sensitive to climate change, not only due to their location in a semi – arid ecosystem where evaporation exceeds precipitation, but a dominant winter season as well (Conly and Van Der Kamp, 2001). Modelling conducted as part of the Lake Winnipeg Basin Initiative and from other sources has revealed that future climate change is likely to produce appreciable changes to the hydrologic and nutrient transport regimes within this basin. From 1895 to 1991 temperatures on the Canadian prairies rose by 1.1 °C with larger increases of up to 3 °C reported for parts of Montana and the Dakotas (Millett et al., 2009). With minimum temperatures warming more in winter than in summer the prairies are getting less cold (Millett et al., 2009). Such warming may, in fact, exceed the global average (Gan, 1998). Along with increasing temperatures, the Polar air masses which dominate prairie winters are predicted to weaken thereby allowing hot dry air from the American

Table I.5: Model calibration coefficients ranges and final values

Name*	Description	Ranges	Final Value
BETA	Fraction of incident solar radiation absorbed at the water surface	0.15–0.9	0.430
EXH20	Extinction for pure water, m^{-1}	0.25–0.45	0.250
DX	Longitudinal eddy diffusivity, m^2 sec^{-1}	1–400	30.01
NH_4DK	Ammonium decay rate, day^{-1}	0–3	0.308
NO_3DK	Nitrate decay rate, day^{-1}	0–2	0.055
NO_3S	Denitrification rate from sediments, m day^{-1}	0–0.5	0.021
PO_4R	Sediment release rate of phosphorus, fraction of SOD	0–0.01	0.001
PARTP	Phosphorus partitioning coefficient for suspended solids	0–1	0.023
O2LIM	Dissolved oxygen half-saturation constant	0–3	0.149
LPOMDK	Labile POM decay rate, day^{-1}	0–0.2	0.022
POMS	POM settling rate, m day^{-1}	0–1	0.273
SOD	Sediment oxygen demand	0–5	0.412

*See manual of CE-QUAL-W2 model

SW and hot moist air from the American SE to more routinely affect the prairies. Drought interspersed with unusually wet conditions is also expected with climate change. Rainfall will be more concentrated in time with larger amounts falling in fewer storms (Waiser, 2013). An increase in the number of extreme weather events is also expected. Other impacts include a greater frost free period, in fact from 2080 to 2099, 20 fewer frost free days on the Great Plains are projected (Millett et al., 2009). Longer warmer winters will reduce snowpack accumulations and this reduction will result in less spring runoff. Based on the fact that nutrient loading during rain events in the Tobacco Creek watershed can be greater than those during the snow melt runoff, increased loadings of N and P can be expected under the climate change scenarios noted above.

This study focused on a small catchment (Brown drain) where no obvious high point loadings were detected. As a result, the water quality modeling did not incorporate non-diffuse discharges. However, high nutrient point loadings in different parts of a catchment can result in non-diffuse discharges, which may have affected the findings from this study for different hydrological design standards, and should be addressed in future work. Channel slope can also have considerable impacts on nutrient loading as the velocity of flow is sensitive to channel slope. However, in this study only data from the Brown drain was available where the channel slope is determined by the prairie slope. Further studies are needed to model

loadings from different catchments with different channel slopes to compare the effects of channel slope on nutrient loading under different hydrological standards.

The current drainage system in the Tobacco Creek study area has been designed in a way to move water quickly off the land to reduce crop damage from inundation. Although data presented here indicate that there was some retention of nutrients between the upstream and downstream sites, a large proportion was still travelling, relatively unchanged biologically, into the Red River and ending up in Lake Winnipeg. Even though this watershed is small, it still contributes nutrients to Lake Winnipeg and exacerbates the eutrophication problem. Any measure that might possibly slow down the transit time or lower the concentration of these nutrients, now and in the future, would ultimately benefit Lake Winnipeg. To this end, the CE-QUAL-W2 water quality model used in this study investigated the effects of different drain sizes for rainfall with 2, 5, 10, 15 and 20 year return periods. According to the results of this modelling exercise, as return periods became larger, nutrient concentrations declined. On average, nutrient concentrations declined about 15%–20% in channels with 20 years design return period compared with those with 2 year return periods.

VI Conclusions

The explosion of eutrophication-related research on Lake Winnipeg and its watersheds has made it clear that a comprehensive nutrient reduction strategy is required to prevent further water quality deterioration now and in the future. One of the first steps in the development of such a strategy is to understand the hydrological processes that drive and contribute to nutrient loading in the small, managed watersheds that feed into Lake Winnipeg. The discussion of how hydrological processes influence nutrient loads to the Tobacco Creek watershed will hopefully contribute to this nutrient reduction strategy. The modelling exercise represents a significant step forward in our understanding of how drain size affects nutrient retention in these small managed watersheds. In fact, based on the results of this study, in an environmental point view it is recommended that the hydrological standard used for future drain design should be based on a 20 year return period, under the modeling results without consideration the effects of nutrient point loading and channel slope. In this manner, a balance can be struck between fast water removal and nutrient retention.

Such steps encourage environmentally sound decisions with regard to nutrient reduction in small managed agricultural watersheds and ultimately facilitate future sustainable economic development in the province of Manitoba.

Acknowledgements

The authors are grateful to Michael Stainton and Paul Martin from the Department of Fisheries and Oceans for the laboratory analyses. As well, many thanks to Les McEwan from Tobacco Creek Model Watershed for the field sampling done during 2013. We would also like to acknowledge the Manitoba Water Stewardship Fund for their funding of this study.

References

AAFC (2013). *South Tobacco Creek/Steppler Watershed. Government of Canada.* Agriculture and Agri-Food Canada. Available at: http://www.agr.gc.ca/eng/?id=1297269073820.

Anteau, M. J. (2012). Do interactions of land use and climate affect productivity of waterbirds and prairie-pothole wetlands? *Wetlands*, 32(1):1–9.

Bourne, A., Armstrong, N., and Jones, G. (2002). *A preliminary estimate of total nitrogen and total phosphorus loading to streams in Manitoba, Canada.* Citeseer.

Burns, D. A. and Kendall, C. (2002). Analysis of δ15N and δ18O to differentiate NO3- sources in runoff at two watersheds in the Catskill Mountains of New York. *Water Resources Research*, 38(5).

Chambers, P., Corriveau, J., Yates, A., Culp, J., Benoy, G., and Elliott, J. (2012). *Transport of nutrients from agricultural watersheds through tributaries in the Lake Winnipeg Basin in Environment Canada.* Environment Canada. Final Project Reports Lake Winnipeg Basin Initiative:2008/09–2011/12. Available at: http://lwbi.cc.umanitoba.ca/media/files/FinalProjectReports_LWpgB_In2008_2012.pdf.

Cole, T. M. and Wells, S. A. (2013). *CE-QUAL-W2: A two-dimensional, laterally averaged, hydrodynamic and water quality model.* Department of Civil and Environmental Engineering, Portland State University, Portland, OR, 3.71 edition.

Conly, F. M. and Van Der Kamp, G. (2001). Monitoring the hydrology of canadian prairie wetlands to detect the effects of climate change and land use changes. *Environmental Monitoring and Assessment*, 67(1):195–215.

Dumanski, S., Pomeroy, J. W., and Westbrook, C. J. (2015). Hydrological regime changes in a Canadian Prairie basin. *Hydrological Processes*, 29(18):3893–3904.

Gan, T. Y. (1998). Hydroclimatic trends and possible climatic warming in the Canadian Prairies. *Water Resources Research*, 34(11):3009–3015.

Glozier, N., Elliott, J., Holliday, B., Yarotski, J., and Harker, B. (2006). Water quality characteristics and trends in a small agricultural watershed: South Tobacco Creek, Manitoba, 1992–2001. *Environment Canada, Ottawa, ON*.

Han, C.-W., Xu, S.-G., Liu, J.-W., and Lian, J.-J. (2010). Nonpoint-source nitrogen and phosphorus behavior and modeling in cold climate: a review. *Water Science and Technology*, 62(10):2277–2285.

Hope, J., Harker, D. B., and Townley-Smith, L. (2002). *Long term land use trends for water quality protection: ten years of monitoring in the South Tobacco Creek Watershed*. Agriculture and Agri-Food Canada, PFRA.

Jensen, T., Tiessen, K., Salvano, E., Kalischuk, A., Flaten, D. N., et al. (2011). Spring snowmelt impact on phosphorus addition to surface runoff in the Northern Great Plains. *Better Crops*, 95(1):28–31.

Long, T., Wellen, C., Arhonditsis, G., and Boyd, D. (2014). Evaluation of stormwater and snowmelt inputs, land use and seasonality on nutrient dynamics in the watersheds of Hamilton Harbour, Ontario, Canada. *Journal of Great Lakes Research*, 40(4):964–979.

LWSB (2006). *Reducing nutrient loading to Lake Winnipeg and its watershed – our collective responsibility and commitment to action. Report to the minister of water stewardship*. Winnipeg, MB, Canada. Available at: http://www.gov.mb.ca/waterstewardship/water_quality/lake_winnipeg/nutrient_literature.pdf.

LWSB (2009). *Manitoba's progress towards implementing recommendations of the Lake Winnipeg stewardship board. Report to the minister of water stewardship*. Winnipeg, MB, Canada. Available at: http://www.gov.mb.ca/waterstewardship/reports/misc/lake_winnipeg_stewardship_board_report_on_progress.pdf.

Millett, B., Johnson, W. C., and Guntenspergen, G. (2009). Climate trends of the North American prairie pothole region 1906–2000. *Climatic Change*, 93(1):243–267.

Oczkowski, A. J., Pellerin, B. A., Hunt, C. W., Wollheim, W. M., Vörösmarty, C. J., and Loder, T. C. (2006). The role of snowmelt and spring rainfall in inorganic nutrient fluxes from a large temperate watershed, the Androscoggin River basin (Maine and New Hampshire). *Biogeochemistry*, 80(3):191–203.

Petzold, H. (2012). Channel morphology of the Tobacco Creek watershed in southern Manitoba. Technical report, University of Manitoba, NSERC.

Sadeghian, A., de Boer, D., Hudson, J. J., Wheater, H., and Lindenschmidt, K.-E. (2015). Lake Diefenbaker temperature model. *Journal of Great Lakes Research*, 41:8–21.

Stewardship, M. W. (2011). State of lake winnipeg: 1999 to 2007. Technical report, Environment Canada and Manitoba Water Stewardship. available at: https://www.gov.mb.ca/waterstewardship/water_quality/state_lk_winnipeg_report/pdf/state_of_lake_winnipeg_rpt_technical_high_resolution.pdf.

Tiessen, K., Elliott, J., Yarotski, J., Lobb, D., Flaten, D., and Glozier, N. (2010). Conventional and conservation tillage: influence on seasonal runoff, sediment, and nutrient losses in the Canadian prairies. *Journal of Environmental Quality*, 39(3):964–980.

Waiser, M. J. (2006). Relationship between hydrological characteristics and dissolved organic carbon concentration and mass in northern prairie wetlands using a conservative tracer approach. *Journal of Geophysical Research: Biogeosciences*, 111(G2).

Waiser, M. J. (2013). Climate Change and Wetlands of the Prairie Pothole Region of North America: Effects, Management and Mitigation. *Climatic Change and Global Warming of Inland Waters: Impacts and Mitigation for Ecosystems and Societies*, pages 219–230.

Appendix II

Modelling Dissolved Oxygen/Sediment Oxygen Demand under Ice in a Shallow Eutrophic Prairie Reservoir

This chapter is a published paper in the journal of Water, and, also, will appear as a chapter in the Ph.D. theses of Julie A. Terry.

Terry, J., **Sadeghian, A.**, Lindenschmidt, K.E. (2017). Modelling dissolved oxygen/sediment oxygen demand under ice in a shallow eutrophic prairie reservoir. *Journal of Water*, 9 (2), 131, DOI: 10.3390/w9020131

The document has been reformatted from the original version for inclusion in the thesis, and no content has changed from the published version. The journal of Water is an open access journal, and the open access license and policy from the publisher (MDPI) are included in Appendix VI.

Contributions of the candidate and co-authors

Julie A. Terry, Amir Sadeghian and Karl-Erich Lindenschmidt conceived and designed the experiments under the latter's supervision. Julie A. Terry set-up and calibrated the Buffalo Pound reservoir model including the water balance, water temperature dynamics and initial DO-BOD kinetics. Amir Sadeghian adapted CE-QUAL-W2 for snow-cover, and, after establishing trends between SOD, Chla and BOD, extended the model to include variable SOD. Julie A. Terry wrote the bulk of the paper with text inputs and conceptual edits from Karl-Erich Lindenschmidt. All authors proofread and approved the manuscript.

Contribution of this chapter to the overall study

The overall objective of this Ph.D. research was to conduct the water quality modeling of Lake Diefenbaker. The model used for different parts of this study was the 2D

laterally averaged water quality model CE-QUAL-W2. During the modeling process, some limitations were found with the model that required attention especially for using the model in the cold regions. Hence, this study can be a post-modeling of the Lake Diefenbaker water quality model for addressing the limitations found during this Ph.D. research with regard to the winter sediment oxygen demand.

I Abstract

Dissolved oxygen is an influential factor of aquatic ecosystem health. Future predictions of oxygen deficits are paramount for maintaining water quality. Oxygen demands depend greatly on a waterbody's attributes. A large sediment–water interface relative to volume means sediment oxygen demand has greater influence in shallow systems. In shallow, ice-covered waterbodies the potential for winter anoxia is high. Water quality models offer two options for modelling sediment oxygen demand: a zero-order constant rate, or a sediment diagenesis model. The constant rate is unrepresentative of a real system, yet a diagenesis model is difficult to parameterise and calibrate without data. We use the water quality model CE-QUAL-W2 to increase the complexity of a zero-order sediment compartment with limited data. We model summer and winter conditions individually to capture decay rates under-ice. Using a semi-automated calibration method, we find an annual pattern in sediment oxygen demand that follows the trend of chlorophyll-a concentrations in a shallow, eutrophic Prairie reservoir. We use chlorophyll-a as a proxy for estimation of summer oxygen demand and winter decay. We show that winter sediment oxygen demand is dependent on the previous summer's maximum chlorophyll-a concentrations.

II Introduction

Oxygen is essential for a healthy aquatic system. The Canadian water quality guidelines for the protection of aquatic life state that dissolved oxygen (DO) is the most important parameter in water (Canadian Council of Ministers of the Environment, 1999). Severe oxygen depletion can lead to fish kills (Meding and Jackson, 2003; Robarts et al., 2005), deformities in fish larvae (Canadian Council of Ministers of the Environment, 1999), and changes in community composition and lake trophic state (Meding and Jackson,

2003; Wetzel, 2001). The prediction of DO concentrations is vital for fisheries, and for aquatic managers responsible for maintaining ecosystem health (Meding and Jackson, 2003).

The shallow lakes and reservoirs of the Canadian Prairies are naturally mesotrophic to eutrophic (Finlay et al., 2010), and display severe fluctuations in DO (Robarts et al., 2005). Large phytoplankton blooms can occur, and the waterbodies are subject to an extreme climate with hot summers and ice-covered winters. DO is additionally important in drinking water reservoirs as dissolved gas supersaturation can be an issue in water treatment (Scardina and Edwards, 2001). Low oxygen can also induce release of nutrients, and sulphide production.

Phytoplankton contribute greatly to DO in reservoirs by photosynthesis, as will macrophytes if present in large volumes (Hosseini et al., 2017; Meding and Jackson, 2003). Periphyton may also contribute (Thornton et al., 1990). Additional DO will enter as inflows and reaeration from the atmosphere. As well as replenishing DO, inflowing waters also transport organic matter into a reservoir. This matter will settle in the sediments along with dead plants and algae. When this material decomposes both chemical oxidation and biological respiration exert a significant oxygen demand to the water column (Cross and Summerfelt, 1987), known as biochemical oxygen demand (BOD), and to the sediments, known as sediment oxygen demand (SOD). Both BOD and SOD have a positive relationship with reservoir productivity in this case. Nitrification also contributes to oxygen demand.

In open water oxygen deficits are replenished through reaeration (Chapra, 2008) to the surface and mixed to the bottom by wind and turbulence. Reaeration is the exchange of gases at the air–water interface. In contrast, ice-covered conditions bring significant changes to the DO dynamics. Under ice-cover atmospheric gas exchange is removed from the oxygen balance (Golosov et al., 2007). If sufficient light penetrates through the ice, plants and algae continue to photosynthesise and produce oxygen (Vehmaa and Salonen, 2009). The cooler winter water temperatures slow the decomposition of organic matter and reduce the consumption of oxygen through bacterial activity (Canadian Council of Ministers of the Environment, 1999; Wetzel, 2001). Breaks in the ice can increase the oxygen balance by allowing gas exchange.

Conversely, heavy snow loads reduce light penetration to a point where photosynthesis is greatly reduced (Fang and Stefan, 2000; Salonen et al., 2009; Wetzel, 2001). The resultant decomposition of dying biota consumes further oxygen supplies (Golosov et al., 2007). Inflow volumes are often low in winter with less new oxygen inflow to offset consumptive processes (Martin et al., 2013). There may be no breaks in the ice and extended ice-cover. The absence of wind on the water surface reduces the chance of oxygen mixing through the water column to deeper waters. Oxygen levels can reach the point of anoxic conditions at the bottom of reservoirs with high oxygen demands (Meding and Jackson, 2003).

Low winter DO concentrations have been linked to shallower lakes with sizeable littoral zones and prolonged ice-cover (Leppi et al., 2016). Shallow waterbodies have a large sediment–water interface relative to water volume. This interface is where the organic matter and bacterial activity tends to be concentrated (Leppi et al., 2016). The relative influence of bottom decomposition on the water column is therefore greater in shallow systems (Chapra, 2008). While open waters are often well-mixed from wind action, under ice-cover the shallow water depth means that the anoxic zone could potentially thicken along the bottom sediments. SOD is highly sensitive to small temperature fluctuations at lower water temperatures, with small increases intensifying oxygen depletion (Kirillin et al., 2012). When modelling DO in a shallow, eutrophic system the ability to simulate SOD and the rate of SOD decay is important.

Water quality modellers usually work in a series of steps: first is a water balance model followed by a water temperature and mixing model to set-up the hydrodynamics for the system. Some modellers then choose to move to a full nutrient and phytoplankton model, and their DO predictions are part of the overall sources and sinks of the model. The danger with greatly increasing the complexity at once is that each additional state variable will require additional parameters and functions to control the escalating number of interacting processes. The result is a large number of parameters in relation to output variables and objective functions. An over-parameterised model is difficult to calibrate due to the greater number of parameter combinations that may provide *non-unique* optima as described by the *equifinality* thesis (Beven, 2006).

Another strategy is to approach the nutrient and phytoplankton modelling with a stepwise approach: building the model complexity in stages rather than adding all the water-quality data at once. This method allows parameters to be constrained at a lower complexity (fewer output variables) before enabling further state variables, parameters and functions.

One of the simplest methods to begin a DO model would be the Streeter–Phelps model, a long-standing model with the state variables BOD and DO (Chapra, 2008). In practice, the relative importance of BOD depends on the system being investigated. In Europe, for example, rivers have high loading of waste water BOD in areas of dense population and industry (Lindenschmidt, 2006; Lindenschmidt et al., 2009; Williams et al., 2012). The Prairie reservoirs in Canada are often in rural areas and BOD inflows can be small. For these shallow, eutrophic systems it is far more important to include SOD when modelling DO.

Water quality models generally fall into two categories for modelling SOD: a full sediment diagenesis model, or a much simplified year-round SOD rate that varies in response to water temperature. A diagenesis model has the advantage that it can be calibrated for specific applications such as wastewater studies. The disadvantage is that, in reality, SOD is fairly difficult to measure in the field. The diagenesis model is useful when sediment core analyses are available, yet few aquatic managers and fisheries would have access to this kind of information.

A full water-quality model is currently being built for Buffalo Pound Lake (BPL), a shallow eutrophic Prairie reservoir in the Canadian province of Saskatchewan. BPL has insufficient sediment data to properly parameterise a diagenesis model. A constant SOD rate, however, is unrepresentative of the processes in a shallow, eutrophic system that spends approximately half of the year under-ice.

Our objective in this study is to test an alternative approach that allows us to increase the complexity in the constant rate SOD formulation with limited data. Our method extends the year-round constant rate by building an empirical model for SOD that considers both ice-on and ice-off periods. Modelling both winter and summer allows us to constrain certain parameters during certain seasons in order to better calibrate other parameters. For instance, setting reaeration to zero under ice-covered conditions allows us to better describe

the SOD parameterisation.

For the DO model, we use CE-QUAL-W2 (W2) (Portland, OR, USA)—a two-dimensional (vertical and longitudinal) coupled hydrodynamic and water quality model. W2 is a complex model suitable for reservoirs. W2 is chosen due to its suitability for BPL as a long, narrow waterbody, and the inclusion of an ice model. A full description of the hydrodynamics and transport processes of W2 is given in the user manual (Cole and Wells, 2015).

The results obtained by our simulations will allow us to constrain our baseline SOD within a sensible range for BPL. We will be able to maintain appropriate SOD rates as the model becomes more complex on incorporating algal-nutrient dynamics.

III Materials and Methods

III.1 Site Description

Buffalo Pound Lake (BPL) is an impounded natural lake located on the Upper Qu'Appelle River in the Saskatchewan Province of Canada (Figure II.1). The reservoir supplies the water demands of the cities of Moose Jaw, Regina, surrounding communities, and an expanding industrial corridor and potash mines. The reservoir forms part of the glacially formed upper Qu'Appelle River system described in detail in Hammer (1971). Annual mean precipitation is 365.3 mm and approximately 30% falls as snowfall (Environment Canada, 2014). Ice cover is typically November to late April. Air temperatures range between a daily minimum of −17.7 °C in January to a daily maximum of 26.2 °C in July (Environment Canada, 2014). Over 95% of the drainage basin is agricultural land (Hall et al., 1999) suggesting that non-point nutrient sources (diffuse pollution, overland run-off) may factor significantly in nutrient loading to BPL. Water quality issues such as eutrophication remain a challenge, and the reservoir has persistent problems with taste, odour, and algal blooms (Kehoe et al., 2015; Slater and Blok, 1983).

III.2 Model Setup

W2 needs full geometric data to operate. A digital elevation model (DEM) was prepared in ArcGIS 10.2.2 (ESRI Inc., Redlands, CA, USA). The DEM includes sonar data collected by

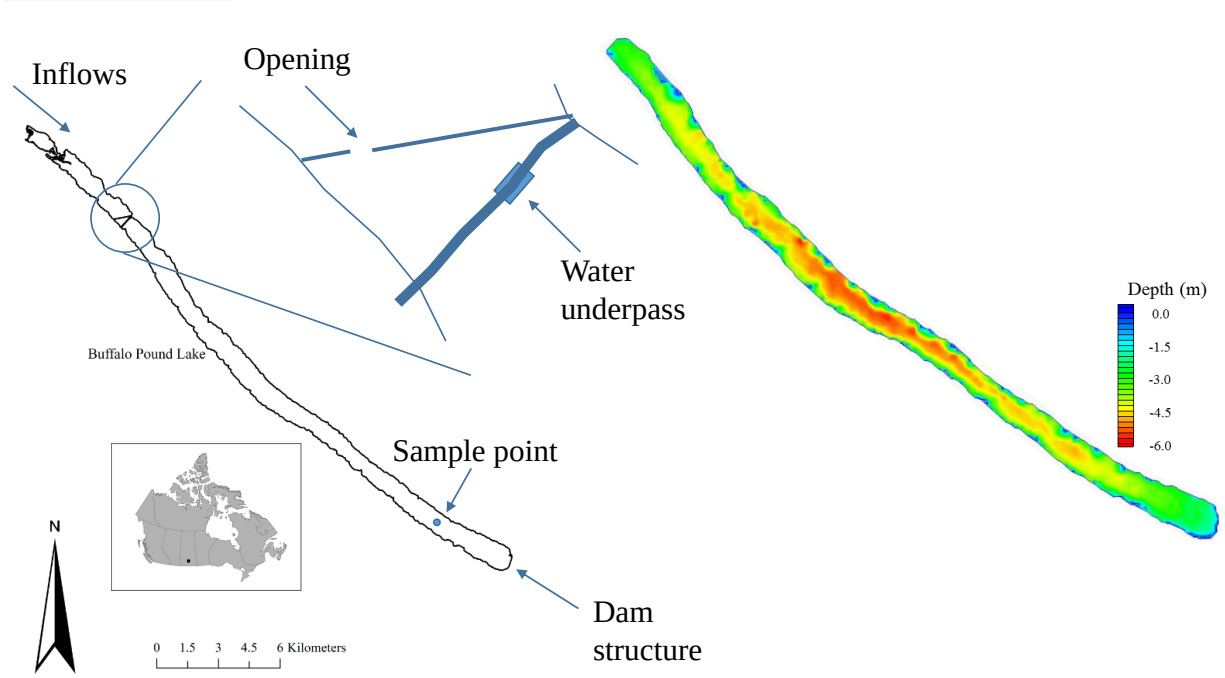

Figure II.1: Buffalo Pound Lake, Saskatchewan, Canada. Mean depth is 3.8 m with a maximum depth of 5.98 m. Mean residence time is highly variable (6 to 30 months). Flow is in a southeast direction. The black reservoir outline is to the provided scale. The digital elevation model (DEM) shows bathymetry for the main body of the lake downstream of the underpass

boat in 2014, and a reservoir extent polygon and shoreline digital elevation data provided by the Saskatchewan Water Security Agency (WSA). The combined GIS data are interpolated using a spline barrier method at 30 m resolution. The Upper Qu'Appelle flows into the northwest end of the reservoir with the dam located at the southeast end. In essence, the upstream area of BPL is split into separate waterbodies by Highway 2, which dams the reservoir down to the reservoir bed (Figure II.1). The first obstacle that the inflows meet is the breaker built to protect the highway. Once the flows are through the breaker they are then squeezed through a gap of 45 m (three connected 15 m sections) under the bridge, and into the main body of the reservoir. The top section of the reservoir is extremely shallow and weed choked, and sonar data could not be collected by boat. The top and main body of the reservoir will likely experience some differences in reservoir conditions making it less realistic to model the reservoir as just one waterbody. Water quality data were available for under Highway 2 and so these are set as boundary data. The

DEM and water quality model covers the whole main body of BPL downstream of Highway 2.

W2 discretises the waterbody into a finite grid of longitudinal segments, vertical layers and cross-sectional widths. The user specifies the space steps in the longitudinal and vertical directions. The cross-sectional widths are determined by the shoreline bathymetry as each cell spans the width of the waterbody. The prepared DEM has been segmented into a numerical grid in the Watershed Modelling System (WMS) (Aquaveo, Provo, UT, USA) for final output as a bathymetry text file for W2. Longitudinal segments average 100.9 m with a total length for all 256 segments of 25,834 m. Vertical layers are 0.25 m with the maximum number of layers being 26 at the deepest part of the reservoir. W2 requires boundary layers and segments that are all zero meters and these are included in these totals. Average width at the surface is 890 m.

III.3 Data Collection and Analysis

Hourly meteorological forcing data have been downloaded from Environment Canada (EC) for the Moose Jaw station located approximately 30 km south from BPL. In order to estimate the wind conditions at the reservoir surface, comparisons have been made of recent EC data against data from an in situ high-frequency data collecting buoy. This buoy has been deployed on BPL by the Global Institute for Water Security since 2014 for open water field seasons. Snowfall figures are also taken from the EC Moose Jaw station, and are monthly totals. The "snow on the ground" measurement is the physical quantity of snow-cover on the last day of each month.

Gauged averaged daily inflows have been downloaded directly from the EC website. Accurate inflow data is not available for the BPL boundary of Highway 2, and flows are from the nearest gauge 19 km upstream on the Upper Qu'Appelle River. This is land distance—the flows will travel further as the channel meanders. Monthly mean estimates of ungauged inflows are provided by the WSA and include minor tributaries located after the EC gauge, as well as overland run-off estimates.

The main outflows from BPL are dam releases and piped withdrawals. The dam releases have been derived using EC data for two downstream flow gauges. The withdrawal volumes

are provided by the on-site Buffalo Pound Water Treatment Plant (WTP) and by SaskWater. Daily averaged water-level measurements are provided by the WSA for an in-reservoir gauge.

Monthly inflow DO and BOD measurements are provided by the WSA for a sample site at the Highway 2 boundary. The in-reservoir observed data are taken from a substantial weekly dataset provided by the WTP laboratory. The WTP weekly samples are normally taken around 07:20 a.m. at a sample site midway between the north and south shorelines near the downstream end of the reservoir, and approximately one meter off the reservoir bed. The reservoir is expected to be well-mixed at the sampling point. Water is withdrawn through an intake pipe at this location to the WTP's pumping station, on the south shore, where sampling takes place before the water is pumped to the WTP itself. These samples are transported to the WTP laboratory for analyses. This procedure is performed weekly in both open water and under-ice conditions. Some spot sample water quality data are available for other locations across the lake, although not all constituents are measured regularly at these additional sites, and they have not been included in this study.

Weekly inflow temperatures are estimated through a linear regression ($R^2 = 0.861$; equation $y = 1.0598x - 2.7747$; 59 samples; no outliers removed) between WTP spot sample temperature measurements over 34 years at the site of the inflow gauge upstream, and the WTP weekly temperature data for the reservoir. Precipitation temperatures are set at dew-point temperature, or zero if the dew-point is negative.

Initial conditions for water temperature and DO are also taken from the WTP weekly dataset. Sediment temperature is set at the mean annual air temperature over the simulation period as per the W2 manual recommendation (Cole and Wells, 2015). Parameter coefficients are set according to knowledge of the reservoir, or are left at W2 default values where data are not available to support a change. The kinetic coefficients for BOD and SOD are W2 defaults (Table II.1).

For quality assurance, the WTP data span the complete simulation period and undergo strict quality control sample procedures. The flow data, water-level data and meteorological data downloaded from the WSA and EC websites are expected to have undergone quality control prior to commencement of the study. Metadata is available for the WSA water-quality

Table II.1: W2 Default kinetic coefficients used in this study for the sediment oxygen demand (SOD) and biochemical oxygen demand (BOD) calculations

Coefficient	Description	Value	Units
TSED	Sediment temperature	10.3 [1]	°C
CBHE	Coefficient of bottom heat exchange	0.3	W m^{-2} $°C^{-1}$
KBOD	5-day BOD decay rate at 20 °C	0.1 [2]	day^{-1}
TBOD	Temperature coefficient (decay rate)	1.02 [2]	
RBOD	Ratio of 5-day BOD to ultimate BOD	1.85 [2]	
CBODS	BOD settling rate	0.0 [2]	m day^{-1}
SODT1	Lower temperature for zero-order SOD or first-order sediment decay	4.0	°C
SODT2	Upper temperature for zero-order SOD or first-order sediment decay	25.0	°C
SODK1	Fraction of SOD or sediment decay at lower temperature	0.1	
SODK2	Fraction of SOD or sediment decay at upper temperature	0.99	
REAERAT	Reaeration formulation	LAKE, 6	

Notes: [1] Where the value is different to the W2 default; [2] W2 uses CBOD as the model group; we are assuming that CBOD makes up the majority of our BOD.

database that details the source and perceived accuracy of the measurements.

III.4 Model Customisation

We have customised two components of the W2 model: SOD and the ice algorithm. This study uses W2 version 3.72, which includes a zero-order, or a limited first-order, sediment compartment for estimating SOD. The latest version of W2 (v4.0) also includes a new sediment diagenesis model; however, with no sediment data to drive a full diagenesis compartment, there would be considerable uncertainty at the large scale of a reservoir. We opted for v3.72 as the complete source code for v4.0 was not available for download on commencement of our study, and we were unable to customise the later version for our specific objective.

W2 uses three different types of data for model calibration: the first group are set prior to the model run and remain constant throughout the simulation—examples being latitude for the calculation of solar radiation, bathymetry, and parameter coefficients. The second group are the time-varying state variables such as inflows, outflows, and meteorological

data. The third group are the variables changing internally in the model at each time step; temperature, shear stress, and horizontal and vertical velocities are examples of this group.

DO is calculated in W2 as per Equation II.1. The complete set of DO equations in W2 are more complex as the model recognises up to thirteen sources and sinks of DO (Cole and Wells, 2015). We present here the W2 equations we use in our own reservoir DO/SOD model.

$$S_{DO} = \underbrace{A_{sur} K_L (\Phi'_{DO} - \Phi_{DO})}_{aeration} - \underbrace{SOD \gamma_{OM} \frac{A_{sed}}{V}}_{zero-order\ SOD} - \underbrace{\sum K_{BOD} R_{BOD} \Theta^{T-20} \Phi_{BOD}}_{BOD\ decay} \tag{II.1}$$

where:

A_{sur}	water surface area, m^2
K_L	interfacial exchange rate for oxygen, m s^{-1}
Φ'_{DO}	saturation DO concentration, g m^{-3}
Φ_{DO}	dissolved oxygen concentration, g m^{-3}
SOD	sediment oxygen demand, g m^{-2} s^1
γ_{OM}	temperature rate multiplier for organic matter decay
A_{sed}	sediment surface area, m^2
V	volume of computational cell, m^{-3}
K_{BOD}	BOD decay rate, s^{-1}
R_{BOD}	conversion from BOD in the model to BOD ultimate
Θ	BOD temperature rate multiplier
Φ_{BOD}	BOD concentration, g m^{-3}

The zero-order SOD is a user-defined constant rate that is temperature dependant. In the original source code the model reads the SOD at the start of the simulation, and uses the same rate in the equation for the whole simulation period. The zero-order SOD is displayed in bold text in Equation II.1. In W2, BOD is imported as a time-varying variable in the inflow constituent file. We modified the W2 code to treat SOD in a similar manner and read SOD as a time-varying temperature-dependent input file. The model checks for new values of SOD during each iteration and updates the zero-order SOD in Equation II.1. The original constant SOD rate in W2 is now a variable rate in the DO equations, although the DO module itself is unchanged.

For the ice model W2 calculates the formation and melting of ice during simulations, and the relevant processes (e.g., light, wind, heat fluxes) are adjusted accordingly by the model. Snow is not considered in the algorithm. Snow depth at BPL is often between 0.1 and 0.3 m as per the supplied WSA long-term data. To account for this lack of snow the ice model has been extended to include two empirical coefficients to the existing W2 algorithms, as have been previously applied (Sadeghian et al., 2015). The first coefficient α extends the ice growth and thickness equations and reduces the heat lost through back radiation from black surfaces. The second coefficient β extends the ice melt equations and reduces the heat conduction between air and ice. Both coefficients are assigned a value between zero and one to be multiplied by the appropriate equation parameter. For BPL, no ice thickness data are available for calibration of α. A 39-year data set of ice-on and ice-off dates has been provided by the WTP, and it is found that W2 predicts the ice-on dates to be closely matched with the observed dates. For this study, the coefficient α is set to have no contribution to the ice growth equation (given the value 1). Ice-off dates were difficult to match as the ice melts too quickly in the W2 simulations—up to a period of several weeks. The optimum value of coefficient β is found to be 0.24 to predict the best spring ice-off dates over the simulation period.

III.5 Model Setup and Application

The model simulates a continuous seven-year period (1 April 1986–31 March 1993). This period is chosen due to the availability of daily flow data recorded by two WSA gauges just above and below BPL that were subsequently discontinued.

The water balance, ice-on and ice-off dates, and the water temperature model were calibrated. The final temperature model shows good results (Figure II.2). Some discrepancy occurs in the winter of 1989/90 and 1991/92 with the model under-predicting the winter bottom temperature and possibly the stratification. The temperature profile can depend on the meteorological conditions at freeze-over. In addition, many of the temperature sensitive parameters and coefficients in W2 (e.g., sediment temperature, bottom heat exchange, surface albedo) are fixed in the model. It is likely that there is some temporal variance in these in-reservoir.

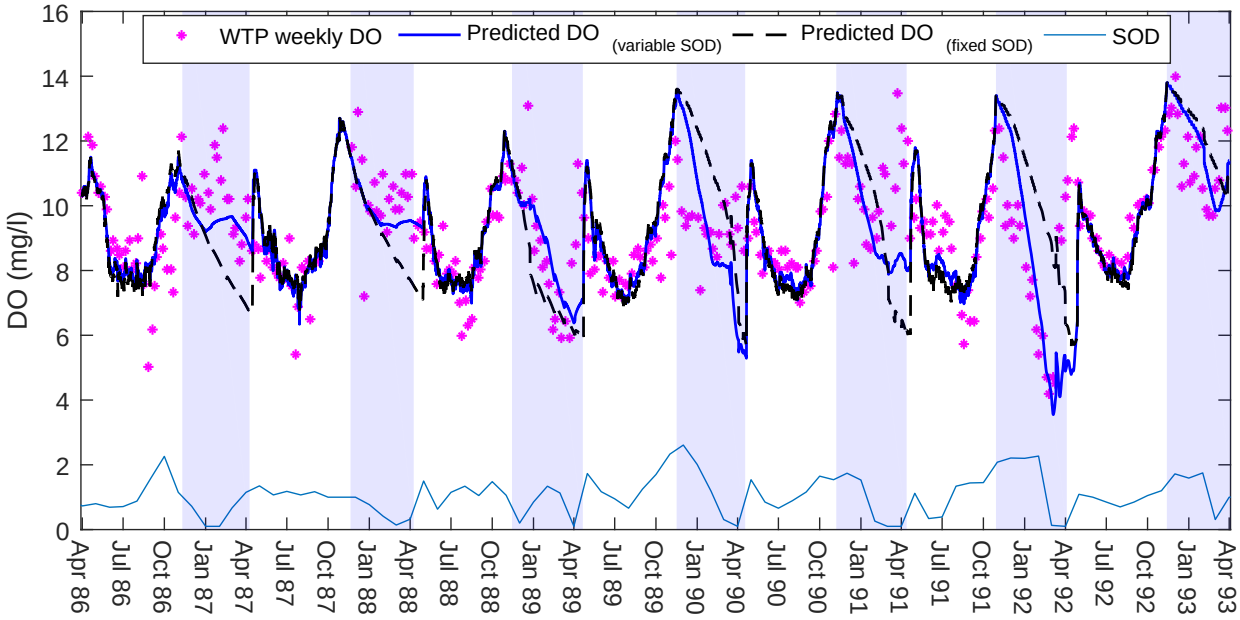

Figure II.2: Results of the water temperature model. Compares predicted temperatures in the same grid cell as the Buffalo Pound Water Treatment Plant weekly observations. Note that CE-QUAL-W2 converts the negative water temperature modelled at the start of each winter to equivalent ice thickness. Root mean square error = 1.46 (to 2 dp); mean absolute error = 1.12 (to 2 dp)

The monthly ungauged inflow estimates provided by the WSA are created to close their own water-balance for BPL, and our respective water-balances differ as a result of methodology and data. We chose not to use the provided estimates due to the uncertainty. Another limitation is that the downstream flow data, which we have included, have room for error due to the presence of wetlands, and the potential for backwater flows during the freshet from a tributary confluence downstream of the reservoir. To close our water-balance we have incorporated a distributary tributary (DT) using the W2 in-built water-balance tool. The total contribution of the DT flows is approximately 1.4% of total inflows and precipitation over the eight-year simulation period, although there are seasonal fluctuations. An exception is the winter of 1992/93 where the maximum contribution of DT flows to total inflows under ice reach 22%. This is likely due to uncertainty attributed to error in the withdrawals to the industrial corridor as they are reported on yearly totals. These final year DT flows equate to an approximate 6.5% of BPL volume based on our initial reservoir volume in the DEM (BPL water levels are controlled within a few cm). We aim to assign the DT flows to ungauged inflows and/or outflows once we calibrate the full water-quality model—based on our chemical and nutrient data. For this study, we are assuming that

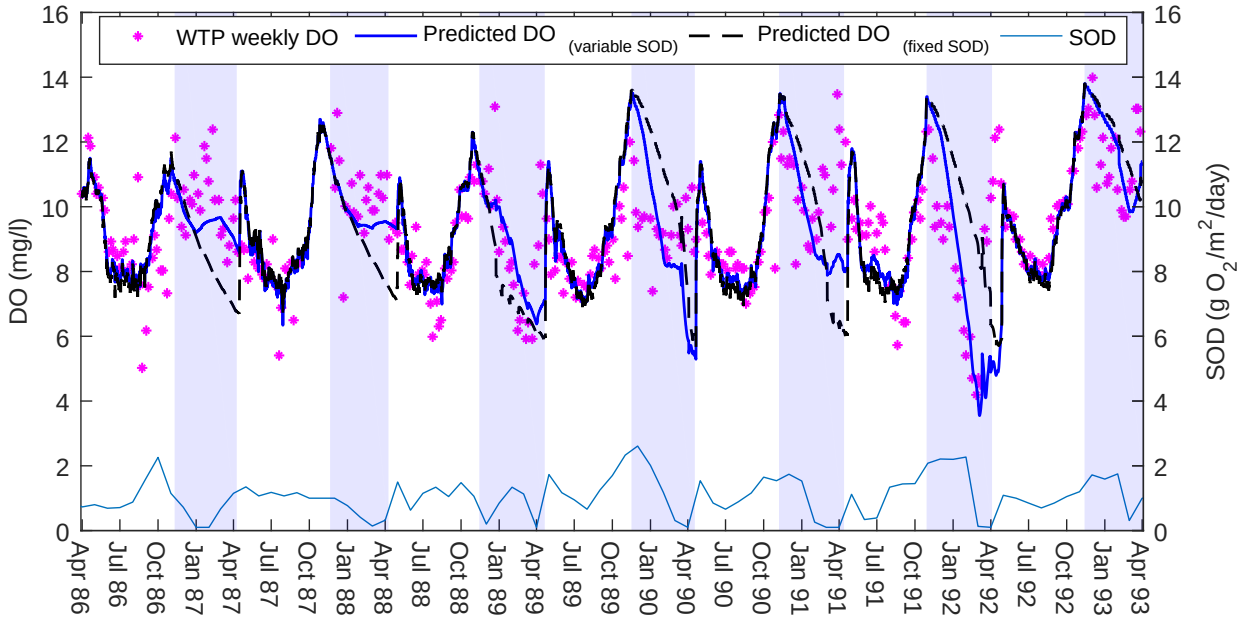

Figure II.3: The dissolved oxygen (DO) model using variable sediment oxygen demand (SOD) rates found through a semi-automated calibration procedure to match weekly predicted and observed DO concentrations (WTP weekly DO). These SOD rates are maximum values, as used by CE-QUAL-W2. The black line represents the best fit we could achieve by Monte Carlo analyses using a constant SOD rate (root mean square error = 1.94 (to 2 dp); mean absolute error = 1.43 (to 2 dp). Ice-cover days shown here in blue stripes are observed data from the Buffalo Pound Water Treatment Plant. Predicted DO concentrations using the variable SOD have root mean square error = 1.58 (to 2 dp); mean absolute error = 1.1 (to 2 dp)

constituent concentrations are primarily introduced in the main river inflows, and that DO and BOD inputs are zero in the DT flows.

We first simulated a simple DO model of BPL with a constant SOD, for comparative purposes. We extended the calibrated temperature model by enabling the water quality variables DO and BOD (BOD as one group) in W2. We proceeded to calibrate the SOD rate as part of a Monte Carlo analyses for several coefficients. We used MATLAB (MathWorks, Natick, MA, USA) to run W2 for these calibration iterations and attempted to fit the predicted DO to observed DO concentrations. Using a constant SOD we were only able to produce a moderately good fit (Figure II.3): with both underestimations and overestimations of DO throughout the simulation period.

To introduce a variable SOD we took the DO model of Figure II.3 and implemented a semi-automated calibration through MATLAB. The code attempted to match W2's predicted DO to the observed data by changing the SOD at weekly intervals. We used simple rules: for each weekly period, if the predicted DO concentrations were overestimated then the MATLAB code increased the SOD to increase consumption. If the predicted DO concentrations were underestimated then the SOD decreased that week. All weeks were changing simultaneously during the iterations and we ran the model until the SOD rates reached a stable condition.

We found that the DO model performed better with the variable SOD rates (Figure II.3). On examining the results of this new model, we noted that SOD followed a relatively consistent seasonal trend. SOD was high over summer, peaking towards the end of the season, and then gradually depleting over winter. The rates of SOD were different in magnitude each year, yet similar in behaviour.

We compared the new SOD results against observed in-reservoir water-quality data to look for trends. We noticed that the predicted SOD appeared to follow a similar pattern to the observed weekly summer chlorophyll-a (Chla) concentrations (Figure II.4) over the first few years: with SOD peaking not long after Chla. In light of this, we investigated if any relationships could be found between Chla abundance, and SOD. Our aim was to determine if Chla might be useful as an alternative measurement for estimating SOD. We approached the open water and under-ice periods differently due to the restriction of ice-cover on reaeration. We wanted to maintain the assumption of having limited data with which to build a model, and we aimed for simple strategies.

For open water seasons reaeration can replenish oxygen as it consumed, and we elected to keep our SOD constant over these periods. We allowed the model to have interannual variability by using individual SOD rates for each year. We began by averaging each summer variable SOD presented in Figure II.3. Taking these averages, we found that the lowest and highest seasonal SOD occurred in the respective years of the lowest and highest maximum summer Chla concentrations in the reservoir. This made it simpler to assume the two SOD values as being our SOD range. We then used an equation based on the apparent relationship of these two variables (summer SOD $= 0.0042 \times$ max summer

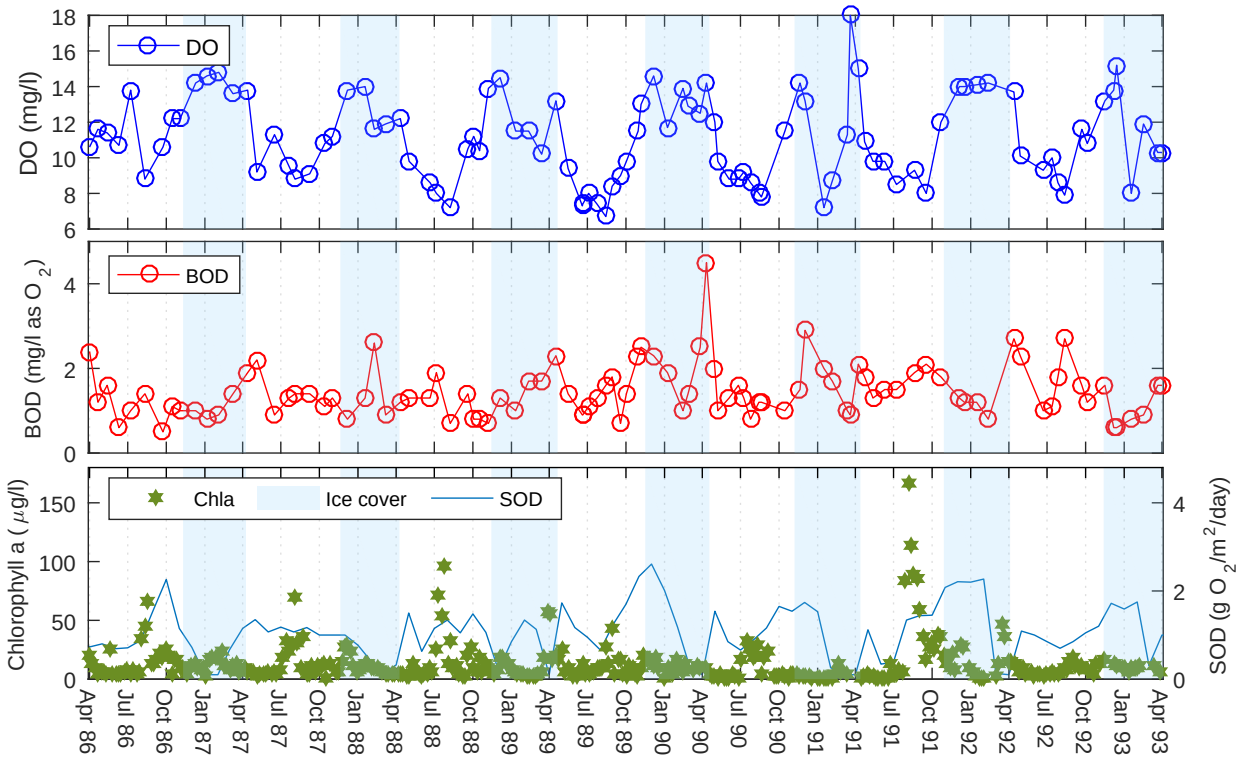

Figure II.4: Observed dissolved oxygen (DO) and biochemical oxygen demand (BOD) inflow data, and in-reservoir Chlorophyll-a (Chla) concentrations in BPL. The DO and BOD data are monthly measurements at the upstream boundary (BOD as the standard five-day BOD at 20 °C), and the Chla data are from the long-term weekly dataset, provided by the Buffalo Pound Water Treatment Plant, at the downstream sample point

Chla + 0.9345) to set the remaining summer SOD rates based on the maximum summer Chla concentrations each year. By this method, we used the previous summer's maximum Chla concentrations as a proxy of the magnitude of biomass production that settled to the bottom sediments by the end of the open water season.

To simulate end of season algal bloom mortality and winter decay we again used MATAB to adjust the SOD rate, so that predicted DO fit to observed DO, from one-month before ice-on occurred until ice-off the following spring. We implemented the same weekly semi-automated calibration process as before, and the SOD rates generally peaked before the ice-on event. Under ice-cover W2 automatically stops any gas exchange, and reaeration equals zero. This allows us to imitate a first-order decay rate during this time.

Once we had both the end of season peak SODs and winter SODs we were then able to back-calculate the winter SOD decay rates (k) for each year based on Equation II.2:

$$SOD = peak\ SOD \times weeks^{-decay(k)} \tag{II.2}$$

where the predicted winter SOD in W2 is assumed to be a function of the predicted peak SOD, and the number of weeks since the start of ice-cover to the decay rate k; With k being the unknown in this equation. These back-calculated decay rates were then plotted against summer Chla.

IV Results

IV.1 Dissolved Oxygen Simulation

The final DO model shows good overall results (Figure II.5). The predicted DO observations follow the pattern of the observed DO measurements in most years. There is some underestimation in the winters of 1986/87, 1987/88 and 1992/93. SOD follows a similar trend for each year with an end-of-season peak, and winter decay. The SOD remains high in the winter of 1991/92 due to a greater than average oxygen depletion that year. There is a clear connection in the model between the predicted DO, and the observed ice-on and ice-off dates provided by the WTP.

IV.2 Sediment Oxygen Demand Relationships

The peak SOD does not fit particularly well with the maximum or average summer Chla. Interestingly, in comparison with observed data for BPL, the peak SODs appear to have a high correlation (R^2= 0.85) with the average BOD inflows included in our model for the open water period. (Figure II.6a). The winter SOD decay rates have a negative, exponential relationship with both the average and maximum summer Chla concentrations of the previous summer. The relationship between SOD decay and the maximum Chla (Figure II.6b) is slightly stronger at $R^2 = 0.88$ (average Chla: $R^2 = 0.84$).

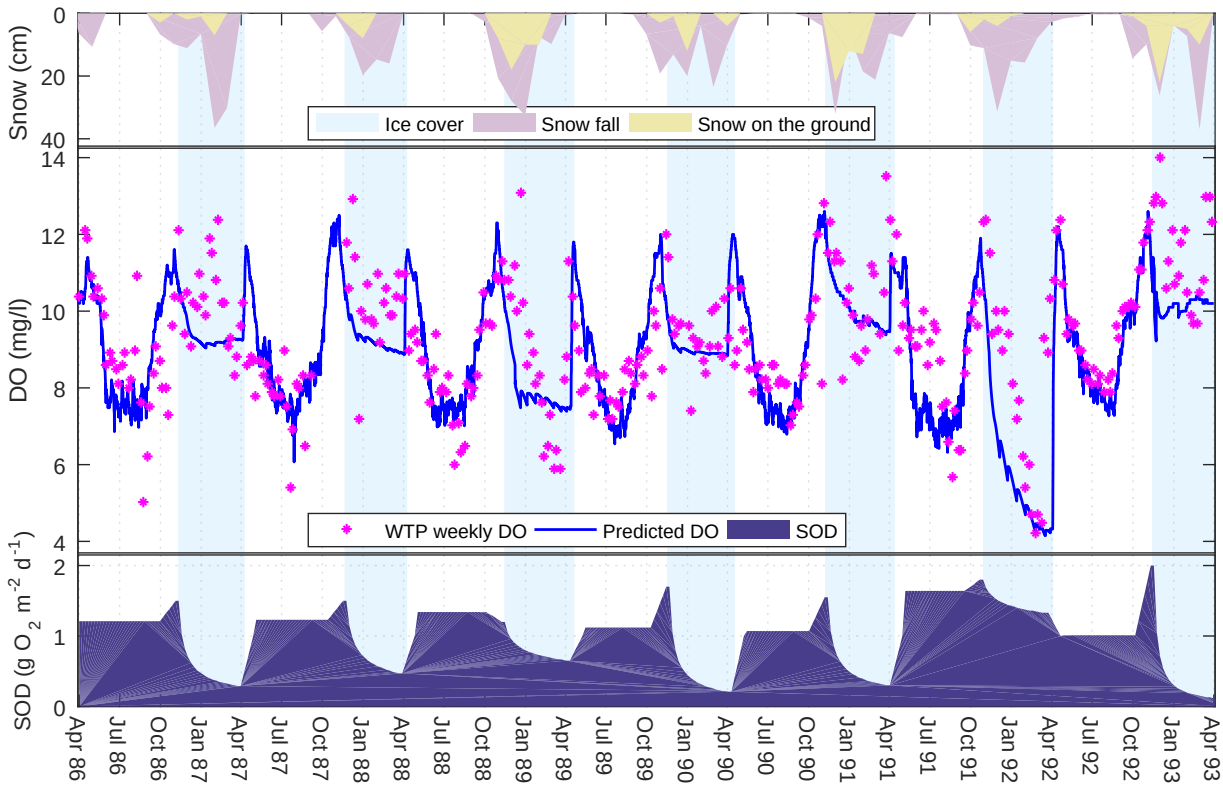

Figure II.5: Dissolved oxygen (DO) model using summer sediment oxygen demand (SOD) rates based on the maximum summer Chlorophyll-a. The end of season peak and winter decay are found through a semi-automated calibration procedure to match weekly observed DO concentrations (WTP weekly DO). Ice-cover days shown here are the observed data from the Buffalo Pound Water Treatment Plant, and snow data are from Environment Canada. Snow on the ground is measured on the last day of each month. Predicted DO have root mean square error = 1.47 (to 2 dp); mean absolute error = 1.09 (to 2 dp)

V Discussion

A zero-order approach for SOD that treats the demand as an input variable rather than a calculated one does not reflect the conversion of organic matter settling during the simulation (Cross and Summerfelt, 1987). Our original intention was to allow the model to find the changing SOD values through matching to observed DO concentrations. For this, the model was calibrated in MATLAB using a semi-automated iterative process that allowed the model to change the SOD weekly. The resulting SOD values were then to be read by W2 as an input file; this would imitate a first-order compartment, in essence, by varying through the simulation. The model indeed predicted DO concentrations more

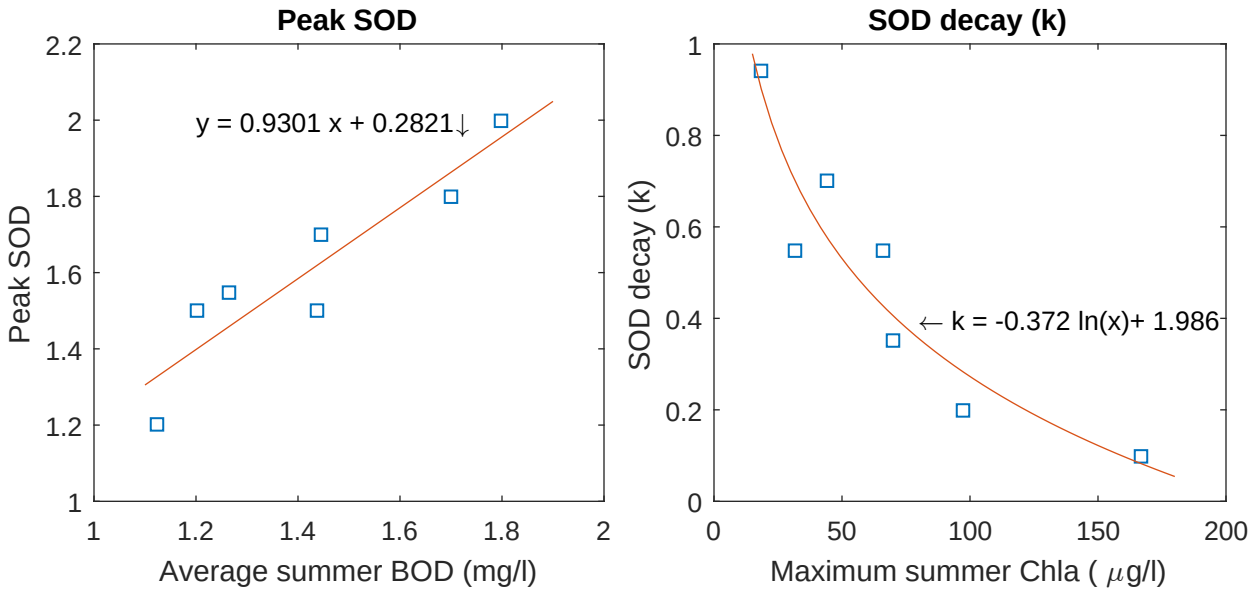

Figure II.6: Relationships between SOD (day^{-1}), and observed BPL measurements, after the final DO model simulation: (**a**) Predicted peak SOD and average open water BOD inflows ($R^2 = 0.85$); (**b**) Back-calculated winter SOD decay, and observed maximum summer Chla concentrations of the previous summer ($R^2 = 0.88$)

closely with this variable SOD file than with the W2's original fixed rate option.

Calibrating the SOD with the purpose that the model's DO predictions match with observed DO measurements can be an unsound technique as it assumes that other parameters such as reaeration and settling rates are already well-known (Chapra, 2008). This method of calibration also combines several reservoir processes that contribute to DO into one net value that is assumed to be SOD. While these points suggest that there are limitations to this approach, there remains the problem that few aquatic managers have sufficient data available to run the full diagenesis model. In view of this, we assessed the initial results to see if there were other trends that matched what we know about BPL, and that might suffice as a proxy measurement or explanatory variable.

The reservoir is a highly eutrophic system with high incidences of algal blooms. Deoxygenation can occur after the collapse of a summer algal bloom due to additional bacterial activity (Robarts et al., 2005). In general, the more enriched the system then the higher the rates of productivity and ultimately the greater the oxygen depletion from decomposition (Meding and Jackson, 2003). Chla has previously been used as a proxy for

estimating in-lake BOD (Fang and Stefan, 2009). Based on this principal, and our knowledge of the reservoir, we are assuming that most of the autochthonous contributions to oxygen demand within BPL are related to algal activity (apart from nitrification and chemical oxygen demand). Any allochthonous inputs to oxygen demand are already included in our BOD time-series data in the inflow constituent file—with the caveat that we are using the W2 default BOD settling rate between upstream and our sample site on the reservoir.

We have found this approach to be successful, as shown in Figure II.5. The summer SOD rates based on a correlation with the summer Chla concentrations act effectively as a substitute to our weekly variable SOD. This suggested link between oxygen depletion and productivity also agrees with our findings relating winter SOD decay to the Chla concentrations of the previous summer. This is noticeable in the results for the winters of 1988/89 and 1991/92 where the SOD remains high under ice-cover following large summer algal blooms.

In contrast, a result of no correlation between Chla and DO consumption is found in other shallow prairie lake sites (Meding and Jackson, 2003). The study in question suggests that the most important predictor of DO consumption is macrophyte biomass due to the large contribution to particulate organic matter (POM). This is found to be also true in sites with abundant phytoplankton, although the authors point out that the algal-derived carbon averages 150 times less than the macrophyte-derived carbon in their study. In BPL, apart from the top section outside of the model boundary, the reservoir is not thought to have many macrophytes. This may explain why we are able to find a relationship between summer Chla and winter SOD decay as the macrophyte contribution to POM is not important in this reservoir.

Our winter SOD decay pattern declines in an exponential manner with a rapid reduction at the onset of winter. This theory fits with the suggestion that the first three months of ice-cover have the greatest oxygen consumption due to the rapid oxidation of certain organic materials over others, for example (Babin and Prepas, 1985)

The apparent connection between peak SOD and the average BOD inflows for the open water season is more surprising as we had suspected that the low values of BOD would

have little impact in the reservoir. SOD and BOD are, in fact, often combined into one demand known as hypolimnetic oxygen demand (Kirillin et al., 2012). In an ideal model BOD and SOD would be kept separate. Our internal BOD is included with our SOD, as is reaeration. In addition, BOD inflows are based on monthly samples. The result is that we cannot ascertain for certain the relative importance of BOD flowing into the reservoir.

In the winters of 1986/87 and 1987/88, the model under-predicted the DO concentrations. However, in these years, it can be seen that although snowfall was still high in both years, there was little snow left on the ground at the end of each month. It is possible that the reservoir winter albedo is relatively low in these years and light can penetrate the ice to allow photosynthesis to take place. This is evident in the observed winter Chla concentrations (Figure II.4). This is a winter phenomenon that we are unable to capture in the model as we do not simulate primary productivity, and our SOD equations are founded on summer Chla. While snow on the ground is also minimal in the winter of 1991/92, this year is different as the intense summer algal bloom preceding this year results in the DO concentrations falling and the SOD remaining high.

What is interesting in the winter of 1992/93 is that the snow cover is high throughout the winter, suggesting low light availability, and yet DO concentrations are high. On examination of the temperature model (Figure II.2), it can be seen that the observed bottom water temperatures are much lower in this year than in previous years. Cold water holds more oxygen than warm water (Wetzel, 2001), and estimating DO inputs based on monthly samples may be missing occasional elevated DO concentrations in cold river inflows during periodic snowmelts. The winter of 1992/93 also has the greatest contribution of the distributary tributary inflows, which indicates that there may be a larger amount of ungauged inflows contributing to the water balance in W2 with no corresponding DO input file.

Another point to consider is that oxygen consumption rates are shown to be temperature dependent with lower consumption rates at lower temperatures (Golosov et al., 2007). Both the summer temperatures of 1992 and winter temperatures of 1992/93 were colder than previous years. This suggests that less heat may be stored in the sediments. The sediment temperature in W2 is a fixed user parameter, and in our model has been set at the

average annual air temperature over the simulation period (where temperature >0 °C). The observed sediment temperature may be colder than this average value in the final winter, and, in reality, the sediment oxygen requirements are lower than we are modelling.

An equation for the effect of water temperature on SOD shows how temperature and SOD have a positive relationship with each other: SOD starts to decline more rapidly after temperatures go lower than 10 °C, and reduces towards zero as water temperatures drop below 5 °C (Chapra, 2008). Part of the pattern of SOD changes in BPL will also be a function of bottom water temperature. Our SOD decays rapidly to near zero levels quite early in the colder water temperatures of winter 1992/93. The temperatures in BPL are fairly consistent year-on-year until the summer of 1992, and the winter decreases and summer increases of SOD in response to temperature are expected to be comparable up to this point. This leaves Chla explaining the SOD variance between the individual years.

W2 uses four SOD temperature-rate multipliers to adjust the rate of SOD decay as a function of temperature in the model. They are model calibration parameters, and can be helpful in reproducing the changing rate of consumption of DO. We have used the default settings in W2 (Table II.1). The variable SOD values that we include in W2 as an input file are maximum SOD rates—the same as the model format for a constant SOD rate. Figure II.7 shows the temperature adjusted rates that W2 is actually using during the simulations based on these default calibration parameters. A contributing reason for the end of summer SOD peaks, for example, might be that the rapid decreases in the temperature adjusted SOD are too extreme. The model may potentially increase the maximum SOD to compensate for this temperature effect when calibrating SOD to match the predicted DO with observed DO. We had no data with which to justify changing the default values. Likewise, we did not wish to increase our model uncertainty by expanding the number of parameters with no additional data. We instead chose to adjust just one parameter (SOD) for our purposes.

There are a few differences between SOD found by using MATLAB to vary SOD each week to fit the predicted and observed DO to each other (weekly model—Figure II.3), and SOD found through basing the demand on summer Chla (final model—Figure II.5). The winter decay in the final model agrees well with the drops in SOD in the weekly model except

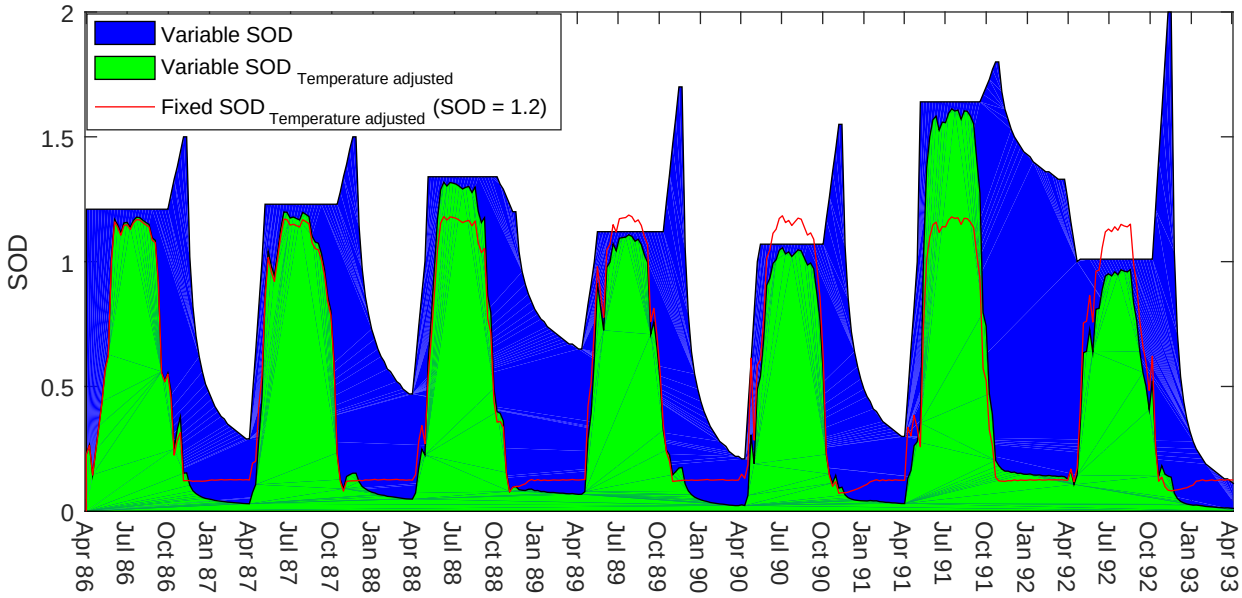

Figure II.7: A comparison of the maximum SOD rates that we input into the model (blue) against the temperature adjusted rates that the model is actually using based on W2 default values for the four temperature-rate multipliers (green). Also shown is the temperature adjusted rates for the fixed SOD simulations

for the winter of 1991/92. In this year, the weekly model drops the SOD to zero when the DO levels are extremely low and then increases SOD as the oxygen levels rise. This is the opposite behaviour to what we would expect in a limnological sense. The behaviour of the final model in this time period is more realistic. The relatively large peak in SOD at the end of this summer may possibly be due to the BOD inputs being higher this year (Figure II.4).

In reality, the rapid peaks in SOD shown in Figure II.5 are also likely a result of our holding the SOD at a constant rate over the summer period. The final model uses average summer rates, and will miss some of the variability that would naturally occur. In the semi-automated calibration of Figure II.3, we show that when the model uses variable weekly SOD rates there is a general (with some fluctuations) increase over the course of the summer. This agrees with our assumption that SOD in BPL cumulates to a peak due to biota dying towards the end of the season. By holding the model at an average seasonal SOD, instead, we are likely overestimating the SOD in spring, and underestimating the SOD in autumn—if we are to assume that SOD increases as suggested by Figure II.3. We found that our winter decay relationship with Chla was

stronger if we allowed MATLAB to adjust SOD so that the predicted DO fits to the observed DO at the onset of ice-on. In order to achieve this, we had to release the model from the fixed SOD rate at the end of the season—thereby simulating the end of season peak. We chose a one-month period prior to ice-on as a sensitivity analysis showed that this gradient of SOD adjustment gave us the best overall results for summer and winter.

This summer averaging method is most likely responsible for the sudden increase in SOD at ice-off in April. There will be natural processes leading to an increase in SOD (e.g., warmer water, spring blooms, and spring turnover) that will be exaggerated by the need for the SOD to instantly increase to the average summer rate at the start of spring. Other methods may be to allow the model to increase gradually over the whole summer duration, either linearly or exponentially, although we would need to consider some way of verifying the manner in which it increased. Our strategy was to approach the problem as if having little to no data to verify the predicted SOD rates (except using DO data). We decided to constrain the model to using an average summer rate based on a relationship found with Chla, and then allow the SOD to decay over winter dependent on a fixed equation. Thus, the aquatic manager would only need to find (and ideally verify) limited points, such as the end of season peak rate, rather than weekly SOD rates.

One limitation to our study is the disconnection between the top and main section of the reservoir. While our inflow constituent file is based on observed data from under Highway 2, and the boundary of our model, the inflows themselves relate to a gauge further upstream on The Upper Qu'Appelle River. It is uncertain at present what effect the top section of the reservoir, the wave-breaker, and the 45 m gap under the highway have on our inflow boundary data.

Finally, while our extended W2 ice model is a suitable model for seasonally ice and snow-covered waterbodies, the W2 model has a fixed albedo coefficient through the simulation. The extension to the ice model stops the ice melting too quickly by keeping the snow on the ground, yet does not help with modelling the correct amount of light penetrating the ice. This will make it difficult to calibrate DO, when primary production is added to the model, with just one value for high and low snow years, and different ice structures. This is due to the influence of light on photosynthesis and oxygen production,

as indicated in the observed data in the winters of 1986/87 and 1987/88. Our future plans include modifying the ice model further to include a function for a variable albedo. We think that this will be an interesting step to take forward and is a missing-link in modelling DO/SOD relationships in ice-covered reservoirs.

VI Conclusions

From the modelling, we show that winter SOD decay is inversely dependent on the previous summer's maximum Chla concentrations. The decay rate is faster when less algae are produced. A constant SOD value suffices during the summer half-year; however, a better DO simulation is obtained in winter when the SOD rate decays during the course of the winter. This implies that the biomass supply during winter is limited and much of the draw on DO is diminished by the end of the winter. This result is backed by several field studies. We have shown that for a Prairie shallow reservoir with few macrophytes and BOD inputs variable SOD can be used in a water quality model to represent additional oxygen demand after an algal bloom. The summer SOD and winter SOD decay can be estimated by treating the open water and under-ice period individually in the model. This variable SOD over-time can be estimated for both summer and winter conditions based on summer concentrations of Chla. This concept can be widely applied to similar systems that do not have data to support a full diagenesis model, yet would benefit from a more representative estimation of SOD than is provided by a zero-order constant SOD rate.

Acknowledgments:

This work is funded through the Natural Sciences and Engineering Research Council of Canada Strategic Project Grant, the Buffalo Pound Water Treatment Plant (WTP), the Water Security Agency (WSA), the Global Institute for Water Security (GIWS), and the School of Environment and Sustainability (SENS). We thank Heather Wilson (DEM preparation), and Helen Baulch (buoy data + funding support) from GIWS, and Paul Jones (boat sonar data) from SENS. We also thank John-Mark Davies (water-quality data), Dave MacDonald (GIS data), and Andrew Thornton (water demands) from the WSA. We are grateful to Curtis Hallborg from the WSA for hydrological data and his time in explaining

the hydrology of the reservoir system. Water-quality data provided by Dan Conrad at the WTP is gratefully acknowledged. We thank the anonymous reviewers for valuable feedback.

References

Babin, J. and Prepas, E. (1985). Modelling winter oxygen depletion rates in ice-covered temperate zone lakes in Canada. *Canadian Journal of Fisheries and Aquatic Sciences*, 42(2):239–249.

Beven, K. (2006). A manifesto for the equifinality thesis. *Journal of hydrology*, 320(1):18–36.

Canadian Council of Ministers of the Environment (1999). Canadian water quality guidelines for the protection of aquatic life: Dissolved oxygen (freshwater). Technical report, Canadian Council of Ministers of the Environment: Winnipeg, MB, Canada.

Chapra, S. C. (2008). *Surface water-quality modeling*. Waveland press.

Cole, T. M. and Wells, S. A. (2015). *CE-QUAL-W2: A two-dimensional, laterally averaged, hydrodynamic and water quality model*. Department of Civil and Environmental Engineering, Portland State University, Portland, OR, 3.72 edition.

Cross, T. K. and Summerfelt, R. C. (1987). Oxygen demand of lakes: sediment and water column BOD. *Lake and Reservoir Management*, 3(1):109–116.

Environment Canada (2014). Climate Normals 1981–2010 Station Data for Moose Jaw a Station. Available at: http://climate.weather.gc.ca/, accessed on 21 November 2014.

Fang, X. and Stefan, H. G. (2000). Projected climate change effects on winterkill in shallow lakes in the northern united states. *Environmental Management*, 25(3):291–304.

Fang, X. and Stefan, H. G. (2009). Simulations of climate effects on water temperature, dissolved oxygen, and ice and snow covers in lakes of the contiguous us under past and future climate scenarios. *Limnology and Oceanography*, 54(6part2):2359–2370.

Finlay, K., Leavitt, P., Patoine, A., and Wissel, B. (2010). Magnitudes and controls of organic and inorganic carbon flux through a chain of hard-water lakes on the northern Great Plains. *Limnology and Oceanography*, 55(4):1551–1564.

Golosov, S., Maher, O., Schipunova, E., Terzhevik, A., Zdorovennova, G., and Kirillin, G. (2007). Physical background of the development of oxygen depletion in ice-covered lakes. *Oecologia*, 151(2):331–340.

Hall, R. I., Leavitt, P. R., Dixit, A. S., Quinlan, R., and Smol, J. P. (1999). Limnological succession in reservoirs: a paleolimnological comparison of two methods of reservoir formation. *Canadian Journal of Fisheries and Aquatic Sciences*, 56(6):1109–1121.

Hammer, U. (1971). Limnological studies of the lakes and streams of the upper qu'appelle river system, saskatchewan, canada. *Hydrobiologia*, 37(3-4):473–507.

Hosseini, N., Johnston, J., and Lindenschmidt, K.-E. (2017). Impacts of climate change on the water quality of a regulated prairie river. *Water*, 9(3):199.

Kehoe, M. J., Chun, K. P., and Baulch, H. M. (2015). Who smells? forecasting taste and odor in a drinking water reservoir. *Environmental science & technology*, 49(18):10984–10992.

Kirillin, G., Leppäranta, M., Terzhevik, A., Granin, N., Bernhardt, J., Engelhardt, C., Efremova, T., Golosov, S., Palshin, N., Sherstyankin, P., et al. (2012). Physics of seasonally ice-covered lakes: a review. *Aquatic sciences*, 74(4):659–682.

Leppi, J. C., Arp, C. D., and Whitman, M. S. (2016). Predicting late winter dissolved oxygen levels in arctic lakes using morphology and landscape metrics. *Environmental management*, 57(2):463–473.

Lindenschmidt, K.-E. (2006). The effect of complexity on parameter sensitivity and model uncertainty in river water quality modelling. *Ecological Modelling*, 190(1):72–86.

Lindenschmidt, K.-E., Pech, I., and Baborowski, M. (2009). Environmental risk of dissolved oxygen depletion of diverted flood waters in river polder systems–a quasi-2d flood modelling approach. *Science of the total environment*, 407(5):1598–1612.

Martin, N., McEachern, P., Yu, T., and Zhu, D. Z. (2013). Model development for prediction and mitigation of dissolved oxygen sags in the athabasca river, canada. *Science of the Total Environment*, 443:403–412.

Meding, M. E. and Jackson, L. J. (2003). Biotic, chemical, and morphometric factors contributing to winter anoxia in prairie lakes. *Limnology and Oceanography*, 48(4):1633–1642.

Robarts, R. D., Waiser, M. J., Arts, M. T., and Evans, M. S. (2005). Seasonal and diel changes of dissolved oxygen in a hypertrophic prairie lake. *Lakes & Reservoirs: Research & Management*, 10(3):167–177.

Sadeghian, A., de Boer, D., Hudson, J. J., Wheater, H., and Lindenschmidt, K.-E. (2015). Lake Diefenbaker temperature model. *Journal of Great Lakes Research*, 41:8–21.

Salonen, K., Leppäranta, M., Viljanen, M., and Gulati, R. (2009). Perspectives in winter limnology: closing the annual cycle of freezing lakes. *Aquatic ecology*, 43(3):609–616.

Scardina, P. and Edwards, M. (2001). Prediction and measurement of bubble formation in water treatment. *Journal of Environmental Engineering*, 127(11):968–973.

Slater, G. P. and Blok, V. C. (1983). Isolation and identification of odourous compounds from a lake subject to cyanobacterial blooms. *Water Science and Technology*, 15(6-7):229–240.

Thornton, K. W., Kimmel, B. L., and Payne, F. E. (1990). *Reservoir limnology: ecological perspectives*. John Wiley & Sons.

Vehmaa, A. and Salonen, K. (2009). Development of phytoplankton in lake pääjärvi (finland) during under-ice convective mixing period. *Aquatic Ecology*, 43(3):693–705.

Wetzel, R. G. (2001). *Limnology: lake and river ecosystems*. Gulf Professional Publishing, 3rd edition.

Williams, R., Keller, V., Voß, A., Bärlund, I., Malve, O., Riihimäki, J., Tattari, S., and Alcamo, J. (2012). Assessment of current water pollution loads in Europe: estimation of gridded loads for use in global water quality models. *Hydrological processes*, 26(16):2395–2410.

Appendix III
Calibration and optimization

Similar to many well-established water quality models, CE-QUAL-W2 normally relies on a trial and error process for calibration, which is not an efficient approach for parameter identification (see Lindim et al., 2011). A limited Monte Carlo analysis (1,000 runs) was applied here to evaluate model performance, followed by automatic optimization. Each model run took two to three hours on a high-performance PC (Intel Core i7–3770S / 8 MB cache 3.4 GHz 5.0 GT/ 12 GB DDR3), with the simulations starting in April 2011 and ending in October 2012. By using all the processors, implemented by additional code to use six CPU cores at the same time, the total calculation time for 1,000 runs was reduced to approximately two weeks. The global sensitivity analysis was based on a Monte Carlo analysis of 1,000 runs, with each simulation having parameters randomly selected from a uniform distribution within defined ranges.

Although the results from the Monte Carlo simulations are extremely useful for sensitivity analysis, the long computational time is a drawback. Therefore, in order to calibrate the model more efficiently, a coupled global and local optimization method was tested, which is well suited for complex systems (Vesselinov and Harp, 2012). Global optimization methods are useful to explore regions with good parameter settings (finding the ranges for each parameter that produce satisfactory results), but need more iterations for fine tuning within those regions. In contrast, local optimization methods are very sensitive to the initial estimates. If the initial estimates for parameter values are close to optimal, they become very efficient (Vesselinov and Harp, 2012).

In our approach, we used the global optimization method "Particle Swarm Optimization" (PSO) to find optimal regions. Subsequently, the parameter settings were fine-tuned using the local optimization method "Levenberg-Marquardt" (LM). The code for PSO calculations was obtained from the MATLAB® code repository (PSO, 2013) and the code for LM was obtained from Gavin (2011).

A swarm is a set of calibration parameters that the PSO model generates randomly at first. Each parameter set has a position and gradient showing the improvement in accuracies. After each iteration, the PSO checks the performance and updates the position and gradient values to generate new parameter values based on their positions in the swarm. One important parameter for the PSO calculations is the swarm size. Swarm size is equal to the number of parameter sets. The larger the swarm size, the longer it takes to run. An optimal swarm size S is suggested to be $S = 10 + 2\sqrt{D}$ (PSO, 2006), where D is the number of calibration parameters (which = 4 in our case). A swarm size of 12 (instead of 14) was used in order to be consistent with the running of six models in parallel, the approach used in the Monte-Carlo simulations. After 12 initial runs for randomly generated values, the code checks the results and generates new parameter estimates, which takes another 12 runs. After these 24 runs, parameter values with the best results were sent as initial estimates for the LM code.

The Levenberg-Marquardt (LM) algorithm is a method for solving nonlinear least squares problems. In each iteration, a new set of parameters is generated and, based on results, an algorithmic parameter (λ) is calculated. For small values of λ, the parameters update using the Gauss-Newton method. Large λ values result in a gradient descent update (Gavin, 2011). If a convergence happens in the gradient, parameters or chi-squared (X^2 = sum of the weighted squares of the errors between the measured data and the curve-fit function), the code will terminate and return the results, otherwise it continues until the threshold for the number of iterations is exceeded. When the number of LM iterations is exceeded (30 in this current work), the code will return the results to the PSO again, to find new regions of potential best performance. This system continues until a convergence happens or the code reaches the threshold of the total number of iterations.

The difference between measured and calculated temperature values of each Monte Carlo simulation was calculated using the sum of squared error (SSE) as:

$$SSE = \sum (O - S)^2 \tag{III.1}$$

where O is the measured value and S is the model output time-series for vertical temperature profiles at the 16 stations shown in Figure 3.3. To calculate SSE, all the temperature measurements from all different depths and locations were sorted in one column and

compared with the simulated values at exactly the same location and depth. In some cases, model performance calculations were divided into smaller groups to draw out comparisons of performance for different years and depths. The "Root Mean Square Error" (Eq. 5.1) was used instead of SSE to account for differences in the number of samples between different groups:

SSE values were used to find the best parameter settings in the Monte-Carlo and PSO simulations; chi-squared was used in the LM simulations. A more detailed description of PSO and LM methods is beyond the scope of this text and readers are referred to Clerc (2010); Gavin (2011) and Vesselinov and Harp (2012) for more information.

Monte Carlo simulations were applied to both the fine and coarse bathymetric models. For the model with 187 segments, 1,000 uniformly random generated values were used for each parameter. For the model with 126 segments, the PSO+LM runs were repeated until a total number of 1,000 runs was achieved. Therefore, the results could be used both for the analyses of parameter sensitivity and model responses related to segment lengths. In addition, the repeated PSO+LM runs were also used to assure the accuracy of the codes. In the PSO+LM runs, instead of continuously running from 2011 to 2012, two models were used: one from April to October 2011 and the second from April to October 2012. This allowed us to check that the reservoir's yearly net heat budget remained balanced (equal to zero) and that no residual heat was added or removed between years. Computational time also decreased without losing accuracy.

The model performances based on PSO+LM for two model coefficients, WSC and SHADE, are shown in Figure III.1 based on the objective function SSE. In the top panel, the results of all the runs are displayed with both the size and color of the spheres indicating the significance of the errors. The bottom panel shows the results for one optimization tried as an example in which the red spheres show the PSO runs (24 runs) and the blue spheres show the LM runs (11 runs). Similar to the top figure, the size of the spheres indicate the significance of the errors. As can be seen in both pictures, the errors are more prominent in some areas in space and smaller in some other regions. Model results were most sensitive to the values of WSC and SHADE, hence combining them in one figure provided a better image of the optimization algorithms' performances. The algorithms were allowed to find

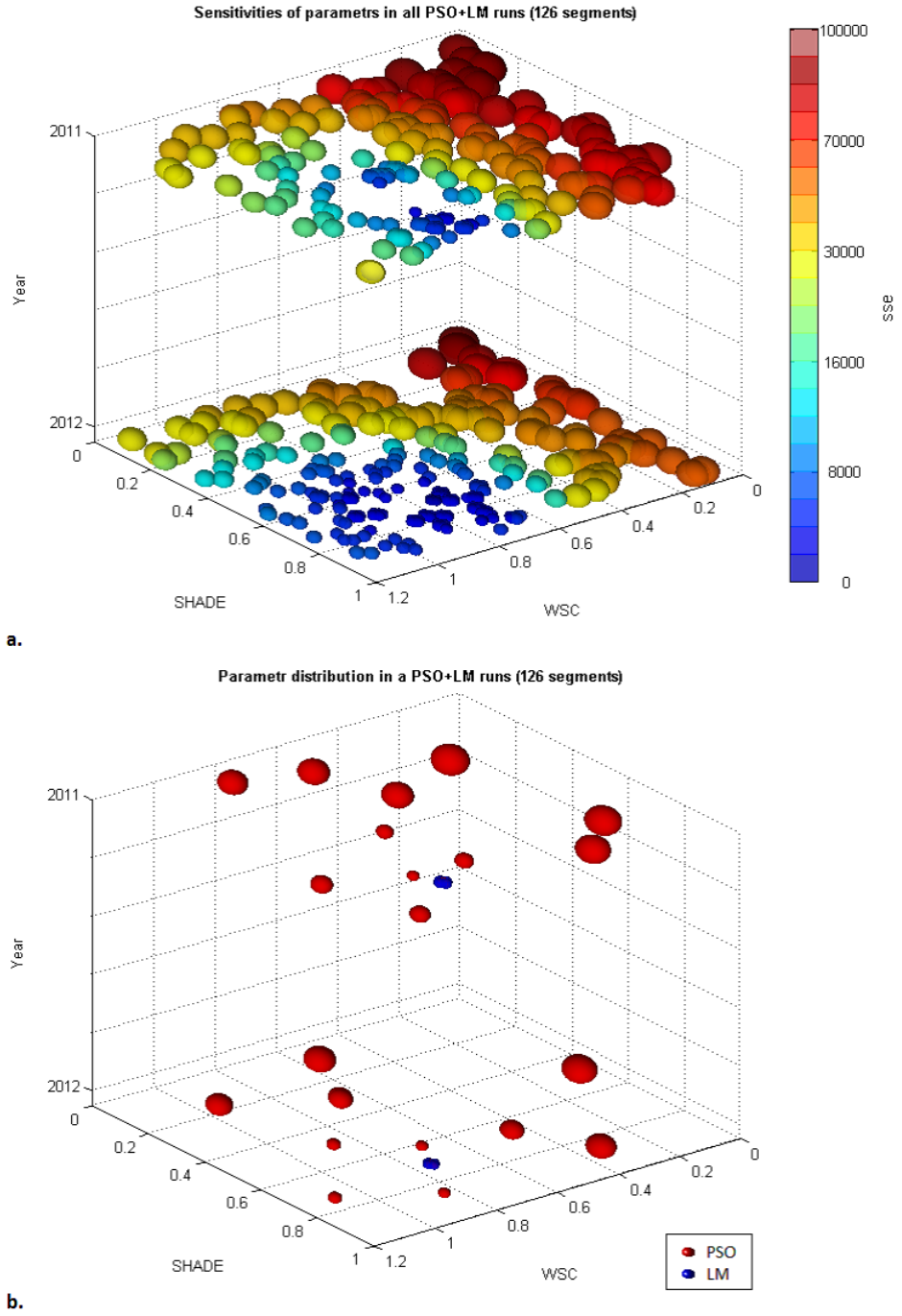

Figure III.1: Optimization method procedure. a: PSO+LM runs for the model with 126 segments in 2011 and 2012. The figure shows the distribution of parameters that are selected by algorithms which is different from the uniform distribution in Monte-Carlo simulations. The size of the circles is also an indicator of errors. The bigger the circles the larger the SSE. b: Model parameter distribution for best PSO+LM run. In each year the total runs are 35 including 24 PSO (red circles) and 11 LM runs (blue circles)

optimum values for each year separately. The global optimization algorithm (PSO) was responsible for finding the areas with the lowest errors and found very similar regions for both years. Then, the local optimization algorithm (LM) could fine-tune the model results within that limited boundaries which have small differences for different years.

References

Clerc, M. (2010). *Particle swarm optimization*, volume 93. John Wiley & Sons.

Gavin, H. (2011). The levenberg-marquardt method for nonlinear least squares curve-fitting problems. Technical report, Department of Civil and Environmental Engineering, Duke University.

Lindim, C., Pinho, J., and Vieira, J. (2011). Analysis of spatial and temporal patterns in a large reservoir using water quality and hydrodynamic modeling. *Ecological Modelling*, 222(14):2485–2494.

PSO (2006). Particle swarm central. Available at: http://www.particleswarm.info/Standard_PSO_2006.c.

PSO (2013). Particle swarm optimization. Available at: http://www.mathworks.com/matlabcentral/fileexchange/41708-particle-swarm-optimization.

Vesselinov, V. V. and Harp, D. R. (2012). Adaptive hybrid optimization strategy for calibration and parameter estimation of physical process models. *Computers & Geosciences*, 49:10–20.

Appendix IV

pH calculation code subroutine in CE-QUAL-W2

```
!**************************************************************************
!**                                 p H   C O 2
!**************************************************************************
ENTRY PH_CO2

! pH and carbonate species
  DO I=IU,ID
    DO K=KT,KB(I)
      CART = TIC(K,I)/12000.0  ! CART=equivalents/liter of C    TIC=mg/l C (MW=12g/mole)
      ALKT = ALK(K,I)/5.0E+04  ! ALK=mg/l as CaCO3 (MW=50 g/mole; EQ=50g/eq))      ALKT=equivalents/l
      T1K  = T1(K,I)+273.15

!**** Ionic strength
      IF (FRESH_WATER(JW)) S2 = 2.5E-05*TDS(K,I)
      IF (SALT_WATER(JW))  S2 = 1.47E-3+1.9885E-2*TDS(K,I)+3.8E-5*TDS(K,I)*TDS(K,I)

!**** Debye-Huckel terms and activity coefficients
      SQRS2  =  SQRT(S2)
      DH1    = -0.5085*SQRS2/(1.0+1.3124*SQRS2)+4.745694E-03+4.160762E-02*S2-9.284843E-03*S2*S2
      DH2    = -2.0340*SQRS2/(1.0+1.4765*SQRS2)+1.205665E-02+9.715745E-02*S2-2.067746E-02*S2*S2
      H2CO3T =  10.0**(0.0755*S2)
      HCO3T  =  10.0**DH1
      CO3T   =  10.0**DH2
      OH     =  HCO3T

!**** Temperature adjustment
      KW = 10.0**(-283.971-0.05069842*T1K+13323.0/T1K+102.24447*LOG10(T1K)-1119669.0/(T1K*T1K))/OH
      K1 = 10.0**(-3404.71/T1K+14.8435-0.032786*T1K)*H2CO3T/HCO3T
      K2 = 10.0**(-2902.39/T1K+ 6.4980-0.023790*T1K)*HCO3T/CO3T

!**** pH evaluation
      PHT = -PH(K,I)-2.1
      IF (PH(K,I) <= 0.0) PHT = -14.0
      INCR = 10.0
      DO N=1,3
        F    = 1.0
        INCR = INCR/10.0
        ITER = 0
        DO WHILE (F > 0.0 .AND. ITER < 12)
          PHT    = PHT+INCR
          HION   = 10.0**PHT
          BICART = CART*K1*HION/(K1*HION+K1*K2+HION*HION)
          F      = BICART*(HION+2.0*K2)/HION+KW/HION-ALKT-HION/OH
          ITER   = ITER+1
        END DO
        PHT = PHT-INCR
      END DO

!**** pH, carbon dioxide, bicarbonate, and carbonate concentrations
      HION      =  10.0**PHT
      PH(K,I)   = -PHT
      CO2(K,I)  =  TIC(K,I)/(1.0+K1/HION+K1*K2/(HION*HION))          ! mg/l as C
      HCO3(K,I) =  TIC(K,I)/(1.0+HION/K1+K2/HION)                    ! mg/l as C
      CO3(K,I)  =  TIC(K,I)/((HION*HION)/(K1*K2)+HION/K2+1.0)        ! mg/l as C
    END DO
  END DO
RETURN
```

Appendix V

Water quality variables in CE-QUAL-W2

Parameter	Value	Description
IMX	87	Number of segments in the computational grid
KMX	23	Number of layers in the computational grid
Latitude	50.71	Latitude, degrees
Longitude	107.28	Longitude, degrees
TM_{STRT}	April 1, 2011	Model simulation starting time
$TEMP_I$	4	Initial temperature, °C
TDS	250	TDS (g/m^3 or mg/l)
ISS	2	Inorganic suspended solids, mg/l
PO_4	0.01	PO_4-P, mg/l as P
NH_4	0.02	NH_4-N, mg/l as N
NO_3	0.01	NO_3-N + NO_2-N, mg/l as N
DSi	2	Dissolved silica, mg/l as Si
LDOM	0.1	Labile dissolved organic matter, mg/l as organic matter
RDOM	0.1	Refractory dissolved organic matter, mg/l as organic matter
LPOM	0.67	Labile particulate organic matter, mg/l as organic matter
RPOM	0.1	Refractory particulate organic matter, mg/l as organic matter
ALG	0.00001	Algae, mg/l as dry weight organic matter
DO	8	Dissolved oxygen, mg/l
TIC	15	Total inorganic carbon, mg/l as C
EX_{H_2O}	0.25	Extinction for pure water, m-1
EX_{SS}	0.1	Extinction due to inorganic suspended solids, $m^{-1}/(g/m^3)$
EX_{OM}	0.1	Extinction due to organic suspended solids, $m^{-1}/(g/m^3)$
EX_A	0.2	Algal light extinction, $m^{-1}/(g/m^3)$
β	0.45	Fraction of incident solar radiation absorbed at the water surface
SSS	1.1	Suspended solids settling rate, m day^{-1}
τ_{cr}	1.9	Critical shear stress for sediment resuspension, $dynes/cm^2$
AG	0.43	Maximum algal growth rate, day-1
AR	0.04	Maximum algal respiration rate, day-1
AE	0.02	Maximum algal excretion rate, day-1

AM	0.05	Maximum algal mortality rate, day-1
AS	0.13	Algal settling rate, m day-1
AHS_P	0.003	Algal half-saturation for phosphorus limited growth, g/m^3
AHS_N	0.014	Algal half-saturation for nitrogen limited growth, g/m^3
ASA_T	114	Light saturation intensity at maximum photosynthetic rate, W m^{-2}
AT_1	6.9	Lower temperature for algal growth, °C
AT_2	22.3	Lower temperature for maximum algal growth, °C
AT_3	35	Upper temperature for maximum algal growth, °C
AT_4	40	Upper temperature for algal growth, °C
ALG_P	0.005	Stoichiometric equivalent between algal biomass and phosphorus
ALG_N	0.08	Stoichiometric equivalent between algal biomass and nitrogen
ALG_C	0.45	Stoichiometric equivalent between algal biomass and carbon
ACHLA	0.05	Ratio between algal biomass and chlorophyll a in terms of mg algae/μg chlorophyll a
A_{POM}	0.8	Fraction of algal biomass that is converted to particulate organic matter when algae die
ANPR	0.001	Algal half saturation constant for ammonium preference
$LDOM_{DK}$	0.02	Labile DOM decay rate, day^{-1}
$RDOM_{DK}$	0.001	Refractory DOM decay rate, day^{-1}
LRD_{DK}	0.001	Labile to refractory DOM decay rate, day^{-1}
$LPOM_{DK}$	0.05	Labile POM decay rate, day^{-1}
$RPOM_{DK}$	0.001	Refractory POM decay rate, day^{-1}
LRP_{DK}	0.011	Labile to refractory POM decay rate, day^{-1}
POM_S	0.25	POM settling rate, m day^{-1}
PO_{4R}	0.001	Sediment release rate of phosphorus, fraction of SOD
NH_{4R}	0.001	Sediment release rate of ammonium, fraction of SOD
NH_{4DK}	0.15	Ammonium decay rate, day^{-1}
NO_{3DK}	0.05	Nitrate decay rate, day^{-1}
NO_{3S}	0.011	Denitrification rate from sediments, m day^{-1}
SOD	0.1	Zero-order sediment oxygen demand for each segment, g O_2 m^{-2} day^{-1}

Table V.1: CE-QUAL-W2 initial and optimal values for different parameters in the *Lite* model. Parameters definitions are from the CE-QUAL-W2 manual (Cole and Wells, 2015)

Table V.2: Derived variables in CE-QUAL-W2 model

$$POC = POM \times ORG_C \tag{V.1}$$

$$PON = POM \times ORG_N + Algae \times A_N \tag{V.2}$$

$$TN = DON + PON + NH_4 + NO_3 \tag{V.3}$$

$$TP = DOP + POP + PO_4 + TP_{SS} \tag{V.4}$$

Algae = Algal biomass
POC = Particulate organic carbon
PON = Particulate organic nitrogen
TN = Total nitrogen
TP = Total phosphorus
POM = Particulate organic matter
ORG_C = Stoichiometric equivalent between organic matter and carbon, $ORG_C = 0.45$
ORG_N = Stoichiometric equivalent between organic matter and nitrogen, $ORG_N = 0.08$
A_N = Stoichiometric equivalent between algal biomass and nitrogen, $A_N = 0.08$
DON = Dissolved organic nitrogen
TP_{SS} = SS $\times$ $PART_P$, SS= suspended solids & $PART_P$ = phosphorus partitioning coefficient for suspended solids.

References

Cole, T. M. and Wells, S. A. (2015). *CE-QUAL-W2: A two-dimensional, laterally averaged, hydrodynamic and water quality model*. Department of Civil and Environmental Engineering, Portland State University, Portland, OR, 3.72 edition.

Appendix VI

Permission for use of published manuscripts

.1 Elsevier License, terms and conditions

ELSEVIER LICENSE

Dec 15, 2016

This Agreement between Amir Sadeghian ("You") and Elsevier ("Elsevier") consists of your order details and the terms and conditions provided by Elsevier and Copyright Clearance Center.

All payments must be made in full to CCC. For payment instructions, please see information listed at the bottom of this form.

License number	4010380724905
License date	Dec 08, 2016
Licensed content publisher	Elsevier
Licensed content publication	Journal of Great Lakes Research
Licensed content title	Lake Diefenbaker temperature model
Licensed content author	Amir Sadeghian, Dirk de Boer, Jeff J. Hudson, Howard Wheater, Karl-Erich Lindenschmidt
Licensed content date	2015
Licensed content volume number	41
Licensed content issue number	n/a
Number of pages	14
Start Page	8
End Page	21
Type of Use	reuse in a thesis/dissertation
Portion	full article
Format	both print and electronic
Are you the author of this Elsevier article?	Yes
Will you be translating?	No
Title of your thesis/dissertation	Water quality modeling of Lake Diefenbaker
Expected completion date	Feb 2017

Estimated size (number of pages)	120
Elsevier VAT number	GB 494 6272 12
Requestor Location	Amir Sadeghian 11 Innovation Boulevard Saskatoon, SK S7N 3H5 Canada Attn: Amir Sadeghian
Billing Type	Invoice
Billing Address	Amir Sadeghian 11 Innovation Boulevard Saskatoon, SK S7N 3H5 Canada Attn: Amir Sadeghian
Total	0.00 CAD

INTRODUCTION

1. The publisher for this copyrighted material is Elsevier. By clicking "accept" in connection with completing this licensing transaction, you agree that the following terms and conditions apply to this transaction (along with the Billing and Payment terms and conditions established by Copyright Clearance Center, Inc. ("CCC"), at the time that you opened your Rightslink account and that are available at any time at http://myaccount.copyright.com).

GENERAL TERMS

2. Elsevier hereby grants you permission to reproduce the aforementioned material subject to the terms and conditions indicated.
3. Acknowledgement: If any part of the material to be used (for example, figures) has appeared in our publication with credit or acknowledgement to another source, permission must also be sought from that source. If such permission is not obtained then that material may not be included in your publication/copies. Suitable acknowledgement to the source must be made, either as a footnote or in a reference list at the end of your publication, as follows:
"Reprinted from Publication title, Vol /edition number, Author(s), Title of article / title of chapter, Pages No., Copyright (Year), with permission from Elsevier [OR APPLICABLE SOCIETY COPYRIGHT OWNER]." Also Lancet special credit - "Reprinted from The Lancet, Vol. number, Author(s), Title of article, Pages No., Copyright (Year), with permission from Elsevier."
4. Reproduction of this material is confined to the purpose and/or media for which permission is hereby given.
5. Altering/Modifying Material: Not Permitted. However figures and illustrations may be altered/adapted minimally to serve your work. Any other abbreviations, additions, deletions and/or any other alterations shall be made only with prior written authorization of Elsevier Ltd. (Please contact Elsevier at permissions@elsevier.com). No modifications can be made to any Lancet figures/tables and they must be reproduced in full.
6. If the permission fee for the requested use of our material is waived in this instance, please be advised that your future requests for Elsevier materials may attract a fee.
7. Reservation of Rights: Publisher reserves all rights not specifically granted in the combination of (i) the license details provided by you and accepted in the course of this licensing transaction, (ii) these terms and conditions and (iii) CCC's Billing and Payment terms and conditions.
8. License Contingent Upon Payment: While you may exercise the rights licensed immediately upon issuance of the license at the end of the licensing process for the transaction, provided that you have disclosed complete and accurate details of your proposed use, no license is finally effective unless and until full payment is received from you (either by publisher or by CCC) as provided

in CCC's Billing and Payment terms and conditions. If full payment is not received on a timely basis, then any license preliminarily granted shall be deemed automatically revoked and shall be void as if never granted. Further, in the event that you breach any of these terms and conditions or any of CCC's Billing and Payment terms and conditions, the license is automatically revoked and shall be void as if never granted. Use of materials as described in a revoked license, as well as any use of the materials beyond the scope of an unrevoked license, may constitute copyright infringement and publisher reserves the right to take any and all action to protect its copyright in the materials.
9. Warranties: Publisher makes no representations or warranties with respect to the licensed material.
10. Indemnity: You hereby indemnify and agree to hold harmless publisher and CCC, and their respective officers, directors, employees and agents, from and against any and all claims arising out of your use of the licensed material other than as specifically authorized pursuant to this license.
11. No Transfer of License: This license is personal to you and may not be sublicensed, assigned, or transferred by you to any other person without publisher's written permission.
12. No Amendment Except in Writing: This license may not be amended except in a writing signed by both parties (or, in the case of publisher, by CCC on publisher's behalf).
13. Objection to Contrary Terms: Publisher hereby objects to any terms contained in any purchase order, acknowledgment, check endorsement or other writing prepared by you, which terms are inconsistent with these terms and conditions or CCC's Billing and Payment terms and conditions. These terms and conditions, together with CCC's Billing and Payment terms and conditions (which are incorporated herein), comprise the entire agreement between you and publisher (and CCC) concerning this licensing transaction. In the event of any conflict between your obligations established by these terms and conditions and those established by CCC's Billing and Payment terms and conditions, these terms and conditions shall control.
14. Revocation: Elsevier or Copyright Clearance Center may deny the permissions described in this License at their sole discretion, for any reason or no reason, with a full refund payable to you. Notice of such denial will be made using the contact information provided by you. Failure to receive such notice will not alter or invalidate the denial. In no event will Elsevier or Copyright Clearance Center be responsible or liable for any costs, expenses or damage incurred by you as a result of a denial of your permission request, other than a refund of the amount(s) paid by you to Elsevier and/or Copyright Clearance Center for denied permissions.

LIMITED LICENSE

The following terms and conditions apply only to specific license types:
15. **Translation:** This permission is granted for non-exclusive world **English** rights only unless your license was granted for translation rights. If you licensed translation rights you may only translate this content into the languages you requested. A professional translator must perform all translations and reproduce the content word for word preserving the integrity of the article.
16. **Posting licensed content on any Website:** The following terms and conditions apply as follows: Licensing material from an Elsevier journal: All content posted to the web site must maintain the copyright information line on the bottom of each image; A hyper-text must be included to the Homepage of the journal from which you are licensing at http://www.sciencedirect.com/science/journal/xxxxx or the Elsevier homepage for books at http://www.elsevier.com; Central Storage: This license does not include permission for a scanned version of the material to be stored in a central repository such as that provided by. Heron/XanEdu.
Licensing material from an Elsevier book: A hyper-text link must be included to the Elsevier homepage at http://www.elsevier.com . All content posted to the web site must maintain the copyright information line on the bottom of each image.

Posting licensed content on Electronic reserve: In addition to the above the following clauses are applicable: The web site must be password-protected and made available only to bona fide students registered on a relevant course. This permission is granted for 1 year only. You may obtain a new license for future website posting.
17. **For journal authors:** the following clauses are applicable in addition to the above:
Preprints:
A preprint is an author's own write-up of research results and analysis, it has not been peer-reviewed, nor has it had any other value added to it by a publisher (such as formatting,

copyright, technical enhancement etc.).
Authors can share their preprints anywhere at any time. Preprints should not be added to or enhanced in any way in order to appear more like, or to substitute for, the final versions of articles however authors can update their preprints on arXiv or RePEc with their Accepted Author Manuscript (see below).
If accepted for publication, we encourage authors to link from the preprint to their formal publication via its DOI. Millions of researchers have access to the formal publications on ScienceDirect, and so links will help users to find, access, cite and use the best available version. Please note that Cell Press, The Lancet and some society-owned have different preprint policies. Information on these policies is available on the journal homepage.

Accepted Author Manuscripts: An accepted author manuscript is the manuscript of an article that has been accepted for publication and which typically includes author-incorporated changes suggested during submission, peer review and editor-author communications.
Authors can share their accepted author manuscript:

- immediately
  - via their non-commercial person homepage or blog
  - by updating a preprint in arXiv or RePEc with the accepted manuscript
  - via their research institute or institutional repository for internal institutional uses or as part of an invitation-only research collaboration work-group
  - directly by providing copies to their students or to research collaborators for their personal use
  - for private scholarly sharing as part of an invitation-only work group on commercial sites with which Elsevier has an agreement
- after the embargo period
  - via non-commercial hosting platforms such as their institutional repository
  - via commercial sites with which Elsevier has an agreement

In all cases accepted manuscripts should:

- link to the formal publication via its DOI
- bear a CC-BY-NC-ND license - this is easy to do
- if aggregated with other manuscripts, for example in a repository or other site, be shared in alignment with our hosting policy not be added to or enhanced in any way to appear more like, or to substitute for, the published journal article.

Published journal article (JPA): A published journal article (PJA) is the definitive final record of published research that appears or will appear in the journal and embodies all value-adding publishing activities including peer review co-ordination, copy-editing, formatting, (if relevant) pagination and online enrichment.
Policies for sharing publishing journal articles differ for subscription and gold open access articles:
Subscription Articles: If you are an author, please share a link to your article rather than the full-text. Millions of researchers have access to the formal publications on ScienceDirect, and so links will help your users to find, access, cite, and use the best available version.
Theses and dissertations which contain embedded PJAs as part of the formal submission can be posted publicly by the awarding institution with DOI links back to the formal publications on ScienceDirect.
If you are affiliated with a library that subscribes to ScienceDirect you have additional private sharing rights for others' research accessed under that agreement. This includes use for classroom teaching and internal training at the institution (including use in course packs and courseware programs), and inclusion of the article for grant funding purposes.
Gold Open Access Articles: May be shared according to the author-selected end-user license and should contain a CrossMark logo, the end user license, and a DOI link to the formal publication

Posting or linking by commercial companies for use by customers of those companies.

20. **Other Conditions:**
v1.9
Questions? customercare@copyright.com or +1-855-239-3415 (toll free in the US) or +1-978-646-2777.

.2 Springer Licenses, terms and conditions

SPRINGER LICENSE

Sep 15, 2017

This Agreement between Amir Sadeghian ("You") and Springer ("Springer") consists of your license details and the terms and conditions provided by Springer and Copyright Clearance Center.

License number	4190160373850
License date	Sep 15, 2017
Licensed content publisher	Springer
Licensed content publication	Environmental Monitoring and Assessment
Licensed content title	Sedimentation and erosion in Lake Diefenbaker, Canada: solutions for shoreline retreat monitoring
Licensed content author	Amir Sadeghian
Licensed content date	Jan 1, 2017
Licensed Content Volume	189
Licensed Content Issue	10
Type of Use	Thesis/Dissertation
Portion	full text
Number of copies	1
Author of this Springer article	Yes and you are a contributor of the new work
Order reference number	
Title of your thesis/dissertation	Water quality modeling of Lake Diefenbaker
Expected completion date	Jul 2017
Estimated size (number of pages)	180
Elsevier VAT number	GB 494 6272 12
Requestor Location	Amir Sadeghian 11 Innovation Boulevard Saskatoon, SK S7N 3H5 Canada Attn: Amir Sadeghian
Billing Type	Invoice
Billing Address	Amir Sadeghian 11 Innovation Boulevard Saskatoon, SK S7N 3H5 Canada Attn: Amir Sadeghian
Total	0.00 CAD

SPRINGER LICENSE

Jul 05, 2017

This Agreement between Amir Sadeghian ("You") and Springer ("Springer") consists of your license details and the terms and conditions provided by Springer and Copyright Clearance Center.

License number	4142720202228
License date	Jul 05, 2017
Licensed content publisher	Springer
Licensed content publication	Environmental Science and Pollution Research
Licensed content title	Sediment plume model—a comparison between use of measured turbidity data and satellite images for model calibration
Licensed content author	Amir Sadeghian
Licensed content date	Jan 1, 2017
Type of Use	Thesis/Dissertation
Portion	full article
Number of copies	1
Author of this Springer article	Yes and you are a contributor of the new work
Order reference number	
Format	both print and electronic
Are you the author of this Elsevier article?	Yes
Will you be translating?	No
Title of your thesis/dissertation	Water quality modeling of Lake Diefenbaker
Expected completion date	Jul 2017
Estimated size (number of pages)	180
Elsevier VAT number	GB 494 6272 12
Requestor Location	Amir Sadeghian 11 Innovation Boulevard Saskatoon, SK S7N 3H5 Canada Attn: Amir Sadeghian
Billing Type	Invoice
Billing Address	Amir Sadeghian 11 Innovation Boulevard Saskatoon, SK S7N 3H5 Canada Attn: Amir Sadeghian
Total	0.00 CAD

SPRINGER LICENSE

Aug 11, 2017

This Agreement between Amir Sadeghian ("You") and Springer ("Springer") consists of your license details and the terms and conditions provided by Springer and Copyright Clearance Center.

License number	4166120554841
License date	Aug 11, 2017
Licensed content publisher	Springer
Licensed content publication	Water Resources Management
Licensed content title	Modelling Scenarios to Estimate the Potential Impact of Hydrological Standards on Nutrient Retention in the Tobacco Creek Watershed, Manitoba, Canada
Licensed content author	Darian Weber
Licensed content date	Jan 1, 2017
Licensed Content Volume	31
Licensed Content Issue	4
Type of Use	Thesis/Dissertation
Portion	Full text
Number of copies	1
Author of this Springer article	Yes and you are a contributor of the new work
Order reference number	
Title of your thesis/dissertation	Water quality modeling of Lake Diefenbaker
Expected completion date	Jul 2017
Estimated size (number of pages)	180
Requestor Location	Amir Sadeghian 11 Innovation Boulevard Saskatoon, SK S7N 3H5 Canada Attn: Amir Sadeghian
Billing Type	Invoice
Billing Address	Amir Sadeghian 11 Innovation Boulevard Saskatoon, SK S7N 3H5 Canada Attn: Amir Sadeghian
Total	0.00 CAD

Terms and Conditions

Introduction

The publisher for this copyrighted material is Springer. By clicking "accept" in connection with completing this licensing transaction, you agree that the following terms and conditions apply to this transaction (along with the Billing and Payment terms and conditions established by Copyright Clearance Center, Inc. ("CCC"), at the time that you opened your

Rightslink account and that are available at any time at http://myaccount.copyright.com).

Limited License

With reference to your request to reuse material on which Springer controls the copyright, permission is granted for the use indicated in your enquiry under the following conditions:
– Licenses are for one-time use only with a maximum distribution equal to the number stated in your request.
– Springer material represents original material which does not carry references to other sources. If the material in question appears with a credit to another source, this permission is not valid and authorization has to be obtained from the original copyright holder.
– This permission

- is non-exclusive
- is only valid if no personal rights, trademarks, or competitive products are infringed.
- explicitly excludes the right for derivatives.

– Springer does not supply original artwork or content.
– According to the format which you have selected, the following conditions apply accordingly:

- **Print and Electronic:** This License include use in electronic form provided it is password protected, on intranet, or CD-Rom/DVD or E-book/E-journal. It may not be republished in electronic open access.
- **Print:** This License excludes use in electronic form.
- **Electronic:** This License only pertains to use in electronic form provided it is password protected, on intranet, or CD-Rom/DVD or E-book/E-journal. It may not be republished in electronic open access.

For any electronic use not mentioned, please contact Springer at permissions.springer@spi-global.com.
– Although Springer controls the copyright to the material and is entitled to negotiate on rights, this license is only valid subject to courtesy information to the author (address is given in the article/chapter).
– If you are an STM Signatory or your work will be published by an STM Signatory and you are requesting to reuse figures/tables/illustrations or single text extracts, permission is granted according to STM Permissions Guidelines: http://www.stm-assoc.org/permissions-guidelines/
For any electronic use not mentioned in the Guidelines, please contact Springer at permissions.springer@spi-global.com. If you request to reuse more content than stipulated in the STM Permissions Guidelines, you will be charged a permission fee for the excess content.
Permission is valid upon payment of the fee as indicated in the licensing process. If permission is granted free of charge on this occasion, that does not prejudice any rights we might have to charge for reproduction of our copyrighted material in the future.
– If your request is for reuse in a Thesis, permission is granted free of charge under the following conditions:
This license is valid for one-time use only for the purpose of defending your thesis and with a maximum of 100 extra copies in paper. If the thesis is going to be published, permission needs to be reobtained.
– includes use in an electronic form, provided it is an author-created version of the thesis on his/her own website and his/her university's repository, including UMI (according to the definition on the Sherpa website: http://www.sherpa.ac.uk/romeo/);

– subject to courtesy information to the co-author or corresponding author.
Geographic Rights: Scope
Licenses may be exercised anywhere in the world.
Altering/Modifying Material: Not Permitted
Figures, tables, and illustrations may be altered minimally to serve your work. You may not alter or modify text in any manner. Abbreviations, additions, deletions and/or any other alterations shall be made only with prior written authorization of the author(s).
Reservation of Rights
Springer reserves all rights not specifically granted in the combination of (i) the license details provided by you and accepted in the course of this licensing transaction and (ii) these terms and conditions and (iii) CCC's Billing and Payment terms and conditions.
License Contingent on Payment
While you may exercise the rights licensed immediately upon issuance of the license at the end of the licensing process for the transaction, provided that you have disclosed complete and accurate details of your proposed use, no license is finally effective unless and until full payment is received from you (either by Springer or by CCC) as provided in CCC's Billing and Payment terms and conditions. If full payment is not received by the date due, then any license preliminarily granted shall be deemed automatically revoked and shall be void as if never granted. Further, in the event that you breach any of these terms and conditions or any of CCC's Billing and Payment terms and conditions, the license is automatically revoked and shall be void as if never granted. Use of materials as described in a revoked license, as well as any use of the materials beyond the scope of an unrevoked license, may constitute copyright infringement and Springer reserves the right to take any and all action to protect its copyright in the materials.
Copyright Notice: Disclaimer
You must include the following copyright and permission notice in connection with any reproduction of the licensed material:
Springer book/journal title, chapter/article title, volume, year of publication, page, name(s) of author(s), (original copyright notice as given in the publication in which the material was originally published) "With permission of Springer"
In case of use of a graph or illustration, the caption of the graph or illustration must be included, as it is indicated in the original publication.
Warranties: None
Springer makes no representations or warranties with respect to the licensed material and adopts on its own behalf the limitations and disclaimers established by CCC on its behalf in its Billing and Payment terms and conditions for this licensing transaction.
Indemnity
You hereby indemnify and agree to hold harmless Springer and CCC, and their respective officers, directors, employees and agents, from and against any and all claims arising out of your use of the licensed material other than as specifically authorized pursuant to this license. No Transfer of License
This license is personal to you and may not be sublicensed, assigned, or transferred by you without Springer's written permission.
No Amendment Except in Writing
This license may not be amended except in a writing signed by both parties (or, in the case of Springer, by CCC on Springer's behalf).
Objection to Contrary Terms
Springer hereby objects to any terms contained in any purchase order, acknowledgment, check endorsement or other writing prepared by you, which terms are inconsistent with these terms and conditions or CCC's Billing and Payment terms and conditions. These terms and conditions, together with CCC's Billing and Payment terms and conditions (which are incorporated herein), comprise the entire agreement between you and Springer (and CCC) concerning this licensing transaction. In the event of any conflict between your obligations established by these terms and conditions and those established by CCC's

Billing and Payment terms and conditions, these terms and conditions shall control.
Jurisdiction
All disputes that may arise in connection with this present License, or the breach thereof, shall be settled exclusively by arbitration, to be held in the Federal Republic of Germany, in accordance with German law.
Other conditions:
V 12AUG2015
Questions? customercare@copyright.com or +1-855-239-3415 (toll free in the US) or +1-978-646-2777.

.3 MDPI Open Access

MDPI Open Access Information and Policy

All articles published by MDPI are made immediately available worldwide under an open access license. This means:

- everyone has free and unlimited access to the full-text of all articles published in MDPI journals, and
- everyone is free to re-use the published material if proper accreditation/citation of the original publication is given.
- open access publication is supported by the authors' institutes or research funding agencies by payment of a comparatively low Article Processing Charge (APC) for accepted articles.

Meaning of Open Access

In accordance with major definitions of open access in scientific literature (namely the Budapest, Berlin, and Bethesda declarations), MDPI defines open access by the following conditions:

- peer-reviewed literature is freely available without subscription or price barriers,
- literature is immediately released in open access format (no embargo period), and
- published material can be re-used without obtaining permission as long as a correct citation to the original publication is given.

Until 2008, most articles published by MDPI contained the note: "year by MDPI (http://www.mdpi.org). Reproduction is permitted for noncommercial purposes". During 2008, MDPI journals started to publish articles under the Creative Commons Attribution License external link and are now using the latest version of the CC BY license, which grants authors the most extensive rights. All articles published by MDPI before and during 2008 should now be considered as having been released under the post-2008 Creative Commons Attribution License.

This means that all articles published in MDPI journals, including data, graphics, and supplements, can be linked from external sources, scanned by search engines, re-used by text mining applications or websites, blogs, etc. free of charge under the sole condition of proper accreditation of the source and original publisher. MDPI believes that open access publishing fosters the exchange of research results amongst scientists from different disciplines, thus facilitating interdisciplinary research. Open access publishing also provides